Final Technical Report

Contract Number:	**DE-FC26-07NT43270**
Title of Project:	**E85 Optimized Engine through Boosting, Spray-Optimized DIG, VCR and Variable Valvetrain**
Submitted by:	**Delphi Automotive Systems, LLC 5725 Delphi Drive Troy, MI 48098-2815**
	Partners: Wayne State University

Points of Contact:

Principal Investigator	**Keith Confer Phone: 248-836-0439 Fax: 248-836-1891 Email: keith.confer@delphi.com**
Project Director	**Harry Husted Phone: (248) 732-1812 Email: Harry.L.Husted@delphi.com**
DOE Project Officer:	**Ralph Nine Project Manager US Department of Energy Phone: 304-285-2017 Email: Ralph.Nine@netl.doe.gov**
Award Recipient:	**Delphi Automotive Systems, LLC 5725 Delphi Drive Troy, MI 48098-2815**

Date of Report:	**8-29-11**

Introduction

The use of biofuels for internal combustion engines has several well published advantages. The biofuels, made from biological sources such as corn or sugar cane, are renewable resources that reduce the dependence on fossil fuels. Fuels from agricultural sources can therefore reduce a countries energy dependency on other nations. Biofuels also have been shown to reduce CO2 emissions into the atmosphere compared to traditional fossil based fuels. Because of these benefits several countries have set targets for the use of biofuels, especially ethanol, in their transportation fuels. Small percentages of ethanol are common place in gasoline but are typically limited to 5 to 8% by volume. Greater benefits are possible from higher concentrations and some countries such as the US and Sweden have encouraged the production of vehicles capable of operating on E85 (85% denatured ethanol and 15% gasoline). E85 capable vehicles are normally equipped to run the higher levels of ethanol by employing modified fuel delivery systems that can withstand the highly corrosive nature of the alcohol. These vehicles are not however equipped to take full advantage of ethanol's properties during the combustion process. Ethanol has a much higher blend research octane number than gasoline. This allows the use of higher engine compression ratios and spark advance which result in more efficient engine operation. Ethanol's latent heat of vaporization is also much higher that gasoline. This higher heat of vaporization cools the engine intake charge which also allows the engine compression ratio to be increased even further. An engine that is optimized for operation on high concentrations of ethanol therefore will have compression ratios that are too high to avoid spark knock (pre-ignition) if run on gasoline or a gasoline/ethanol blend that has a low percentage alcohol.

An engine was developed during this project to leverage the improved evaporative cooling and high octane of E85 to improve fuel economy and offset E85's lower energy content. A 2.0 L production Direct Injection gasoline, (DIg) engine employing Dual Independent Cam Phasing, (DICP) and turbo charging was used as the base engine. Modified pistons were used to increase the geometric compression ratio from 9.2:1 to 11.85:1 by modifying the pistons and adding advanced valvetrain to proved control of displacement and effective compression ratio through valve timing control. The advanced valvetrain utilized Delphi's two step valvetrain hardware and intake cam phaser with increased phasing authority of 80 crank angle degrees.

Using this hardware the engine was capable of operating knock free on all fuels tested from E0 –E85 by controlling effective compression ratio using a Late Intake Valve Closing, (LIVC) strategy. The LIVC strategy results in changes in the trapped displacement such that knock limited torque for gasoline is significantly lower than E85. The use of spark retard to control knock enables higher peak torque for knock limited fuels, however a loss in efficiency results. For gasoline and E10 fuels, full effective displacement could not be reached before spark retard produced a net loss in torque.

The use of an Early Intake Valve Closing, (EIVC) strategy resulted in an improvement of engine efficiency at low to mid loads for all fuels tested from E0-E85. Further the use of valve deactivation, to a single intake valve, improved combustion stability and enabled throttle-less operation down to less than 2 bar BMEP. Slight throttling to trap internal residual provided additional reductions in fuel consumption.

To fully leverage the benefits of E 85, or ethanol blends above E10, would require a vehicle level approach that would take advantage of the improved low end torque that is possible with E85. Operating the engine at reduced speeds and using advanced transmissions (6 speeds or higher) would provide a responsive efficient driving experience to the customer. The vehicle shift and torque converter lockup points for high ethanol blends could take advantage of the significant efficiency advantage of down-speeding and operating at higher loads to deliver the required power.

Additional fuel efficiency for E85 could likely be achieved by a further increase in compression ratio, however problems arise with compatibility with low ethanol blends plus the resulting increased cylinder pressures would require building heavier engines which would detract from vehicle level fuel economy. Peak pressures for this engine would be limited under boosted operation, requiring spark retard to limit peak pressure and further reducing efficiency.

The use of ethanol blends as high as E85 in transportation does not provide the optimal balance between the performance potential of the ethanol compared to ethanol's reduced energy density. The use of moderate blends, E20 to E30, provides a better balance of improved performance potential with a reduced energy density penalty.

Program Overview

During the program, the following series of activities were carried out during the development of the flex fuel optimized engine. Details of these activities are presented in the attached quarterly reports. The activities are listed in chronological order.

Modeling
- Engine simulation (GT Power)
- Spray modeling
- In-cylinder CFD Modeling

Spray Testing
- Targeting characterization
- Droplet size distributions
- Spray structure (MIE, Schlieren)
- Vapor plume (Schlieren)

Hardware fabrication
- Valvetrain
- Injectors
- Pistons
- Engine control integration

Engine validation
- Load control
- Knock management
- Engine stability

Engine calibration optimization
- Cam phasing optimization
- Injection timing optimization

Vehicle drive simulation
- Down-speed, shift schedule optimization

Charge motion evaluation
- Valve deactivation for improved stability
- Valve deactivation for soot management.
- Optical engine evaluation
- CFD modeling

Fuel blend evaluation
- Knock limited torque
- Peak torque
- Emissions

Result Highlights

<u>Throttle-less control</u>

The use of Delphi's 2 Step Variable Valve Activation (VVA) system in conjunction with an extended authority cam phaser allowed throttle-less load control from as low as 2 bar BMEP up to peak torque (see Figure 1). Difficulties arose due to combustion stability at low loads with increasing speed. This difficulty was addressed during the project by increasing in-cylinder charge motion through deactivation of one of the intake valves at low load while operating in an Early Intake Valve Closing, (EIVC) strategy.

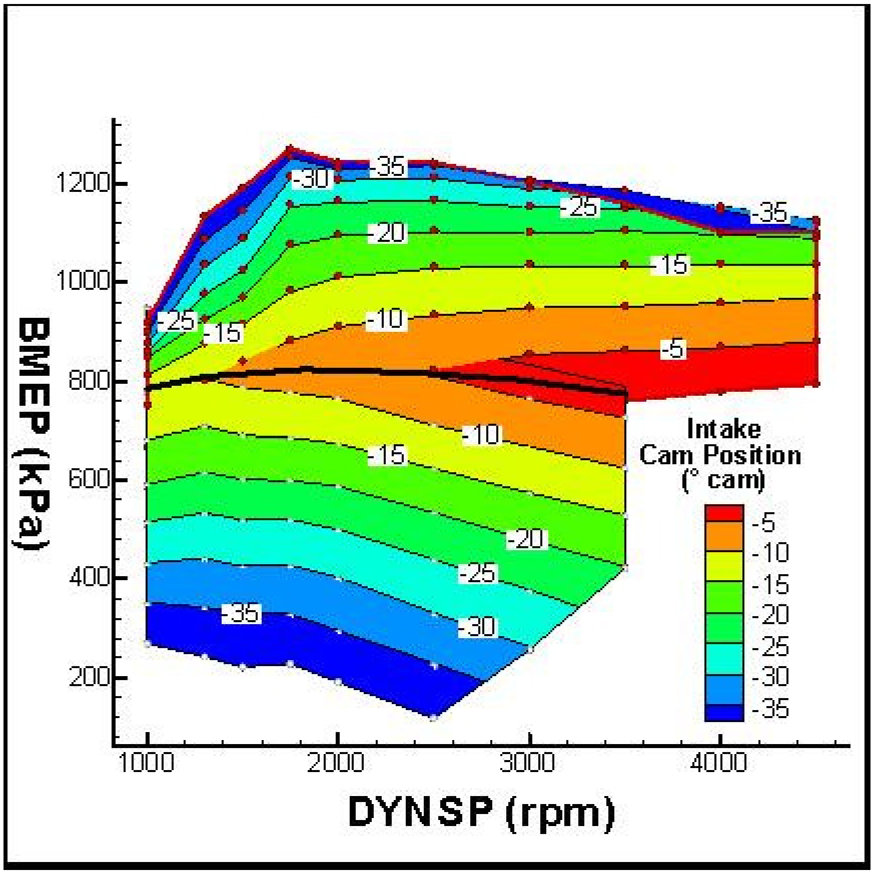

<u>Figure 1</u> Un-throttled load control domain, contours indicate cam phasing location, 0=park, 40 =max phasing in cam degrees, Black Line Switch point

<u>Cam optimization</u>

Cam phasing optimization was conducted to minimize fuel consumption and emissions while maintaining good combustion stability. It was found that optimal efficiency could be established using slight throttling which trapped internal combustion residuals. A cam optimization map is shown in Figure 2 for operation with EIVC and intake valve de-activation (single intake valve open).

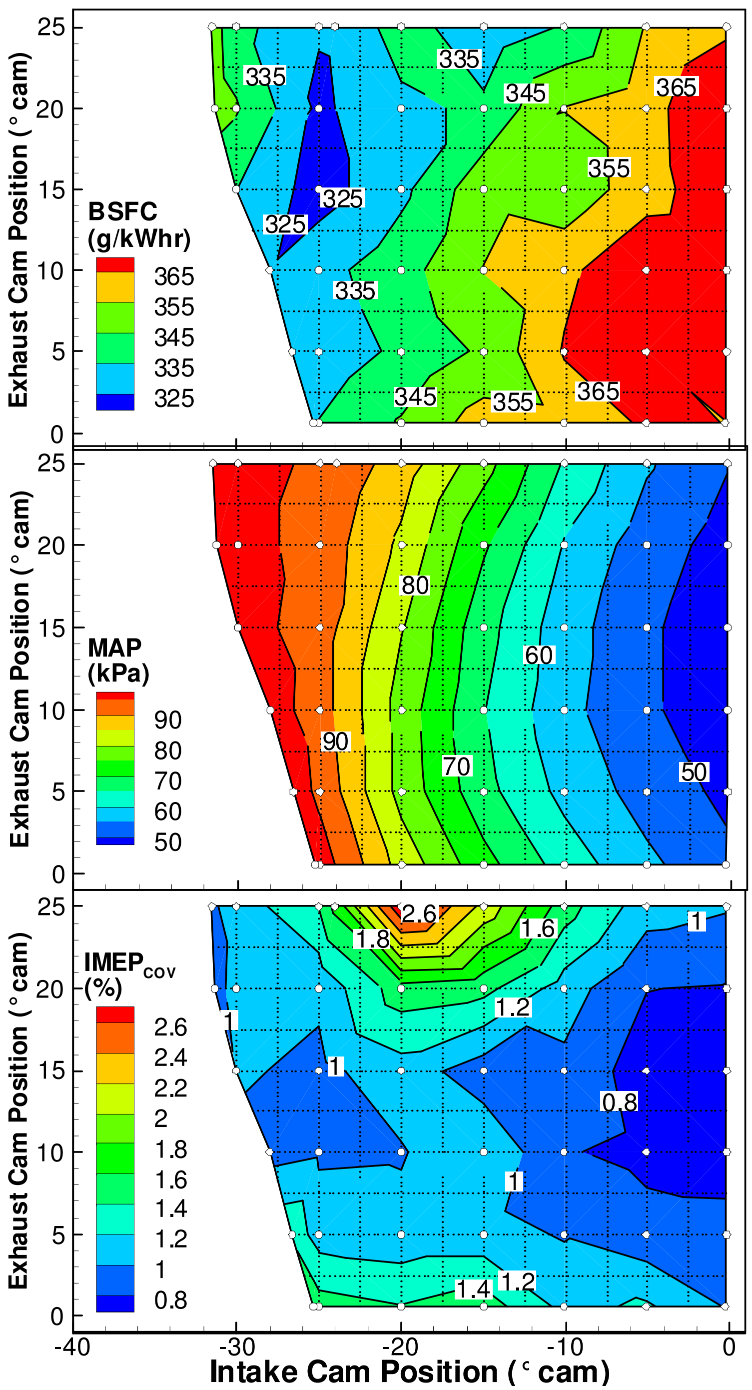

Figure 2 *Cam phasing optimization map with EIVC with valve deactivation, 2000 RPM, Fixed fuel 9,95 mg/cyl, Nominal load 2 Bar BMEP, 91 RON E0 gasoline*

Fuel Economy Improvements

Fuel economy was improved on the engine as a result of increased compression ratio and reduced pumping losses from advanced valve train with cam timing optimization. E85 was able to maintain optimal spark timing due to its high octane number such that benefits were achieved over the entire speed load range tested (see Figure 3). The most significant benefits were achieved at low loads using Early Intake Valve Closing (EIVC) with one valve deactivated to promote improved charge mixing, which significantly improved stability. At low loads efficiency improvements from this approach were also realized while operating on gasoline however efficiency did suffer at high loads on gasoline due to spark retard to control knock (see Figure 4). Gasoline and low ethanol blends also suffered from high particulate levels. An attempt to reduce particulates with increased mixing resulting from single valve deactivation was detrimental to peak power and efficiency due to an increase in knock sensitivity (see Figure 4). The preferred method of operation would be to utilize 1 valve EIVC at low loads and switch to 2 Valve LIVC operation for high load and high speeds.

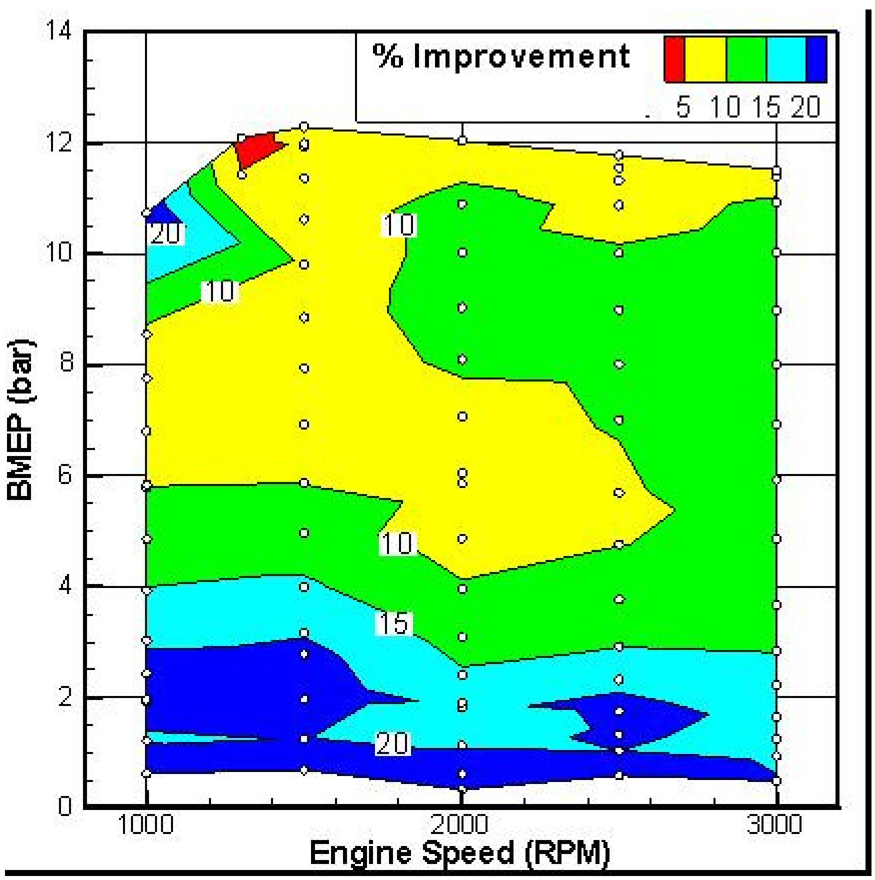

Figure 3 E85 Speed load map showing relative thermal efficiency improvement over base engine data.

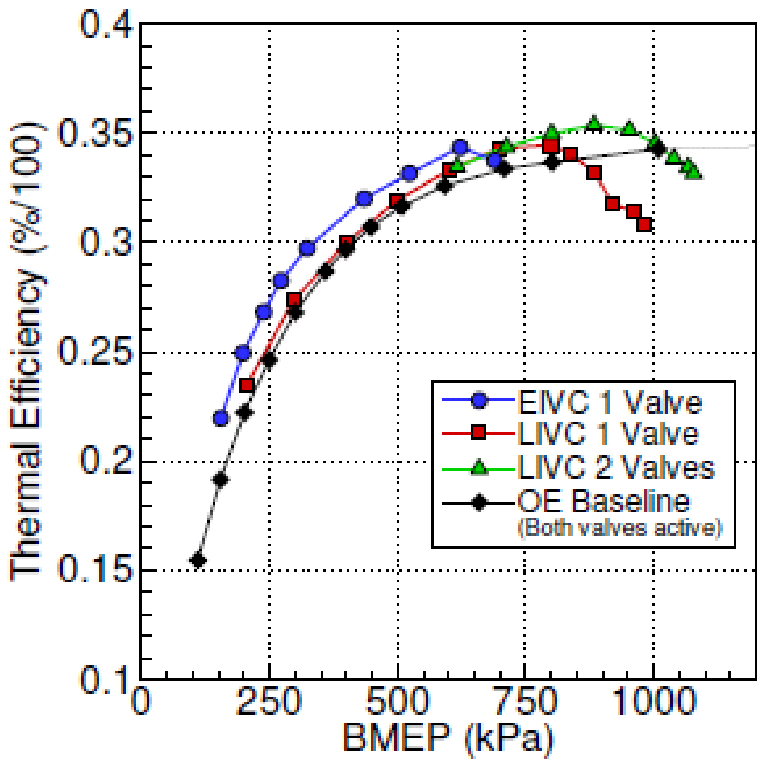

Figure 4. *Thermal efficiency at 2000 RPM, 91 RON Gasoline, strategy comparison.*

Fuel Blend knock Limited compression ratio and peak torque

Fuel blends from E0 to E85 blended using 91 RON gasoline were evaluated to determine their knock limited compression ratio. For reference a 96 RON gasoline was also tested. An effective compression ratio sweep was conducted from 1000-4000 rpm for each of the fuels until trace knock was detected at MBT with a combustion phasing near 9 cad aTDC. Figure 3 shows the knock limited effective compression ratio for the fuels. By using spark retard to retard combustion phasing peak torque could be increased for the knock prone fuels however this results in a loss of efficiency. Peak knock limited torque is shown in Figure 4 under naturally aspirated conditions.

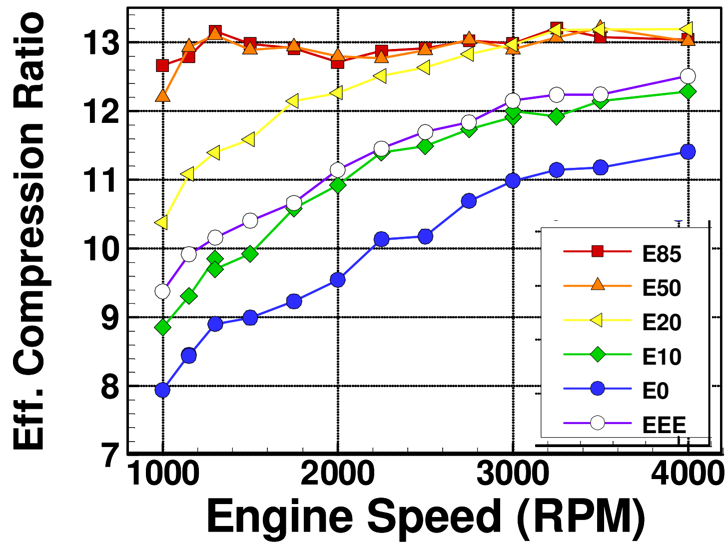

Figure 5 Knock limited compression ratio

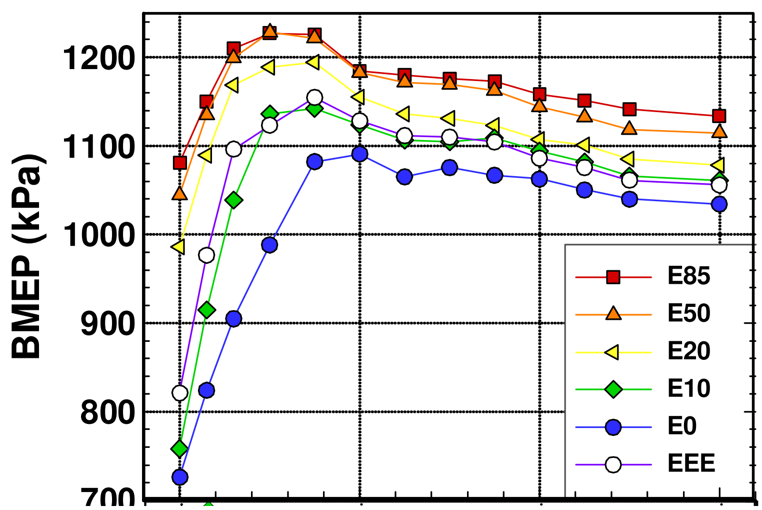

Figure 6 Peak Torque

Charge motion evaluation

The use of valve deactivation under high load conditions was found to reduce particulate and hydrocarbon emissions. Although E85 was very resistant to particulate formation, intermediate blends still produced unacceptable particle emissions under low RPM, high load conditions. Figure5 shows a comparison of particle emissions from E20 during a 1500 RPM load sweep for both a deactivated intake valve system (one valve open) and a fully active system. A significant reduction in both the particle emissions as measured by an AVL 415 smoke meter and the engine out hydrocarbons is observed. The additional charge motion did however produce a detrimental effect due to knock sensitivity, resulting in a reduction of peak power and retarded combustion phasing.

Predictions from CFD indicated an increase in average charge temperature which would explain the observed result of lower volumetric efficiency and increased knock sensitivity. This sensitivity was more severe with lower ethanol blends or straight gasoline.

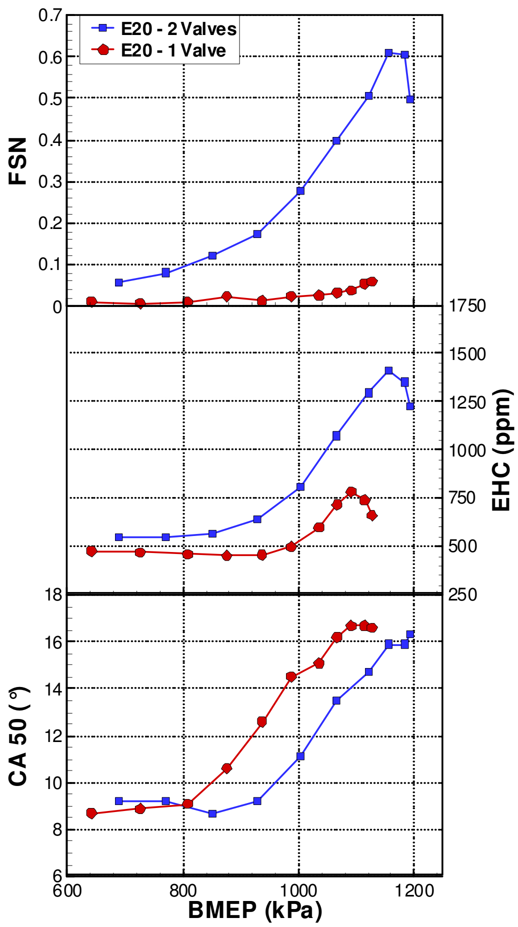

Figure 7 *1500 RPM Un-throttled LIVC sweep, (a)Soot (FSN), (b) Hydrocarbons, (c) Combustion phasing (CA50)*

Fuel blend sensitivity

Fuels samples were pulled from the blends tested to quantify the fuel properties. Testing of the RON index showed a significant nonlinear response to ethanol content. Figure 6 shows the effect of measured ethanol content on measured RON for this study as well as test data reported in literature. From these results it appears that the majority of the knock resistance is achieved with moderate ethanol addition, under 50%, and over half of the benefit is achieved with the addition of 20% ethanol to the 91 RON gasoline.

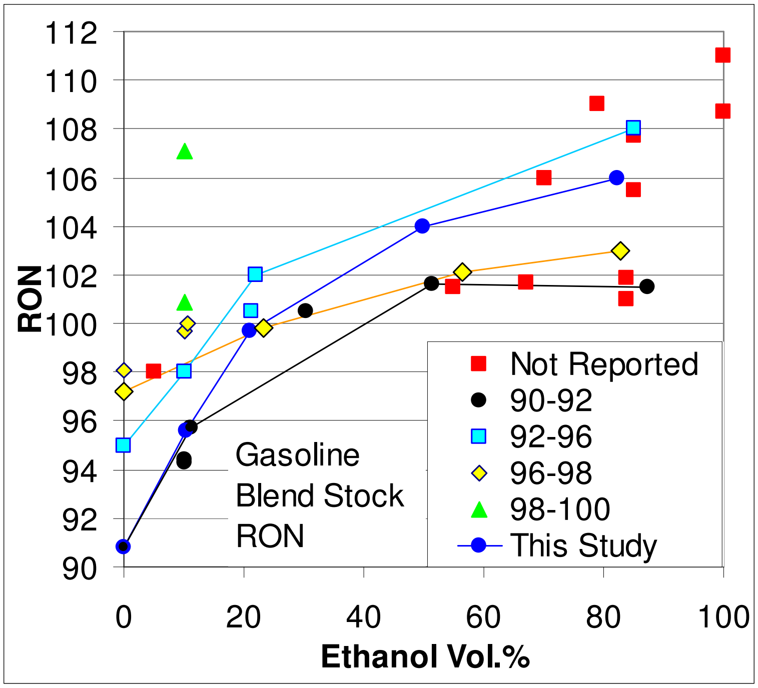

Figure 8) RON sensitivity to ethanol content

Vehicle simulation

Vehicle simulation was used to determine the potential benefits of using an engine specifically designed to take advantage of E85. Many of the improvements to the engine benefited not only E85 operation but gasoline operation as well. The use of high ethanol blends however presented an opportunity to leverage the superior low end torque of E85 by down-speeding the engine and operating at higher load with more aggressive shift schedules. Figure 6 shows the benefits of vehicle level changes including addition of a 6 speed transmission and a lower final drive ratio to reduce engine speed. Compared to the base engine, significant improvement can be realized using E85. The use of intermediate blends E20 toE30 offer the potential to take advantage of the same strategies while reducing the energy density penalty associated with E85 and appear to be the best compromise between octane increase and energy density reduction.

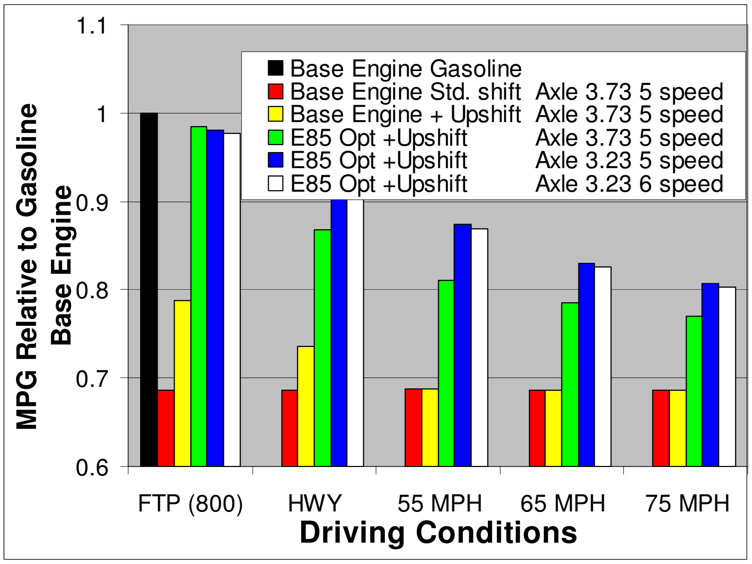

Figure 9) *Relative fuel economy to base engine operating on E85 for various operating modes and effect of transmission axel ratio and shift strategy.*

Fuel Policy Strategy

Ethanol can be integrated into the US fueling infrastructure in a method that maximizes it potential benefits rather than simply as an energy substitute for gasoline. Ethanol offers significant potential as an additive to meet the octane requirements of engines while reducing refining cost of other octane enhancing treatments. This has been done historically for creating blends up to E10 that are compatible with current engines for producing current pump gasoline. An additional octane improvement can be achieved with moderate ethanol blends, E20-E30. These higher blends could provide improved octane levels, enabling the production of engines that are optimized for these fuels. Blends above E50 however offer very little additional benefit but suffer significantly due to lower energy density. The use of blend pumps to supply a nominal 87 Octane gasoline at E10, with additional ethanol blending for higher octane fuels, from the same gasoline blend stock, would give consumers the opportunity to buy ethanol for its performance benefits instead of being penalized for it's lower energy content. Development of engine-vehicle systems offer the potential to leverage this performance potential to provide increased performance and improved fuel economy to the end user.

Application Strategy

Utilization of ethanol offers fuel economy potential in the transportation sector through intelligent selection of the fuel, engine and vehicle architecture. The improved low end torque enabled by the knock resistance of ethanol blends can be leveraged with modern transmissions using 6 or more speeds to operate at lower engine RPM. This provides the opportunity for improved transient response and fuel economy to the end customer. The vehicle shift points could be optimized for the knock resistant of the ethanol blend to take advantage of the significant efficiency advantage of down-speeding and operating at higher loads to deliver the required power.

Another natural fit for using high ethanol fuels is in the agriculture sector. Typical agricultural uses, i.e. tractors, require excellent low end torque which ethanol can provide. Likewise building dedicated engines for E85 or even denatured E100 do not pose the drawbacks that occur in the transportation sector. Increased mass is not a detriment and these engines would have structural requirements closer to conventional diesel engines which are the workhorse of large agricultural machines. The use of ethanol for agricultural production, especially in the corn belt, would also result in a reduction of transport cost and associated fuel usage. Evaluation of the agricultural fuel demand from EIA data indicates that current ethanol production can meet this need with additional production available for use in the transportation sector. Figure 8 shows that on an energy adjusted basis the U.S. ethanol supply surpassed the demand for agricultural petroleum distillate (Diesel and Gasoline) in 2007. This also presents the opportunity to secure the US food supply from disruptions in petroleum supply due to natural or political disasters.

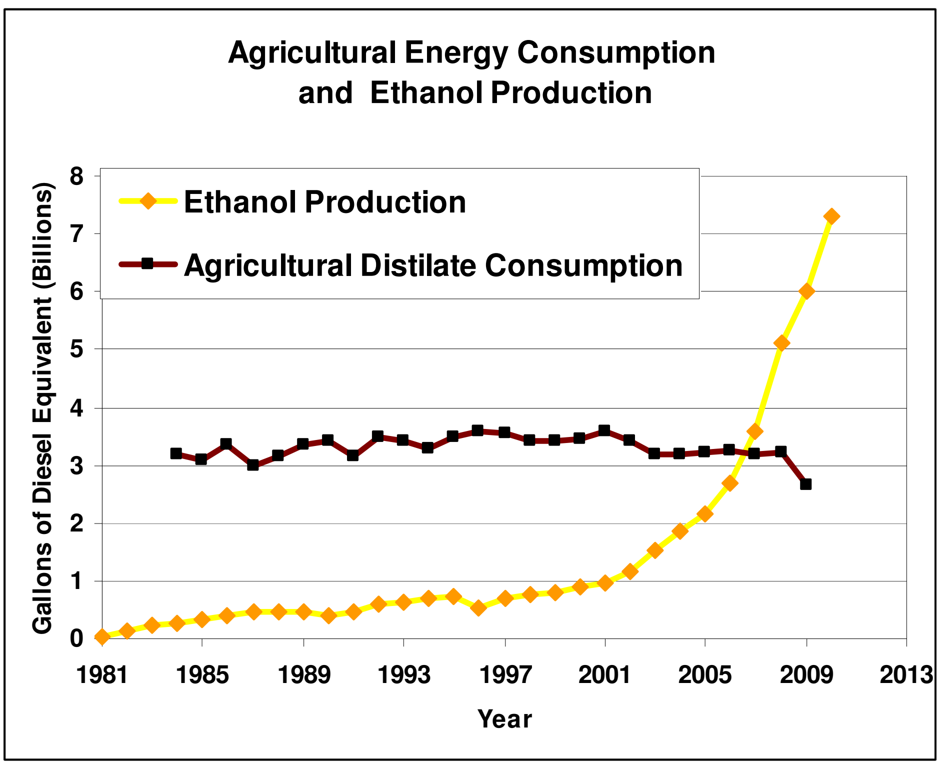

Figure 10) Us Ethanol Production and Farm distillate consumption, adjusted energy basis.

US Agricultural distillate consumption source:
http://www.eia.gov/dnav/pet/hist/LeafHandler.ashx?n=PET&s=KD0VFMNUS1&f=A

US Ethanol Production Source:
http://www.eia.gov/dnav/pet/hist/LeafHandler.ashx?n=PET&s=M_EPOOXE_YOP_NUS_1&f=A

Recommendations for future work with ethanol blends

Mid level ethanol blends offer the opportunity for providing a better tradeoff between the beneficial effects of ethanol to improve octane versus ethanol's reduced fuel energy density. A complete well to wheels analysis of the use of mid level E10-E40 blends in conjunction with flex fuel vehicle design and the refinery implication is needed. The use of ethanol may enable more economical gasoline blend stocks with an E10 nominal meeting the 87 Pump octane specifications while increased ethanol levels could provide fuels for higher performance flex fuel vehicles.

Dedicated ethanol engines could also be optimized for running on E85 or E100. Wet ethanol provides an additional energy savings by reducing energy consumed in converting distilled to anhydrous, (neat) ethanol. These applications may be best suited for agricultural applications where readily available local supplies of ethanol are produced.

Publications/ Presentations related to this program

1. Hoyer, K., Moore, W., Confer, K., "A Simulation Method to Guide DISI Engine Redesign for Increased Efficiency Using Alcohol Fuel Blends," SAE Technical Paper 2010-01-1203, 2010.
2. Matsumoto, A., Zheng, Y., Xie, X.B., Lai, M.C., Moore, W., "Characterization of Multi-hole Spray and Mixing of Ethanol and Gasoline Fuels under DI Engine Conditions" SAE Technical Paper 2010-01-2151, 2010.
3. Moore, W., "Development of en SIDI ethanol optimized flex fuel engine using advanced valve train", Presentation DEER conference 2010 http://www1.eere.energy.gov/vehiclesandfuels/pdfs/deer_2010/wednesday/presentations/deer10_moore.pdf
4. Moore, W., Foster, Hoyer, K., 'Engine Efficiency Improvements Enabled by Ethanol Fuels, in an GDI, VVA Flex Fuel Engine". SAE Technical Offer Number: 2011-01-0900, 2011.

Moore, W., Foster, M., Matsumoto, A., Lai, M.C., Zheng, Y., Xie, X.B., 'Charge motion benefits of valve deactivation design to reduce fuel consumption and emissions in a GDi VVA engine". SAE Technical Paper 2011-0

Project record

The following is a record of the project progress listed chronologically by quarter and year:

Quarter 1 2008

Task 1.0 –Development of Overall Model for 'Ecotec' Engine (1/1/08 thru 3/31/08)

Many GT power simulations using the Ecotec engine model previously developed were run during this reporting period. The objective of these simulations is to determine the compression ratio and valve profiles and cam phasers that should be used for the engine builds.

As described in the previous quarter report valve phasing sweeps are simulated to map the performance in terms of brake mean effective pressure (BMEP), brake specific fuel consumption (BSFC), exhaust trapped residual mass fraction (residuals) and a calculation of the fractional amount of unburned fuel in-cylinder at the point of auto ignition (knock strength). Intake cam profiles having lifts of 6 mm, 8 mm, and the production lift approximately 10 mm are evaluated at steady state speeds from 1000 to 5000 rpm. For each cam lift the duration is also treated as a parameter so that the duration between intake valve opening and intake valve closing is varied as shown in Figure 3.0-1. The objective is to determine two cam profiles, lift and duration, that can cover the range of speeds and loads the engine is expected to deliver with the range of fuels. Analysis results to date show the 6 mm cam will be used for low speed load range points and the 8 or 10 mm lift cam will be employed for the engine to operate at high speeds and loads.

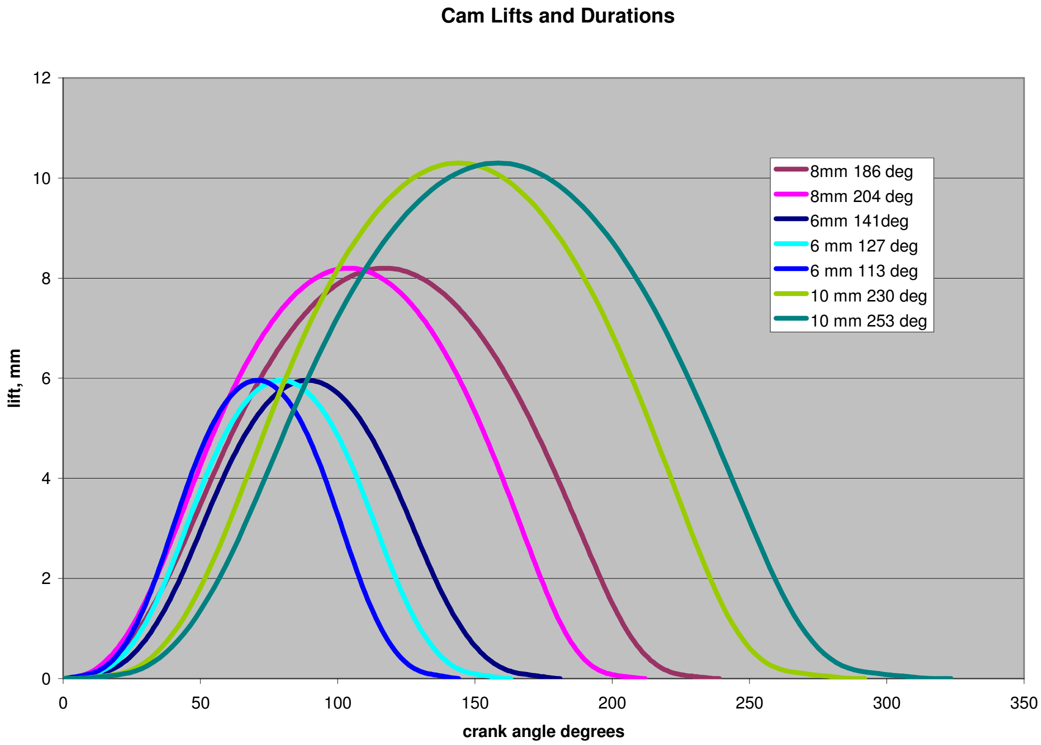

Figure 3.0-1: Lift and Duration profiles of various cams

Evaluation of performance over the entire range with all cam phase-lift-duration combinations allows for identification of tradeoffs in an idealized simulation. Limitations of computer simulations and model assumptions allow overcoming constraints that will realistically be encountered when hardware is to be made and the performance is to be evaluated on an actual engine. Constraints that must be considered are physical interference of mechanical parts and maximum forces parts can withstand, as well as limits to combustion due to autoignition or misfire.

Physical interference of the engine valves and piston must be avoided. To increase compression ratio the clearance around the intake and exhaust valves is reduced. As the clearance height is reduced there are more restrictions on the valve lift and phasing to avoid interference. Figure 3.0-2 shows an example of how the phasing limits for a 10 mm lift valve change with clearance height. As the piston approaches TDC the piston clearance from the seated valve location becomes minimum, defined here as the clearance. As the exhaust valves close and intake valve lift to allow air into the cylinder the maximum phasing conditions are shown.

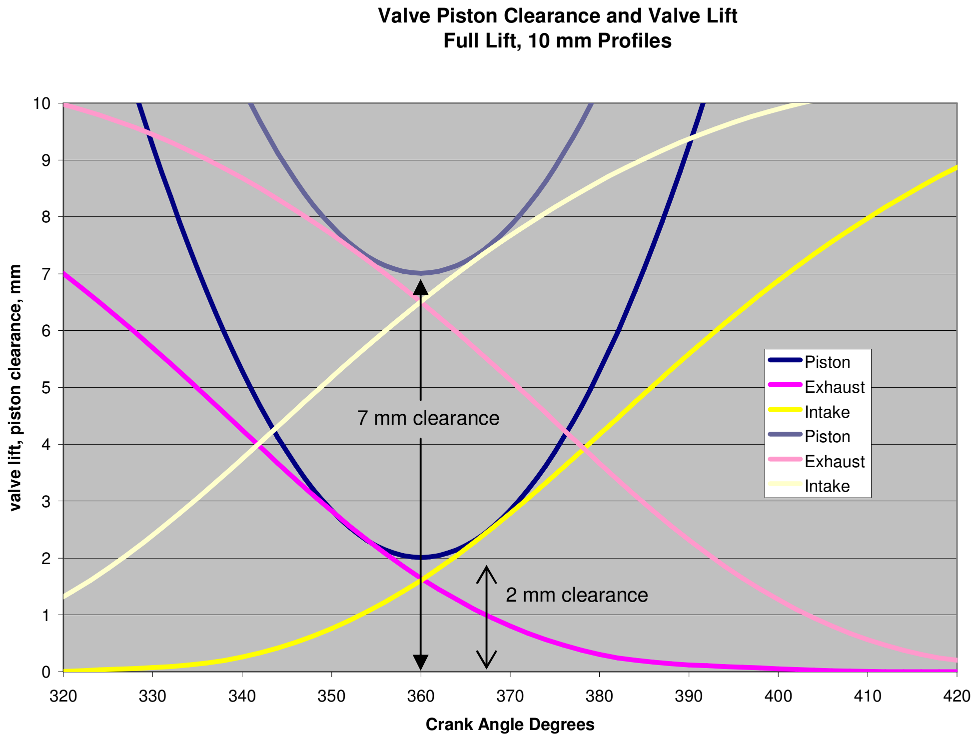

Figure 3.0-2: Piston-Valve clearance near piston TDC conditions for production (approximately 10 mm lift) at two values of piston-seated valve TDC clearance

Interference phasing requirements are for 10 mm and 8 mm lift cams are shown in Figure 3.0-3. Simulation results indicate very early intake valve phasing requirements for the 6 mm lift cam are required to control load at low speeds. Maximum phase of the intake cam is determined by the high lift cam, 8 mm or 10 mm, since the two-step valve train hardware requires the low lift 6 mm cam profile to lie inside of the high lift profile.

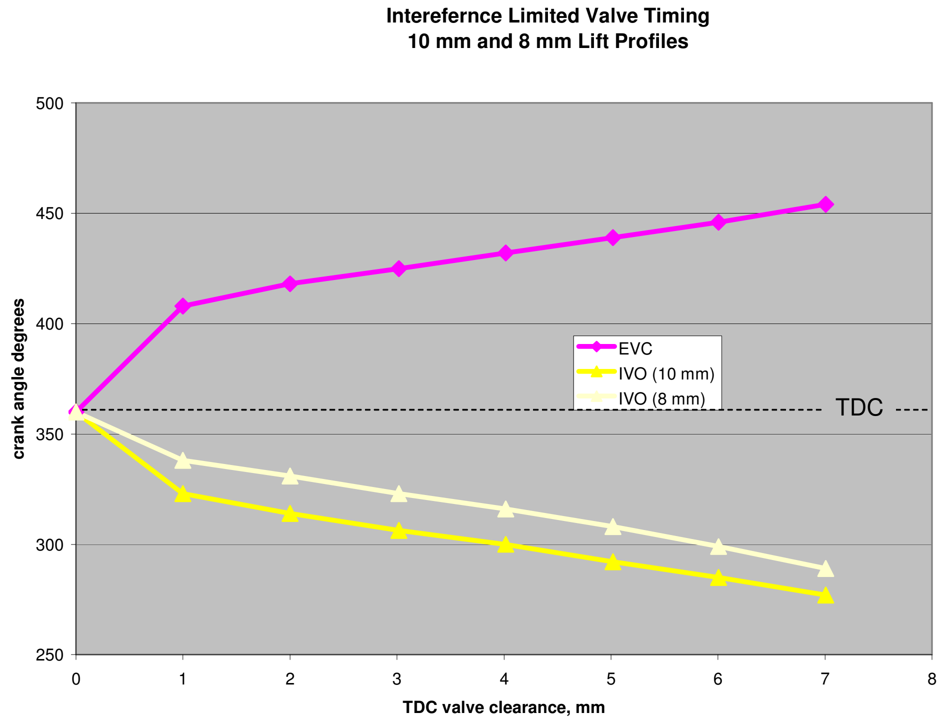

Figure 3.0-3: Intake and exhaust valve phase at Piston-Valve interference

Figure 3.0-4 shows the intake valve interference constraints on a contour performance overlay chart. Intake valve phasings to the left of the identified vertical lines will result in interference. For example, a 4 mm clearance value will allow for phasing the intake valve opening as early as 300 crank angle degrees. To get to lower load values on the optimum bsfc track requires more piston to seated valve TDC clearance. Larger values of TDC clearance result in lower compression ratio combustion chamber designs or less optimum combustion chamber geometry.

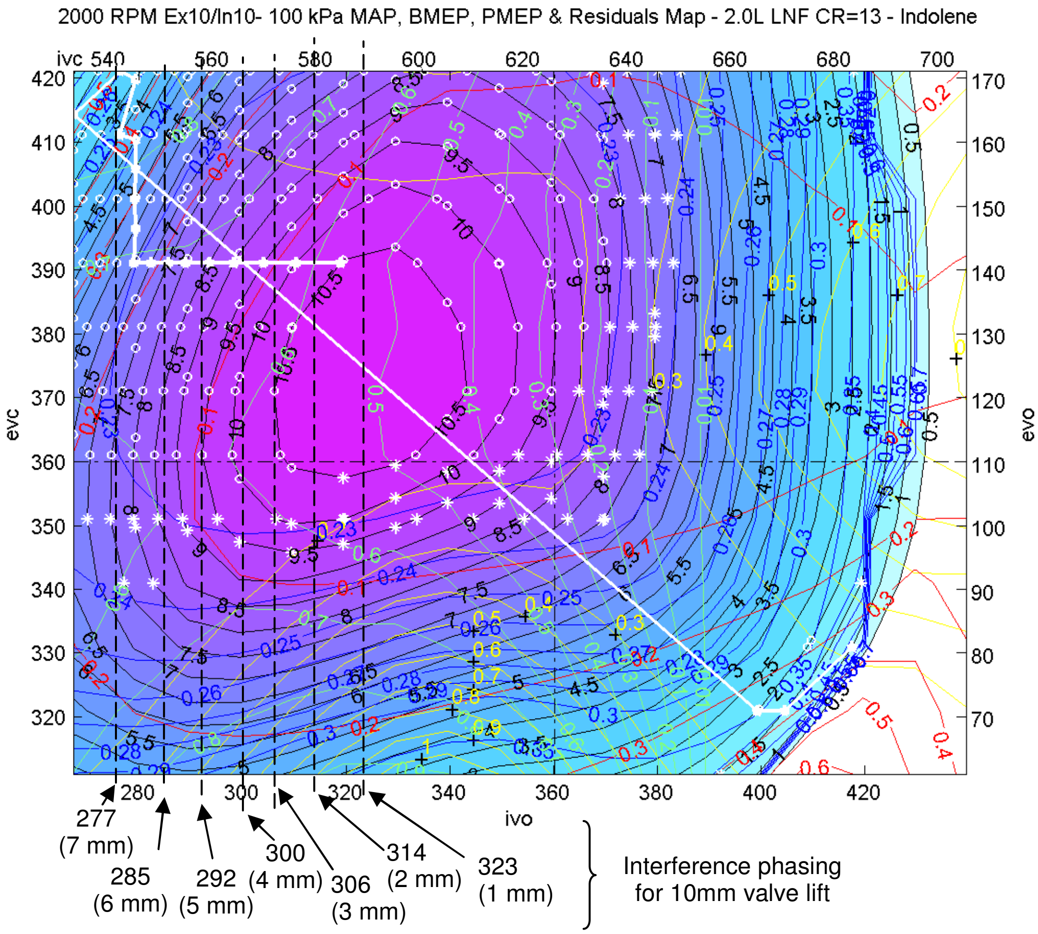

<u>Figure Contour Key</u>:

- BMEP [bar]
- PMEP [bar]
- Residuals (Mass Fraction Trapped)
- BSFC [kg/kW-h]
- Knock Strength

Figure 3.0-4: Engine performance overlay contours with interference phasing constraints shown for 10 mm valve lift

The engine simulation is able to operate where a real engine would fail due to physical interference, and is also able to predict performance where a real engine may not run due to poor combustion quality. On the speed phasing result maps areas contours of knock strength are shown ranging from 0 to 1. By this definition of knock strength a value of .5 means that there is 50% of the fuel unburned in the cylinder when pressure and temperatures of the unburned gases in the cylinder reach conditions where autoignition is possible. A standard knock calculation is used for this calculation so there is no correlation available to know how the knock strength value relates to real engine knock. This standard knock calculation (Douaud and Eyzat) is able to predict the effect of several parameters on knock, as shown in figure 3.0-5. A threshold of 0.1 has been assumed as a knock strength limit at this stage of the work, but engine testing will be needed to determine how well the calculation correlates the to engine knocking behavior.

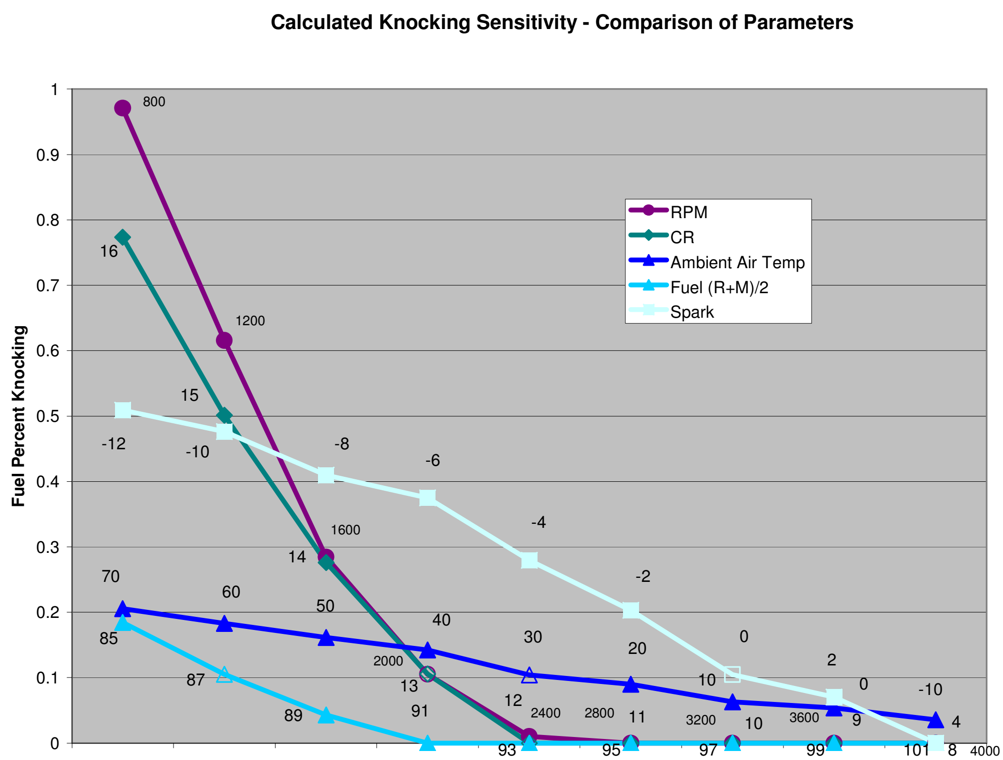

Figure 3.0-5: Knock strength calculation sensitivity to engine speed (RPM), compression ratio (CR), ambient air temperature (deg C), fuel octane number, and relative spark timing.

Whereas knock indicates the mixture in the cylinder will auto ignite, without spark, at the other extreme the mixture may not ignite (misfire) or only weakly combust (partial-fire). These mis- and partial-fire combustion conditions occur when the air-fuel mixture is near or outside the flammability limits for the fuel. A cause for misfire is too little fresh air charge due to high amounts of residual exhaust gas. Without engine data to determine the tolerance for residual gases it is assumed that 0.25 is an approximate upper residual limit to still expect combustion to occur. Again, it is expected that engine test data will help to determine the tolerance to residual gases and enable better definition of this constraint.

Peak cylinder pressure is another physical constraint that will exist on the real engine but is ignored in the engine simulation. The combustion chamber, piston and piston rings, and connecting rod are all designed to withstand a maximum in cylinder pressure of around 100 MPa during combustion. This constraint will limit the amount of boost the compressor can supply and affect the strategy to achieve high loads with boosting. More physical constraints exist, such as mass and balance of the piston, and need to be addressed to determine maximum engine speed once a piston design is finalized.

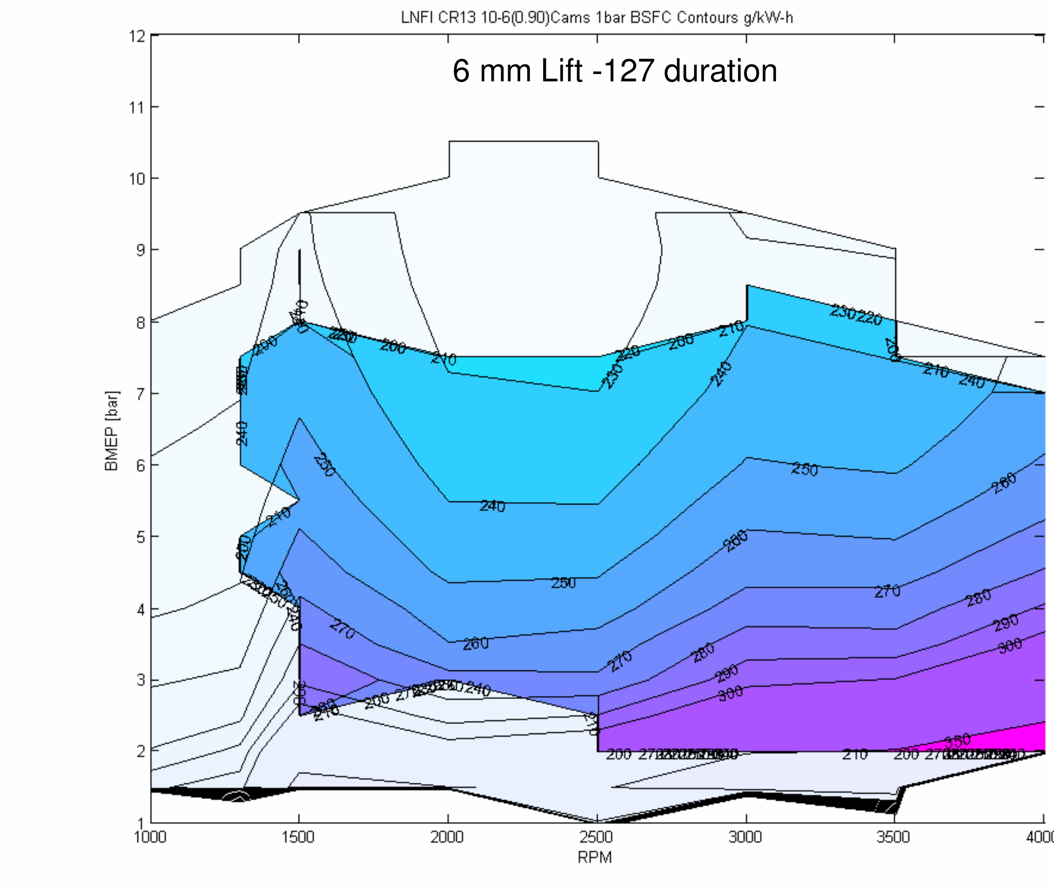

Figure 3.0-6: Speed-load map for 6 mm lift cam with 127 crank angle degrees duration fueled with indolene.

The outline of the contour represents the unconstrained speed-load map and the filled domain represents the area of the map where none of the constraints are violated. In the example figure shown the low speed – low rpm range is constrained due to high residuals that exceed the 0.25 threshold mentioned. To allow the engine to operate in this region is expected that throttling will be required at the cost of less than optimum fuel consumption efficiency. At the high loads the knock strength exceeds the 0.1 threshold. To extend the engine operation in this region perhaps spark timing may be altered. Maps are made for each cam lift/duration profile and with pure indolene and an assumed E85 blend fuel. As mentioned in the previous discussion, the constraints of operation need to be verified with engine data using the chosen fuels.

Task 2.0 –Spray Modeling of Ethanol-Gasoline Blended Fuel (1/1/08 thru 3/31/08)

Injector Spray Test

In the last quarter (Jan 1st – March 31st), additional spray characterization tests were done for E85, Stoddard and n-Heptane under atmosphere pressure and room temperature conditions. The laser diffraction results showed slightly larger droplets for Stoddard solvent and E-85 than for n-Heptane. This is consistent with the higher surface tension found in Stoddard and E-85 when compared to n-Heptane as shown in the following table.

Table 2.0-1: Material properties of typical fluids used in Technical Center Rochester (TCR)

	Density(g/mL)	Viscosity(cP)	Surf.Tension.(mN/m)	Source
Butanol	0.81	2.59	24.3	www.trimen.pl
Ca-RFG-Ph3	0.74	0.46	21.6	TCR
NA E-10	0.76	0.49	22.1	TCR
E-85	0.78	1.07	22.1	TCR
E-100	0.79	1.20	22.3	TCR
Methanol	0.80	0.55	22.1	www.trimen.pl
n-Heptane	0.68	0.44	20.6	TCR
Stoddard	0.79	1.01	25.4	TCR

(Courtesy of Bill Humphrey, TCR)

Figure 2.0-1 summarizes results of major droplet size parameters for the tested injector part number and fuel combinations. DV10, DV 50 and DV90 represent the diameters at accumulative volume fractions of 10%, 50% and 90% of the total injected volume. D43 is the mean droplet size measure weighted by the droplet volume. D32 or Sauter Mean Diameter (SMD) is the average droplet size calculated by taking the total volume of all droplets divided by the total surface area of all droplets. SMD, weighs more on small droplets for their larger surface areas per unit volume, is typically less than DV50 while D43 favors larger droplets and is typically larger than DV50 as evident in the summary chart. The droplet size measurements were made with a Malvern laser diffraction instrument using a 5 mW and 13 mm beam diameter Helium-Neon laser at 633 nm wavelength intersecting the spray plume at 50 mm below injector tip. All tests were conducted according to SAE J-2715 or Delphi TCR standards at the same injection conditions as reported in the previous quarter.

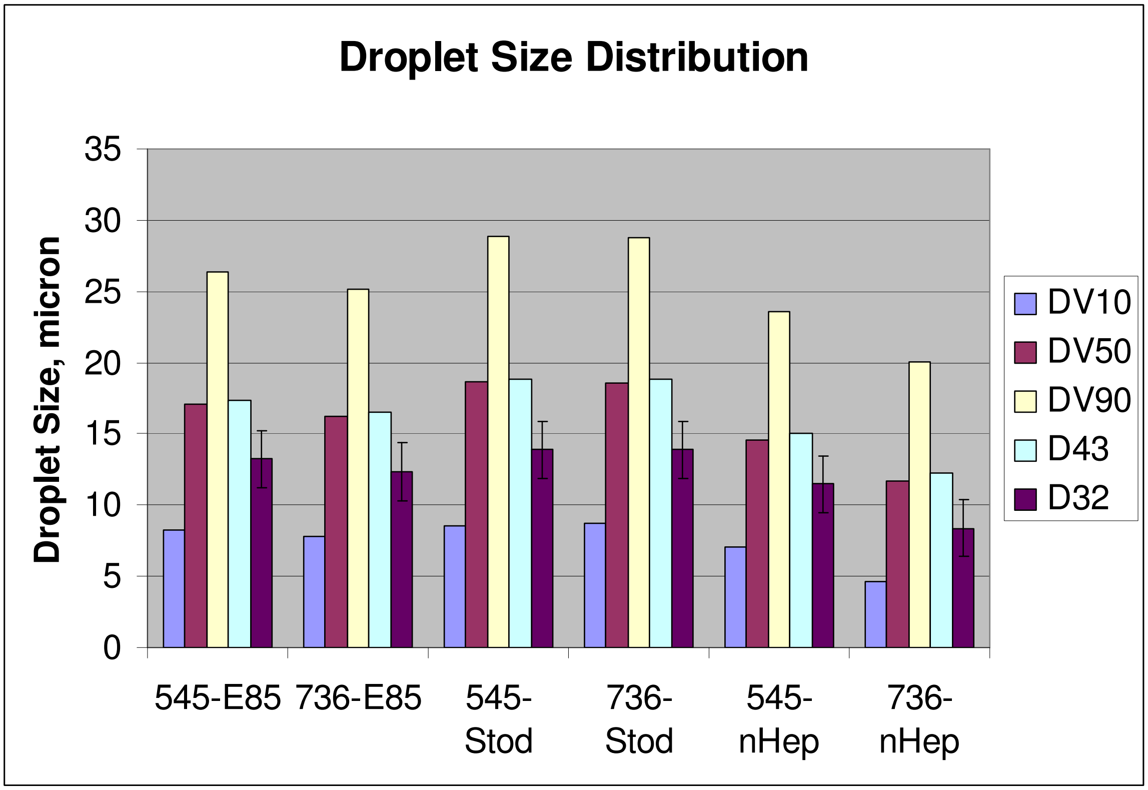

Figure 2.0-1: Laser diffraction droplet size measurement results for E85, Stoddard and n-Heptane

The spray imaging pictures, taken at 1.5 ms after Start Of Logic (aSOL) for n-Heptane, E85 and Stoddard, are shown in Figure 2.0-2. These images were captured with a Kodak MEGAPLUS CCD camera as the spray was illuminated by a strobe light against a dark background. The camera and the strobe light were synchronized relative to the start of injection logic signal. Each picture shown is a composite of 30 images. These images were then processed with Optimas 6.2 image analysis software to construct the Liquid Probability Image as shown. All the spray tests were performed at 10 MPa injection pressure and 1.5 ms pulse width in atmosphere conditions.

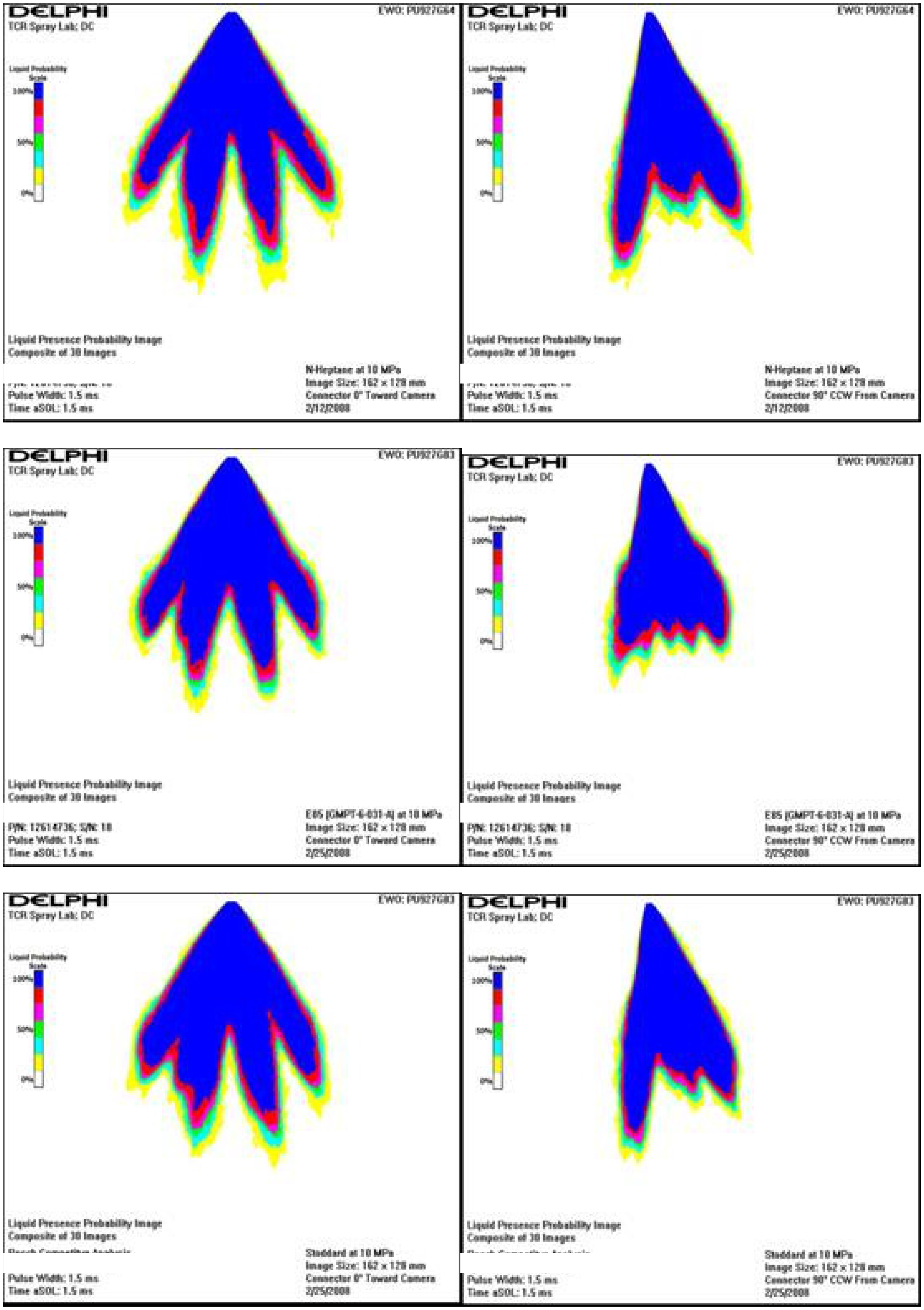

Figure 2.0-2: Spray patterns of a 6-hole injector (Part Number: 736, Serial Number: 18) viewed from two angles in spray tests with n-Heptane, E-85 and Stoddard as the injection fluids

Spray Model Development

Extensive modeling work is done in the last quarter using AVL-Fire to develop predictive spray models that can be used in phase 2 to optimize engine performance by incorporating various fuel injection strategies. The baseline model has been set up as a single plumed spray injecting vertically into a spray chamber 100 mm in diameter and 150 mm in length. The spray chamber is quiescent at room temperature and atmosphere pressure. The injector diameter is 0.23 mm, the same as measured from the Ecotec engine. The injection pressure is modeled indirectly by the corresponding flow rate of 2.45 gram/second/hole as measured from the flow tests at 10 MPa. The injection pulse width is set at 1.5 ms. The total modeled spray time is 3 ms or up to 1.5 ms after the end of injection. Penetration, SMD and %evaporation are calculated at the end of the 3 ms simulated spray time.

Mesh Size Sensitivity Study:

Three meshes of 1x1x3, 2x2x3 and 4x4x6 (all dimensions in mm) were constructed to evaluate the mesh size effect on computed spray penetration, SMD, and % evaporation. The simulation domain is an open spray chamber 100 mm in diameter and 150 mm in length. The results as summarized in Figure 2.0-3 clearly show the mesh size sensitivity, i.e., as the mesh becomes finer, the computed penetration and the SMD become larger while % evaporated becomes less. This trend is consistent with what has been reported in the literature [1] and is attributed to the “numerical” diffusion between liquid spray droplets and the surrounding gas phase. In other words, the mass, momentum and energy transfer between gas and liquid are over estimated when the mesh size is bigger than the real “sphere of influence” of the liquid droplet, resulting in less penetration, smaller SMD and more evaporation for coarser mesh models. It may appear attractive to refine the meshes until the gas-liquid interaction is properly resolved. However, very fine mesh would violate a basic assumption of the Eulerian-Lagrangian spray model, i.e., the volume fraction of liquid droplet must be small in each cell. Another serious drawback of very fine meshes is of course the exponential increase in computational time. Many well developed CFD codes, including AVL-Fire, are fine tuned to produce acceptable results within their recommended range of mesh sizes. In this sensitivity study, the penetration result of the 2x2x3 mesh matches the measured value while SMD is clearly over-estimated. Further model parameter tuning would be needed to address this discrepancy.

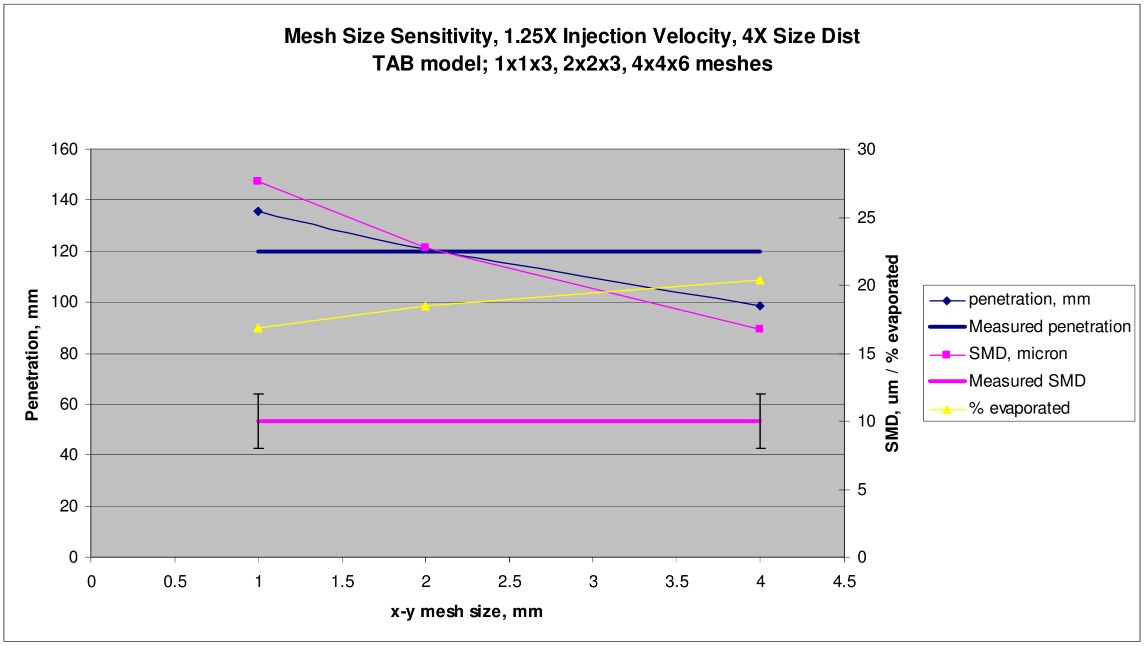

Figure 2.0-3: Mesh size sensitivity for penetration, SMD and % evaporated

Time step and Z-Dimension Mesh Sensitivity:

Additional sensitivity study was done to evaluate the effects of timestep between 50 microseconds and 100 microseconds and two meshes of 2x2x3 versus 2.5x2.5x7.5. The results as compiled in Figure 2.0-4 show practically the same computed penetration, SMD and %evaporation for all three cases. This indicates that acceptable results can be expected for a 100-microsecond timestep and a longer Z-dimension mesh. The Z-dimensional sensitivity however is predicated on the alignment of spray axis with Z. This rule should be modified for multi-hole injectors where injection directions in general are not in line with Z-axis at all.

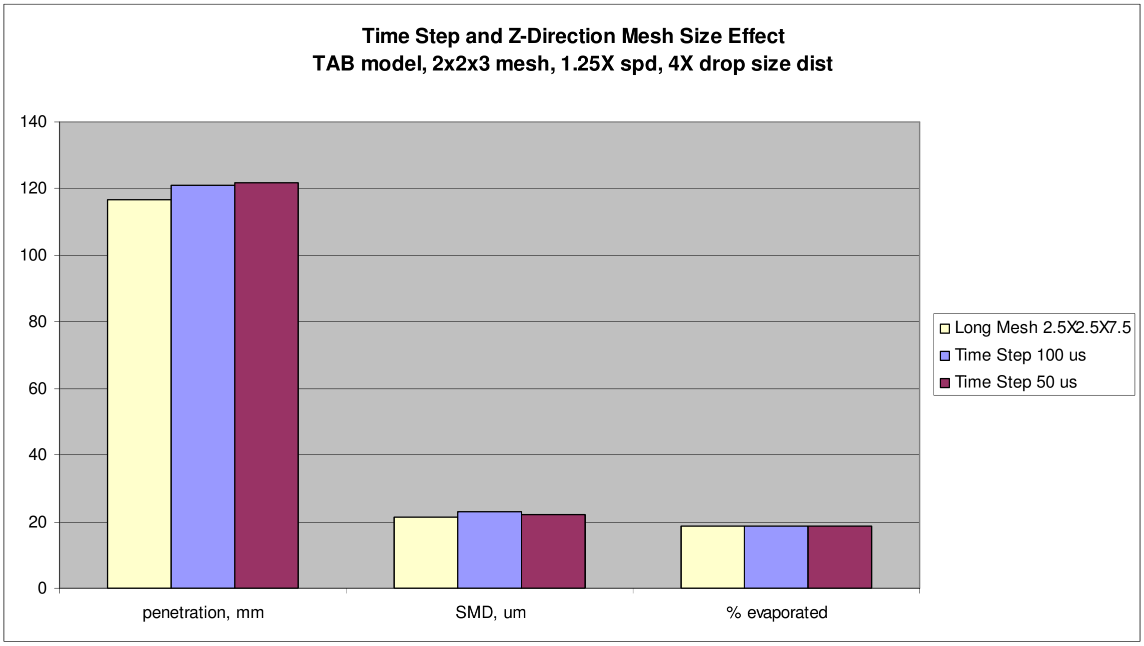

Figure 2.0-4: Timestep and Z-dimension mesh size sensitivity for penetration, SMD and % evaporated

Injection Velocity Effect:

The spray models used in AVL-Fire assume a Fully Atomized Jet (AFAJ) at the nozzle exit and rely on users to prescribe the droplet size distribution as input parameters. This method avoids the uncertain and highly nozzle dependent phenomena of cavitation and primary breakup near the nozzle exit, but produces results under-estimate the penetration according to Levy, et.al.[2]. Levy recommended an injection velocity multiplier of 1.5-10 for diesel spray. Our own injection velocity study however shows a multiplier of about 1.25 best matching the n-Heptane spray data. As shown in Figure 2.0-5, the general effects of increased injection velocity are increased penetration, reduced SMD and increased %evaporation.

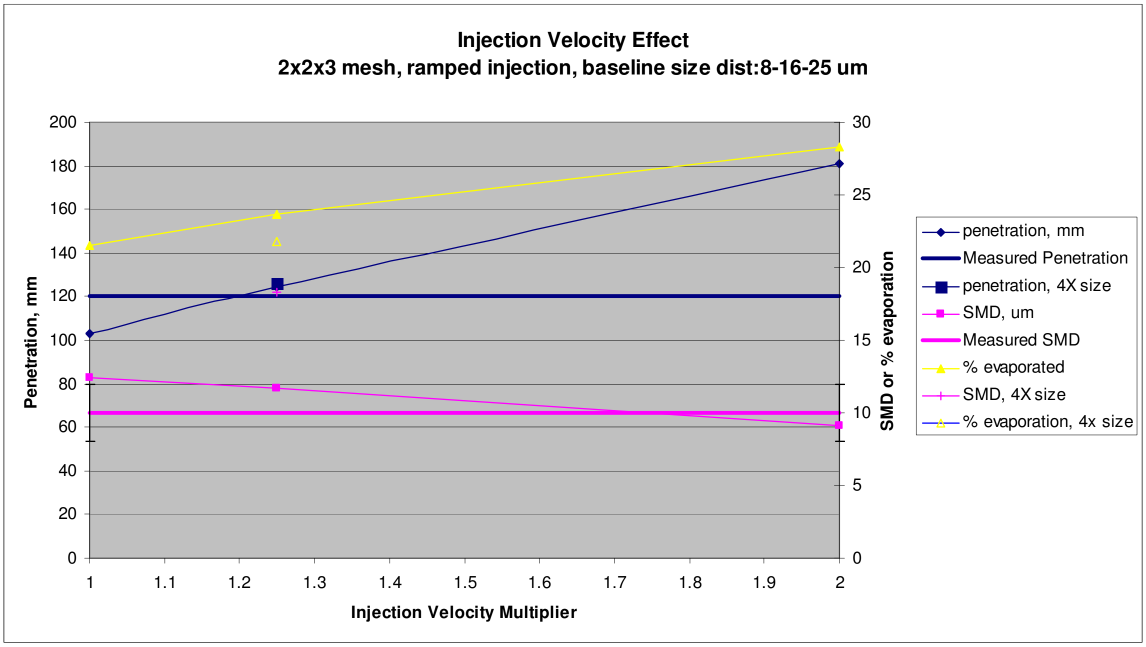

Figure 2.0-5: Injection velocity effect for penetration, SMD and % evaporated

Injection Rate Profile Effect:

Real injection event includes delays in valve opening and closing of up to 500 microseconds. In the following, we studied the effect of a linearly ramped opening and closing of 300 microseconds for a total injection time of 1.5 milliseconds. The total injected fuel is kept the same for both cases. The results show an increased penetration, reduced SMD, and increased evaporation due to higher injection velocity during the main injection period for the ramped open/close case.

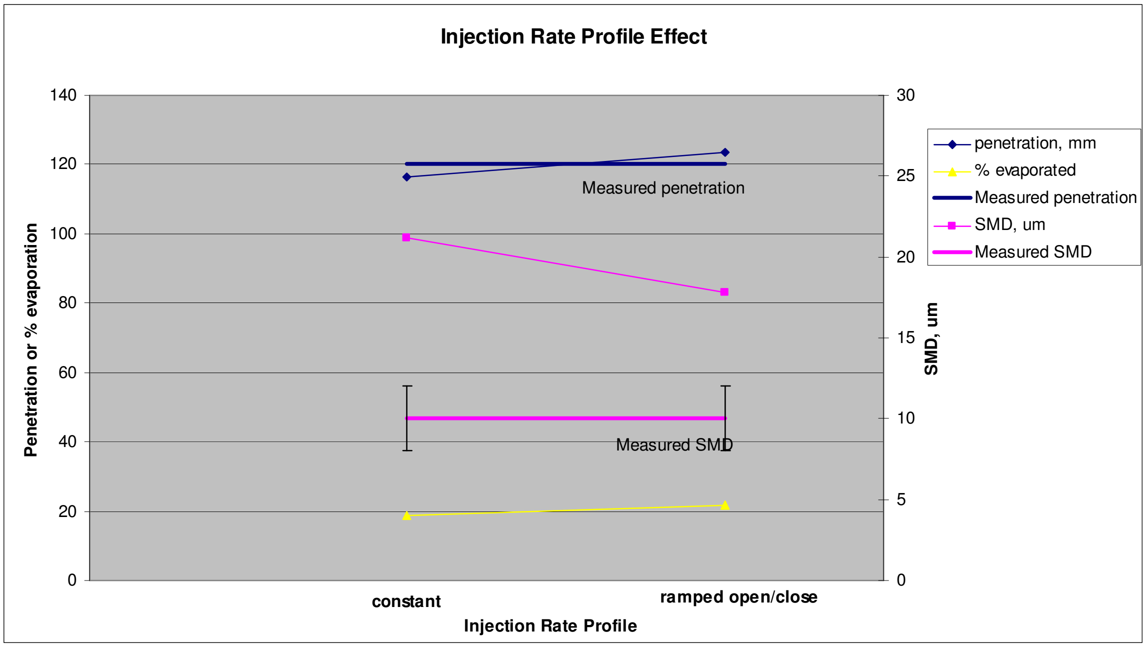

Figure 2.0-6: Injection rate profile effect for penetration, SMD and % evaporated

<u>Task 3.0</u> –Development of Vehicle Level Model (1/1/08 thru 3/31/08)

Speed-load maps, as discussed in Phase 1 Task 1 above, are useful for more than identification of the relative domain where the cams can operate. The speed-load maps can be input to a vehicle level model to determine how the mapped engine performs in a vehicle under driving conditions. For this phase of the project a GT Drive vehicle model has been made for this purpose. The vehicle chosen to be modeled is a 2007 Pontiac Solstice GXP, a vehicle in production that uses the 2.0 L engine modeled. The model is constructed from reported physical dimensions from the manufacturer and other sources and dynamometer coefficients supplied to the EPA with fuel economy data. Results from the vehicle simulation include a miles per gallon fuel measurement and the second-by-second speed load trace of the engine output over an input driving cycle.

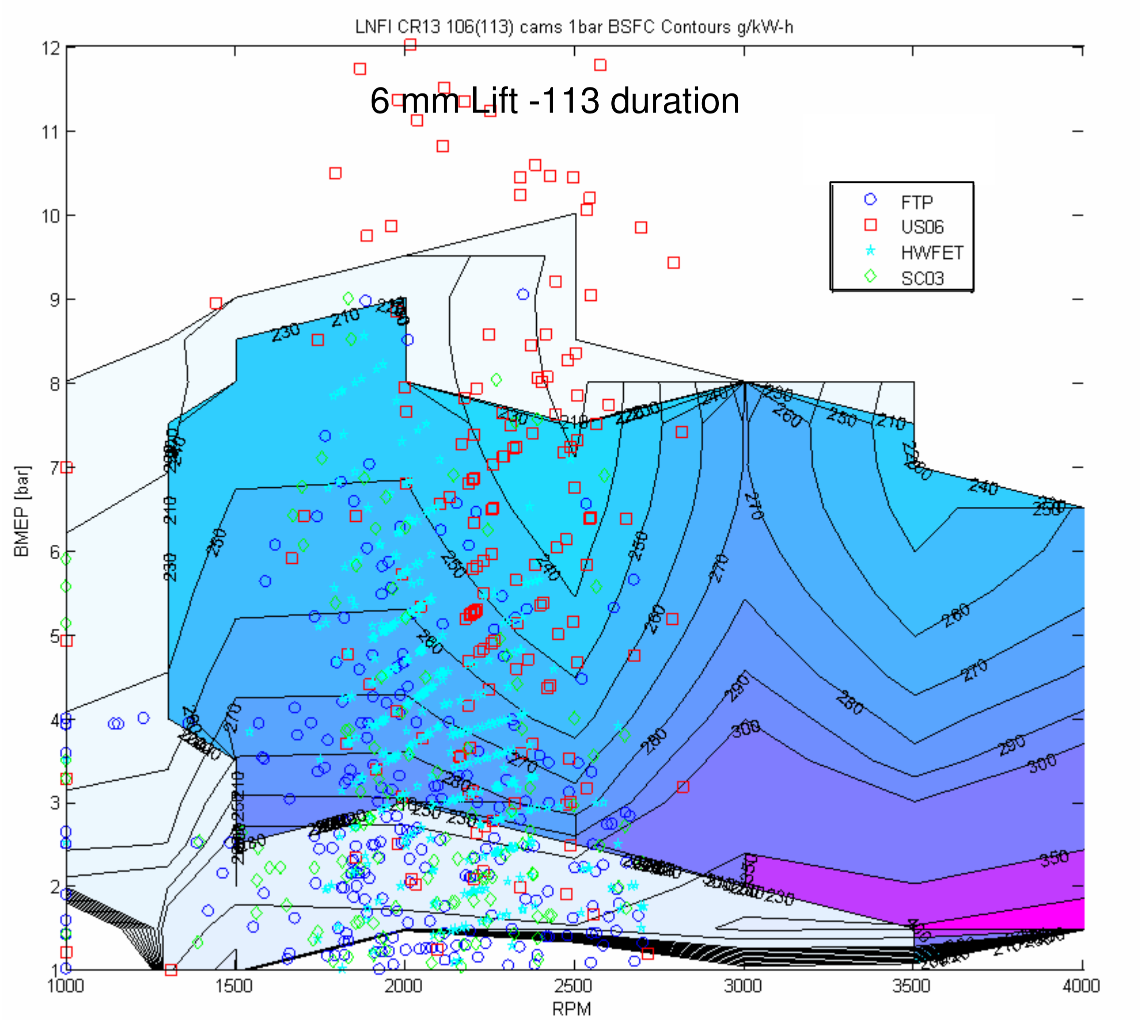

Figure 3.0-7: 2007 Pontiac Solstice GXP vehicle simulated driving cycle speed-load points superimposed on engine speed-load map.

Figure 3.0-7 shows some instantaneous speed-load points from several driving cycles superimposed on the speed-load map for a 6 mm lift cam. Points that fall on the filled contour are achievable with the cam while the points in the outline area require either throttling or changing the cam. This figure shows that for the majority of the FTP, HW-FET and SC03 driving cycles the shown cam is capable of meeting the power requirements for the engine on indolene fuel if throttling is used. There are some limitations of the transmission control in the model that do not allow for a realistic shift schedule to be modeled. The same drive cycle can be run for a variety of shift cycles to determine the envelope of speed-load points expected to be encountered by the vehicle that the engine is required to supply.

In summary, the quarter modeling efforts focused on continued mapping steady state performance for a range of cam lifts and durations. Effort is made to identify, quantify and understand constraints that limit the design and areas where the engine performance is not expected to be accurately predicted by the simulation. Speed load maps are assembled using estimates of the constraints and used with a vehicle model to identify a hardware set (compression ratio, low and high valve lift and duration profiles for two step valve train) that will be used on the engine. Going forward the effort will focus on model refinement and improvement in areas where more data is gained from spray analyses, for example.

Quarter 2 2008

Phase 1 Task 1.0 –Development of Overall Model for 'Ecotec' Engine (4/1/08 thru 6/30/08)

In this quarter the Phase 1 modeling task was completed with selection of the initial valve train configuration to be used on the engine. Performance simulations using the GT power model of the Ecotec engine were used to quantify the performance of the valvetrain among the design considerations. The design with the best combination of compression ratio and lift profiles to be used with the two step valvetrain is identified to be used for the initial engine build, Task 4 of Phase 2 of this project.

Simulation progressed this quarter continuing on from the model built and discussed in the previous quarter reports. Maps of performance quantities load and fuel consumption are constructed for steady-state sweeps of valve phases to locate regions where best to operate for maximum fuel economy. Valid operating points are chosen in regions where exhaust residuals mass fraction does not exceed 25 percent and the knock strength does not exceed a value of 0.1. The operating points of the best performance are compared for different profiles. Figure 3.0-1 is an example of the simulation results for an engine speed of 2000 rpm, with a compression ratio of 11, a production exhaust cam, and intake cams of nominal lift 10 mm and 6 mm using E85 fuel operating at 1 bar (unboosted), at 1.5 bar and at 2 bar manifold pressures.

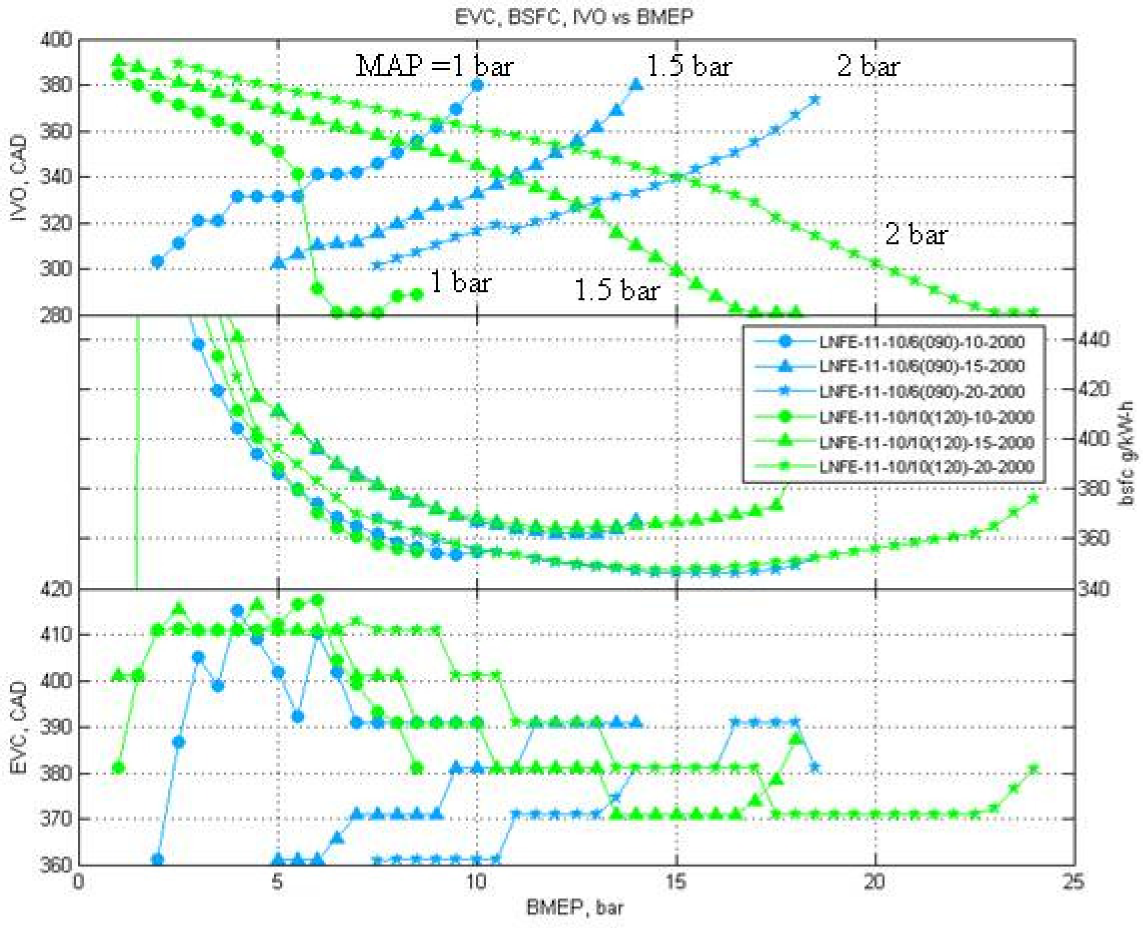

Figure 3.0-2: Minimum bsfc values of Intake valve opening (IVO), Brake specific fuel consumption (bsfc), and Exhaust valve closing (EVC) values versus load for CR 11 engine using E85 fuel with 10 mm nominal lift intake cams (green) and 6 mm nominal lift intake cams (blue) at 2000 rpm and boosted as indicated.

In this figure is evident that a strategy exists that allows to increase load with the engine (move left to right across the load axis). Starting on the low lift cam, blue circles, the load can be increased by later phasing of the intake valve. This continues until the load reaches about 5.5 bar at which point the transition to the high lift cam can be made (green circles). The load can continue to be increased by earlier phasing of the high lift intake valve. The transition from low to high lift is expected to be smooth since the load is equal at the intersection of the curves. This load path also is the most economical as the middle plot shows - the minimum bsfc points are always being used.

At this speed, 2000 rpm, to increase load beyond the 8.5 bar maximum seen with the high lift cam would require manifold pressure boost from the turbocharger. From the middle plot it can be seen the path staying on the high lift cam is just about as economical as if the low lift cam is used with boost. Selecting the high lift cam, however, allows for using less cam phasing authority. If only the low lift cam is used there is a limit to the bmep that can be reached and additionally since the low lift cam uses later phasing to get to higher loads there is more phasing authority required.

The exhaust phasing appears to be somewhat erratic. Looking at the steady state maps from which these curves are extracted shows that constraining the exhaust will not have much impact on performance. The exhaust phasing can be held constant with less than a one percent penalty in fuel consumption for each speed map. Exhaust phasing is required, however, since the phase at each speed is different.

Only a small portion of the operation is captured in Figure 3.0-1. The engine operates over a range of speeds and must be able to run with both gasoline (E00) and E85 fuels. This leads to a different set of curves at each speed and for each fuel for each cam profile. Two lift profiles are chosen based on sets of curves similar to Figure3.0-1 at speeds of 1000 to 4000 rpm with gasoline and e85 fuels. The high lift intake cam profile selected is 10 mm nominal lift (same as production intake), with an extended duration 20 percent longer than the production or about 280 degrees. The low lift intake cam is chosen based on the duration of 127 crank angle degrees. The low lift cam is based on a lift profile that has 6 mm nominal lift. Delphi advanced valvetrain engineering is evaluating the profiles to determine what an achievable lift can be with the given duration that meets manufacturing and operating constraints. Maximum lift of the low lift cam will be less than 6 mm and will need to be evaluated in the model. The exhaust cams are chosen to represent the current production profiles.

Full speed load maps of the lift strategy have been constructed. Figure 3.0-2 shows the lift strategy for the engine operating on e85 fuel blend. Several areas of interest are shown in the figure. The dark blue shaded area at very low loads is an area where throttling will be required. The engine cannot operate in these low load areas by cam phasing alone without violating the residual gas constraints that are assumed. This area will operate on the low lift cam. The pink shaded area indicates where the low lift cam will operate unthrottled. The yellow and light blue shaded areas are regions where the high lift cam is used. Yellow areas indicate unboosted operation and to attain the loads in the light blue zone some boost will be required. The boost will vary in the light blue zone from just above atmospheric at the bottom of the zone to higher as the load goes higher. Since this map is for gasoline there is a propensity for autoignition, or knock, to occur as was discussed in the previous quarter report. The gray area is where the engine is expected to experience knock. If measures are available to mitigate knock the engine could operate using the high lift cam to the extent of the gray shaded area.

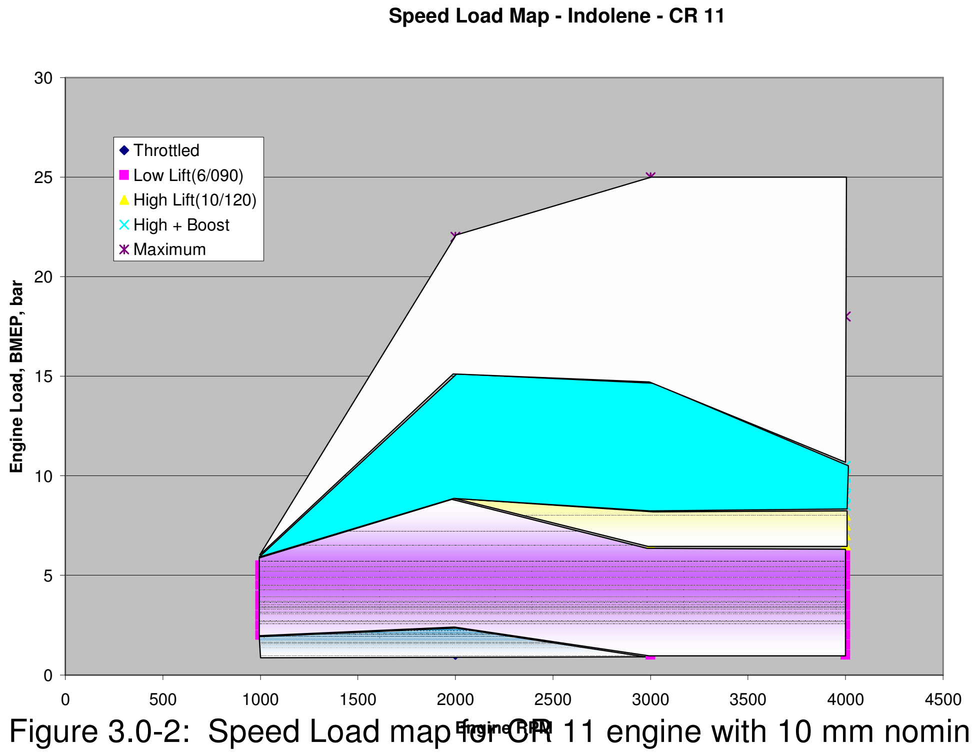

Figure 3.0-2: Speed Load map for CR 11 engine with 10 mm nominal lift high cam and 6 mm nominal low lift cam using gasoline (E00) fuel

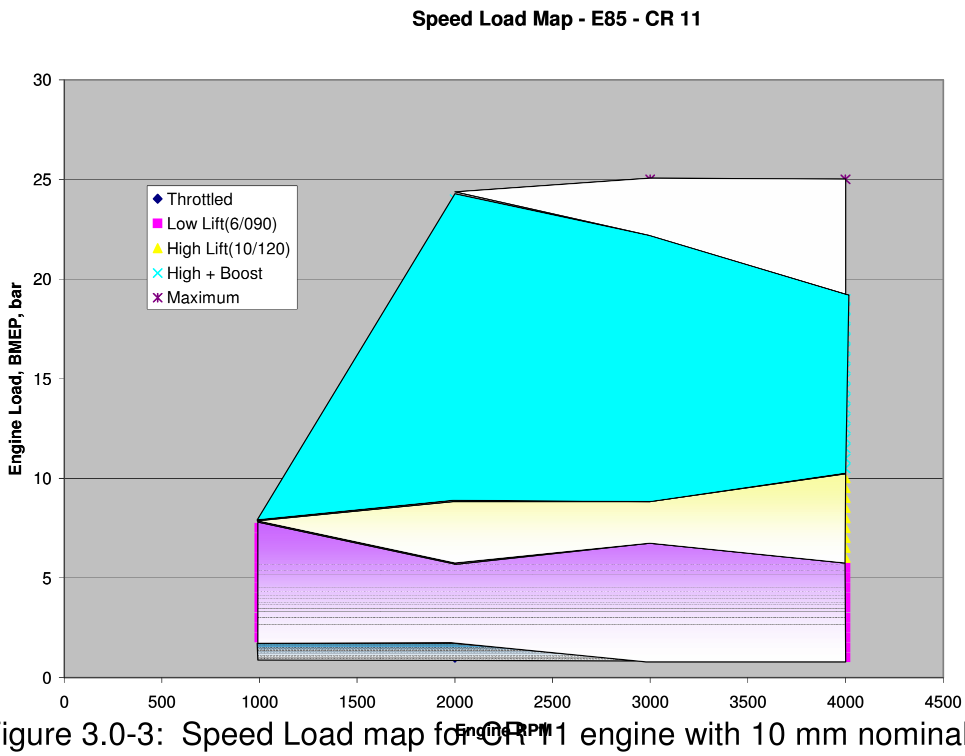

Figure 3.0-3: Speed Load map for CR 11 engine with 10 mm nominal lift high cam and 6 mm nominal low lift cam using E85 fuel blend

In Figure 3.0-3 it can be seen that the lift strategy speed load map of the engine withE85 blend fuel shows similar trends as the engine operating on gasoline. There are throttled (dark blue) and unthrottled (pink) low lift operating regions and unboosted (yellow) and boosted (light blue) high lift cam operating regions. The transition points are different between the low lift and high lift at different loads. The amount of gray area on the E85 fuel plot is much smaller, showing the benefit of the ethanol to achieve higher loads than gasoline at the same speeds without knocking.

Both of the previous two figures are for a compression ratio of 11. Profiles were also chosen based on a compression ratio of 13. The final compression ratio is expected to be in the range of 11 to 13 depending on the exact shape of the piston which the design is currently being finalized. The 2 step profiles chosen will not vary significantly if the compression ratio changes in the range of 11 to 13. The gray area where there is a tendency for knock to occur would be less as the compression ratio is lower. There is a fuel economy penalty for lowering the compression ratio as is discussed in the task 3 vehicle level model results.

<u>Phase 1 Task 2.0</u> –Spray Modeling of Ethanol-Gasoline Blended Fuel (4/1/08 thru 6/30/08)

In the last quarter (April 1st – June 30th), our efforts in spray modeling were concentrated on developing and validating spray models with experimental data obtained from standard flow and spray tests at TCR (Technical Center Rochester). Most of the work in this quarter focused on model parametric study of the KHRT secondary breakup model. The KHRT model was chosen based on its superior ability to model bag and strip breakup modes compared to the other models available in AVL-FIRE.

KHRT Model:

As the result of an extensive literature review, it is determined that KHRT breakup model is the best for the solid cone type spray of a multi-hole injector. KHRT model actually is a composite of KH (Kelvin-Helmholtz) model and RT (Rayleigh-Taylor) model. KH model accounts for breakups due to the instability of surface waves caused by aerodynamic disturbances. It is characterized by a bimodal distribution of droplet sizes as the initial large droplets from the primary breakup stage slowly reduce their sizes, many much smaller droplets form vigorously by stripping off from their parents due to the air drag forces. KH breakup model is controlled by two parameters, C1 and C2. C1 is the wavelength coefficient, relates the dominant wavelength to child droplet size. C2 is the breakup rate coefficient as a function of frequency and wavelength of the dominant unstable surface wave.

RT model represents a sudden breakup due to deceleration of the droplet caused by air drag and gravity. The RT breakup is characterized by two parameters, C4 and C5. C4 determines the child droplet size. C5 is the breakup rate constant, typically set to 1.

C3 determines the breakup length of the KHRT model, for distances less than the breakup length, KH mode dominates. For distances larger than the breakup length, KH and RT both are active and they compete with each other in breaking up the droplets. The rates of breakup and resulted droplet sizes of the two modes are determined by their respective parameter settings.

In the following, the effects of four parameters (C1-C4) in KHRT model will be analyzed in detail based on their influences on penetration, droplet size and % evaporated. Given this information, the best combination of these parameters could be determined from model calibration against test data.

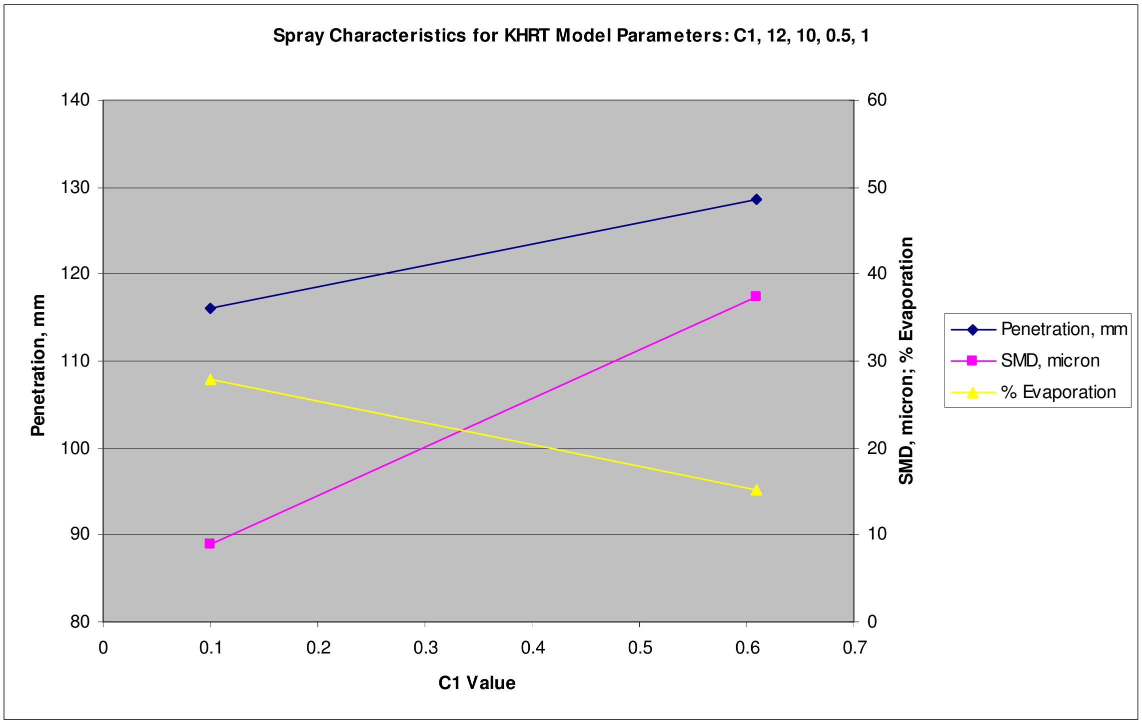
Spray Characteristics for KHRT Model Parameters: C1, 12, 10, 0.5, 1
Penetration, mm
SMD, micron; % Evaporation
C1 Value
140
130
120
110
100
90
80
60
50
40
30
20
10
0
0
0.1
0.2
0.3
0.4
0.5
0.6
0.7
Penetration, mm
SMD, micron
% Evaporation

The figure above shows the effect of C1 on penetration, SMD and % evaporation. When C1 is reduced from the typical setting of 0.61 to 0.1, SMD is significantly reduced accompanied by a moderate reduction in penetration and a moderate increase in evaporation. Relatively speaking, C1 is not a terribly sensitive parameter to various spray conditions. Most authors keep it at the recommended value of 0.61 at which it produces quite consistent spray behavior.

The following figure shows the transient response of penetration, SMD and %evaporation for C1 set to 0.61 and 0.1. Since both cases are dominated by the KH mode only, the reduction of C1 causes reduced child droplets and smaller SMD in a quite predictable fashion.

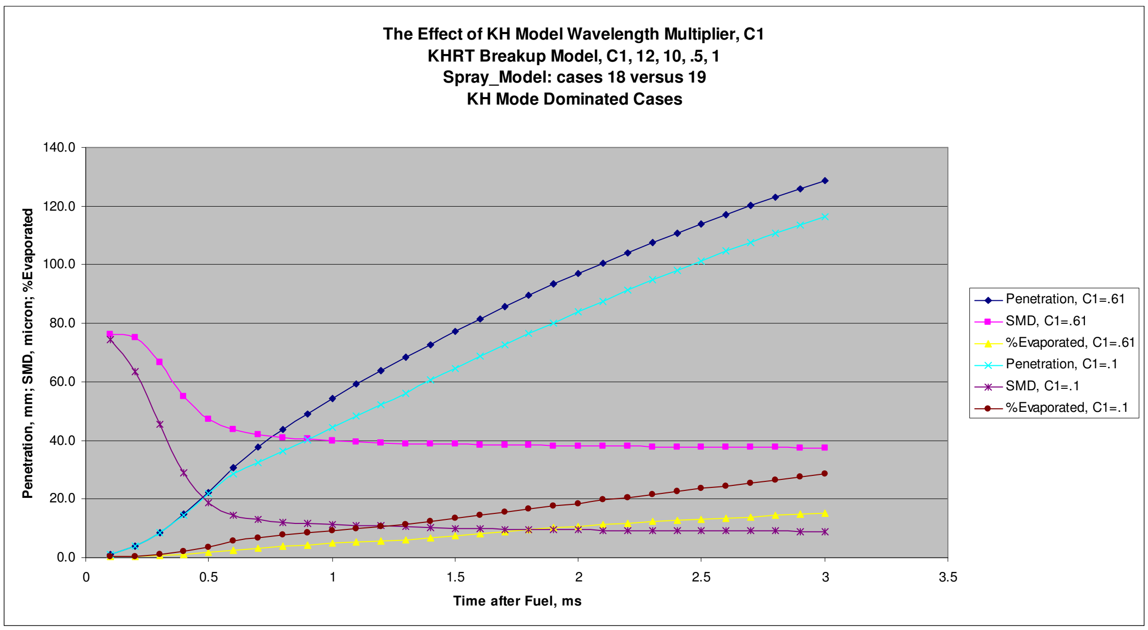

C2 has only mild effects on SMD, penetration and % evaporation in cases (for C4 >= 0.5) where KH mode dominates. Smaller C2 produces smaller SMD with accompanying changes in penetration (reduced) and evaporation (increased). The effect is nonlinear as evident in the following graph. The smaller C2 values of 2.47 and 6.7 are recommended by a Toyota paper.

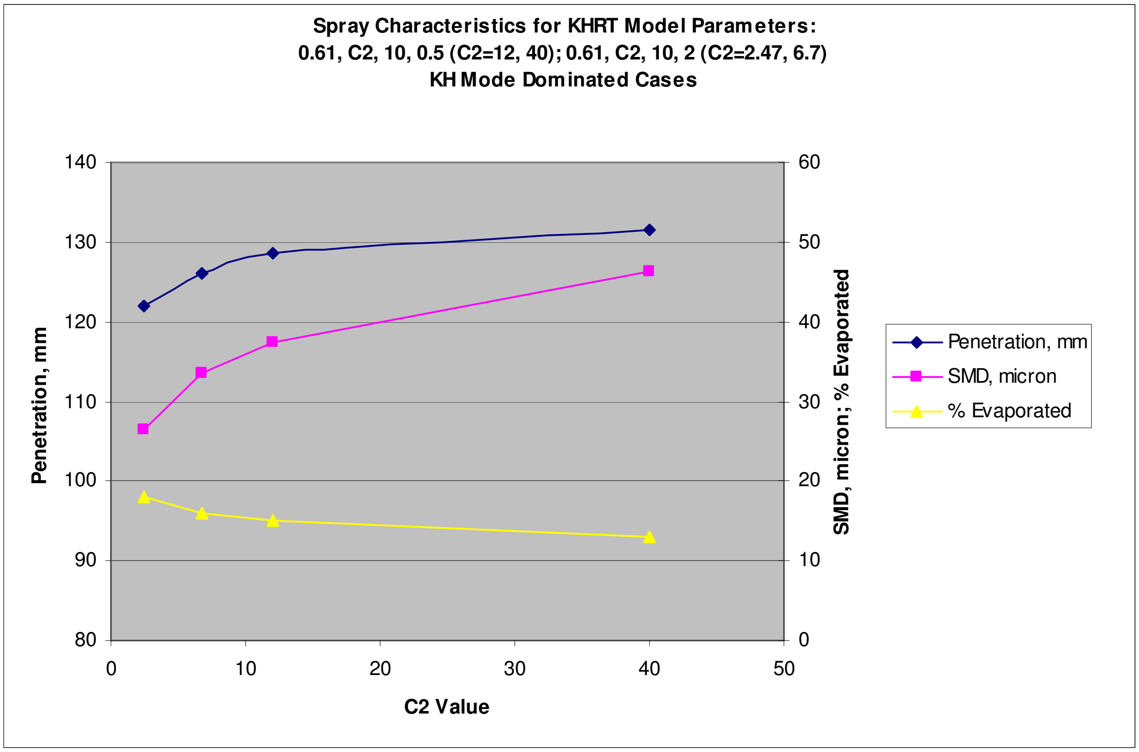

Detailed transient responses for the KH mode dominated cases are shown in the following figure. All trends are very predictable.

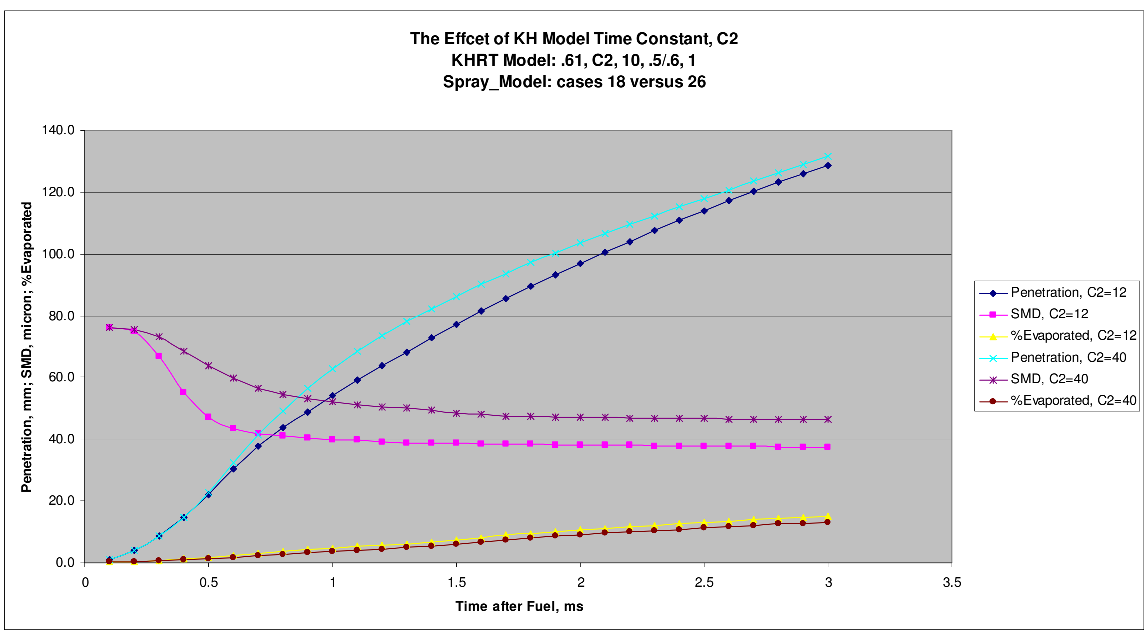

For cases where RT mode becomes active, the effect of C2 reverses the trend seen in the KH mode dominated cases as shown in the previous figures.

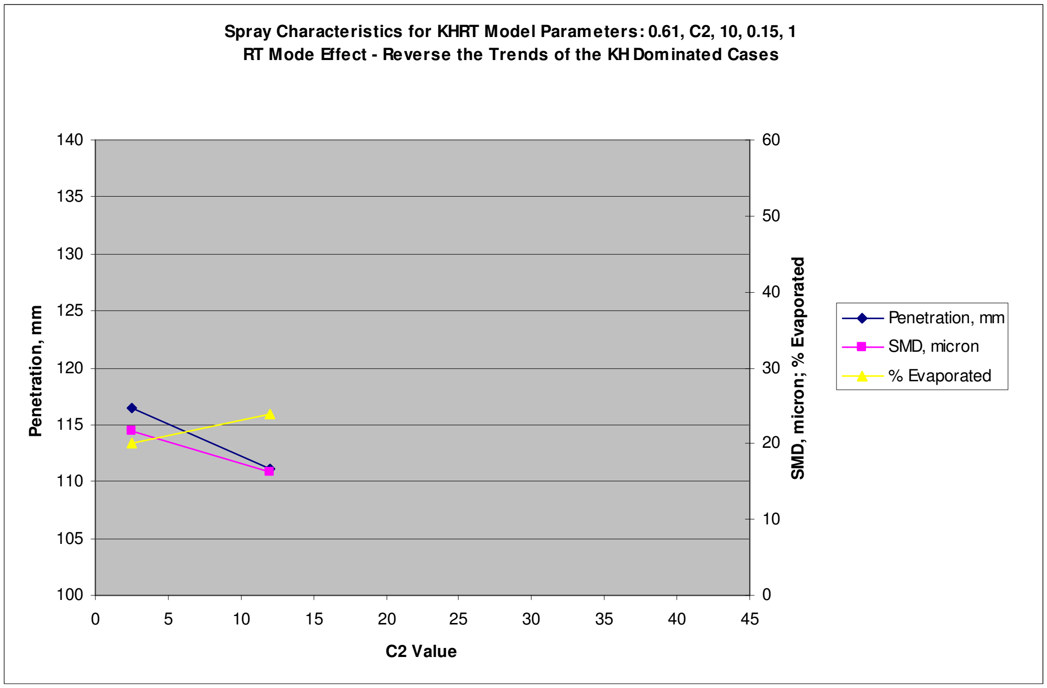

Detailed transient responses for the RT mode effect are shown in the following figure. The pink curve shows how larger C2 (=12) generates smaller SMD through RT mode breakup. The contrasting case is KH dominated due to a more competitive KH breakup mode with a smaller C2 (=2.47). This graph shows the reason for the reversed trend in the above figure.

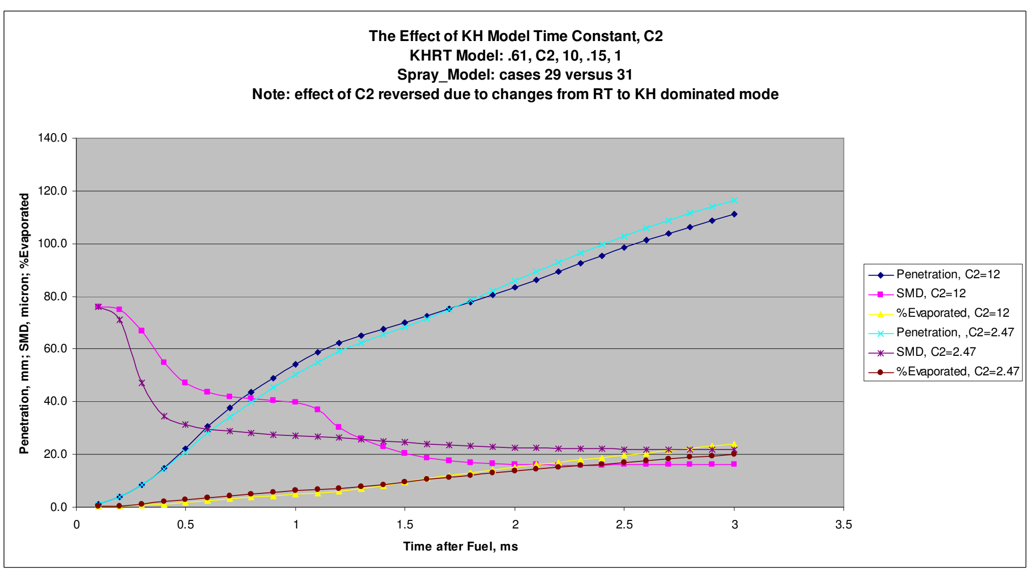

C3 is of no consequence when the KH mode dominates.

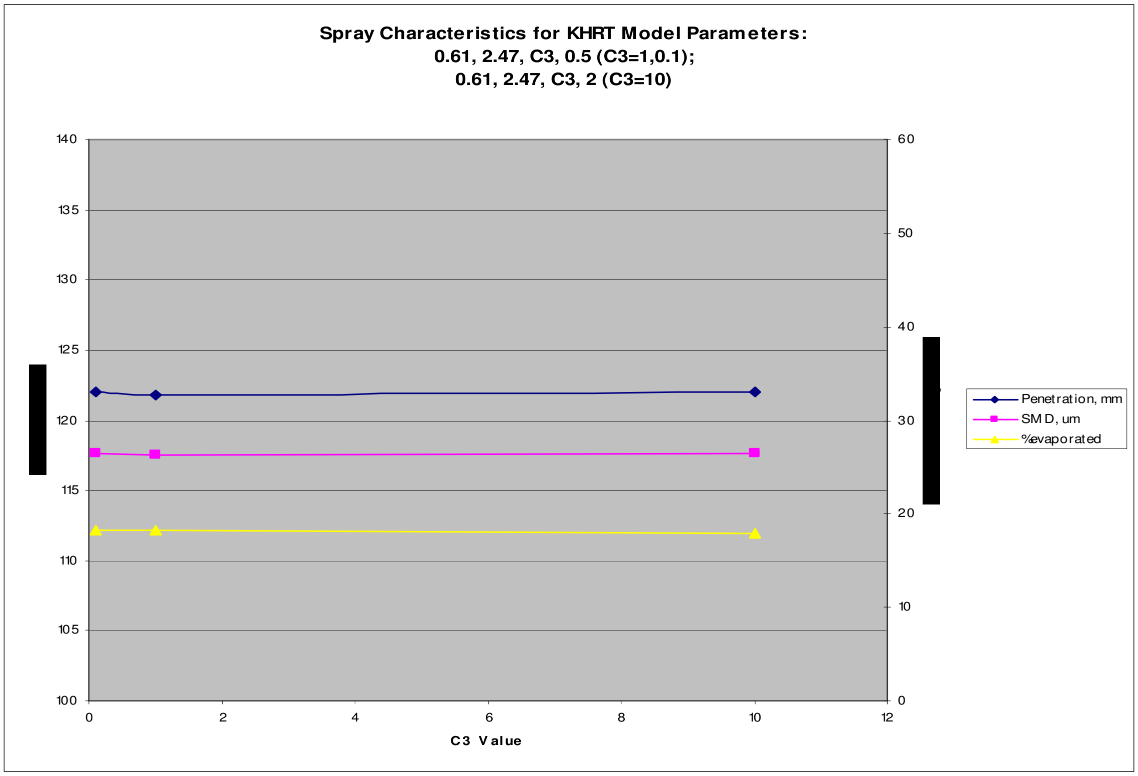

C3 however becomes important when RT starts to compete for C4 < 0.15. Smaller C3 makes the RT mode competitive earlier thus produces smaller SMD and higher evaporation.

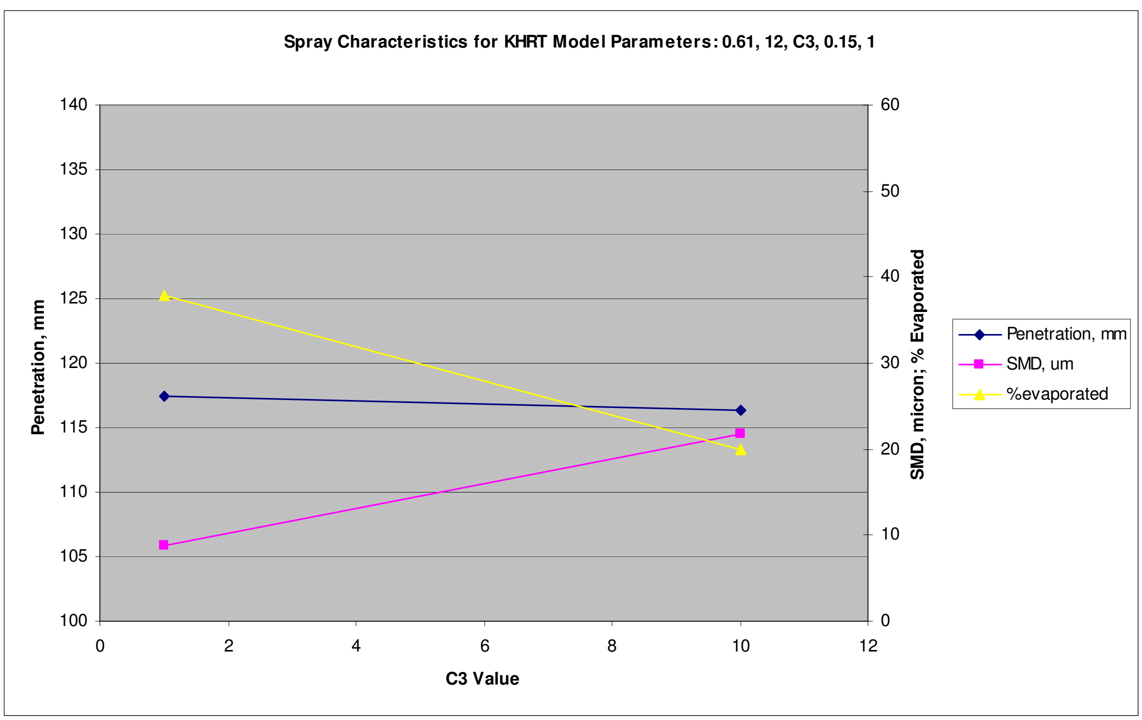

Adding a center point in the following figure shows the C3 effect is nonlinear, even for cases where only KH is active.

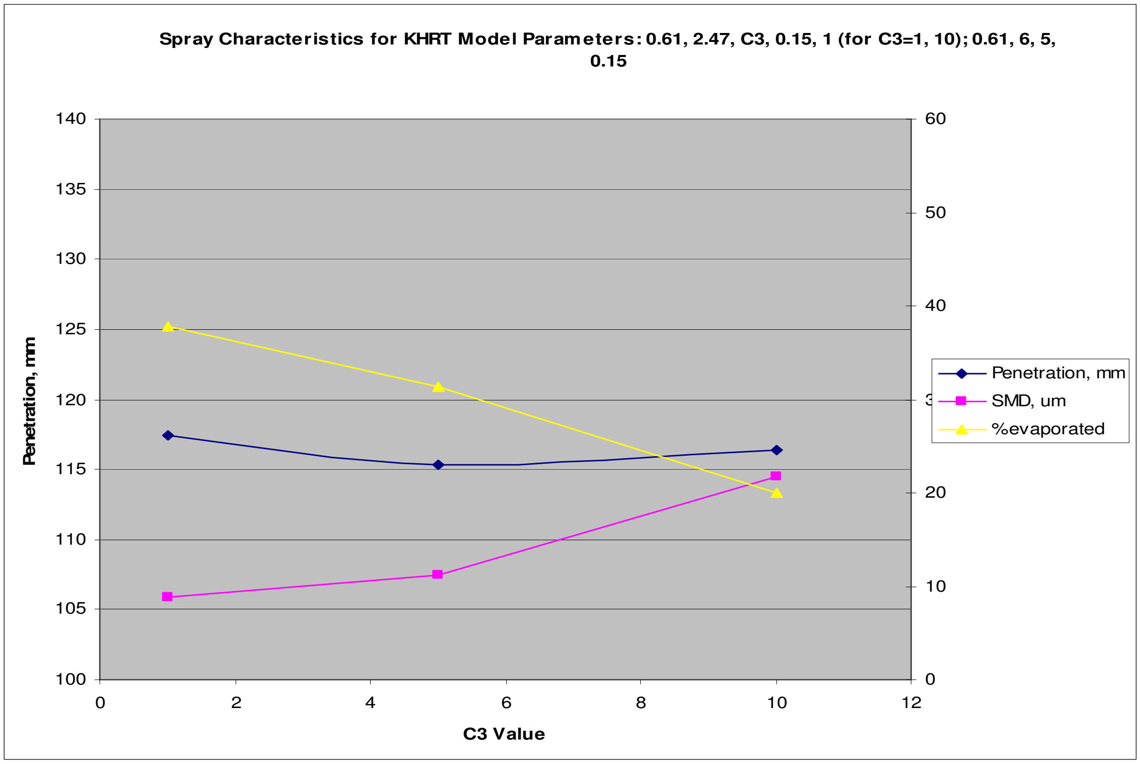

The pink curve in the following figure clearly shows the RT mode competing after the breakup length. The contrasting case (the brown curve) also has RT mode competing, it does not show a two step drop because the RT mode kicks in early, around 0.2-0.3 ms tick marks.

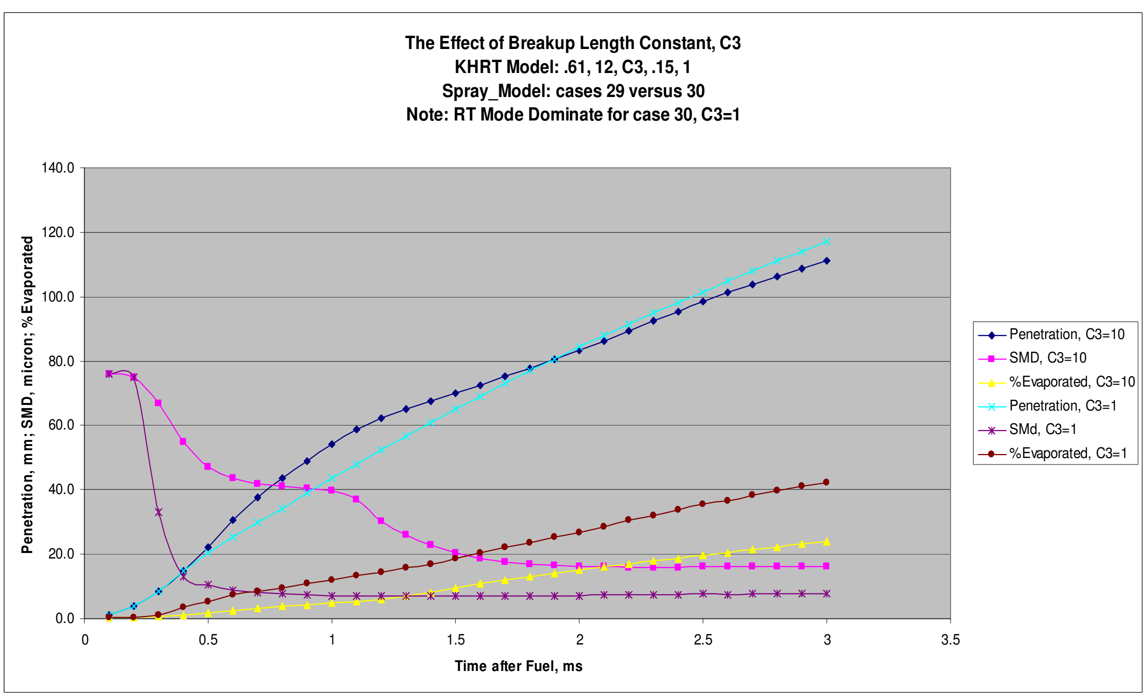

As an interesting comparison to the previous case, the pink curve in the following figure shows a lot less visible RT mode effect than the corresponding curve in the previous figure due to a more competitive KH mode with C2=2.47.

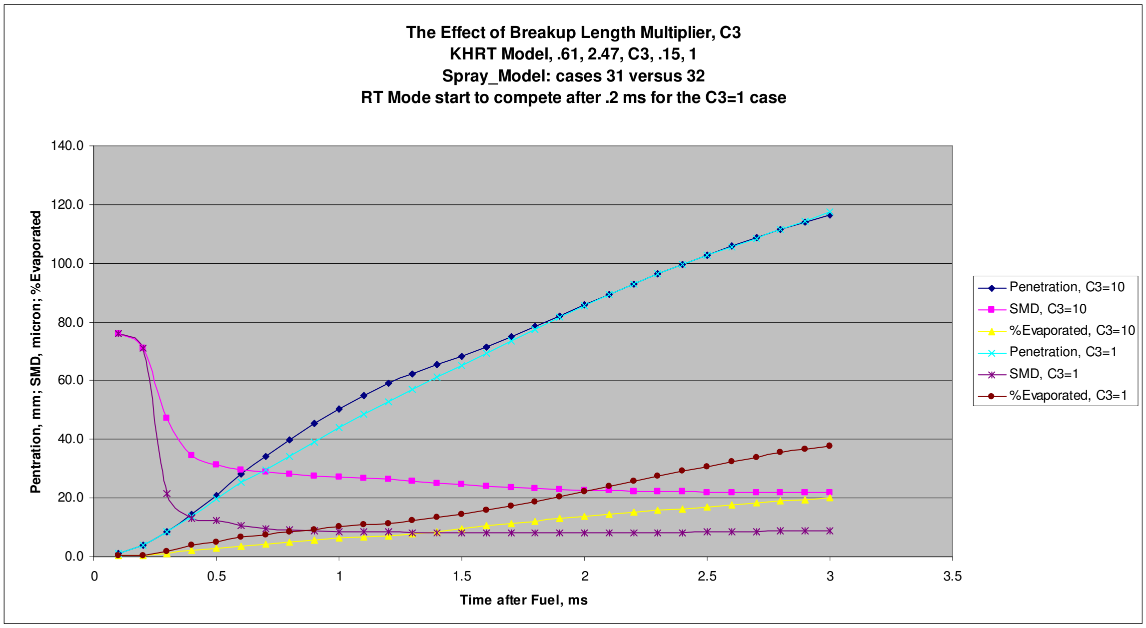

As shown in the following figure, C4 is monotonic down to 0.2, then the change becomes highly nonlinear from 0.15 to 0.1.

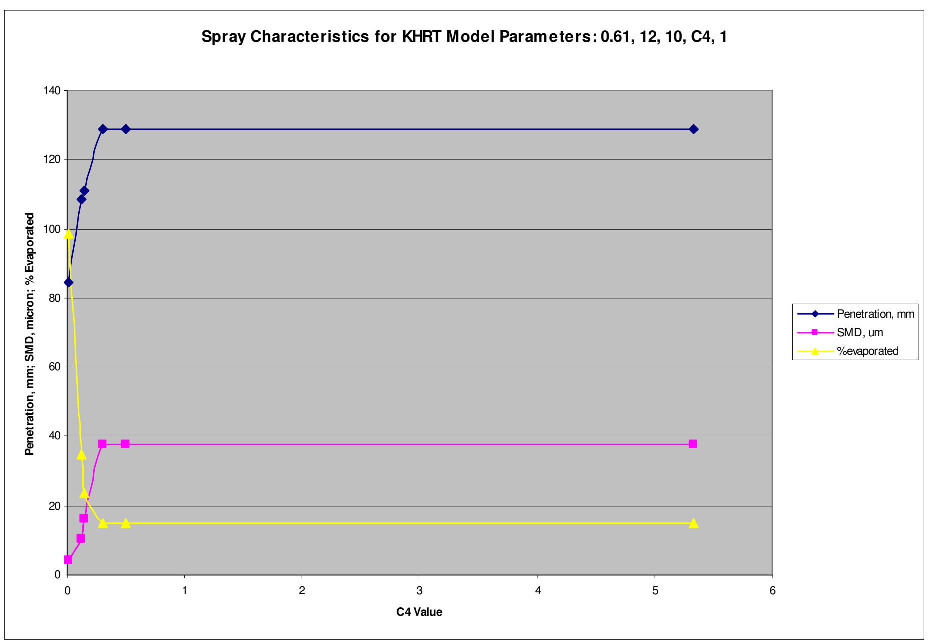

The corresponding transient responses are shown here for the three cases of C4 = 0.15, 0.12 and 0.1. We can see the effects of RT modes with progressively more competitive strength. In the case of C4=0.01, the solution becomes unstable and is not reliable.

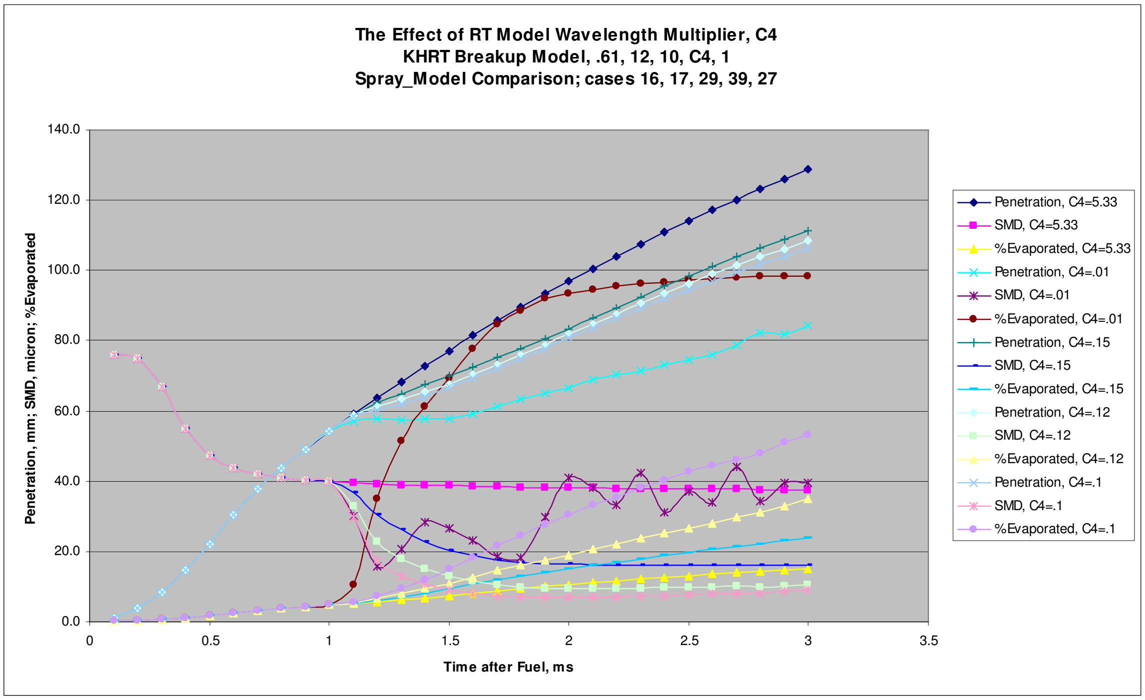

Comparison with Experimental Data in Transient Penetration Curves for n-Heptane and E85 and Lessons Learned for Further Improvements of the Spray Model

Given the parametric study, a model parameter setting of .61, 12, 10, .12, 1 for C1-C5 was chosen on the basis of penetration and SMD at 3 ms. However, detailed comparison of the transient penetration curve with experimental data in the following figure provides a few more clues for better model tuning. A close examination of the curves shows that the discrepancy in the first 0.3 ms may be attributable to the linearly ramped opening of injection flow. An accurately measured flow rate data will be helpful to resolve this discrepancy. The second area of discrepancy is the overall level of penetration is underestimated. This might be due to the smaller velocity correction factor used in the study (1.25 versus 1.5-10 recommended by Levy). Having a time resolved SMD measurement will be helpful in resolving this issue too. The same parameter setting has been used for modeling n-Heptane, gasoline and ethanol. We had also tried but failed to model E85 with the current version of AVL-Fire (version 5) at this point. AVL technical consultant confirmed that the flex-fuel capabilities are not implemented in version 5 but will be available in the next release expected by the end of July. The analyses for gasoline and ethanol however do not show much difference in penetration, SMD and % evaporated for the two fuels, practically bracketed E85 quite tightly within the two sets of solutions for gasoline and ethanol. The evaporation for n-Heptane does show a much higher value than for gasoline and ethanol. This is consistent with the low octane number for n-Heptane. The model also predicts large differences in SMDs for the three fuels around the characteristic breakup length. This prediction needs to be verified with time-resolved droplet size measurements which we plan to do in next quarter.

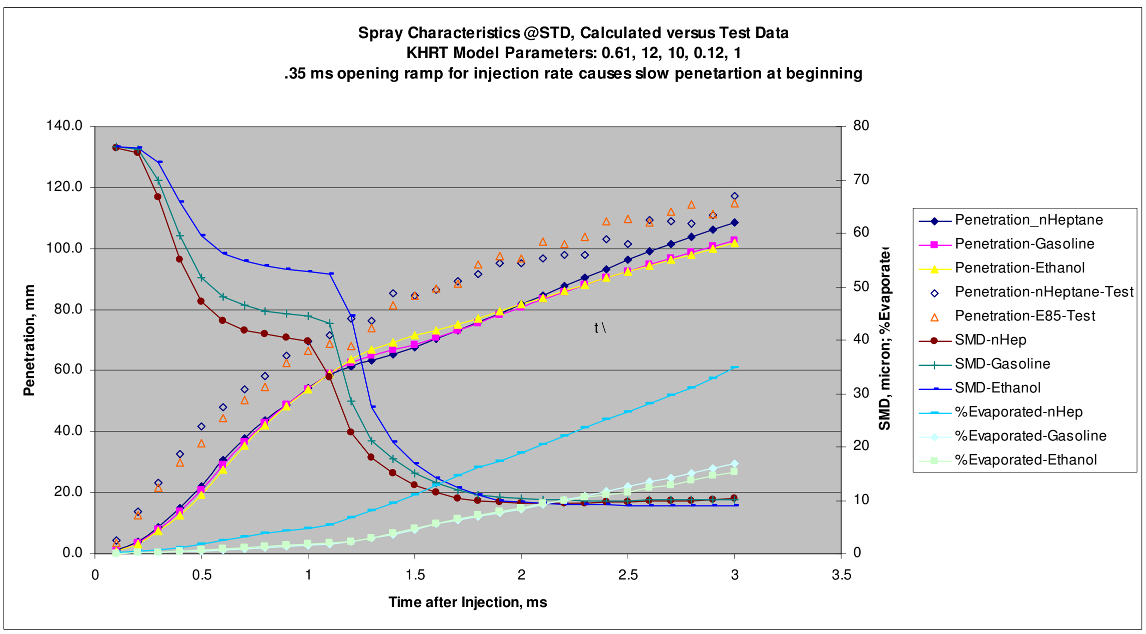

Spray Chamber Tests at High Temperature and Pressure

To support the validation of spray models, we have completed the basic flow/spray tests at room temperature and atmosphere pressure for stoddard, n-heptane and E-85. We are planning more tests next quarter for elevated temperature and pressure conditions that are close representation of realistic engine operating conditions.

The following figure shows the cylinder pressure and temperature traces with respect to Crank Angle under various engine operating conditions obtained from GT-Power simulation

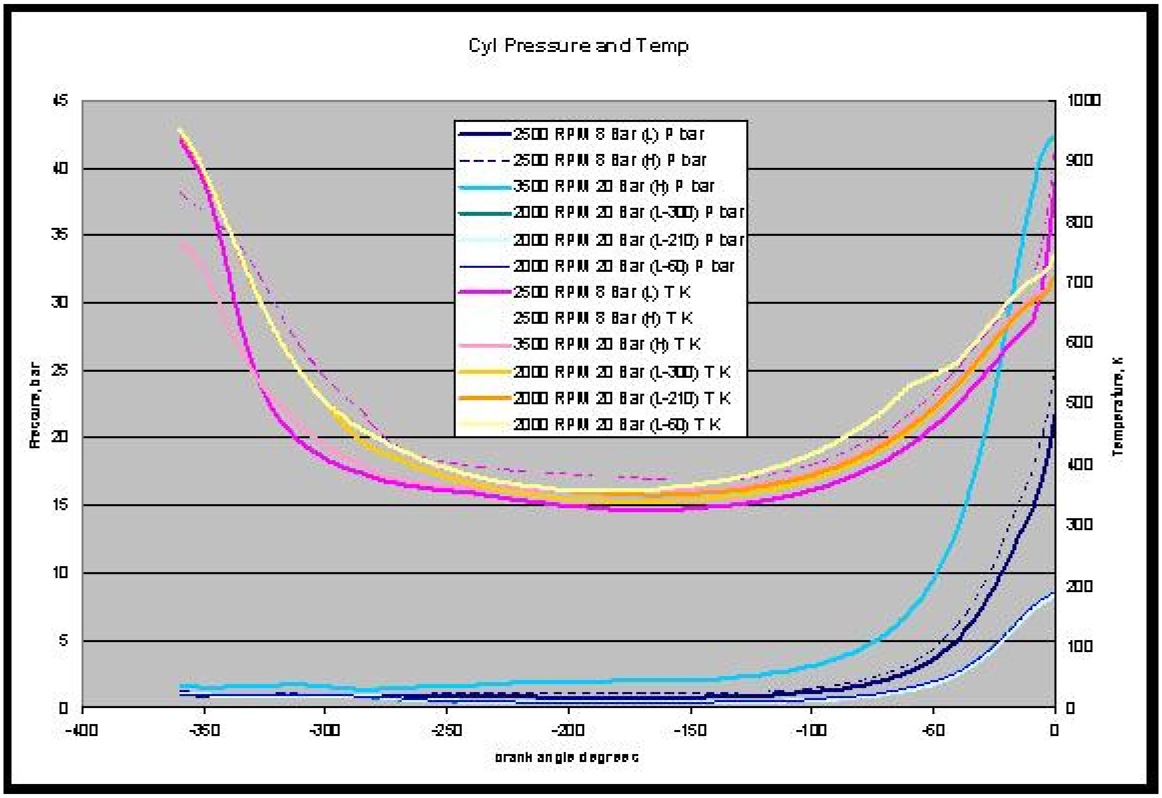

The following figure shows mapping of these traces onto a temperature-pressure chart, overlaid on these mapped traces are the corresponding crank angle positions for various cases and a red box indicating the operating window of the High T/P spray chamber currently being set up at Wayne State University. We will try to obtain time resolved and spatially resolved droplet size data and try to measure liquid and vapor phase distribution in the elevated temperature /pressure spray tests. These data will help ensure that our spray models work at temperature and pressure conditions expected in the E-85 Ecotec engines.

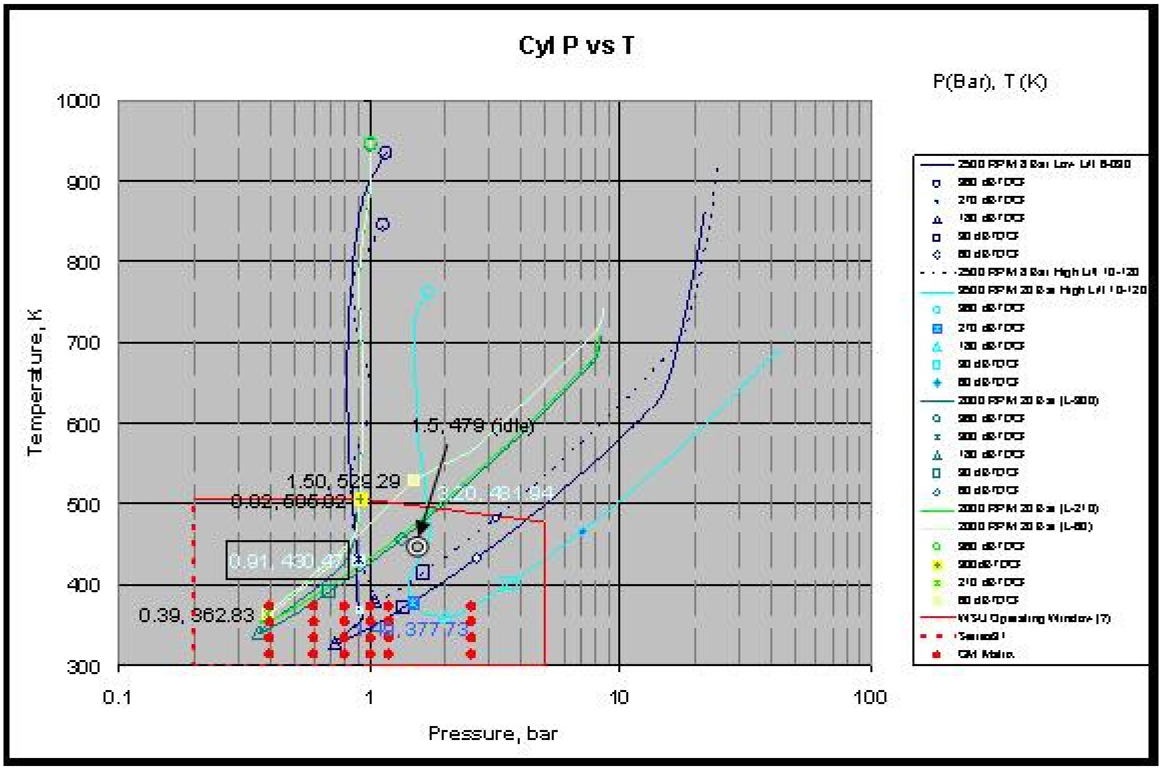

<u>Phase 1 Task 3.0</u> –Development Vehicle Level thru Model (4/1/08 6/30/08)

The GT Power engine model was used under task 1 to evaluate the steady-state operating points for the purpose of selecting two cam profiles for the two step valvetrain. Also a strategy for using the profiles and phasing to operate the engine over a range of speeds and loads has been constructed. The speed load maps generated from the engine simulations are used in the GT Drive vehicle model to quantify fuel economy performance over driving cycles. The vehicle level model for a model year 2007 Pontiac Solstice is as described in the previous quarter report.

A relative fuel consumption speed load map is shown in Figure 3.0-4. Relative fuel consumption is defined here as the fuel consumption of the modified engine relative to the fuel consumption of the baseline engine. The relative fuel consumption of the modified engine at compression ratio of 11 is better than the baseline where the value is less than unity. Over most of the map the modified engine is better than the baseline. In very low load regions where there is significant throttling the modified engine exceeds the fuel consumption of the baseline engine but that is due to a poorly simulated throttle strategy used in the model that would not be used on the engine.

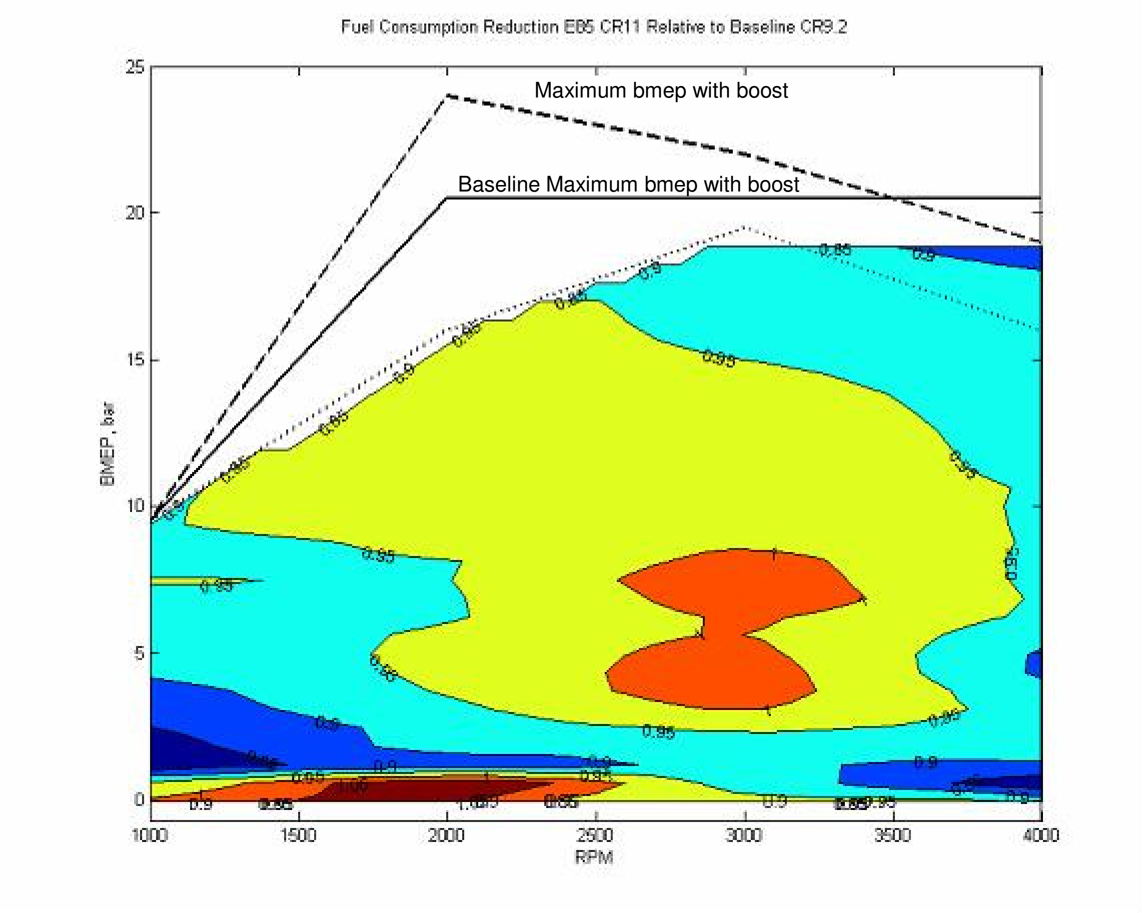

Figure 3.0-4: Relative fuel consumption map for CR 11 engine with 10 mm nominal lift high cam and 6 mm nominal low lift cam using E85 fuel

The engine map shown in Figure 3.0-4 underestimates the predicted fuel consumption benefit in another assumption also. In the model it is assumed the spark timing of the engine using E85 fuel is the same as is used for the engine operating on gasoline. Over much of the speed load map the engine using gasoline has some spark retard built in to prohibit knock. Since E85 fuel is more knock tolerant than gasoline there will be opportunity to leverage to optimize the spark timing to MBT timing and gain more efficiency. Figure 3.0-5 is an estimate of the relative fuel consumption map when the MBT timing is used for E85 fuel. This shows there is an appreciable increase in economy when best spark timing can be used. Exactly how close to optimum the spark timing can be set must be determined with the engine once the final piston design is complete and combustion performance is evaluated.

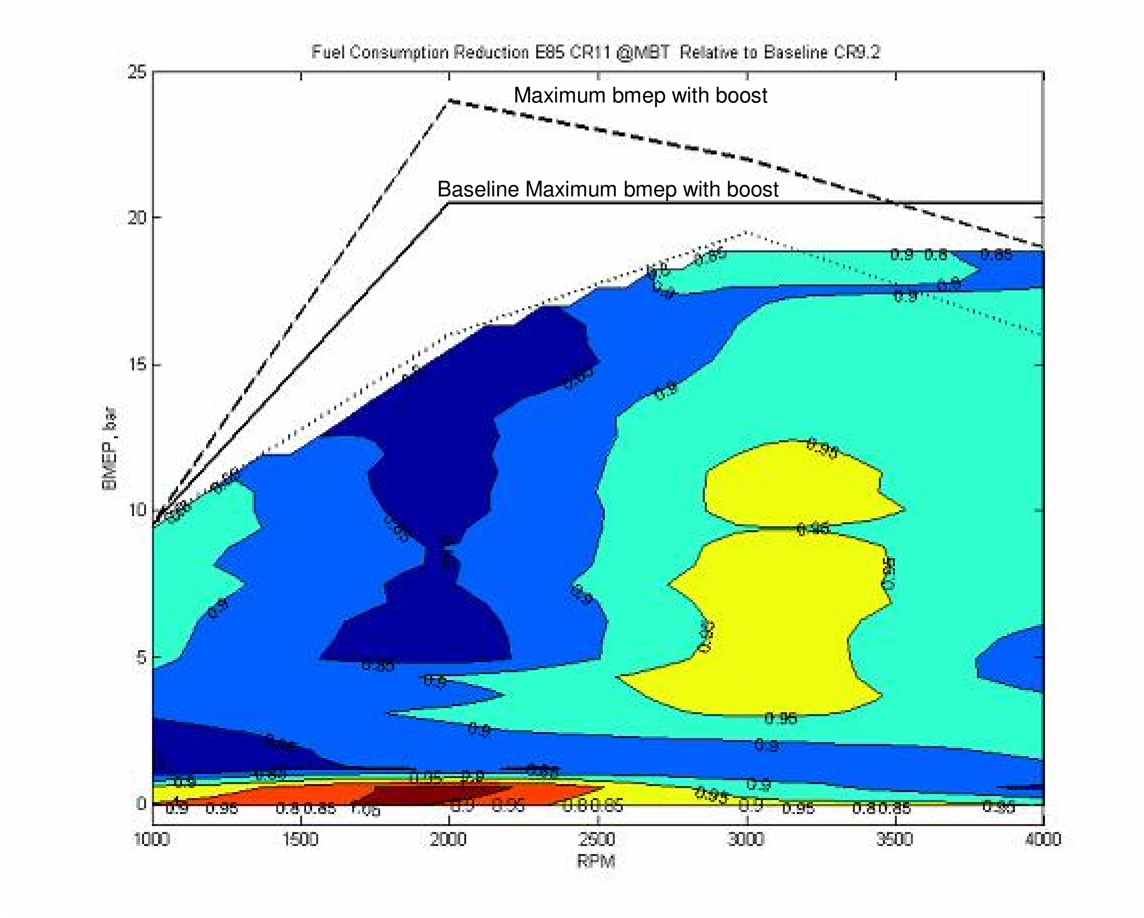

Figure 3.0-5: Relative fuel consumption map for CR 11 engine with 10 mm nominal lift high cam and 6 mm nominal low lift cam using E85 fuel and MBT spark timing

When the fuel consumption maps are put into the GT Drive vehicle simulation a total fuel consumed value is reported for each drive cycle simulated. The bars in Figure 3.0-6 show relative fuel economy gains compared to the baseline engine. A higher bar indicates lower fuel consumption than the baseline engine running on the same fuel over the given cycle. The comparison shows that the modified engine with compression ratio 11 is expected to improve about 8 percent on the FTP driving schedule using the unmodified spark timing. The fuel consumption depends on the driving cycle and which portions of the speed load map are used. Simulation results for the modified compression ratio 11 engine improvement ranges from about 5 percent improvement for the highway fuel economy test driving schedule (HWFET) to 12 percent for the EPA Southern California driving cycle (SC03). An additional 4 to 8 percent improvement is expected from the CR 11 engine (yellow bars) when the fuel economy benefit if MBT spark timing is used with the E85. A CR 13 combustion chamber is expected to deliver an additional 2 percent higher fuel economy benefit so the final piston design may result in economy higher than in this figure.

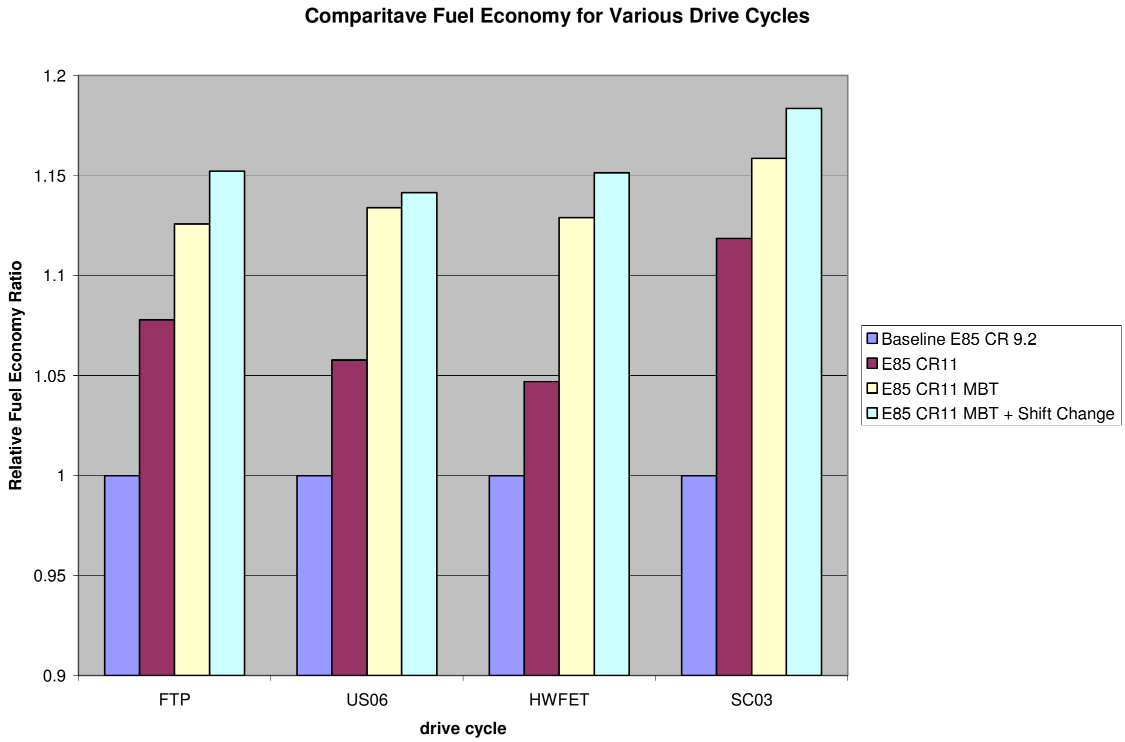

Figure 3.0-6: Relative fuel economy improvement results for various driving cycles in vehicle simulation

Additionally, altering the engine shift schedule could be used to utilize the areas of the fuel economy map where the economy gains are greatest. For comparison purposes an alternate shift schedule was input to the vehicle simulation. This is not an optimized shift schedule but simply an illustration that another few percent in fuel economy gains can be gained by using this technique. Other research in this area has suggested that changing final drive ratio and transmission gearing produces performance benefits as well. Such hardware changes can compromise performance (e.g. 0 – 60 mph acceleration times) and are outside the scope of this project but could ultimately be used in an effort to maximize fuel economy gains.

Phase 1 Gate review in Washington DC

On May 28th a presentation was given to the DOE in Washington DC on cam phasing strategy, showing an EIVC-LIVC strategy for load and compression ratio control. Spray model development, piston geometry and spray targeting status were also covered in the presentation. Simulated fuel economy improvements on E85 over base engine on drives cycles were presented showing 12-15%

improvement. Gate review presentation material is available upon request from Keith Confer at keith.confer@delphi.com

Phase 2 Task 1.0 – Develop Baseline Fuel Specifications (4/1/08 thru 6/30/08)

Plans are being made to blend the fuels as needed. Fuel blends will be sent out for testing and characterization before tests are run.

Phase 2 Task 2.0 – Base Line Definition/Evaluation of Prototype Flex-Fuel Injectors (4/1/08 thru 6/30/08)

During this quarter the GT Power engine model was used to support fuel injection work that falls under this task. While developing the optimum cam lift profiles to be used for the two step hardware there was some modeling work done to preliminarily define fuel injection requirements. Figure 3.0-7 shows model prediction of how the fuel injection timing affects the engine performance, in this figure volumetric efficiency (VE) is plotted. For a fixed exhaust valve closing intake valve opening is varied along the x-axis. The different curves show fuel injection timing is swept from 15 crank angle degrees after TDC to 235 degrees after TDC. With all injection timings there is a strong effect on intake valve phasing as each of the curves shows a maximum VE when the IVO is 230 – 235 degrees. Fuel injection timing has an effect on VE as well. VE is a maximum when 55 to 75 degrees after TDC. Improved flow is due to the charge cooling effect of the fuel. When the fuel is injected so it evaporates during the intake flow event the lower in-cylinder pressure assists the flow. For fuel is injection later than this there is less improvement in VE. The fuel injection timing effect on VE is not so strong with gasoline as the heat of vaporization of the fuel is less than the heat of vaporization of E85 fuel.

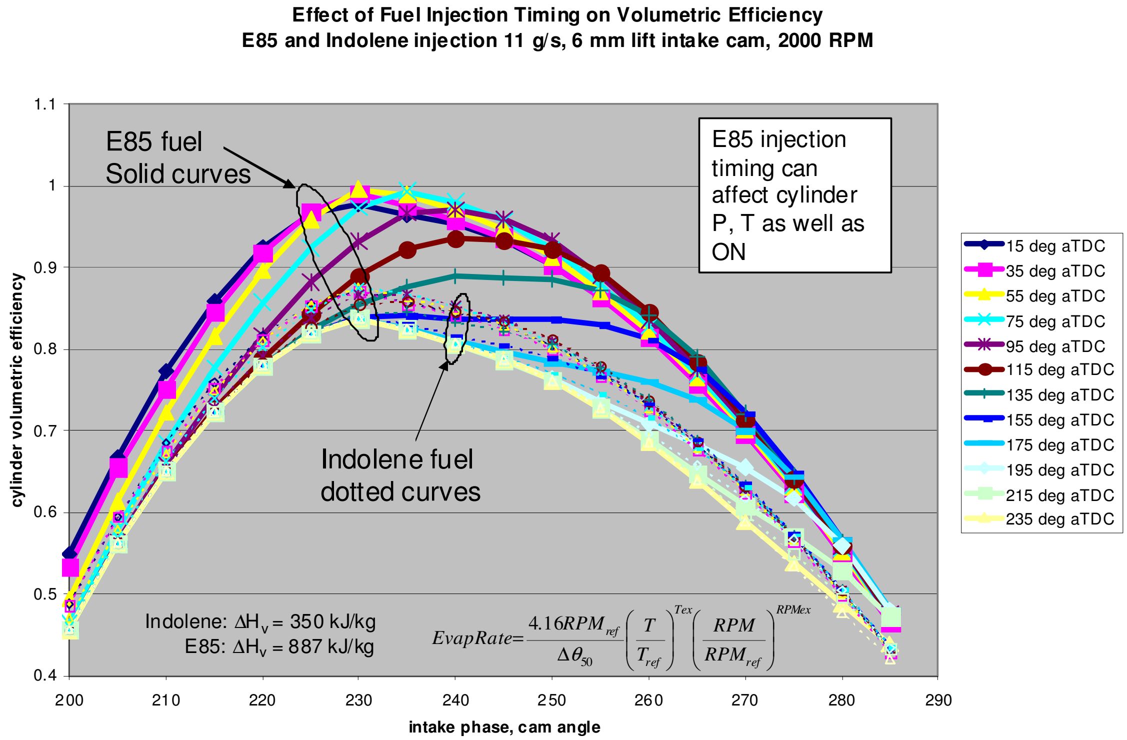

Figure 3.0-7: GT Power model of volumetric efficiency as a function of intake valve opening and fuel injection timing.

The fuel injection model used in the GT Power model is zero dimensional, so it can not comprehend phenomena such as fuel spray interaction and wall wetting. The previous figure assumes a single fuel injection pulse and there may be advantages to evaporation and combustion arising from use of a split injection strategy. These issues indicate a need for three dimensional spray modeling and spray testing to investigate details of the behavior of the fuel injection.

In order to support more detailed spray modeling and spray testing the GT Power engine model is used to determine appropriate in-cylinder pressure and temperature. Several operating points were investigated with the engine model and pressures and temperatures during the engine cycle are plotted in Figure 3.0-8.

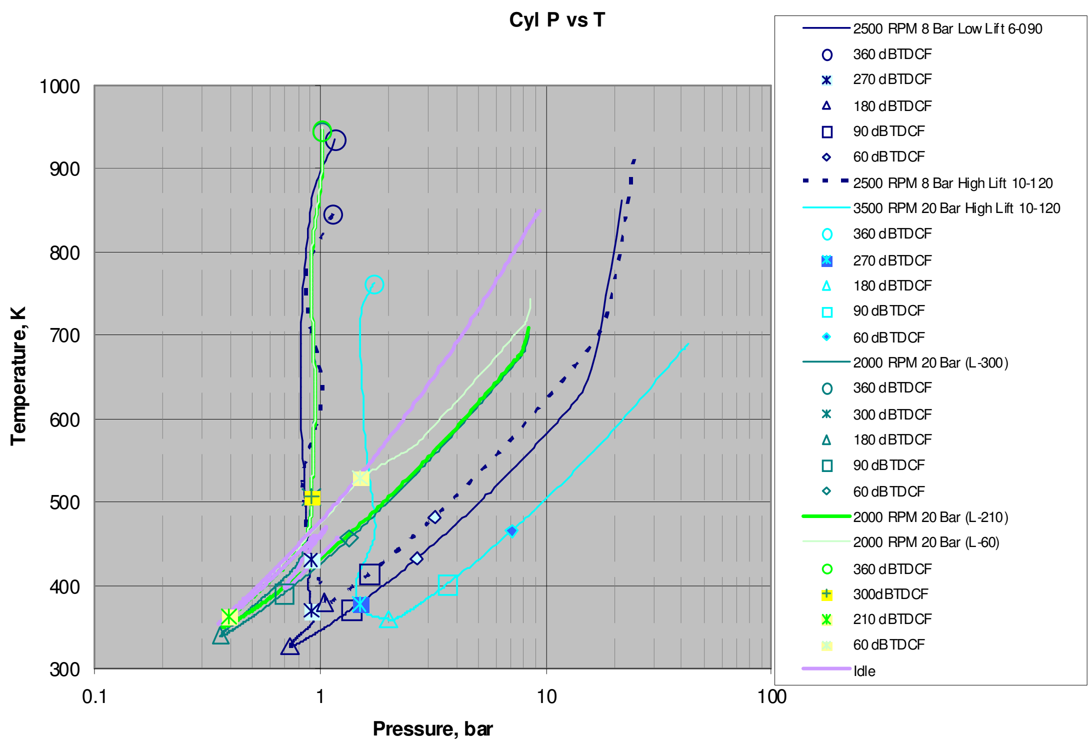

Figure 3.0-8 GT Power simulation results of in-cylinder temperature versus in-cylinder pressure

Cylinder pressure is plotted along the x-axis and cylinder temperature is plotted on the y-axis in this plot. The different curves represent a range of speed load points of engine operation. Time progresses along the curves as indicated by the markers shown at some crank angle increments. The figure shows that late fuel injection will occur at high pressure and temperature. Test conditions to concentrate the testing and three dimensional modeling that will be pursued in Phases 2 and 3 of the project are identified from the results of this figure and others.

The piston crown geometry and spray targeting interaction was designed using Unigraphics modeling geometric representations of the spray. The attached figures show the spray interaction with the piston bowl at a stratified injection timing Figures 1 and 2 and a homogeneous injection timing Figure 3. The inner cone (4 deg.) represents the liquid core and the outer cone 12 deg. Represents the 95%ile spray. The injection penetration is representative of the spray 1.5 msec after Start of injection (SOI). Spray is well retained in the central piston bowl feature for stratified operation and dispersed for injection timings compatible with homogeneous operation. Some piston impingement still occurs even during homogeneous timings due to spray penetration.

The base compression ratio of the piston after design of the piston bowl feature and allowing required valve recesses for the valves to permit valve phasing is 11.9. Figure 4 shows the targeting geometry to specify the fuel injector prototype.

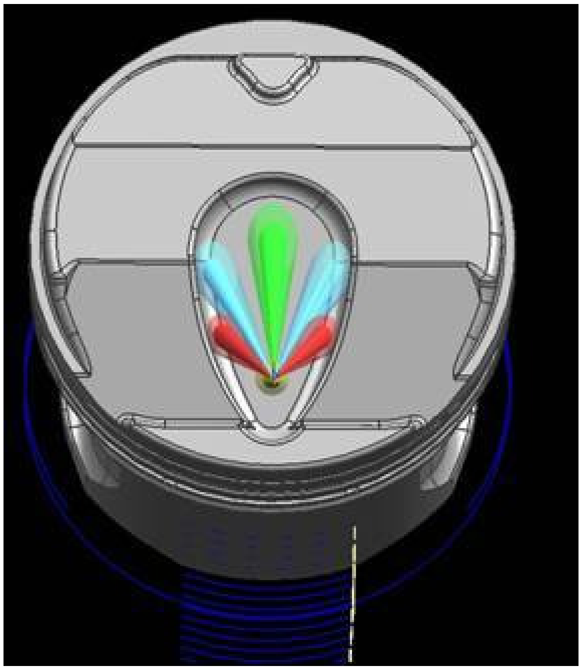

Figure 1 Top view of injection with Piston 20 mm below TDC (Stratified)

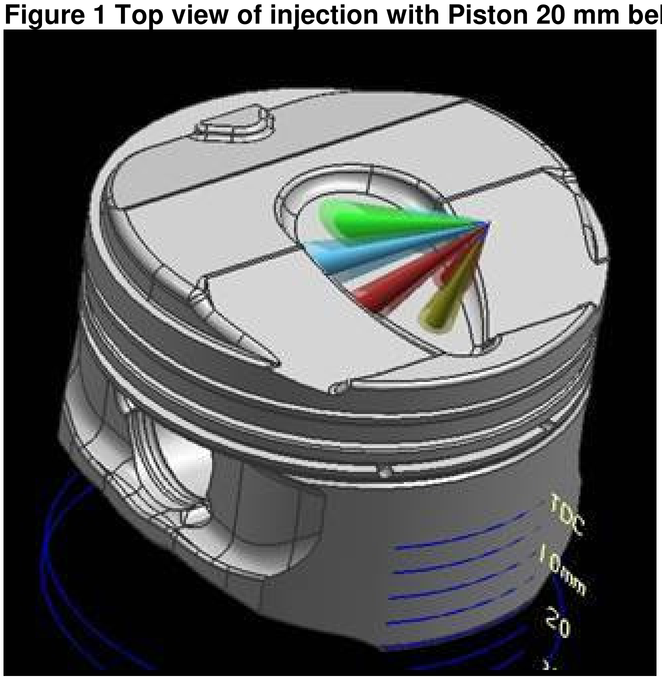

Figure 2 Side view of injection with Piston 20 mm below TDC (Stratified)

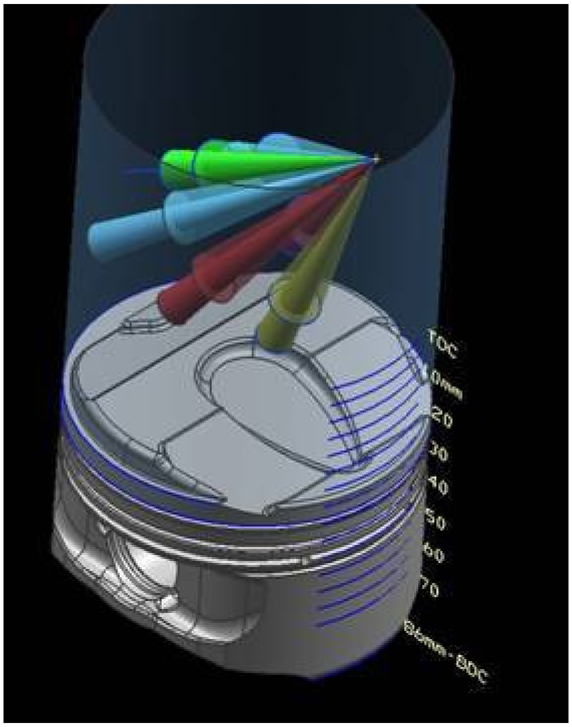

Figure 3. View of piston at BDC during homogeneous injection.

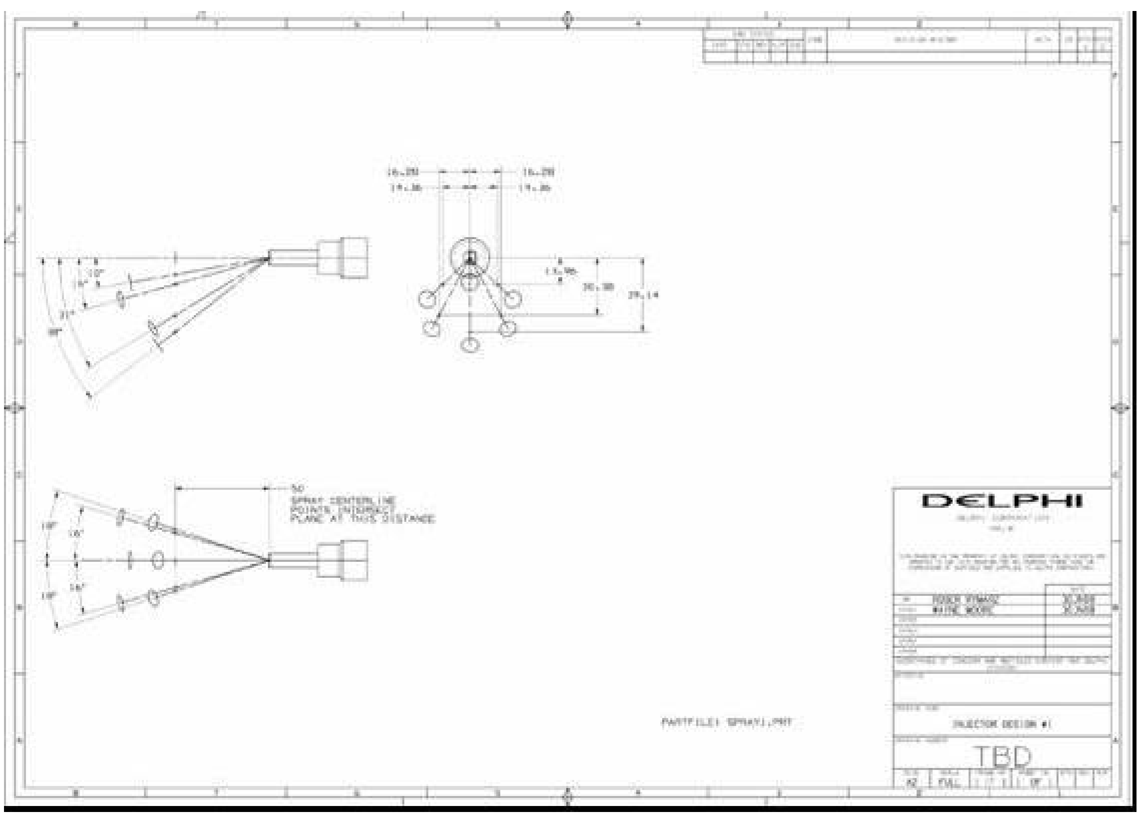

Figure 4. Fuel injector spray targeting at 50 mm normal to the injector axis.

<u>Phase 2 Task 3.</u>0 – Test Chamber Construction (4/1/08 thru 6/30/08)

The injector spray chamber at Wayne State University is being reconfigured for the GDI spray characterization tests in this project. Work began on the lab and is progressing to plan. The chamber is designed for spray visualization and phase Doppler Interferometry (PDI) measurements. The layout for the chamber with PDI is as shown in the figure below.

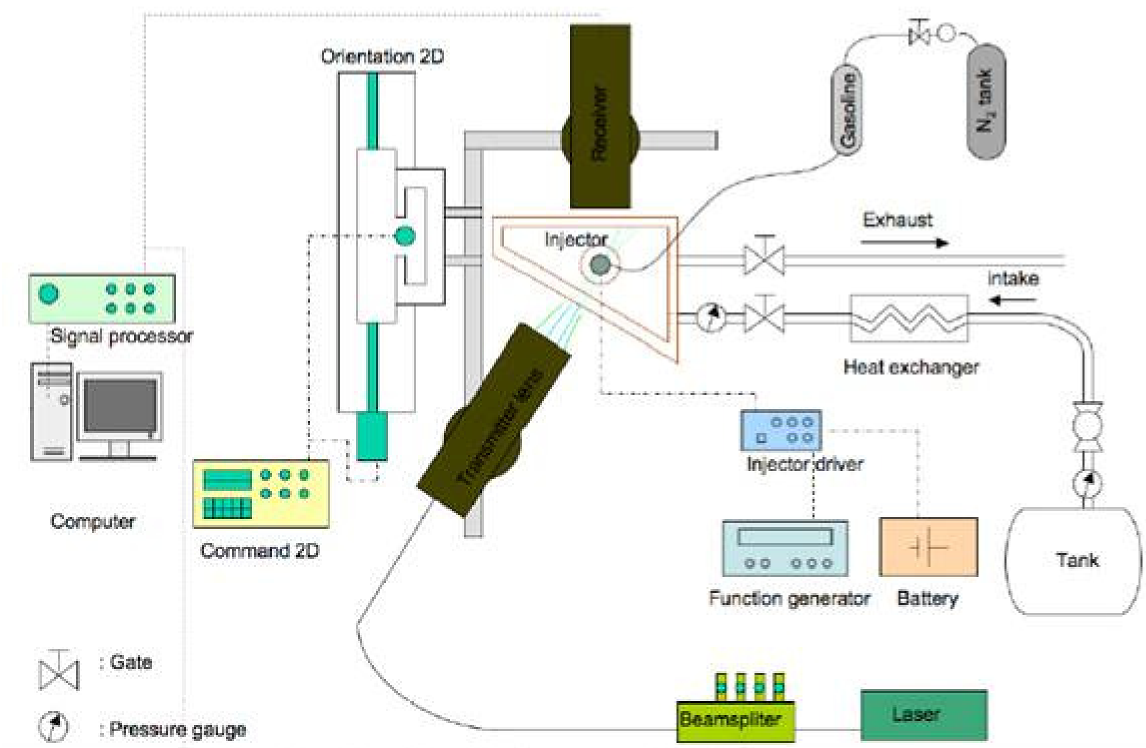

<u>Quarter 3 2008</u>

<u>Phase 2 Task 1.0</u> –Develop Baseline Fuel Specifications for Subsequence Tasks (7/1/08 thru 8/29/08)

A range of ethanol blends will be evaluated in the experimental program but with primary focus on E85 and E0. The ethanol blends will represent a range of ethanol-gasoline that would be used in actual vehicle operation. The baseline fuels shown below will be used.

Name	Definition
Lab E0	Gasoline 100% 87 Octane (R+M)/2
Lab E10	Gasoline 90% & 10% Ethanol
Lab E50	Ethanol 50% Gasoline 50% - Simulates E85 & Gasoline Blending
Lab E85	Ethanol 85% Gasoline 15% - E85 All Zones, Summer Season

The project will use commercially representative fuels comprising splash blends of 87 PON (R+M)/2 with E85. Samples of the fuel will be drawn to have analysis done to document the fuel properties. An additional supply of 87 PON (91 RON) E0 and E100 will be procured to produce an E85 blend. Intermediate blends will be splash blended and evaluated. Blends will be evaluated at E0, E10, E50, and E85.

<u>Phase 2 Task 2.0</u> –Baseline Definition / Evaluation of Prototype Flex-Fuel Injectors (7/1/08 thru 9/30/08)

Injector spray targeting with a 6 hole injector spray pattern, see pattern figure below, was completed to complement both homogeneous operation and interaction with the piston bowl geometry to support light stratified operation to reduce cold start emissions. The targeting was co-designed along with the piston bowl to allow fuel retention during late stratified operation. Attention was also paid to minimize spray interaction with the cylinder bore and avoid impingement with the intake valves during peak lift on the high lift cams.

The orifice plate and injector package design was completed to provide the desired targeting and to meet the specified 20.4 g/s Static flow at 10 MPa injection pressure.

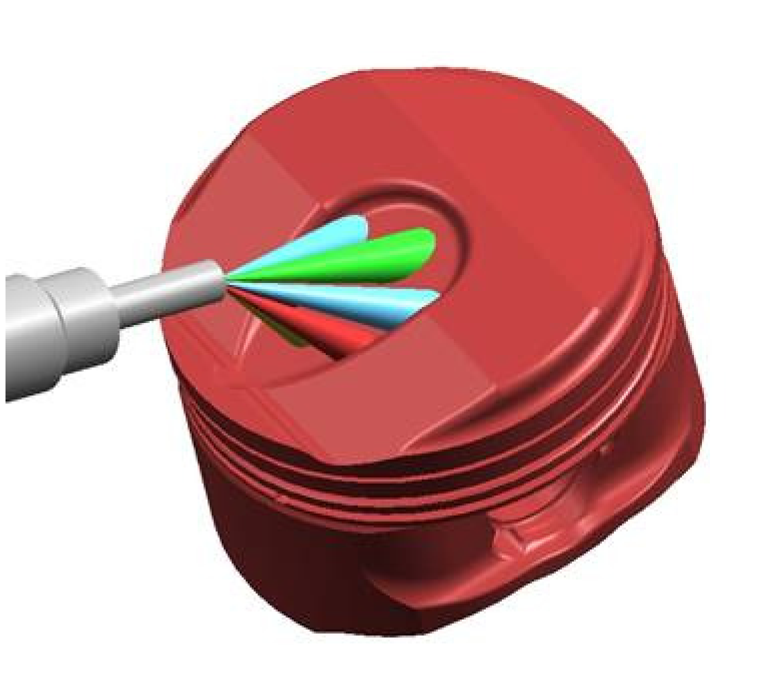

Figure 1: Injector spray targeting with a 6 hole injector spray pattern

Phase 2 Task 3.0 –Test Chamber Construction (7/1/08 thru 9/30/08)

The design of the Spray Chamber has been modified to achieve the following objectives:

- Chamber pressure from 0.3 (partial vacuum) up to 4 bar or higher,
- Chamber air temperature up to 200°C or higher,
- Direct Spray visualization with side- or back-lighting,
- Schlieren spray visualization of both liquid and gaseous phases
- Phase Doppler Interferometry measurement at 135° forward scattering angle,
- 2-D traversing stand for
- Temperature-controlled Injector holder to decouple fuel temperature from chamber temperature.
- Extension for future spray-wall interaction investigation for piston and cylinder surfaces

Further improvements include the minimization of heat loss, insulation, thermocouple and temperature control. The layout for the chamber is shown in

Fig. 2 with the photograph of the setup shown in Fig. 3. In order to facilitate Schlieren visualization, another chamber body was built as shown in Fig. 4.

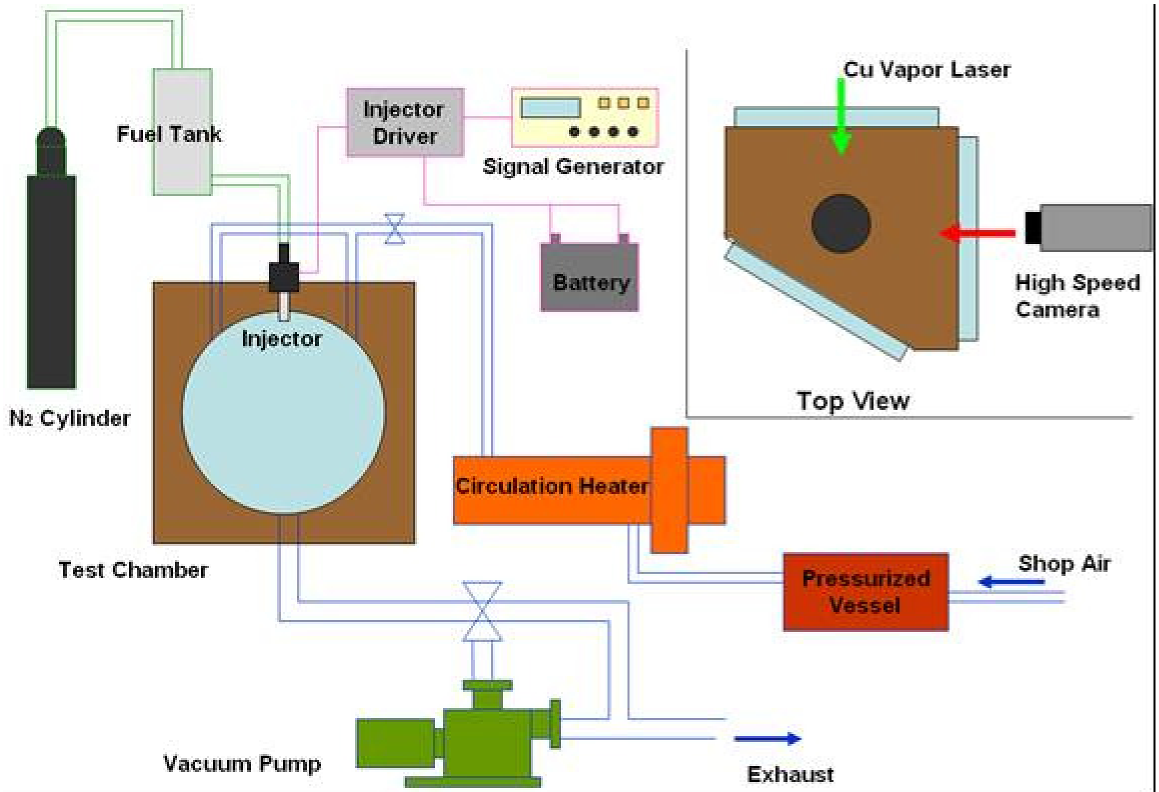

Figure 2: *Test chamber layout spray-visualization with the PDI chamber*

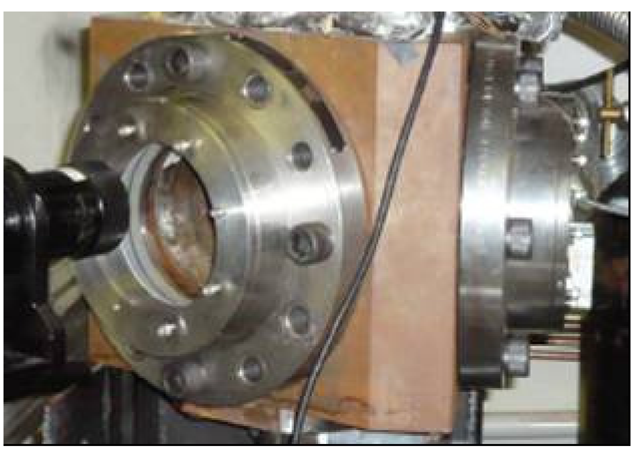

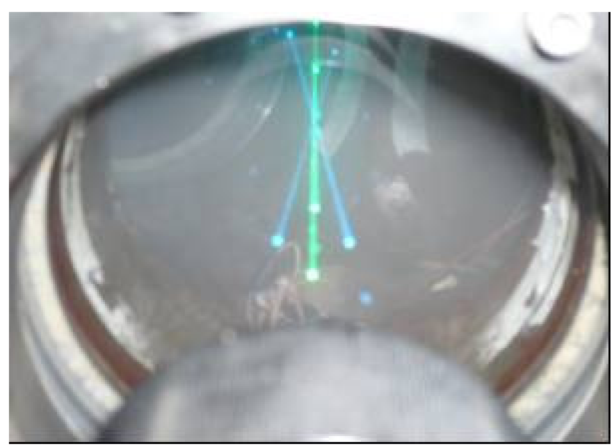

Figure 3: *Test chamber and PDI laser setup*

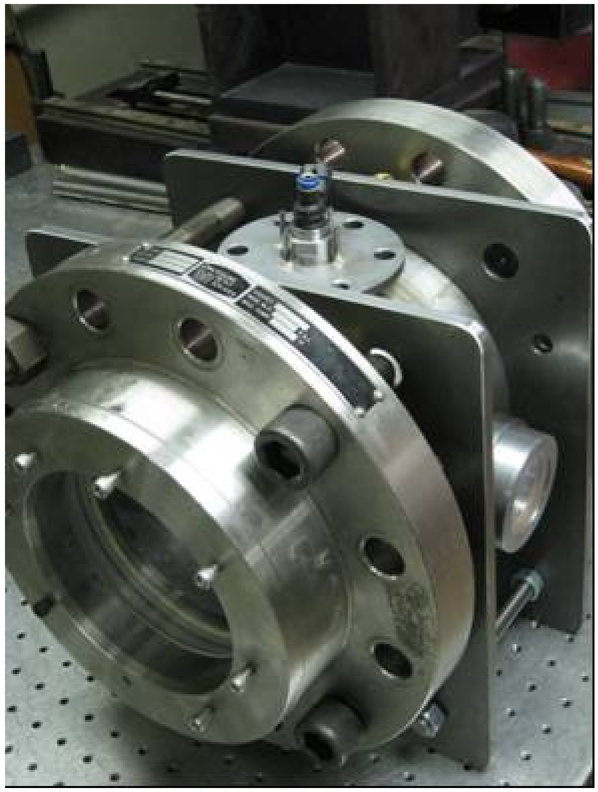

Figure 4: Photograph of the Schlieren chamber and Injector holder (with coolant and thermal couple inlets)

Trial tests were run using a production injector. The DI-G injector tested has a 6-hole nozzle, with offset designed to be side-mounted between and below the intake valves. Preliminary visualization using high-speed digital camera (Phantom 7.1) of the E100 spray from DI injector under the conditions listed in Table 1 will be summarized in the following:

Table 1: Test conditions

Injector Type	736						
Fuel	E100						
Density @ 20ºC [kg/m^3]	789						
Dynamic Viscosity @ 20ºC [Pa•s]	1.2E-3						
Boiling Point [ºC]	78.4						
Chamber Temperature [ºC]	28~150						
Chamber Pressure in absolute [bar]	0.4	0.6	0.8	1	2	3	4
Injection Pressure [MPa]	5						
Injection Signal Duration [ms]	3						

The spray geometry and its orientation are shown in Fig. 5, with the hex cell patternizer measurements (top left) and camera view (bottom left) and the side view (bottom right) through the laser-lighting window. From the spray penetration calculation corrected for the spray geometry and viewing angle, it can be shown in Fig. 5 (top right) that the spray pairs that have the straightest streamline, the (green) spray #1, penetrate the fastest, while the rest seem to be about equal in penetration. This finding has not been reported previously in the literature and show that internal flow structure has significant influence on the spray structure.

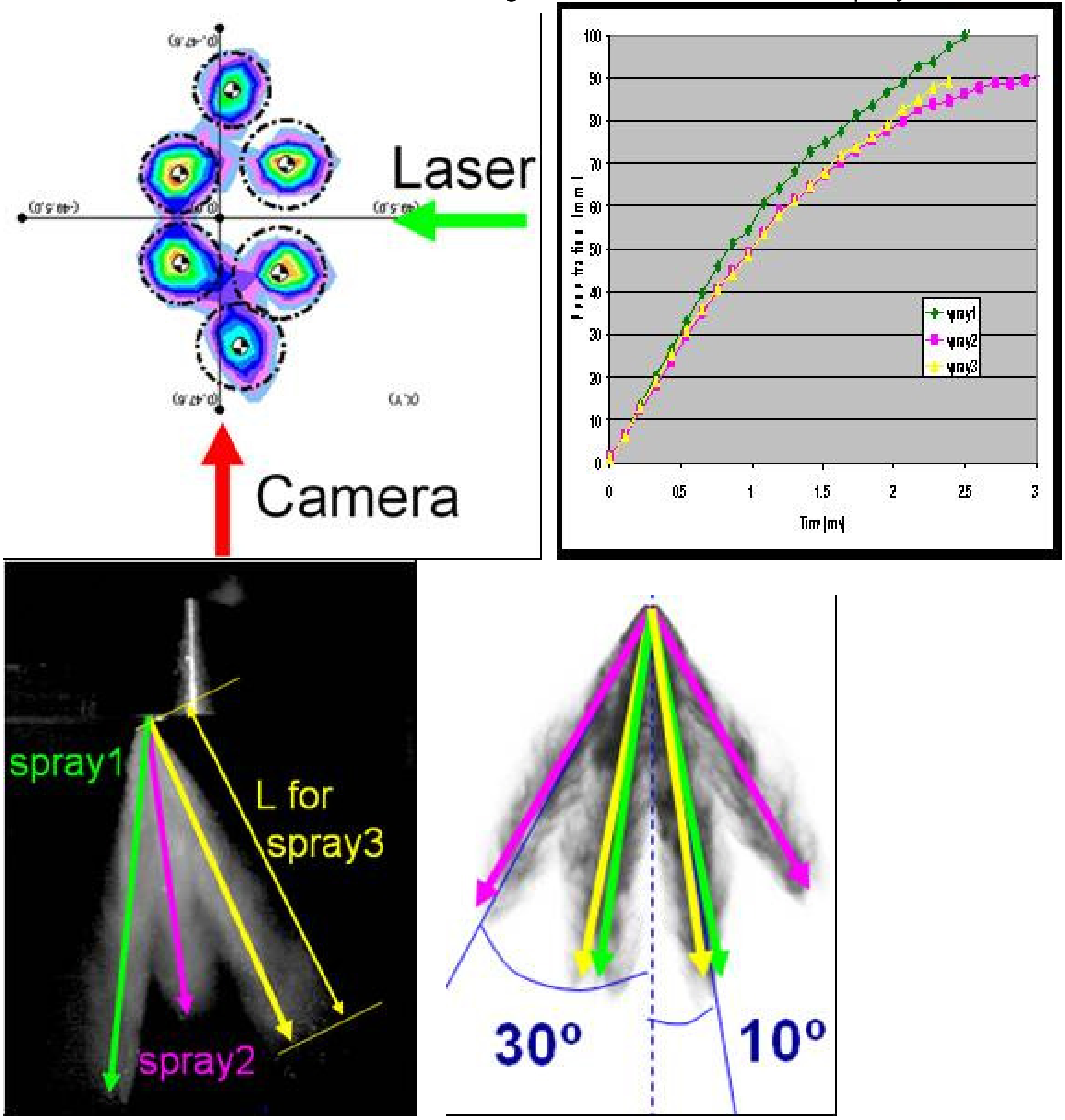

<u>Figure 5:</u> Spray pattern from the Hex-Cell (top left), spray penetration (top right), and spray geometry from the camera view (bottom left) and side window (bottom right)

The effect of chamber pressure on the spray penetration is obvious in Figure 6. It shows that the penetration (of spray #2 which is the closest to the camera) is slower for higher chamber pressure due to increased drag force. The effects of ambient temperature on the spray structure are shown in Figure 7. Below the boiling temperature, the degree of vaporization increases with ambient temperature due to enhancement in heat and mass transfer. Above the boiling temperature, “Flash Boiling” phenomena may arise, which collapse the 6 spray into a coherent spray with enhanced penetration and mixing. The resultant spray structure resembles that of the air-assisted DI spray. The complexity of the flash boiling in spray is that it is a function not only of temperature, but of pressure , and a combination of other effects, including injector design, cavitation, and multiple component effects.

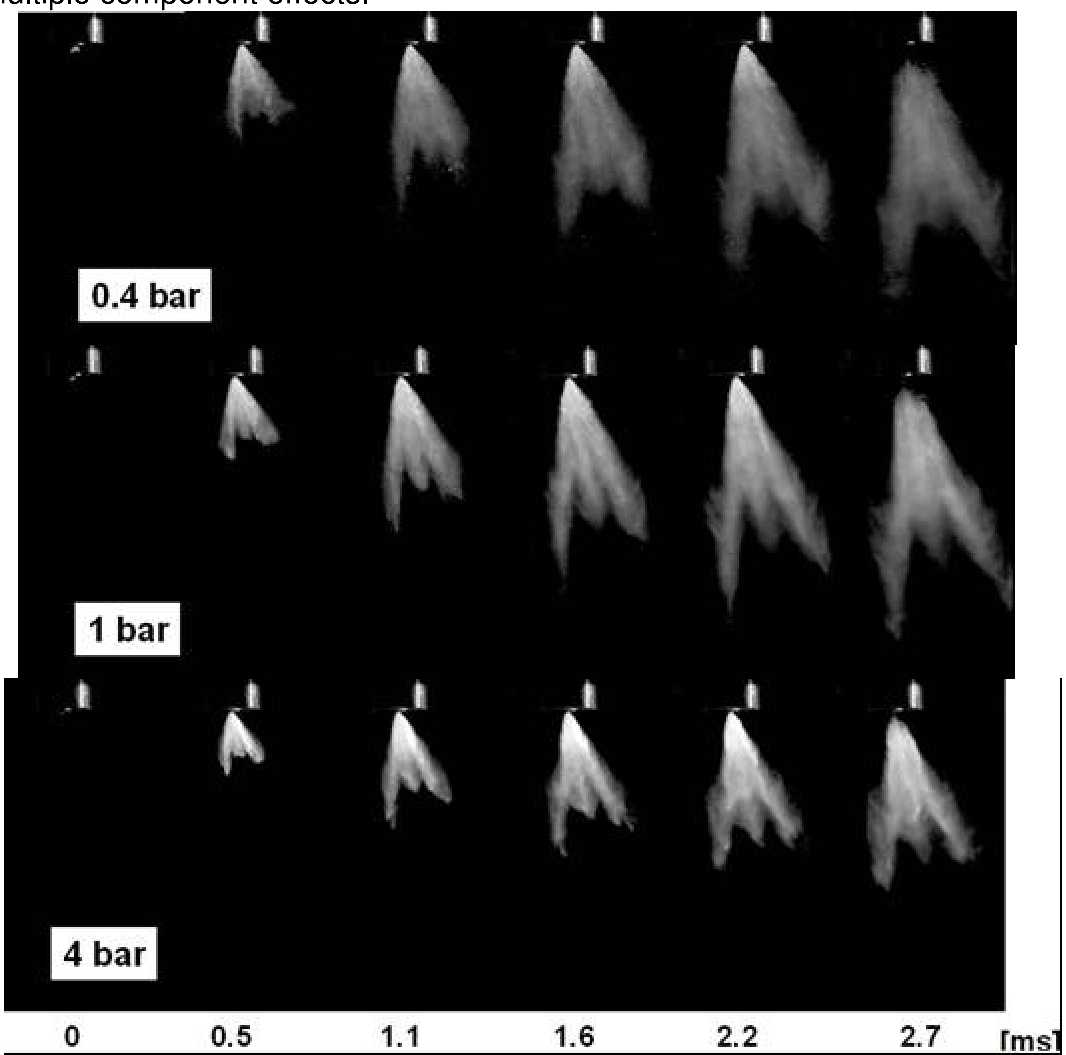

<u>Figure 6a:</u> Effects of ambient pressure on spray structure and penetration (#2, at 28ºC)

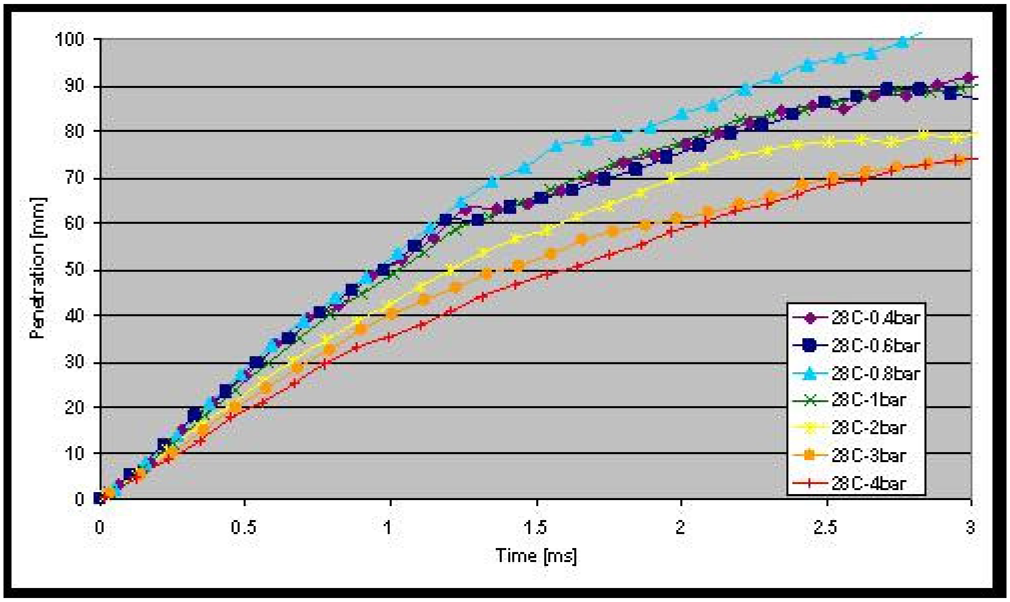

Figure 6b: Effects of ambient pressure on spray structure and penetration (#2, at 28ºC)

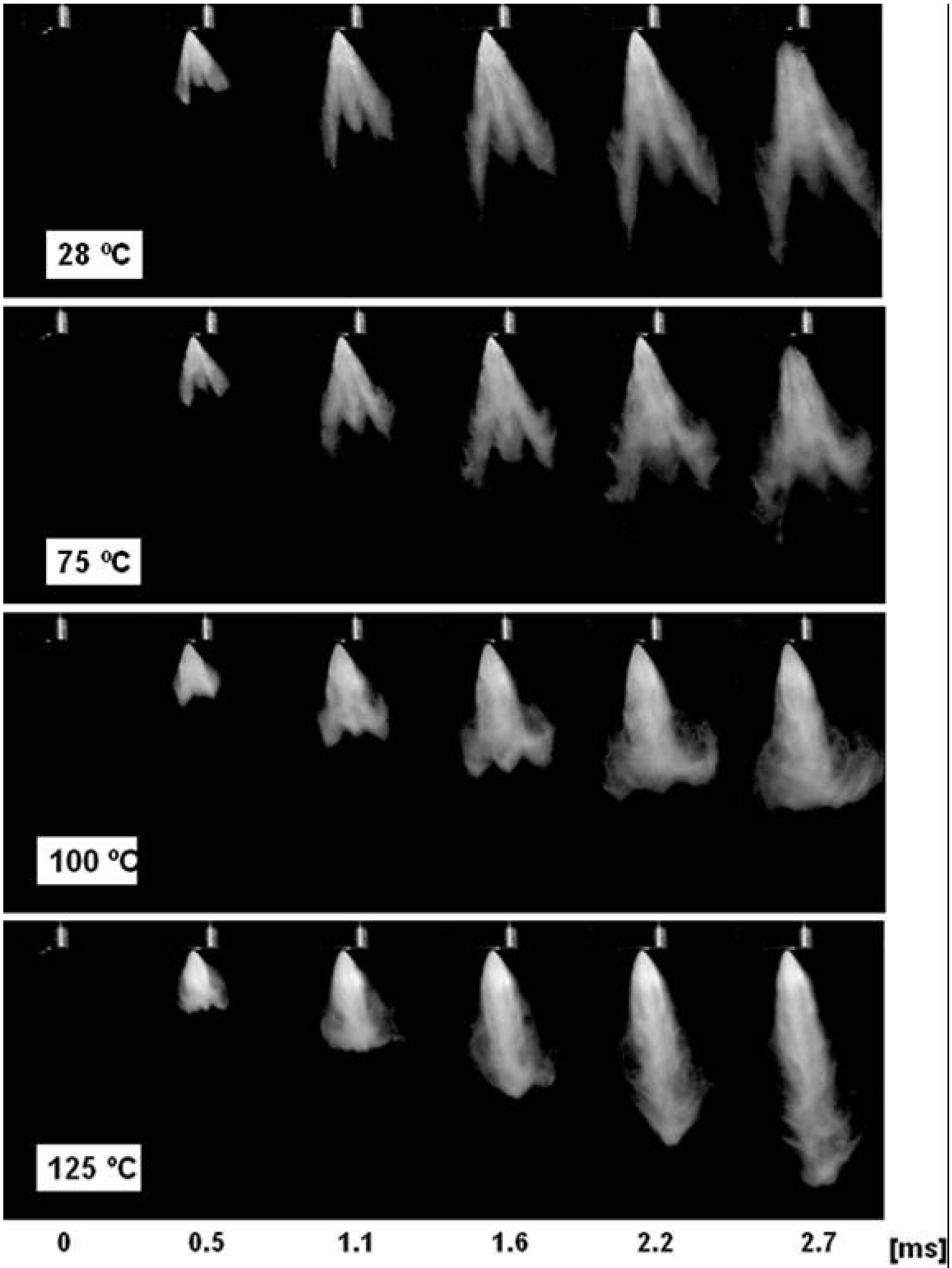

Figure 7a: Effects of ambient temperature on spray structure (at 1 bar)

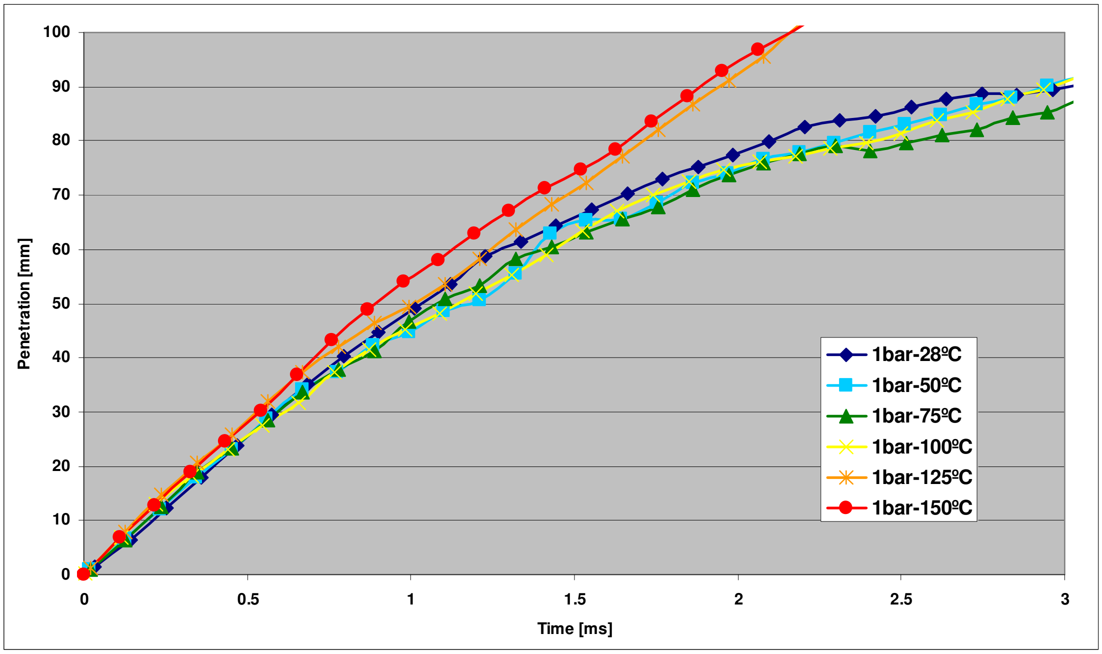

Figure 7b: Effects of ambient temperature on spray penetration (#2, at 1 bar)

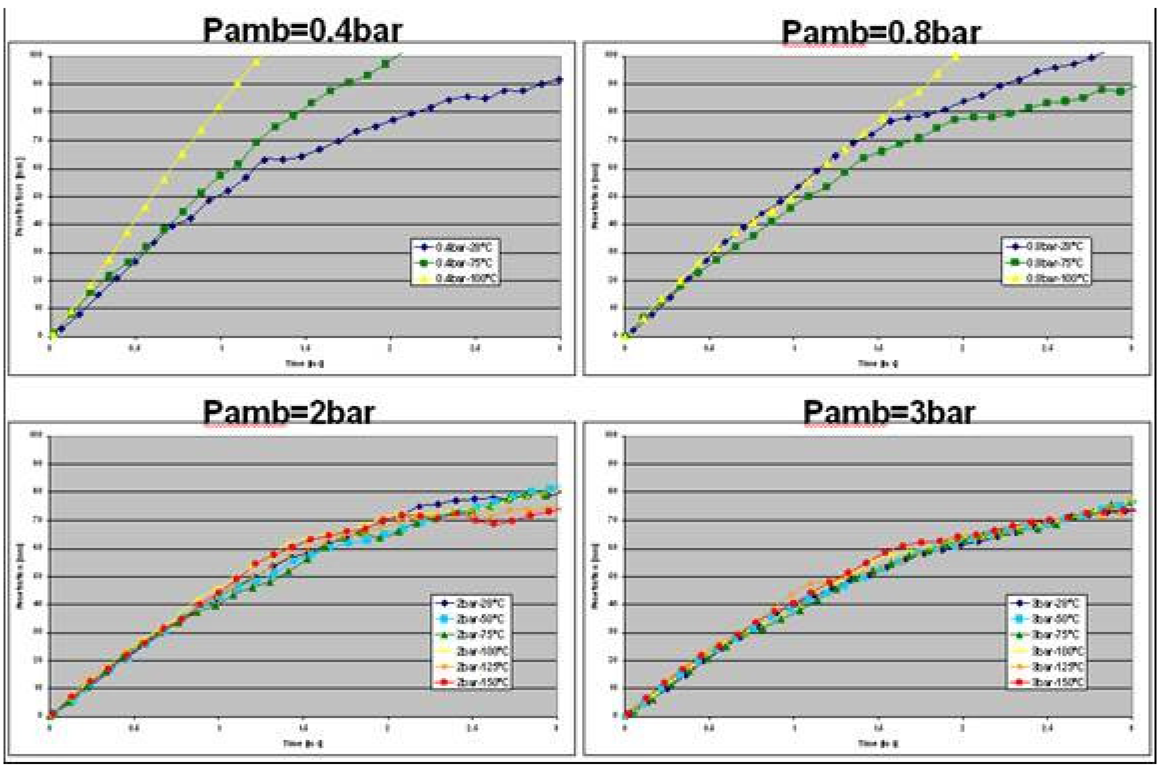

Figure 8: Effects of ambient temperature and pressure on spray penetration (#2)

These experimental results were useful and will be used to validate spray submodels, which include atomization, vaporization, mixing, and multi-component effects. This is a great challenge to be overcome, in order to successfully predict the engine mixing and combustion performance.

Simulation correlation based on new experimental data

The initial comparison of spray simulation model results, from Phase 1, with experimental data from the variable temperature and pressure tests shows appreciable directional sensitivity in the spray analyses. Out of the six holes in the injector, holes number 1 and 2 always produce higher penetrations than the other four. This phenomenon is repeatable but does not have any physical basis since, contrary to spray experiments, the directional effect from different internal flow paths are not included in our secondary breakup model. This discrepancy is being addressed and will be detailed in future reports.

Phase 2 Task 4.0 –Baseline Definition and Build of Valvetrain and Other Engine Hardware (7/1/08 thru 9/30/08)

2-step valve lift

The project will utilize a Delphi 2-step valve lift system. 2-step is an advanced variable valve actuation technology that changes valve lift, duration and timing when opening and closing intake and/or exhaust valves during engine operation. The Delphi 2-Step Valve Lift System is designed specifically for overhead cam engines that include hydraulic lash adjusters and roller finger followers and works in conjunction with the dual independent cam phasers on this engine.

The Delphi 2 Step valve train hardware utilizes dual roller followers for the low lift cam which offer lower friction at typical driving conditions. The high lift cam is engaged by a locking pin that eliminates the lost motion of the high lift slide. The pin is actuated via a hydraulic circuit controlled by an electronic oil control valve.
The rocker arm incorporates an integral oil jet to provide film lubrication to the slider. The cam shaft consists of a Tri-Lobe cam with symmetric outer lobs that define the low lift profile and a central high lift cam. To allow proper actuation of the 2-step mechanization the low lift cam must be inside of the high lift cam profile thus dictating the relative phasing between cams. Optimized profiles for these cam lobes have been a significant accomplishment during this past quarter.

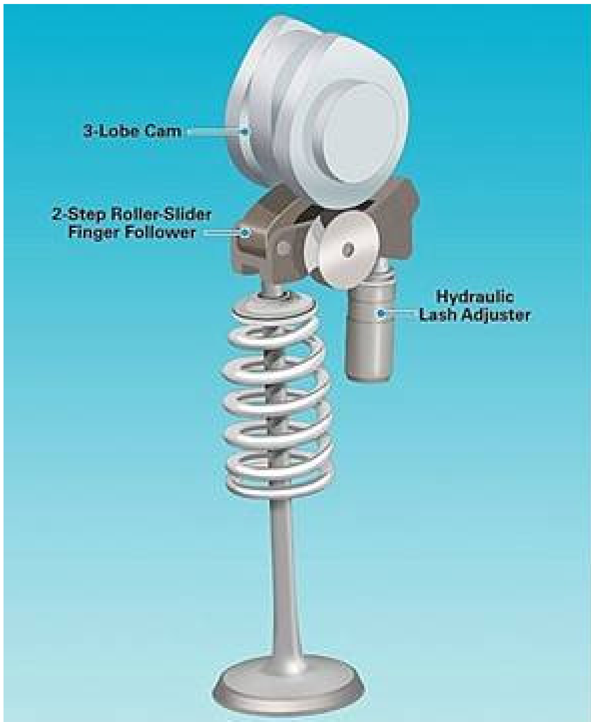

<u>Figure 9:</u> Delphi 2-step Valve Lift System

To fit the two-step valve system on the production cylinder head some machining and modifications was required. The cylinder head that will be used on the optical engine is nearing competition of these modifications and will be available in November. The figure 10 shows the 2-step valve system on the cylinder head.

<u>Figure 10:</u> Delphi 2-step valve system on engine cylinder head

Intake cams

The intake cam profiles were refined to allow efficient load control and stay within limits for maximum stresses and dynamic stability. The low lift cam profile will have a 5.6 mm lift with a 162 cad deg duration (0mm to 0mm). The low lift intake cam is capable of up to 4000 RPM for efficient load control at the majority of real world engine operating conditions. The low lift valve also allows effective CR control during boosted operation to limit knock using an early intake valve closing strategy.

The long duration high lift cam has a 10.2 mm lift with a 320 cad deg duration (0mm to 0mm). The long duration cam is capable of maximum engine speed, (6300 RPM) and provides effective compression ratio control using a late intake valve closing strategy

The initial acceleration ramps of the two profiles are planned to be commonized to reduce friction by using rollers during initial high acceleration. A friction and stack up analysis is in process to estimate the potential for reduced friction and to estimate adverse effects of a discontinuity in the cam profiles due to manufacturing tolerances on the final grind.
A targeted completion date of mid November is anticipated for the 2 step intake cams.

Figure 11 shows the valve lift profiles that were selected. The profiles will be aligned at the intake valve opening ramp. The shown profiles are prior to the modification for the common ramp profile.

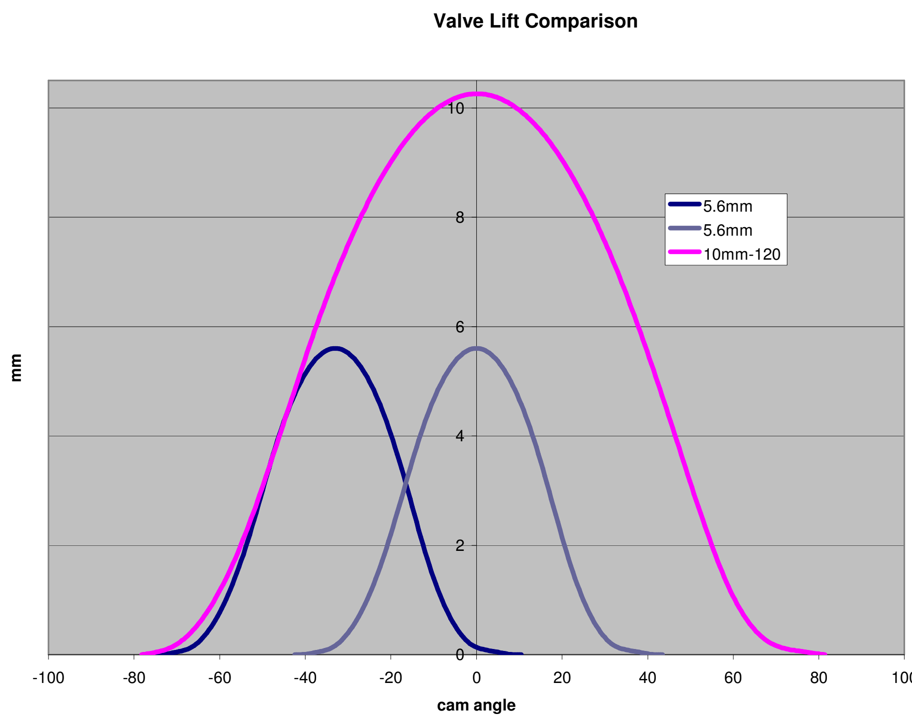

Figure 11: Intake valve lift profiles for 2-step tri-lobe cam

Exhaust cams

The exhaust cams will retain the profile from the production engine, analysis of alternative exhaust cam profiles and durations did not show any benefits.

Valve clearances

Figure 12 shows the allowable phasing as a function of TDC Valve clearance. Based on the phasing required from the GT power simulation this constraint was used in the piston design when trying to maximize the compression ratio. An additional 2 mm clearance above the interference limit was allowed for tolerance stack up and to allow additional phasing if combustion stability is sufficient. The intake clearance is currently 7mm while the exhaust clearance is 5mm.

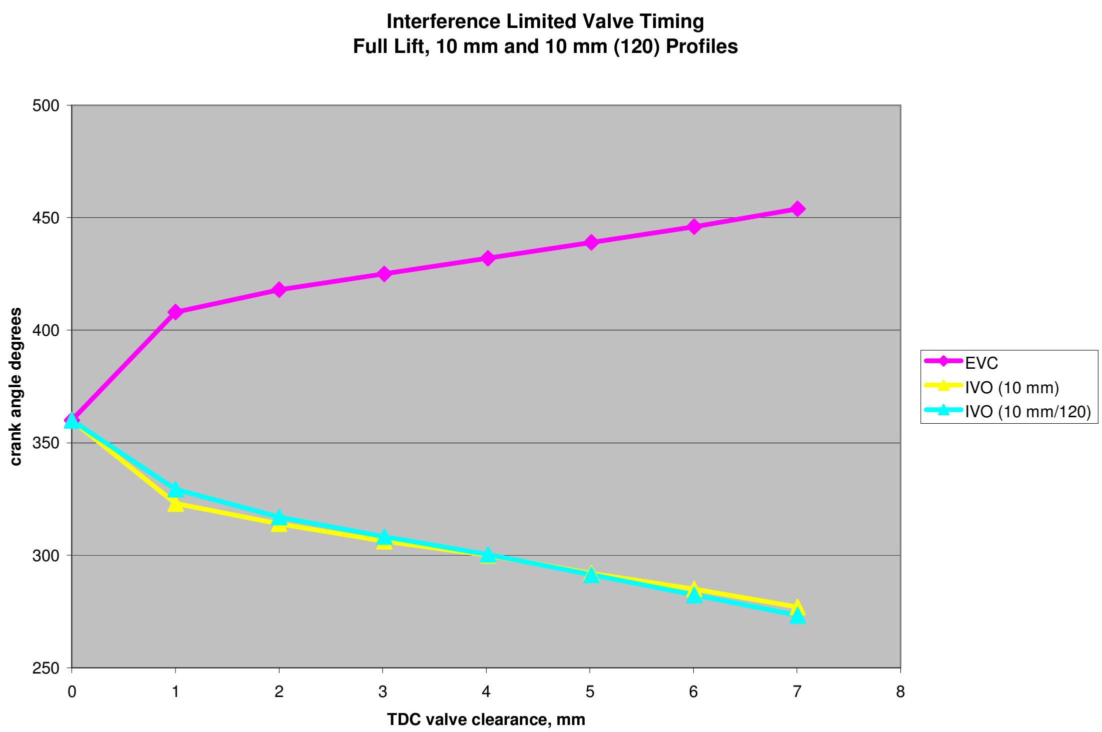

<u>Figure 12:</u> Allowable phasing as a function of TDC Valve clearance

<u>Cam Phasers</u>

Modified versions of Delphi's hydraulic cam phasers were built to increase the phasing authority to 80 degree for the intake. The new phasers are to be completed in early November 2008. The exhaust will retain the production cam phaser with 50 degrees of authority.

<u>Piston</u>

The piston design to increased compression ratio was further refined. The current design (Version 2.3) is completed with reduced surface to volume area to minimize hot spots/ heat transfer. Radii were also eased to reduce deposit formation and simplify machining. Version 2.3 has a geometric compression ratio of 11.85 with 2 mm valve clearance. Based on initial testing to identify knock tolerance, dilution tolerance and maximum pressure limitations additional pistons can be designed. The current squish region, which is small has a squish height of 2 mm. A small, (+0.5CR), increase in geometric compression ratio is possible by reducing the squish height to 1-1.5 mm and valve clearances below 2 mm if the dilution tolerance does not allow earlier intake cam phasing.

The piston includes an integral piston bowl feature to allow mild stratification and net lean cold starts for reduced emissions.

Piston blanks were received in September. A set of pistons including a piston crown geometry blank for spray chamber testing are being built with expected competition in November 2008.

Quarter 4 2008

Phase 2 Task 2.0 –Baseline Definition / Evaluation of Prototype Flex-Fuel Injectors (10/1/08 thru 12/31/08)

Injector spray targeting has been prescribed. The injectors were targeted to avoid the valves and to minimize wall wetting. Additionally the interaction with the piston bowl was a key consideration for injector targeting as well as piston bowl design. While this relationship is not critical to the steady state operation as proposed in this project it does become extremely important under real world light stratified operation to reduce cold start emissions.

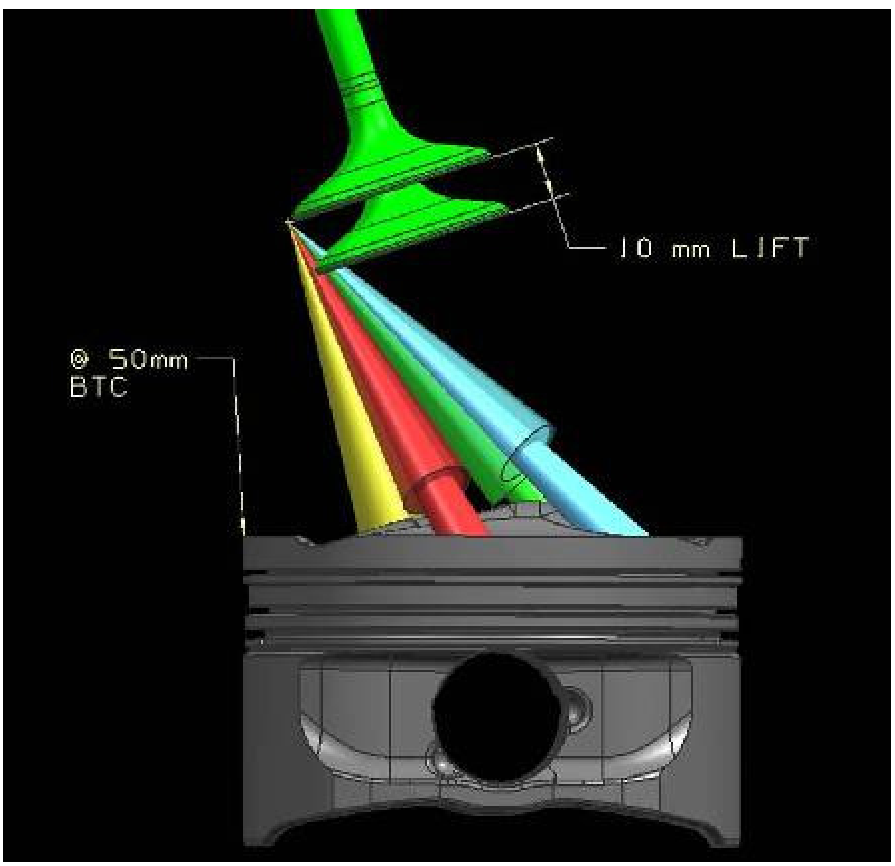

Figure1: Injector targeting to avoid wall wetting

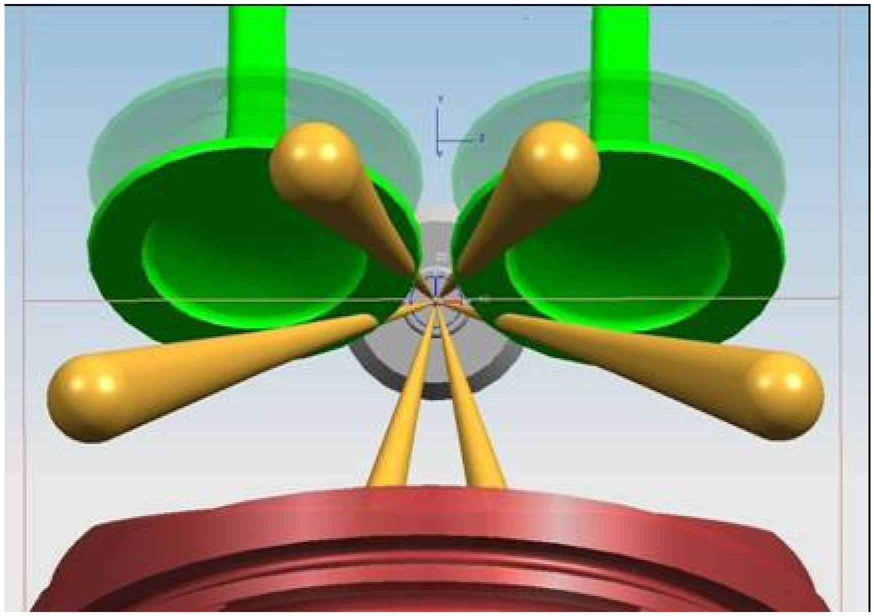

Figure 2: Injector targeting to avoid valves

The injector seat design was then completed. The seat design is the primary control factor for injector targeting. Ethanol compatible injector samples were then completed at Delphi's Technical Center Rochester.

Figure 3: E85 injector for optimization project

Injectors for Phase3 Task1.0 were characterized using laser diffraction, hex cell, image analysis and flow.

DELPHI **Laser Diffraction Drop Size Measurement Summary**

Test Description: Char Delphi Bravo V2 GDi inj's(J79) for GMPT Ecotec

EWO#	PU927M90	Part No.:	28197532A		Fuel Type:	n-Heptane	
Date:	17-Nov-08	Driver Type:	DI Scheme_B2110350.S		Fuel Pressure:	10,000	kPa
Requester:	J.Brosseau	Pulse Flow:	~15	mg/pulse	Injector Height:	50	mm
Operator:	C.Ospina	Pulse Period:	50	ms	Laser Beam Diam:	13	mm

Note: All drop diameters are in microns

Inj Description										
Inj P/N	**Dir P/N**	**Inj S/N**	**PW (ms)**	**# of Tests**		DV10	DV50	**DV90**	D43	**D32**
28197532A	28194723A	J79-01	1.5	10	Average	7	15	**24**	16	**12**
					Std.Dev.	*0.1*	*0.1*	*0.1*	*0.1*	*0.1*
		J79-05			Average	7	15	**25**	16	**12**
					Std.Dev.	*0.1*	*0.1*	*0.1*	*0.1*	*0.1*

	DV10	DV50	**DV90**	D43	**D32**
Overall Average	7	15	**25**	16	**12**
Max	7	15	25	16	12
Min	7	15	24	16	12
Range	0	0	1	0	0

Figure 4: Laser diffraction data summary

Test Description

EWO # : PU27M90
Date : 11/13/2008
Requester : Justin Brosseau
Operator : Fritz Brado
Part # : DI_BRAVOV2_28197532A
Serial # : J79-05
Fuel Type : N-HEPTANE
Injector Driver Type : DI_Bravo2_B2110350.S
Part Descriptor : GDi_Bravo V2_GMPT_Ecotec

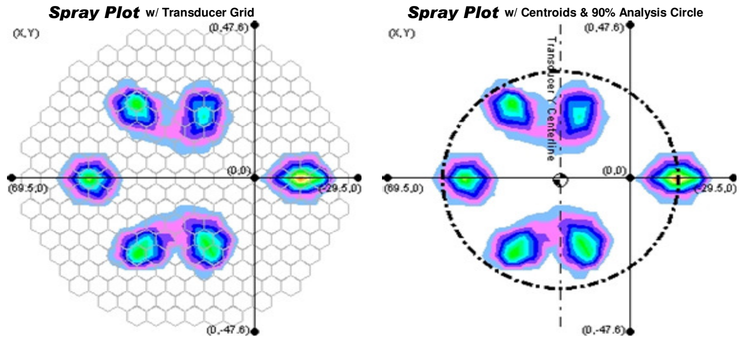

Spray Parameters

Injector Height : 50 mm
Connector Angle (θ) : 0°
Fuel Pressure : 10000 kPa
Pulse Width / Period : 1.5 / 40.0 ms
# of Pulses : 438
Captured Volume : 10.7 ml
Diameter : 67.6 mm @ 90%
Cone Angle α : 64.2° @ 90%
50% Mass Diameter : 49.9 mm
50% Cone Angle : 49.6°
Bend (Skew) Angle (β) : 22.0°
Centroid Location (x,y)* : (20.2 mm, -0.4 mm)
Centroid Location (r,θ)* : (20.2 mm, 358.8°)

Cone Angle (α) vs. Mass %

Mass%	α
60	52.4
70	55.3
80	59.0
90	64.2
96	69.3

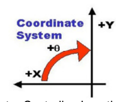

*Injector Centerline Location

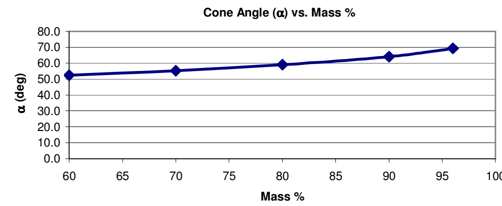

% Transducer Volume		
0.0	to	6.3
6.3	to	12.5
12.5	to	18.8
18.8	to	25.0
25.0	to	31.3
31.3	to	37.5
37.5	to	43.8
43.8	to	50.0
50.0	to	56.3
56.3	to	62.5
62.5	to	68.8
68.8	to	75.0
75.0	to	81.3
81.3	to	87.5
87.5	to	93.8
93.8	to	100.0

Figure 5: Hex cell test data summary

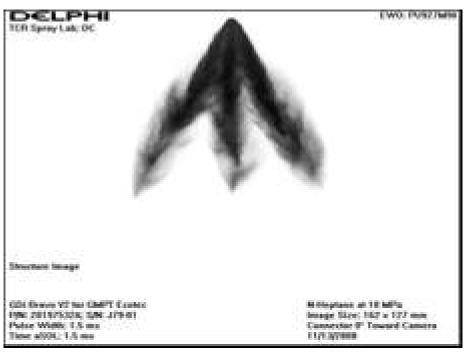

	Penetration (mm)	Spray Angle (°)	Bend Angle (°)
Average	67	59	1
StdDev	2.4	1.7	0.8
Max	73	62	3
Min	63	55	0

Note: Analysis based on SAE standard J2715; Statistics from 30 Images.

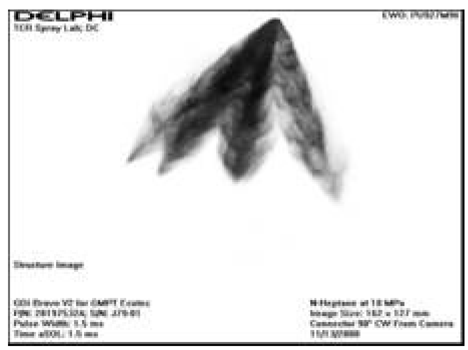

	Penetration (mm)	Spray Angle (°)	Bend Angle (°)
Average	68	70	13
StdDev	2.4	1.8	1.1
Max	75	76	15
Min	64	67	10

Note: Analysis based on SAE standard J2715; Statistics from 30 Images.

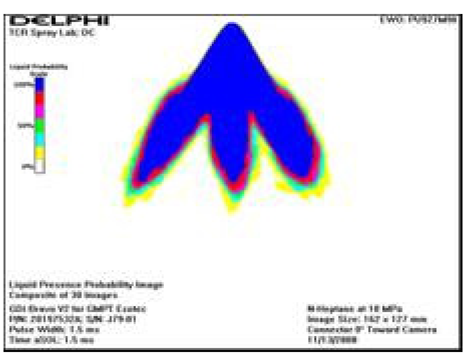

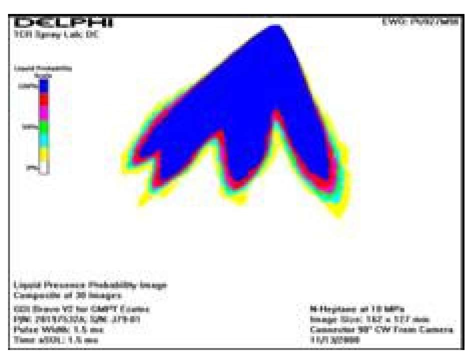

Figure 6: Image analysis data summary

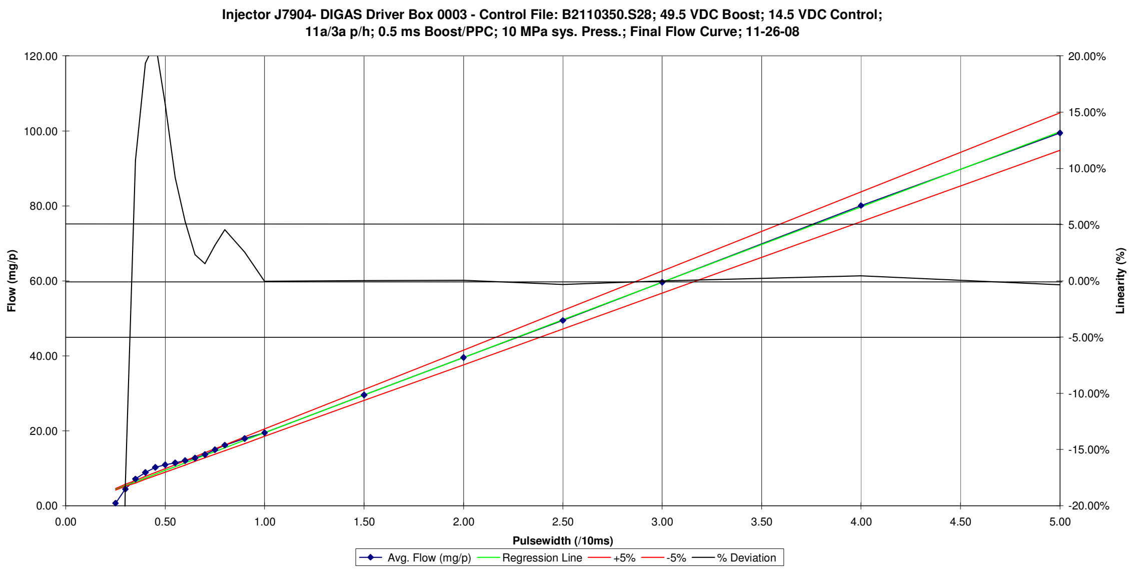

Figure 7: *Flow curve spray characterization data*

These injectors will be used in the Wayne State spray chamber to not only characterize the spray at various pressure and temperature but also to analysis the interaction of the spray with the piston bowl.

The injector drive signal will also be optimized during the course of the project in order to extend the operational range.

Phase 2 Task 3.0 –Test Chamber Construction (10/1/08 thru 12/31/08)

During the course of this task the design of the spray chamber has been modified to achieve the following objectives:

- Chamber pressure from 0.3 (partial vacuum) up to 4 bar or higher,
- Chamber air temperature up to 200^{o}C or higher,
- Direct Spray visualization with side- or back-lighting,
- Schlieren spray visualization of both liquid and gaseous phases
- Phase Doppler Interferometry measurement at 135^{o} forward scattering angle,
- 2-D traversing stand for

- Temperature-controlled Injector holder to decouple fuel temperature from chamber temperature.
- Extension for future spray-wall interaction investigation for piston and cylinder surfaces

During the fourth quarter, the temperature control capabilities were further improved. Insulation was improved to raise the maximum temperature capability. A new isolated fuel injector fixture was also made to improve injector tip temperature control.

Further tests were run during Q4 to try out these new capabilities in preparation for Phase III. All tests were run with a production 6-hole nozzle direct injection gasoline injector.

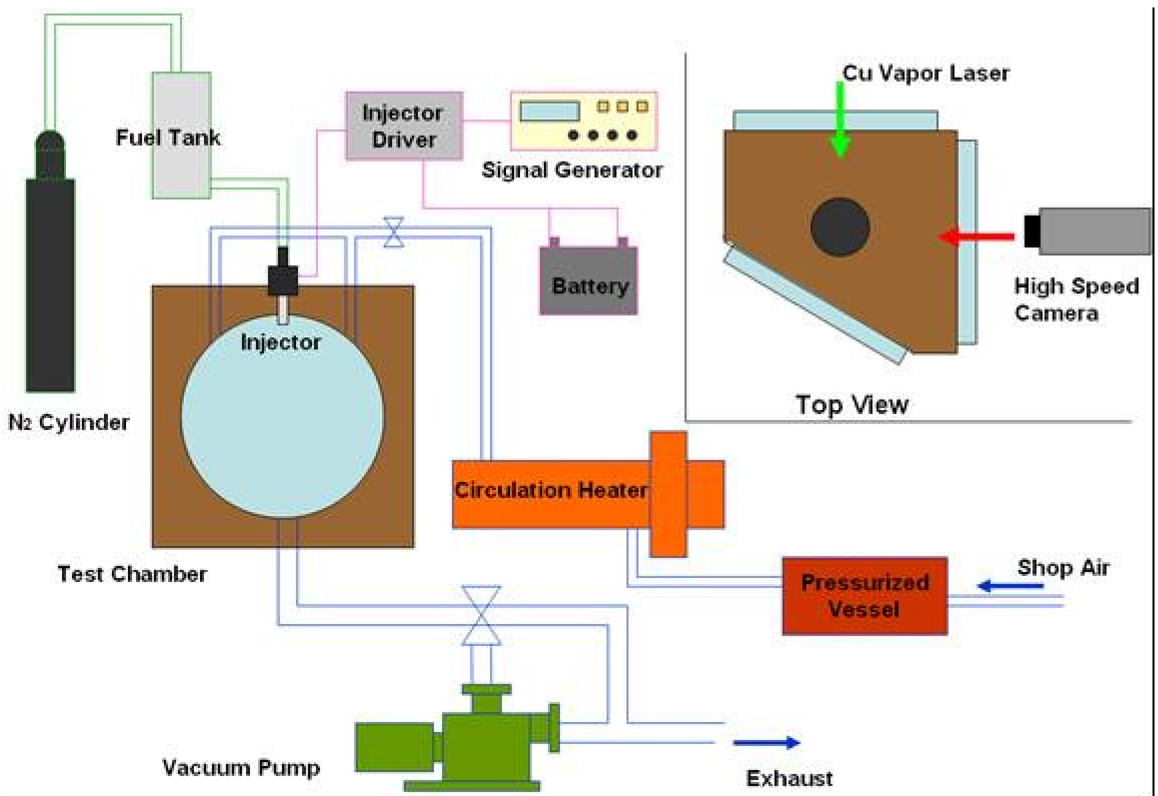

Figure 8: Test chamber layout spray-visualization with the PDI chamber

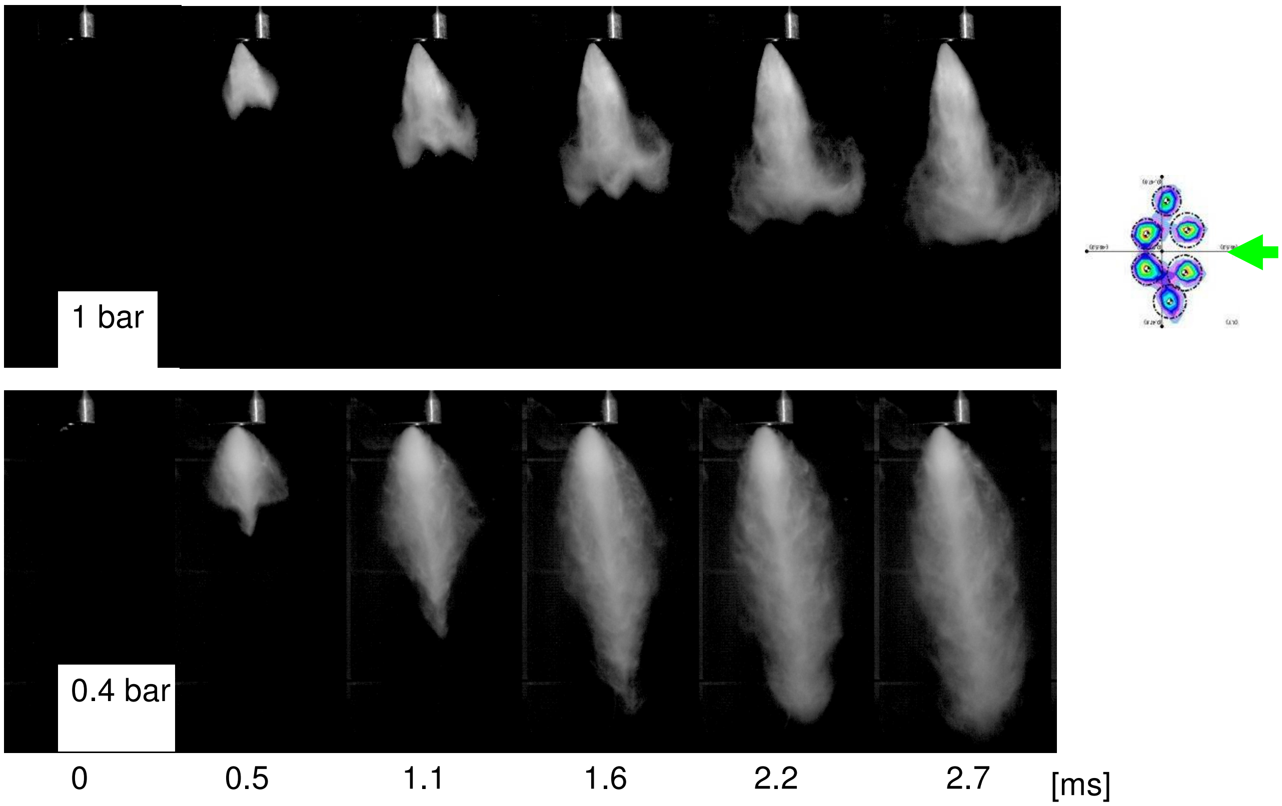

<u>Figure 9a</u>: Spray characterization – effect of ambient pressure on spray structure and penetration

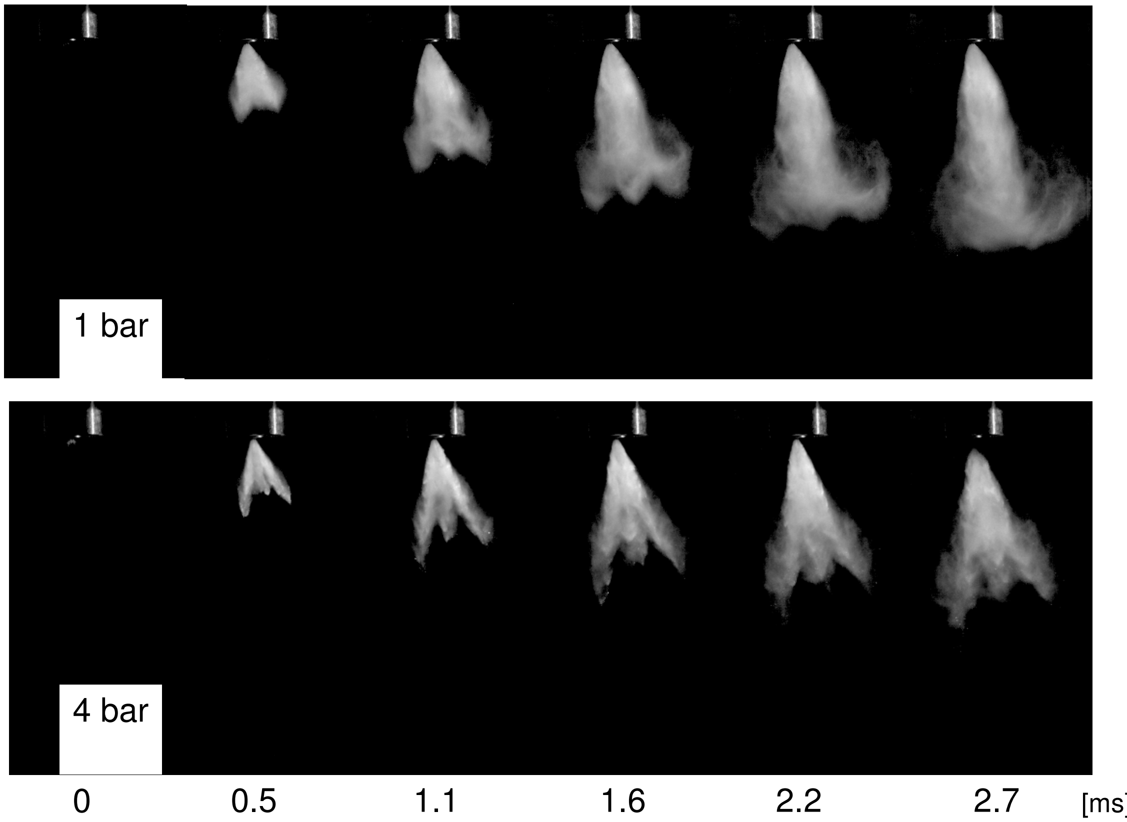

Figure 9b: Spray characterization – effect of ambient pressure on spray structure and penetration

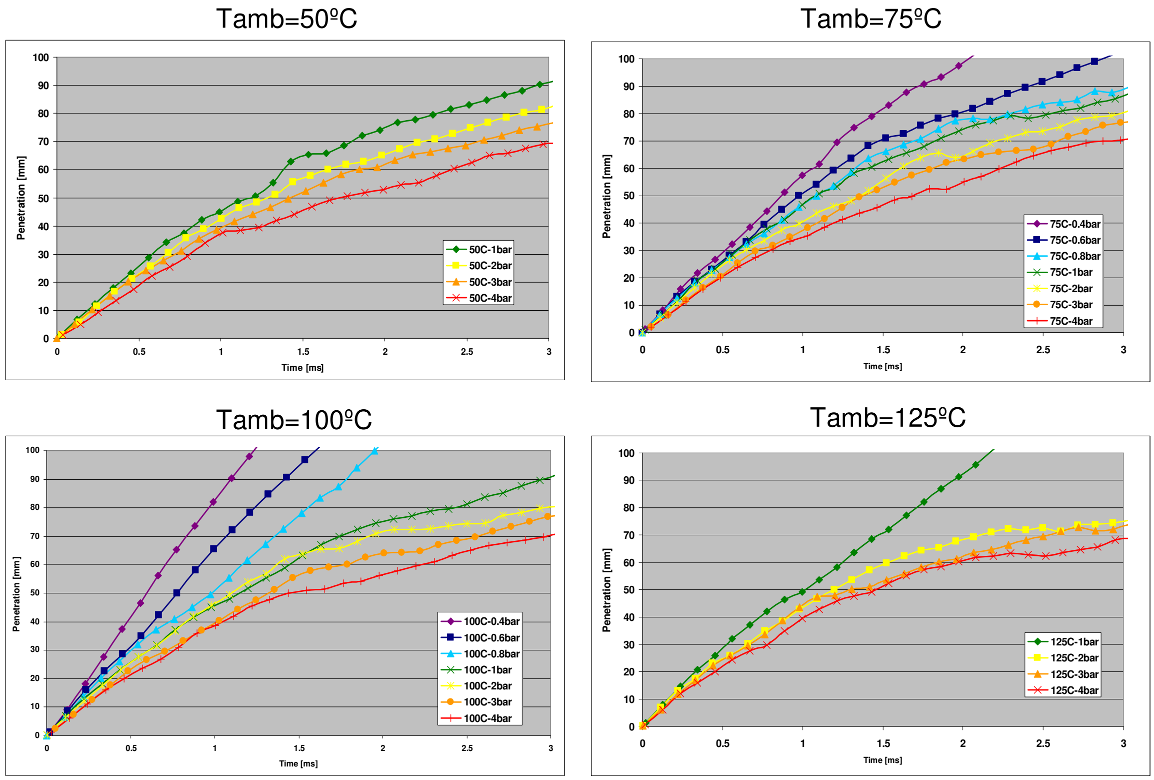

<u>Figure 10</u>: Spray characterization – effect of ambient temperature on spray penetration

<u>Phase 2 Task 4.0</u> –Baseline Definition and Build of Valvetrain and Other Engine Hardware (10/1/08 thru 12/31/08)

<u>2-step valve lift</u>

The project will utilize a Delphi 2-step valve lift system. 2-step is an advanced variable valve actuation technology that changes valve lift, duration and timing when opening and closing intake and/or exhaust valves during engine operation. The Delphi 2-Step Valve Lift System is designed specifically for overhead cam engines that include hydraulic lash adjusters and roller finger followers and works in conjunction with the dual independent cam phasers on this engine.

The Delphi 2 Step valve train hardware utilizes dual roller followers for the low lift cam which offer lower friction at typical driving conditions. The high lift cam is engaged by a locking pin that eliminates the lost motion of the high lift slide. The pin is actuated via a hydraulic circuit controlled by an electronic oil control valve. The rocker arm incorporates an integral oil jet to provide film lubrication to the slider. The cam shaft consists of a Tri-Lobe cam with symmetric outer lobs that define the low lift profile and a central high lift cam. To allow proper actuation of the 2-step mechanization the low lift cam must be inside of the high lift cam profile thus dictating the relative phasing between cams.

<u>Figure 11:</u> Delphi dual roller for the optimized E85 project

The cylinder head that will be used on the optical engine is completed. Fixed cams and manual phasing will be used for the work on this engine in place of 2step valvetrain and cam phasers. These fixed cams will be used to verify the analytical cam optimization that was done in this task during Q3 of 2008.

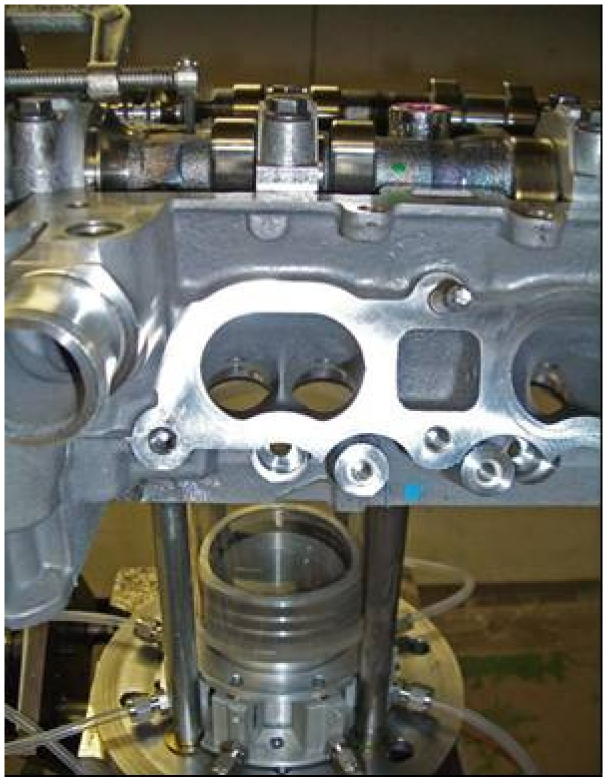

Figure 12: Optical engine at WSU lab with 2.0L LNF head

Intake cams

The intake cam profiles were refined to allow efficient load control and stay within limits for maximum stresses and dynamic stability in this task during Q3. The profiles were then used to design the cam shafts. Long lead times at the cam shaft supplier have delayed completion of this task until Q1 2009. This delay is not expected to cause significant overall project delays of upcoming tasks.

Exhaust cams

The exhaust cams will retain the profile from the production engine, analysis of alternative exhaust cam profiles and durations did not show any benefits.

Cam Phasers

Modified versions of Delphi's hydraulic cam phasers were built to increase the phasing authority to 80 degree for the intake. The required authority was defined using GT Power simulation to meet load control window for throttle-less control above 2 Bar BMEP. The exhaust will retain the production cam phaser with 50 degrees of authority.

Figure 13: Delphi increased authority cam phaser for optimized E85 project

Piston

The new pistons for the project have a compression ratio of 11.85 with 2 mm valve clearance. This piston was designed based on initial testing to identify knock tolerance, dilution tolerance and maximum pressure limitations. Extra pistons blanks were obtained which allows additional pistons to be machined if further optimization is required. The current squish region has a height of 2 mm. A small, (+0.5CR), increase in geometric compression ratio is possible by reducing the squish height to 1-1.5 mm and valve clearances below 2 mm if the dilution tolerance does not allow earlier intake cam phasing.

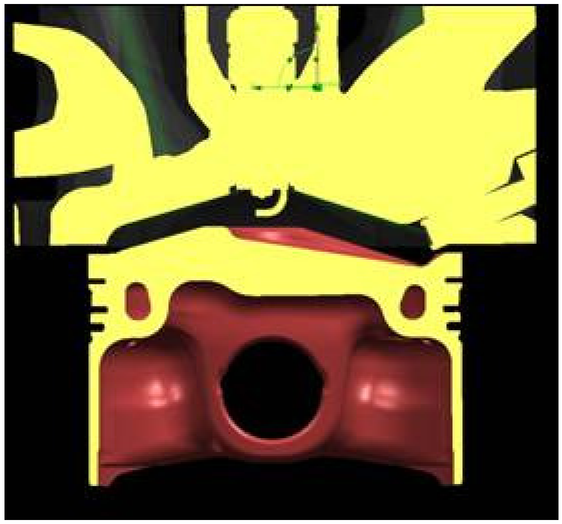

<u>Figure 14:</u> Cross section of combustion chamber at TDB with E85 piston

The piston design includes an integral piston bowl feature to allow mild stratification and net lean cold starts for reduced emissions. While cold start is not within the scope of this project the pistons were designed to take this feature into count and could be used for future development in this area.

Piston blanks were received in September. A new set of pistons, which represent the E85 optimized design, were machined from these blanks during this quarter. A piston blank was also machined for spray chamber testing at Wayne State University.

<u>Figure 15:</u> Piston designed for the E85 optimized project

Quarter 1 2009

Phase 3 Task 1.0 –Injector Optimization under Simulated Engine Conditions (1/1/09 thru 2/28/09)

The chamber developed in Phase II Task 1 will be employed to further optimize the prototype flex-fuel injector designs under highly controlled simulated engine conditions. Spray characteristics for the injector designs identified in Phase II will be established at a matrix of chamber temperatures and pressures as well as with E0, E50 & E85 blends. Refined designs to be used for final selection of Phase IV test hardware.

Spray Characterization

For this report period, high-speed spray visualization was used to characterize the spray structure of the six-hole DI injectors. The experiment was performed for 3 injectors. Injector A is the OEM injector for our test engine and therefore is also referred to as “baseline” injector. Two other new project specific injectors were used as comparison and are summarized in Table 1.

Table 1 Specifications of injectors

	Injector A	Injector B	Injector C
Hole Diameter [mm]	0.23	0.263	0.104
Hole Length [mm]	0.31	0.3	0.23
L/D	1.36	1.14	2.21
Number of holes	6	6	6
Static mass flow with N-Heptane [g/s]	15.9	20.5	4.00

The spray chamber is capable of

- *Chamber pressure from 0.4 (partial vacuum) up to 4 bar,*
- *Chamber air temperature up to 250^{o}C or higher,*
- *Fuel temperature from 10C up to 100C*
- *Direct spray visualization with side- or back-lighting,*
- *Schlieren spray visualization of both liquid and gaseous phases*

Free Spray Testing

Direct spray visualization utilizing bulk lighting was employed for the baseline injector only. Since the fuel temperature was not controlled during the direct visualization testing, it is assumed to be the same as the chamber temperature. The Schlieren testing conditions however were selected based on the realistic engine operating condition. During the Schlieren testing, the fuel temperature was fixed at either 90C or 25C. Only Schlieren testing was performed for the injector B and C. For all the free spray testing, the injection duration was set to 1.5ms.

Some examples of images are shown in Table 2 and 3. First, the individual plume was investigated and the results show that the penetrations of the spray which has more streamline curvature due to the in-sac fluid dynamics are slower. And it is obvious that the plume of larger L/D develops faster and thinner. By the Schlieren visualization, slower evaporation from “inner” surfaces of the sprays, which is the surfaces contact with the air trapped inside the cage of sprays, was observed. Below the boiling temperature, the degree of vaporization increases with ambient temperature due to enhancement in heat and mass transfer. Above the boiling temperature, “Flash Boiling” phenomena could collapse the multiple-hole sprays into a coherent spray with enhanced penetration and mixing, with a resultant spray structure resembling that of the air-assisted DI spray. The complexity of the flash boiling in spray is that it is a function not only of ambient temperature and pressure, but of fuel temperature and pressure, and a combination of other effects, including injector design, cavitation, in addition to other multiple-component effects.

<u>Table 2.</u> Injector A, (T=150C P=1bar)

	Side-lighting Pinj=5MPa	Schlieren Pinj=5MPa	Schlieren Pinj=10MPa
0.5ms ASOI	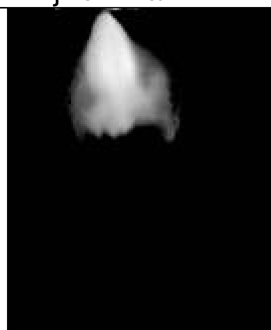		
1.5ms ASOI			

<u>Table 3.</u> Schlieren (T=200C P=3bar Pinj=10MPa Mass=5mg)

	Injector B	Injector C
EOI	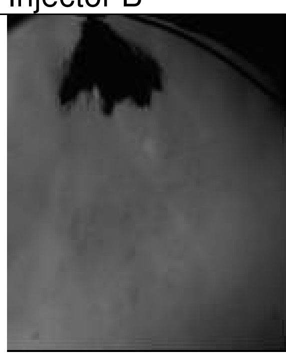 0.3ms ASOI	 1.3ms ASOI

0.5ms AEOI		

<u>Piston Impingement Testing</u>

Piston impingement testing was carried out for simulating the realistic in-cylinder spray behavior during stratified operating conditions. The injector and the piston was mounted in the pressurized chamber so that the relative position of the injector and the piston is the same as the real engine, a GM 2.0L ECOTEC Turbo. The piston can be moved from the TDC position to 20 mm down from TDC along the cylindrical axis. The moving piston surface allows observe of the effect of spray timing. The baseline injector A utilized the “baseline” piston, and the injectors B and C were tested with the prototype piston which was specially designed for the prototype injector. The comparison of the piston designs is shown in Fig. 1. For piston impingement testing, the injection duration was varied from 0.3 to 1.5ms.

<u>Fig. 1</u> Picture of pistons for Injector A (Right) and Injector B and C (Left)

It was generally observed that the fuel stuck and stayed on the piston bowl causing piston wetting when the piston surface was cool (*Figure 2*). However, as the piston surface temperature increased, the fuel in the spray tip could bounce along with the curvature of the piston bowl and form a bunch of droplet bullets or a splash (*Table 4*). These bounces have massive momentum and will travel across the combustion chamber until they hit the roof. In order to avoid this effect, spray targeting, geometry of the piston bowl, and the operating conditions such as the injection timing and pressure must be determined comprehensively.

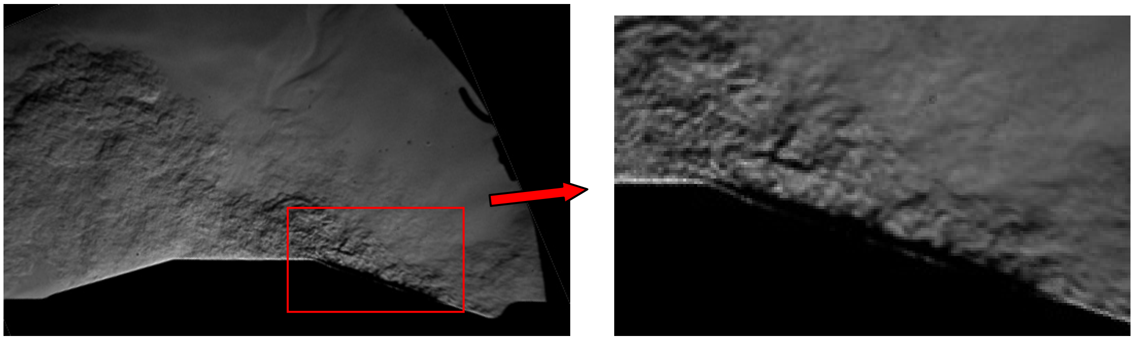

Fig. 2. Piston impingement, Injector B, 15mm, 10ms ASOI (T=100C P=3bar Duration=0.5ms). Injector is on the right side, next to the thermocouple.

Table 4. Piston impingement (T=200C P=3bar Duration=0.5ms)

	Injector A, TDC	Injector C, 15mm
2ms ASOI		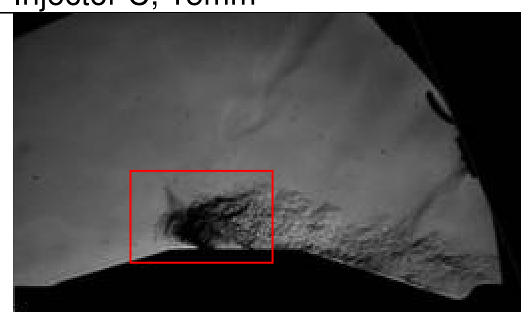
Zoom		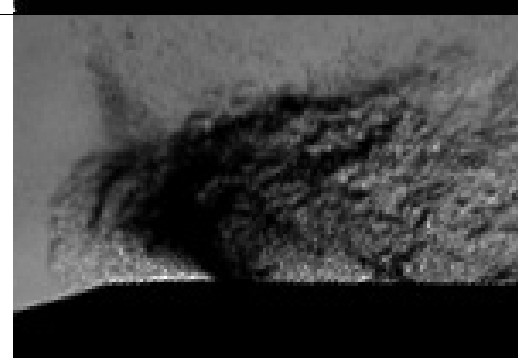

Sprays were evaluated in several studies to evaluate the importance of injector design, operating conditions, injector driver settings and the injection interaction with the piston. Schleiren imaging was used to observe the vapor formation progression in addition to the liquid spray penetration characteristics. To improve the visualization resolution for this initial segment of the work E100 was used as a surrogate fuel. This provides higher evaporative cooling to provide higher contrast. In addition it proved to be a clean fuel that did not promote film or deposit formation on the optical apparatus.

Stratified Spray Piston interaction.

The interaction of the piston geometry, spray quantity and piston location was evaluated. It is desirable to provide a slightly rich equivalence ratio in the spark plug gap at the time of injection. By varying the injection timing the relative piston position and the confinement bowl are changed relative to the spray. The increased temperature and pressure are also beneficial for reduced penetration and vaporization of the fuel. The decreased distance to the piston surface offsets the advantage in the spray behavior and careful design of the injection spray interacting with the piston is necessary to develop a robust wall guided combustion system to support stratified operation. The images in *Figure 3* show injector B at room temperature conditions characteristic of early injection, (top images) and elevated temperature conditions to simulate late injection, (lower images). The elevated temperatures promote fuel vaporization, although the basic spray structure is similar. The image at 2 ms is typical of the delay necessary to provide stratified operation for the late injection case. Of interest is the images 20 ms after injection. Spray impingement that is not confined within the piston bowl redirects the spray tangent to the impinging surface and directs it outward to the cylinder bowl. Impingement of fuel droplets on the optical chamber is apparent in the later image for both early and late simulated injection cases. Thus refinements of the piston bowl and spray geometry to confine the droplets is desirable to minimize wall wetting and its detrimental effects on oil dilution. Also of interest is the area of vaporization that continues long after the initial injection within the piston bowl. This will contribute to reduced charge density and increased HC and particulate emissions due to diffusion flames from pool fires on the piston. These attributes of the spray images are noted below.

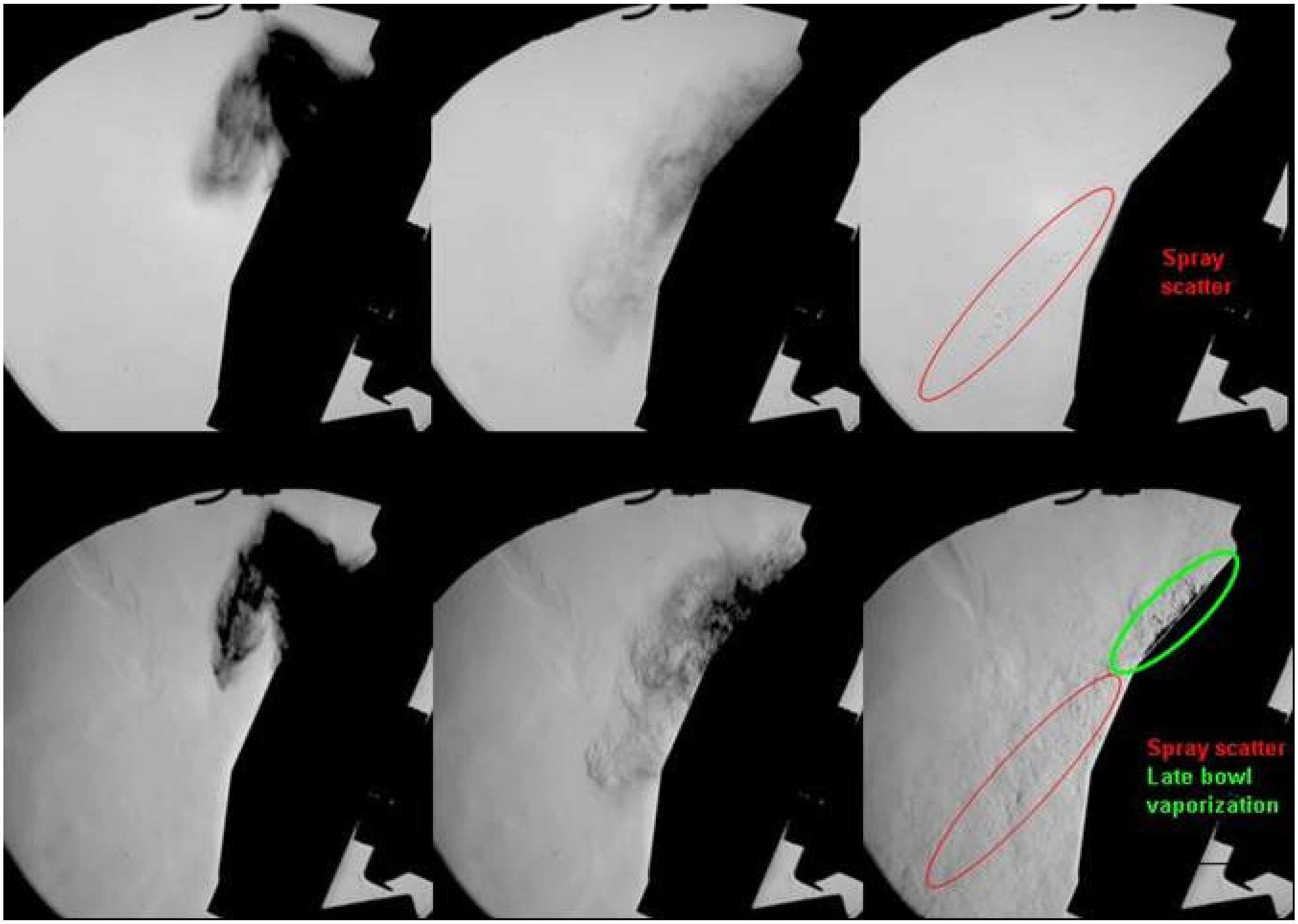

1 ms 2 ms 20 ms

12 mg pulse width, 0.5 milliseconds, Fuel E100, Tf 25 C, Pf 100 Bar Injector B
Top images 25 C, 1 Bar
Lower images 100 C, 3.2 Bar
Figure 3 Spray images showing piston 15 mm below TDC

Spray Targeting Refinement

The targeting of the designed injectors was evaluated to identify the accuracy of individual spray beam targeting. The initial injector (Injector B) showed a wider spray pattern and considerable deviation from target for one of the sprays. This spray resulted in liquid impingement outside of the piston bowl which was then directed outwards toward the cylinder bore and produced liquid impingement on the bore during simulated stratified sprays. The same phenomena would also exist during early injections on the intake stroke and would likely contribute to lube oil degradation.

One of the spray beams deviated significantly from the intended targeting and would result in impingement of the spark plug. This is undesirable since impingement may increase the tendency for spark plug fouling with gasoline blends (*see Figure 4*).

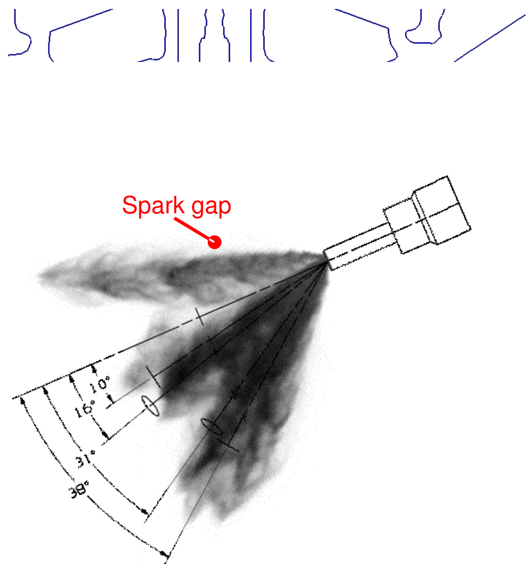

Figure 4. Injector B spray geometry

The deviated spray beam also compromised the ability to provide a stratified charge centered on the spark plug but instead carried the vapor cloud to the exhaust valve side of the combustion chamber see *Figure 5.*

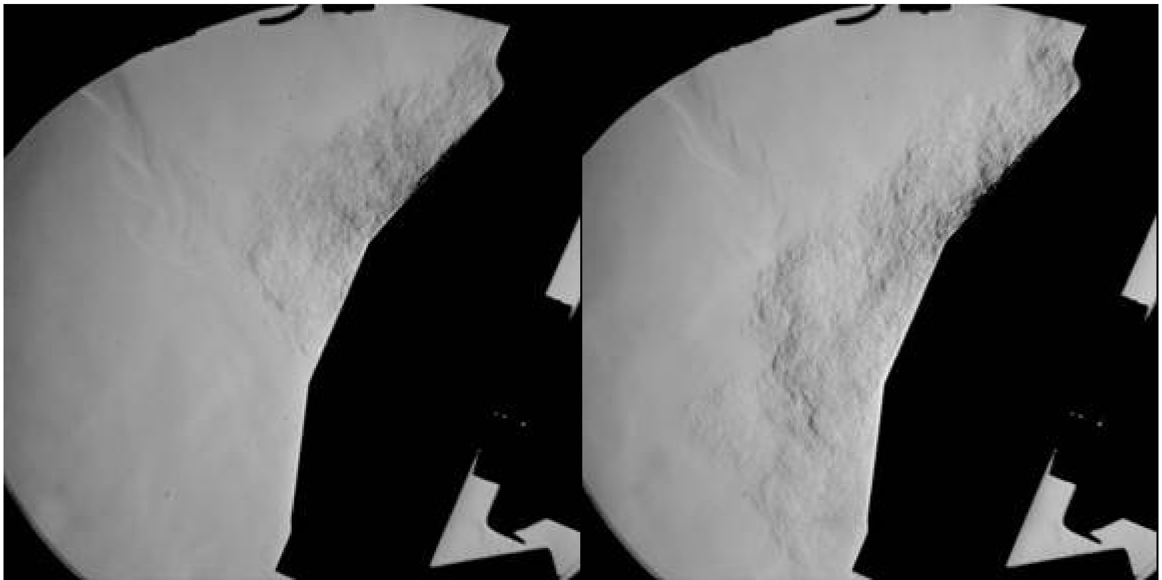

0.3 ms PW 5 mg **0.5 ms PW 12 mg**

***Figure 5* Vapor penetration at 5 ms**

To confirm targeting, additional injectors were evaluated with targeting closer to the intended spray pattern. Injectors with revised targeting were built for this purpose. The new injectors, Beta, also support operation at higher injection pressures and allowed the maximum flow rate specification to be based on 20 MPa vs. 15MPa peak injection pressure allowing for smaller orifice diameters which will provide better atomization. The revised injectors are still in the refinement stage, the spray targeting data is shown in *Figure 6*.

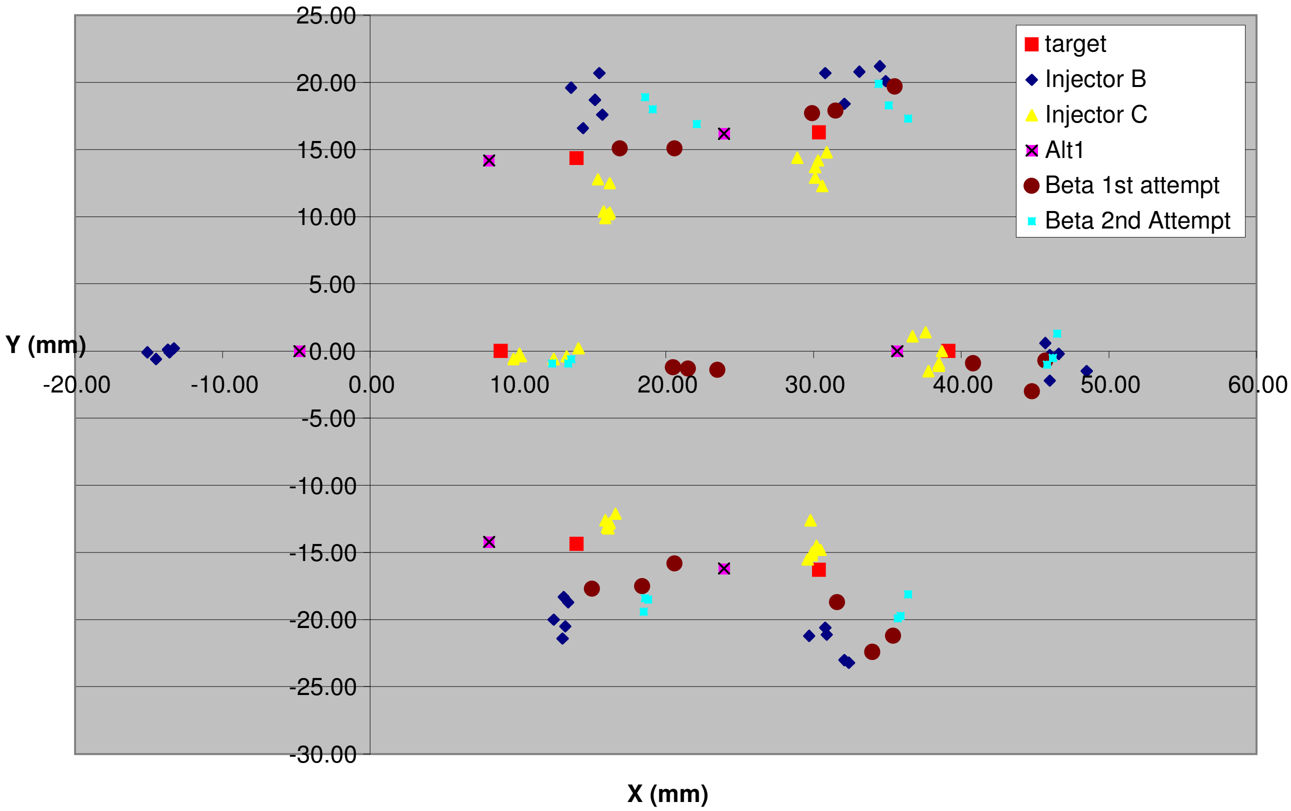

Figure 6 Spray pattern targeting refinement

Influence of Injection Duration on Penetration and Vapor Formation

During testing the spray penetration and vapor formation was significantly dependant on the injection duration. An experiment was conducted in a free chamber without the piston, to quantify the impact of injection duration and spray quantity on the penetration of the liquid core as well as the leading and trailing edges of the vapor plume. Two different injectors, Injector B and Injector C, were used for the evaluation. The injectors were chosen since they had significantly different fuel delivery rates as a function of injection duration. The flow rate at equivalent pulse widths was approximately 5 times higher for the Injector B vs. Injector C. Other design changes in the internal nozzle geometry also played a role in the spray behavior. Testing was conducted at both constant injection durations of 300, 400 and 500 microseconds and also equivalent fuel quantities of 5, 10 and 15 mg/pulse.

Evaluating the data at equivalent fuel delivery demonstrated the significant differences in behavior for the 2 injectors. Images are presented showing the spray development for a 5 mg pulse at different times in *Figure 7*. Data analysis approaches to quantify the liquid and vapor penetration profiles is ongoing. The images illustrate how the longer duration injection results in increased penetration of the vapor plume. This information is being utilized to refine the injector design and guide multiple injection strategies to provide better stratification of the vapor charge in the area of the spark plug at the time of ignition.

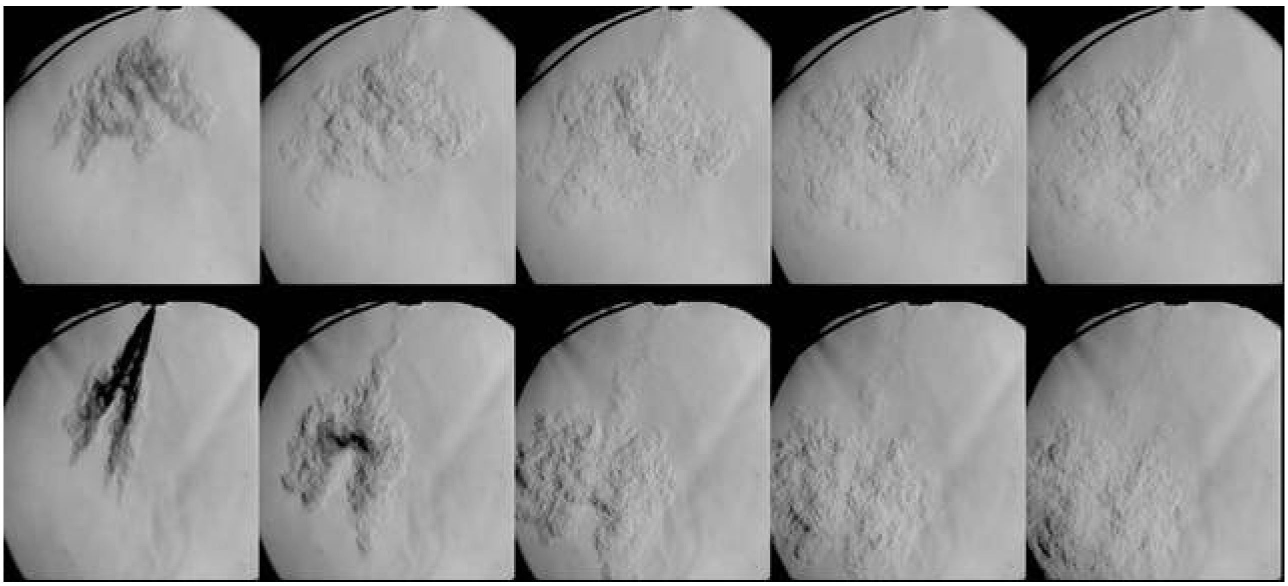

1 ms 2 ms 3 ms 4 ms 5 ms

5 mg pulse width, Tc 210 C, Pc 3.2 Bar pressure, Fuel E100, Tf 60 C, Pf 100 Bar
Top images J79 Injector 0.3 ms Duration
Lower images N01 Injector 1.3 ms Duration

Figure 7 Injector Penetration Comparison

Robust study of spray chamber tests

An important goal of our spray model development is to validate the analytical CFD flow model for conditions that are as close to realistic engine operating conditions as possible. Based on the improved spray chamber capability at Wayne State University, an updated orthogonal test matrix has been designed as part of a robust engineering study for spray optimization.
Table 5) Orthogonal spray test array for CFD validation

	Factors				Factors			
	Engine Operating Condition	Fuel Temp	Injector Design	Fuel Composition	Engine Operating Condition	Fuel Temp	Injector Design	Fuel Compositi on
Run 1	1	1	1	1	P=0.4 bar, T=20 C	25 deg C	736OE	E100
Run 2	1	2	2	2	P=0.4 bar, T=20 C	60 deg C	532A	91-RON
Run 3	1	3	3	3	P=0.4 bar, T=20 C	90 deg C	098A	E50
Run 4	2	1	1	2	P=.4 bar, T=200 C	25 deg C	736OE	91-RON
Run 5	2	2	2	3	P=.4 bar, T=200 C	60 deg C	532A	E50
Run 6	2	3	3	1	P=.4 bar, T=200 C	90 deg C	098A	E100
Run 7	3	1	2	1	P=1 bar, T=200 C	25 deg C	532A	E100
Run 8	3	2	3	2	P=1 bar, T=200 C	60 deg C	098A	91-RON
Run 9	3	3	1	3	P=1 bar, T=200 C	90 deg C	736OE	E50
Run 10	4	1	3	3	P=4 bar, T=20 C	25 deg C	098A	E50
Run 11	4	2	1	1	P=4 bar, T=20 C	60 deg C	736OE	E100
Run 12	4	3	2	2	P=4 bar, T=20 C	90 deg C	532A	91-RON
Run 13	5	1	2	3	P=4 bar, T=200 C	25 deg C	532A	E50
Run 14	5	2	3	1	P=4 bar, T=200 C	60 deg C	098A	E100
Run 15	5	3	1	2	P=4 bar, T=200 C	90 deg C	736OE	91-RON
Run 16	6	1	3	2	P=1 bar, T=20 C	25 deg C	098A	91-RON
Run 17	6	2	1	3	P=1 bar, T=20 C	60 deg C	736OE	E50
Run 18	6	3	2	1	P=1 bar, T=20 C	90 deg C	532A	E100

The L18 test runs are scheduled for April after the multi-pulse tests. Validation of the spray analytical model as well as optimization of injection timing and pulsing strategies will be carried out thereafter based on the test data.

Injector driver waveform studies

One potential way to impact spray quality is through injector driver optimization. Delphi's developmental injector driver box, along with the spray chamber at Wayne State University, are being used to evaluate how the driver waveform might be used to further enhance spray quality. Sprays are evaluated for penetration, spray formation and breakup to evaluate the effects of injector driver parameters. The baseline injector driver profile that has been developed for Delphi's latest generation gasoline direct injectors was used as the starting profile.

Delphi's prototype injector has been tested using Schlieren imaging techniques to see if differences can be detected between different driver profiles. As an example, the images shown in *Figure 8* show the impact of changing boost voltage from 50 V to 65 V at room temperature conditions. The Schleiren images show no appreciable difference at this set of conditions.

300us Pulse Width with 50V Boost

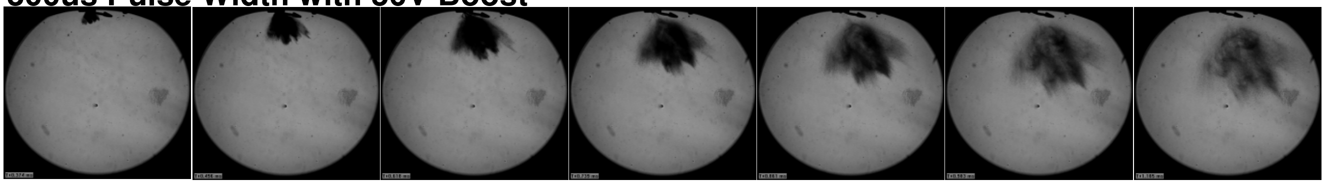

300us Pulse Width with 65V Boost

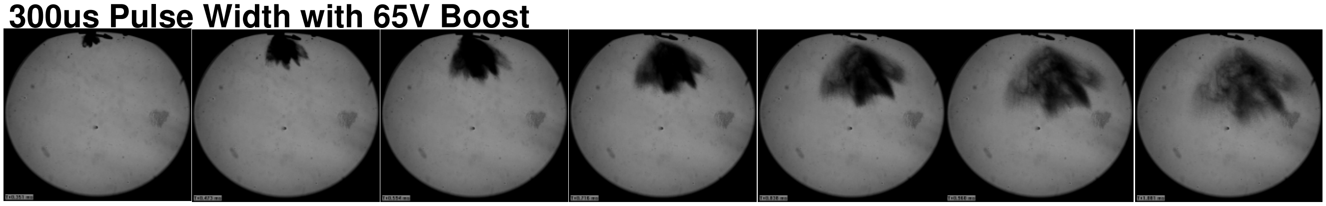

The top row shows time lapsed images with the boost voltage set to 50 V. The bottom row shows time lapsed images with the boost voltage set to 65 V.

Figure 8: Schleiren images of injector spray – 50V Boost vs. 65 V Boost

Future planned work includes testing at higher chamber temperatures and pressures with single injections and multi-pulse injections, as well as assessing potential differences using Laser Mie techniques. The results of these planned evaluations will be used to determine what parameters of the driver profile can be leveraged to increase injector atomization as well as determine the potential benefits of multi-pulse injection strategies.

Piston Bowl Revision

The data collected on the influence of the spray piston interaction is being used to provide guidance for revised piston bowl geometry to improve spray confinement during injection for stratified operation. An increased back wall height and angle is being investigated to provide these benefits.

Phase 3 Task 2.0 –Single-Cylinder Test Engine Modifications for Flex Fuel (1/1/09 thru 2/28/09)

A multi-cylinder engine head will be built up with dual cam phasing, 2-step variable lift, ethanol sensor, and a direct injection fuel system. The head will be fitted to an existing single-cylinder optical engine. The engine system will then be instrumented to obtain appropriate data on combustion temperatures, pressures, emissions etc.

Optical Engine Modification

The optical engine at Wayne State University was modified to accept a multi-cylinder head that matches the test engine for this project. The head is DI gas and will use fixed cams in place of the actual 2step valvetrain hardware.

The new liner for the optical engine was delayed significantly by the supplier. It was not received in Q1 of 2009 as expected. It was finally received by Wayne State in mid April 2009 and work can finally proceed on the optical engine. The optical engine layout is shown in the *Figure 8* below. The liner as installed in the photo was not a high temperature material and could therefore only be used for low-speed initial testing.

Figure 8) Optical engine setup for E85 project

Phase 3 Task 3.0 –Steady State Engine Characterization using Optical Engine (2/1/09 thru 4/30/08)

Optical Engine Operation

Initial low-speed testing were carried out; *Figure 9* shows the picture sequences of the DI spray injection as visualized via the Bowditch piston window from below, and *Figure 10* shows the visualization from the side (front view). The quartz liner has now been installed in the optical engine and further tests will be run at higher speeds and firing.

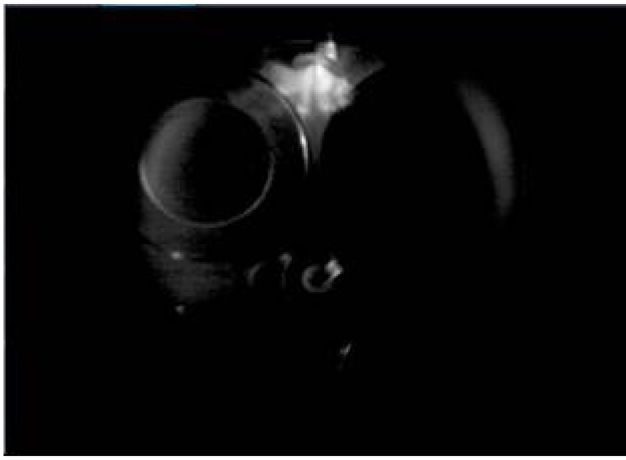
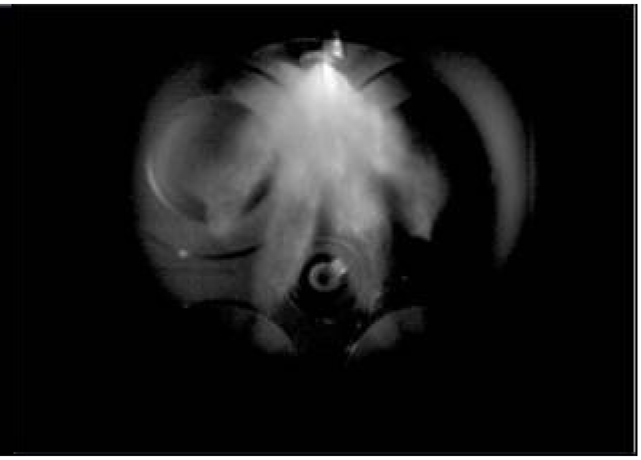
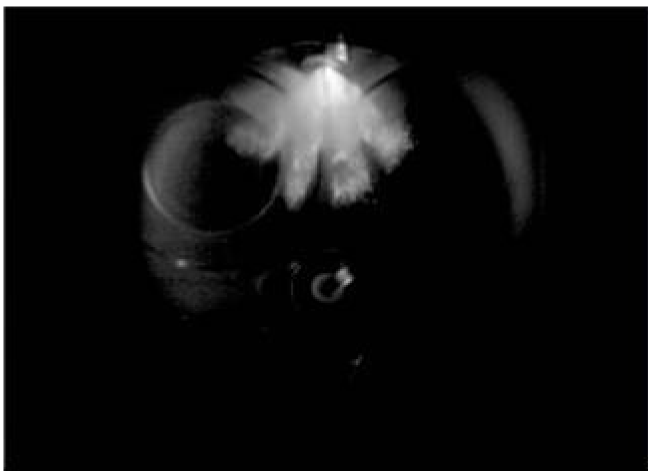
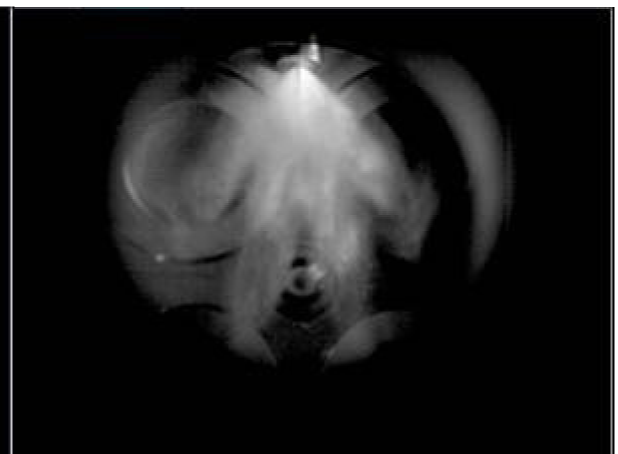
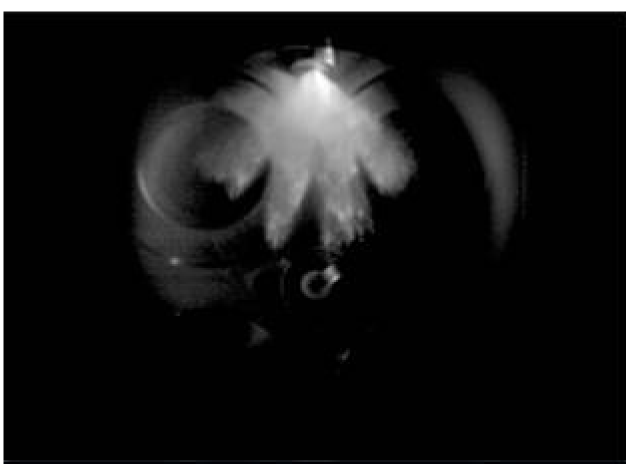
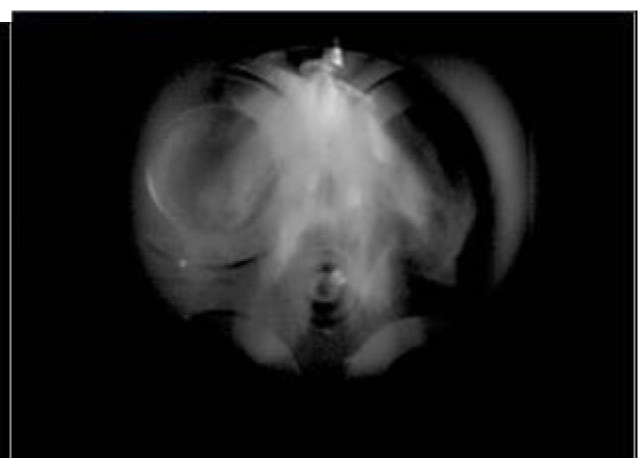

Figure 9) Bottom view of DI injection visualization sequences in motoring optical engine.

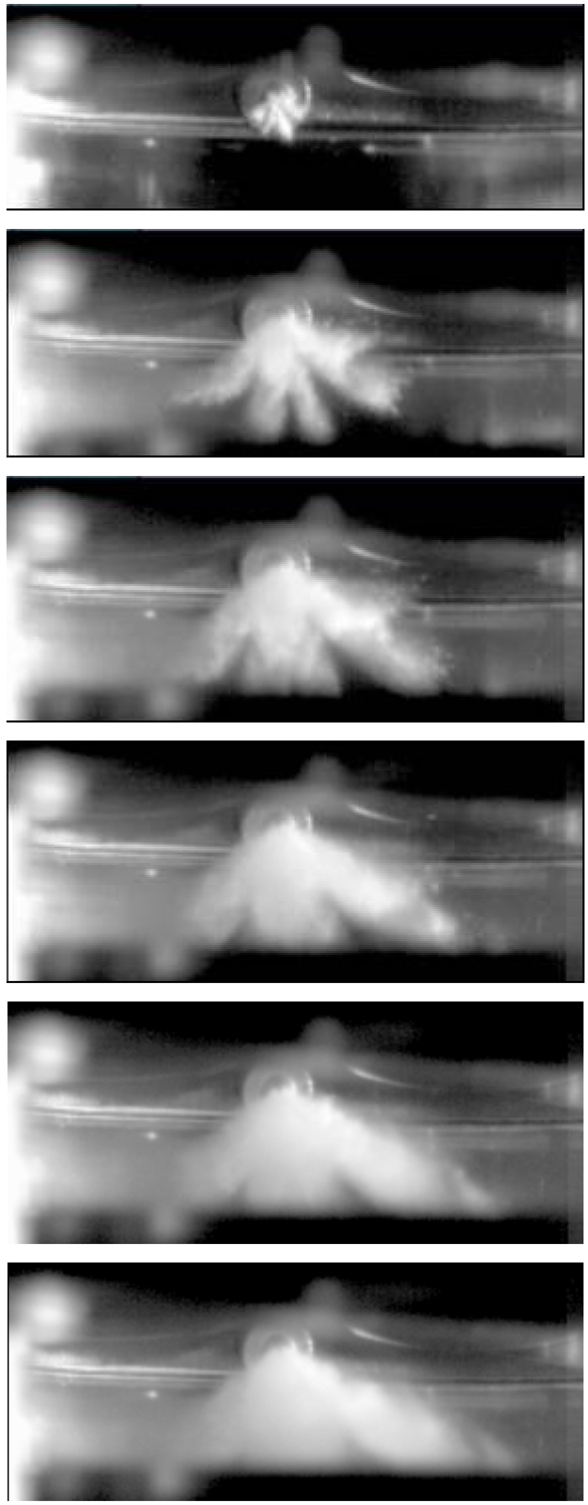

Figure 10) Front views of DI injection visualization sequences in motoring optical engine.

Quarter 2 2009

Phase 3 Task 1.0 – Injector Optimization under Simulated Engine Conditions

The chamber developed in Phase II Task 1 will be employed to further optimize the prototype flex-fuel injector designs under highly controlled simulated engine conditions. Spray characteristics for the injector designs identified in Phase II will be established at a matrix of chamber temperatures and pressures as well as with E0, E50 & E85 blends. Refined designs to be used for final selection of Phase IV test hardware.

Spray Characterization

For this report period, high-speed spray visualization continued to be utilized to characterize and refine the spray structure of the six-hole DI injectors. The injectors used in the assessments are shown in Table 1.

Table 1 Specifications of injectors

	Injector A	Injector B	Injector C
Hole Diameter [mm]	0.23	0.263	0.104
Hole Length [mm]	0.31	0.3	0.23
L/D	1.36	1.14	2.21
Number of holes	6	6	6
Static mass flow with N-Heptane [g/s]	15.9	20.5	4.00

The spray chamber is capable of

- *Chamber pressure from 0.4 (partial vacuum) up to 4 bar,*
- *Chamber air temperature up to 250^{o}C or higher,*
- *Fuel temperature from 10C up to 100C*
- *Direct spray visualization with side- or back-lighting,*
- *Schlieren spray visualization of both liquid and gaseous phases*

Piston Impingement Testing

Piston impingement testing was further carried out simulating the in-cylinder spray behavior during stratified operating conditions. The injector and the piston were mounted in the pressurized chamber so that the relative position of the injector and the piston was the same as the multi-cylinder engine. The piston was moved from TDC position to 20 mm below TDC, along the cylinder axis, to observe the effect of the spray timing change on the control of the vapor plume at the spray-piston interface.

Figure 1 shows some typical results that were observed. The red arrows point to the spray exiting the bowl. Refinement of the spray pattern and timing will be used to improve the AF distribution.

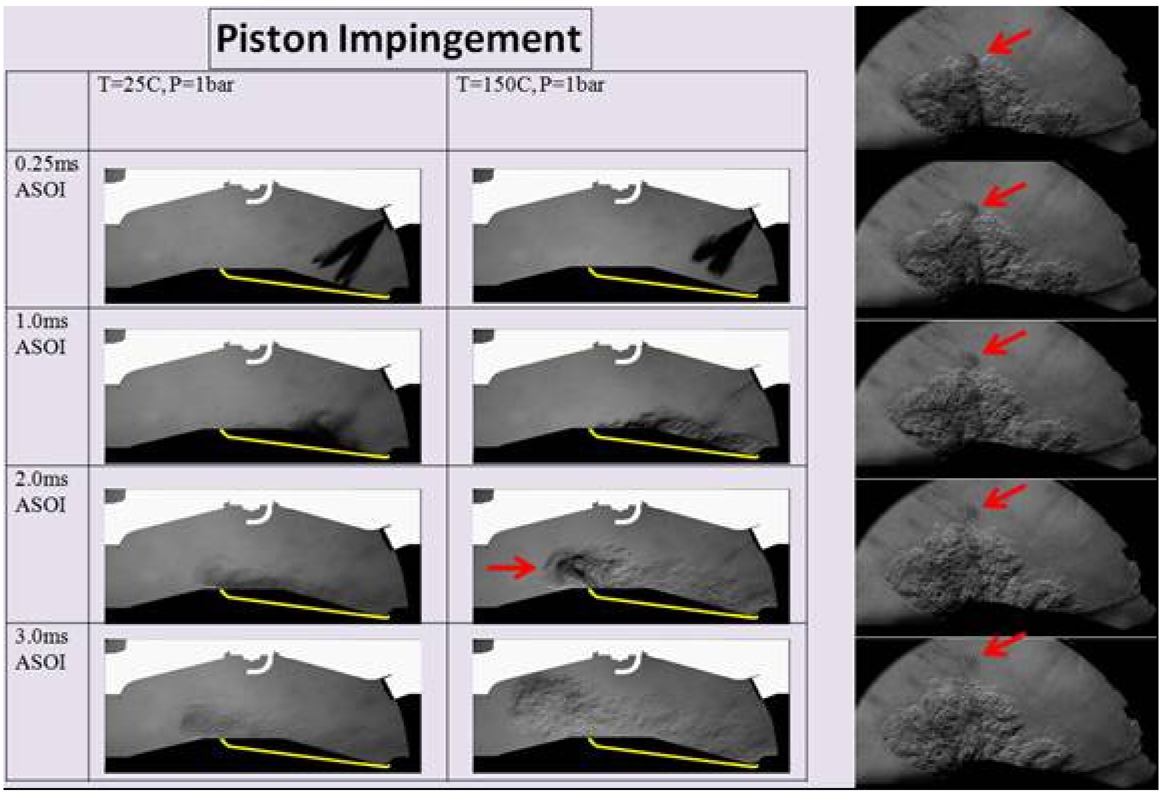

Figure 1: Spray pattern targeting refinement

Spray Pattern Targeting Refinement

To confirm targeting, additional injectors were evaluated. Injectors with revised targeting were built for this purpose. These new injectors use next generation of Delphi GDi design, which supports operation at higher injection pressures. This allowed the maximum flow rate specification to be based on 20 MPa (vs. 15MPa) peak injection pressure allowing for smaller orifice diameters. The smaller orifice size will provide better fuel atomization. Injector spray targeting data is shown in Figure 2.

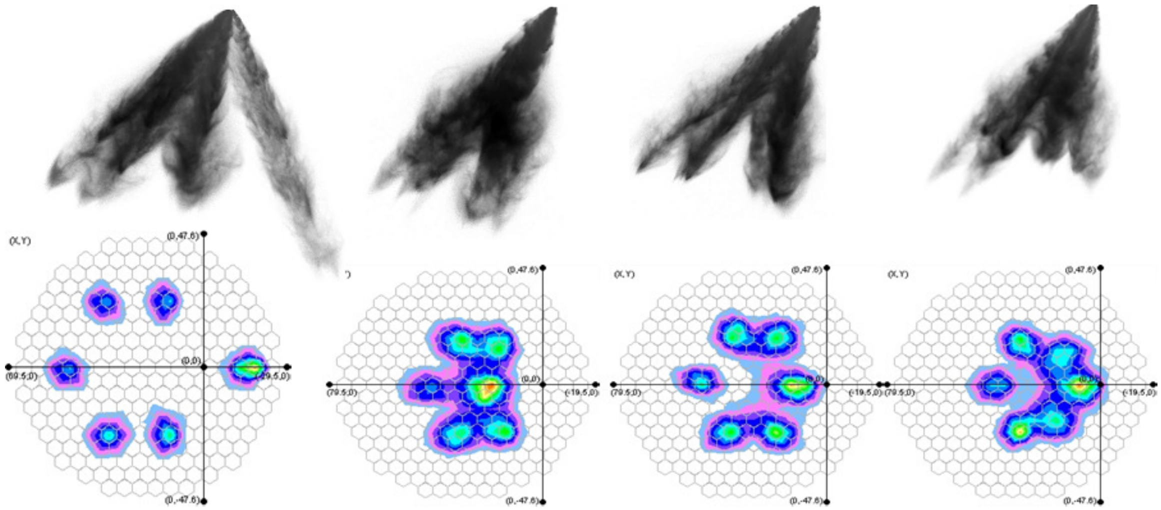

<u>Figure 2:</u> Spray pattern targeting refinement

Visualization of Multiple Pulse Injections

The spray chamber was used to visualize how spray formation would be affected by multiple injections. Preliminary tests of double injections and triple injections were performed to assess the effects of fuel injection quantity and dwell time on spray formation. First injection quantities of 1 mg, 5 mg, 10 mg and dwell times of 0.5 ms, 1.0 ms, and 1.5 ms were evaluated. For the shortest dwell time, it was observed that the fuel from the second (or third) injection could 'catch up' to the previous injection before the previous injected fuel could fully vaporize. A subsequent injection had additional penetration resulting from both induced charge motion and reduced charge temperature that limited vaporization. Additional work will be conducted to shape the injection pulse widths and dwells to concentrate the vapor during stratified operation or disperse it during homogeneous operation. This study will continue in both the spray chamber and optical engine to help define injection strategies.

Figure 3 shows a double injection of 10 mg of fuel separated by 0.5 ms of dwell time.

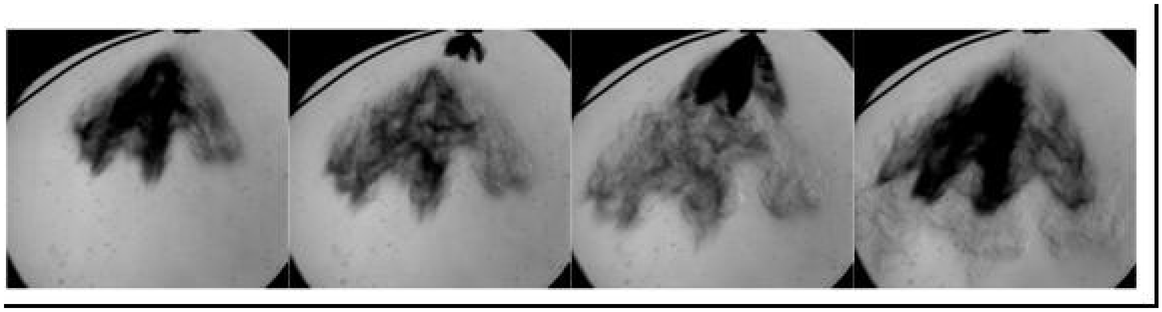

Figure 3: *Double Injection Schlieren Image (10 mg fuel – 0.5 ms dwell – 10 mg fuel)*

Short Pulse Evaluation

A study was conducted to evaluate the effect of short injection duration on spray penetration and vapor generation (see *Figure 4*). Injector B is shown with pulse width delivering from 1-5 mg with time after start of injection (SOI) of 1-5 ms. The penetration curves are depicted in the associated chart. Injection quantities under 3 mg had insufficient penetration to reach the region of the spark plug. Further work will continue with refined spray patterns to produce a more compact spray for stratified operation during cold starts. Split injections will also be evaluated to aid flame propagation during stoichiometric operation. Multiple injections will also be evaluated to aid in injection strategy calibration on the multi-cylinder engine.

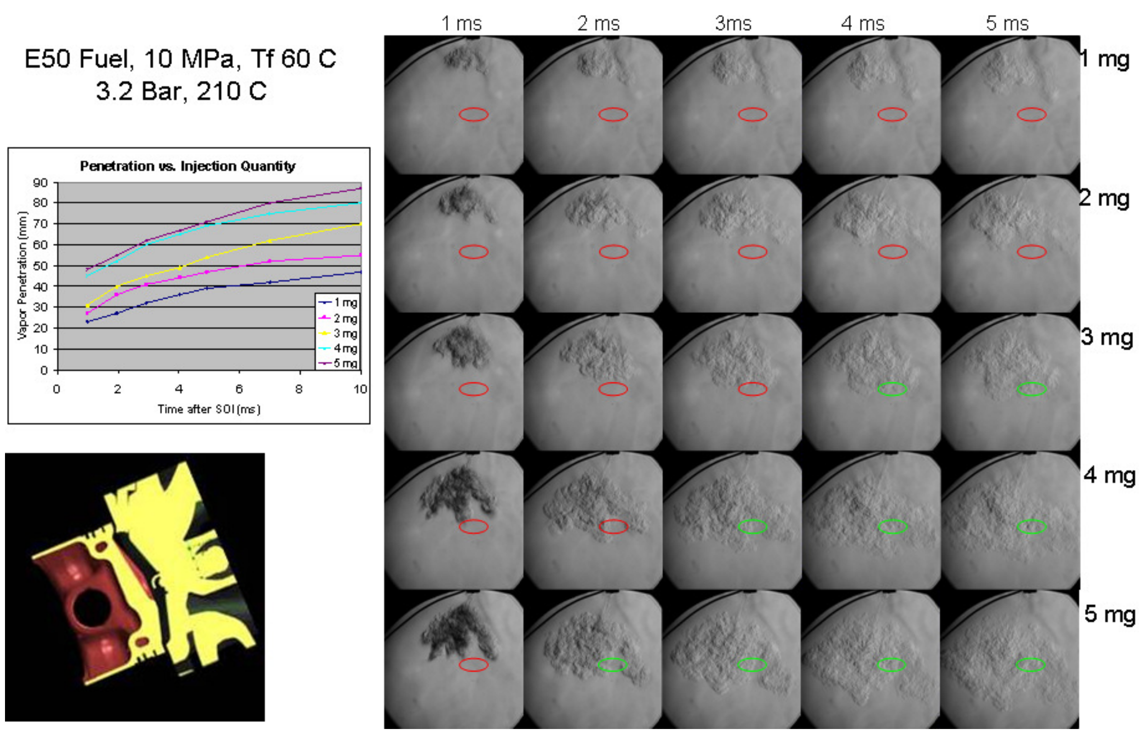

Run	Engine Operating Condition	Fuel Temp	Injector Design	Fuel Composition
1	P=1 bar, T=25 C	90 deg C	B	E100
2	P=4 bar, T=25 C	60 deg C	A	E100
3	P=.4 bar, T=25 C	25 deg C	A	E100
4	P=4 bar, T=200 C	60 deg C	C	E100
5	P=1 bar, T=200 C	25 deg C	B	E100
6	P=.4 bar, T=200 C	90 deg C	C	E100
7	P=1 bar, T=25 C	60 deg C	A	91-RON gasoline
8	P=4 bar, T=25 C	25 deg C	C	91-RON gasoline
9	P=.4 bar, T=25 C	90 deg C	C	91-RON gasoline
10	P=4 bar, T=200 C	25 deg C	B	91-RON gasoline
11	P=1 bar, T=200 C	90 deg C	A	91-RON gasoline
12	P=.4 bar, T=200 C	60 deg C	B	91-RON gasoline
13	P=1 bar, T=25 C	25 deg C	C	E50
14	P=4 bar, T=25 C	90 deg C	B	E50
15	P=.4 bar, T=25 C	60 deg C	B	E50
16	P=4 bar, T=200 C	90 deg C	A	E50
17	P=1 bar, T=200 C	60 deg C	C	E50
18	P=.4 bar, T=200 C	25 deg C	A	E50

Table 2) Orthogonal spray test array for CFD validation (re-ordered in run sequence)

Methods to quantify the Schlieren image results were developed to determine what factors have the largest impact on spray geometry and dispersion. Once the image processing techniques are complete, the results of the tests will be summarized to show the effects of each parameter on spray formation.

Figures 5 thru 8 show some of the different spray geometries that have been observed. Some preliminary observations include:

- High pressure environments promote sprays with distinct individual plumes (see Runs 2, 3, 16).
- Low pressure environments, even with long injection times, promote sprays that coalesce (see Runs 6, 9, 12, 15).

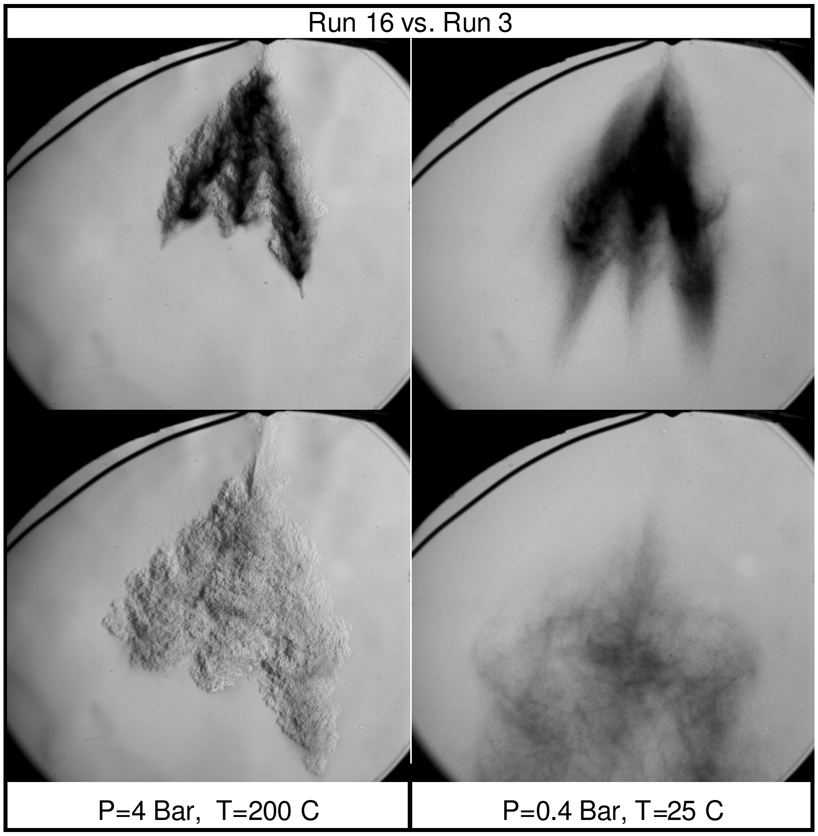

<u>Figure 5</u> Spray images from Injector A at approximately 1 and 2 ms after start of injection (ASOI). The left column images show fuel injected into a high pressure and high temperature environment. The right column images show fuel injected into a low pressure and low temperature environment.

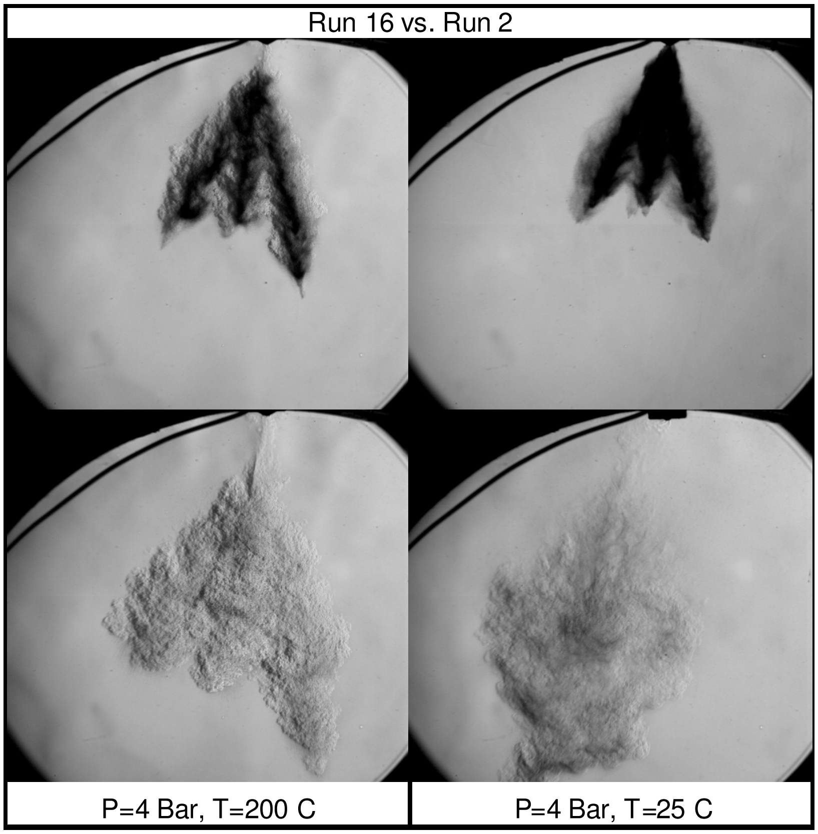

<u>Figure 6</u> Spray images from Injector A at approximately 1 and 2 ms after start of injection (ASOI). The images show the effect of high pressure on spray formation.

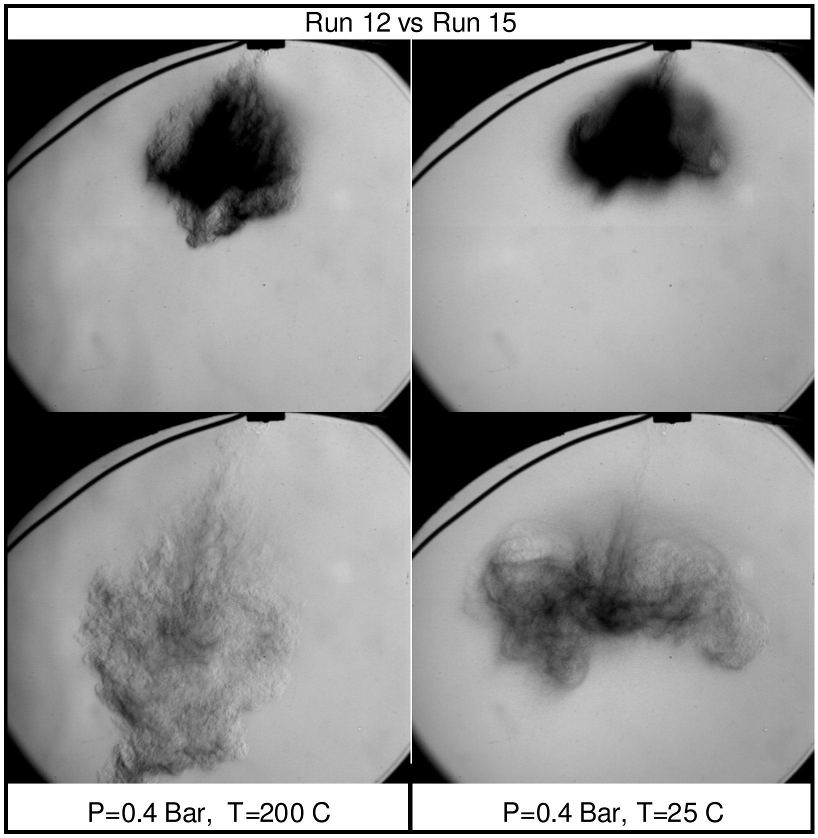

Figure 7 Spray images from Injector B at approximately 0.75 and 1.5 ms ASOI. The images show the effect of low pressure on spray formation.

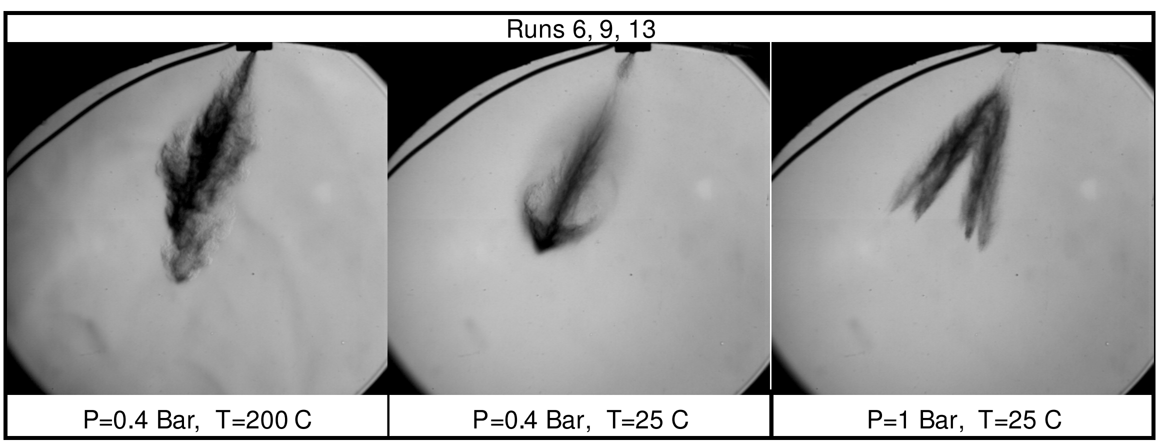

Figure 8 Spray images from injector C at approximately 0.75 ms ASOI. The first 2 images show injection into a 0.4 Bar chamber. The third image shows injection into a 1.0 Bar chamber. The spray formation appears to be sensitive to chamber pressure.

Spray Comparisons of Various Fuel Blends

In addition to the tests outlined in Table 2, additional tests were performed to explicitly evaluate the effect of fuel blend on spray formation. Figure 9 shows the spray formation of 91-RON gasoline, E50, and E100 at 0.5, 1.0, 1.5 and 2 ms after start of injection. Qualitatively, the fuel blend did not appear to have much influence over spray formation.

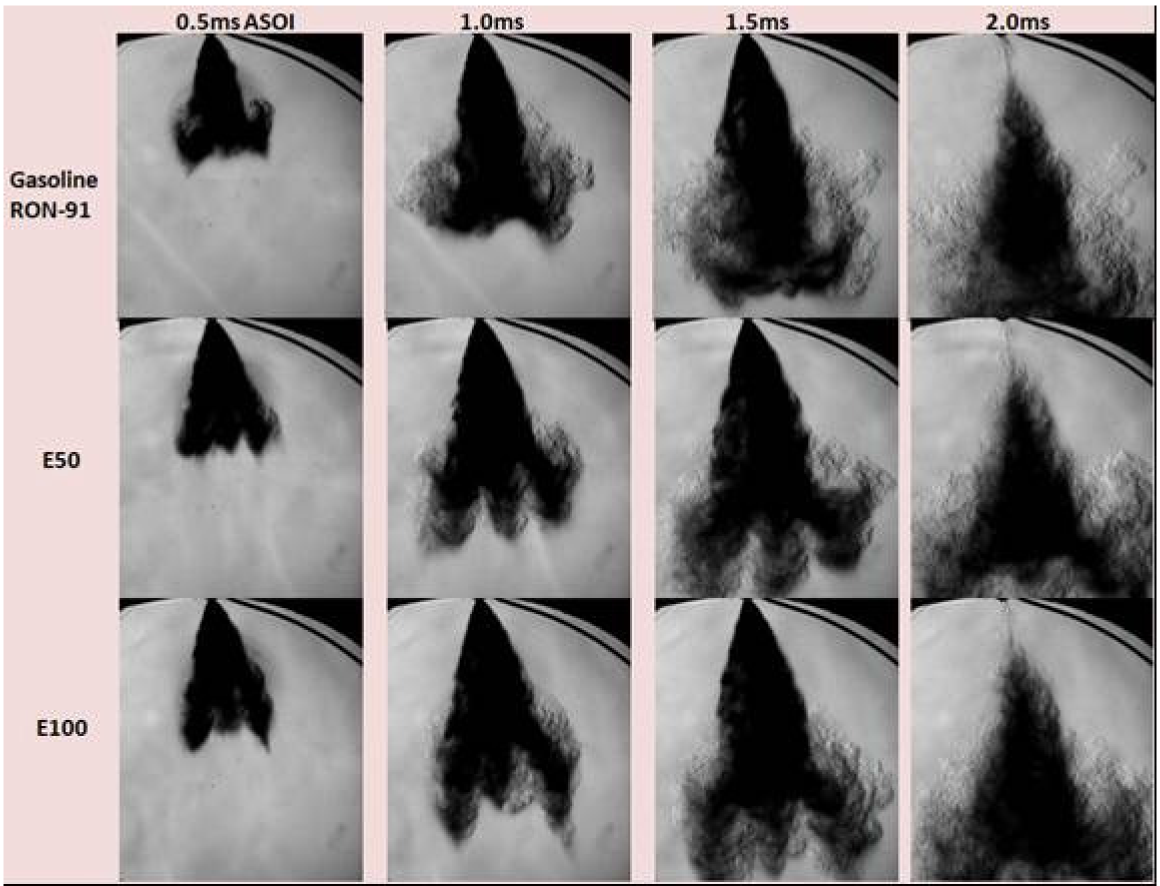

<u>Figure 9:</u> Spray Formation of 91-RON Gasoline, E50, and E100

CFD Model Optimization

CFD model refinement continued during this phase of the project. Three runs of the spray chamber tests were selected as cases to use for the optimization of the CFD injector spray model using Taguchi methods. The input parameters were selected, and they include the following:

- Turbulence model
- Initial droplet size distribution
- Initial velocity

- Evaporation model
- Break up model parameters

<u>Phase 3 Task 2.0</u> –Single-Cylinder Test Engine Modifications for Flex Fuel (Revised date 4/31/09 as reported in Q1 2009)

A multi-cylinder engine head was built with dual cam phasing, 2-step variable lift, ethanol sensor, and a direct injection fuel system. The head will be fitted to an existing single-cylinder optical engine. The engine system will then be instrumented to obtain appropriate data on combustion temperatures, pressures, emissions etc.

Optical Engine Modification

The optical engine build at Wayne State University was completed and debugged during this quarter. The system uses the head from a 2.0L Ecotec engine with fixed cams and a direct injection gas fuel system. Labview programs were completed to control the visualization, fuel injection, and data acquisition systems. Figure 10 shows the completed optical engine.

The engine was balanced for operation up to 1200 rpm.

Figure 10   Optical engine at Wayne State University

Phase 3 Task 3.0 –Steady State Engine Characterization using Optical Engine (Revised date 5/31/09 as reported in Q1 2009)

The optical engine was operated up to 1200 rpm during the debug phase. Figure 11 shows a typical visualization result.

To complement the optical engine experimental work, CFD models were developed and used to simulate the charge motion inside the cylinder. Further work will be performed using injectors with refined spray patterns operating with the low lift cams to simulate cold start and low load conditions.
.

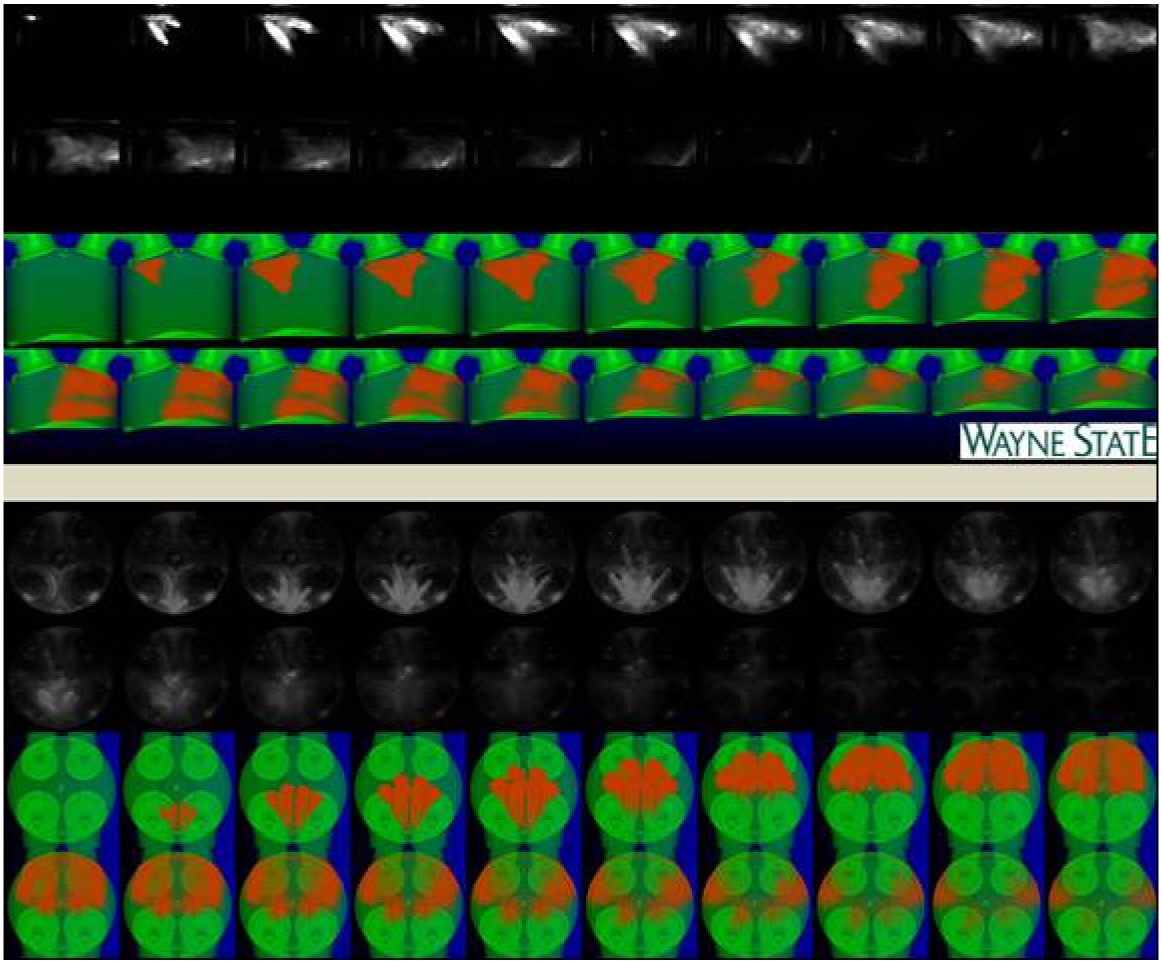

Figure 11: *Optical engine and CFD Visualization*

Once cams with the final profiles and injectors with the final spray pattern are available, the optical engine will be retrofitted and these new systems verified.

<u>Phase 3 Task 4.0</u> –On Engine verification of Injector Spray Optimization (4/15/09 – 8/31/09)

Determination of the effect of key injector factors on specific fuel consumption and emissions with both boosted and non-boosted strategies. Tests will be done for baseline steady state measurements on the multi cylinder engine with a standard sampling system & emission analyzer benches.

An engine retrofitted with 11.85 CR pistons, 2-step VVA and extended range phasers was tested on the engine dyne to map load control with the E85 Optimized engine.

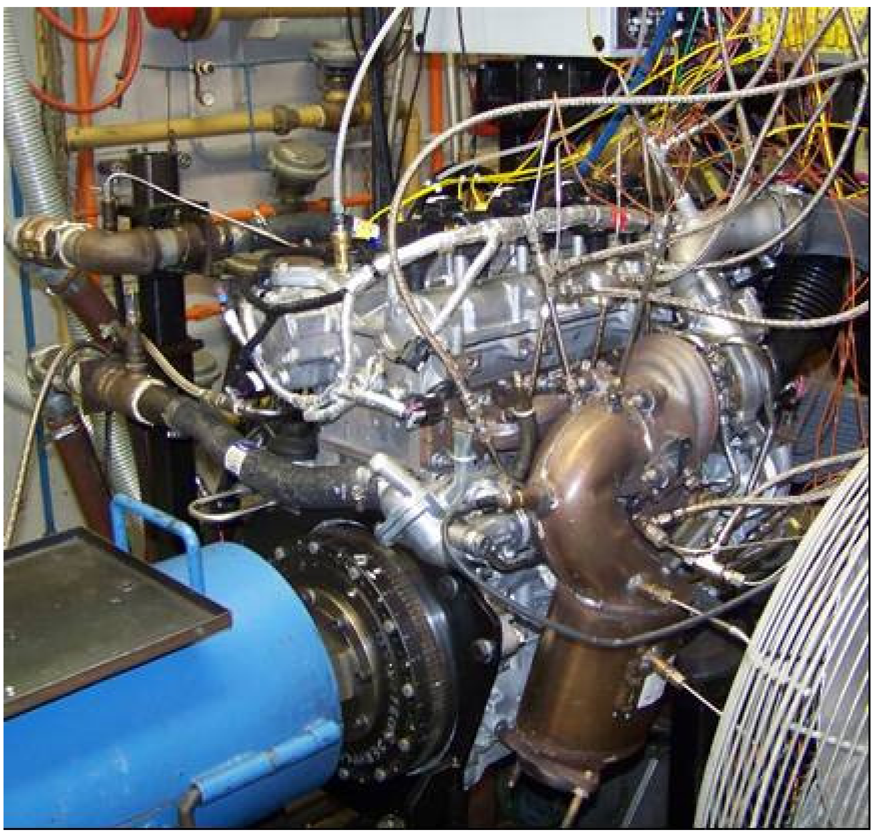

<u>Figure 12</u> Ecotec engine outfitted with E85 project hardware

Figure 13 shows the range of load control via cam phasing using the High Lift cam during WOT operation. MBT Spark is indicated by the color contours. The red test points are at stoichiometric, and the blue test points are 0.96 Lambda. The intake cam position is indicated by the numbered contour lines. The results indicate better than expected low end torque which should be beneficial for operation on E85. The initial testing was done during engine break-in and utilized 100 PON fuel to avoid knock while the initial control map was identified.

A single injection fuel strategy was utilized with SOI of -420 deg (300 deg. btdc firing), which provided a good tradeoff between smoke and combustion stability.

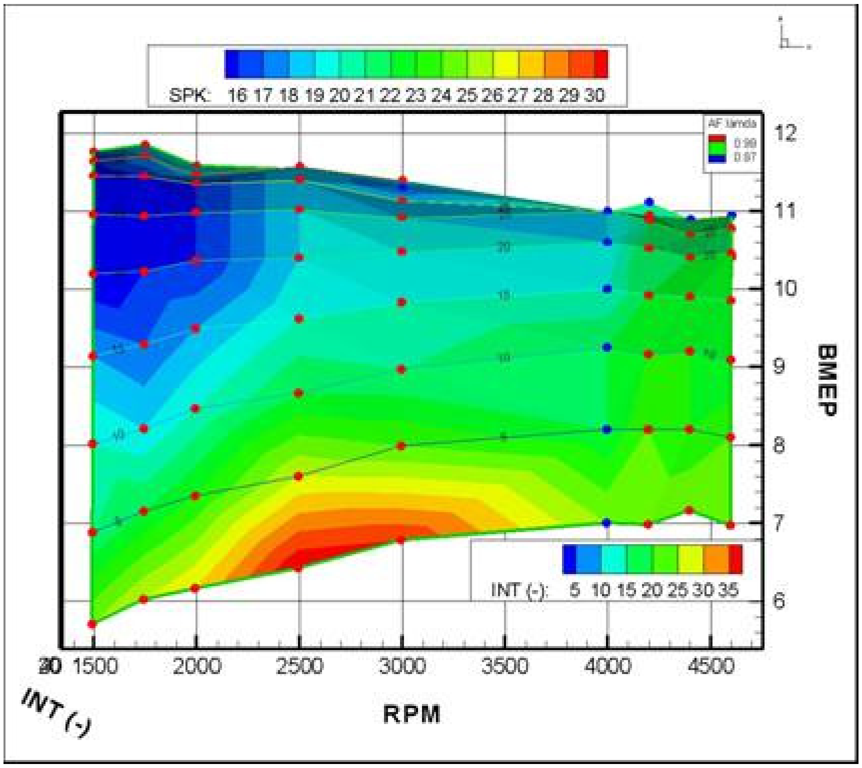

Figure 13 *High lift cam load control map.*

Quarter 3 2009

Phase 3 Task 1.0 – Injector Optimization under Simulated Engine Conditions (1/1/09 thru 2/28/09 original target)

Part of the results and experimental techniques for this work have been summarized in an SAE paper under review for 2010 Congress (Matsumoto, A., Zheng, Y., Xie, X, Lai, M.-C., Moore, W., Yen, D., Hopkins, E., Foster, M., Confer, K. “spray Characterization of Ethanol-Gasoline Blends and Development of a Robust CFD Model for a Gasoline Direct Injector, “SAE 10PFL-0587)

The chamber developed in Phase II Task 1 continued to be employed to further optimize the prototype flex-fuel injector designs under highly controlled simulated engine conditions. Two particular tasks were carried out during this phase:

- Injection to Injection variability
- New Injector spray characterization

Injection-to-Injection Variability

It is found that the more Ethanol content, the more variation was observed at the later stage of injection penetration, but the spray angle has less variability.

The following example summarized variability of 5 injections with identical conditions: Pch=1bar, Tch=200C.

- Pinj=10MPa, Tinj=60C
- PW=1.5ms, Injector type = 736
- Fuel= E100, E50, E0

Definition of penetration and spray angle are illustrated in Figure 1 The penetration is an average of plume A and C because plume B is superimposed by plume A or C and not detectable in some conditions. The angles were measured at three planes, 5mm 10mm and 20mm down from the tip.

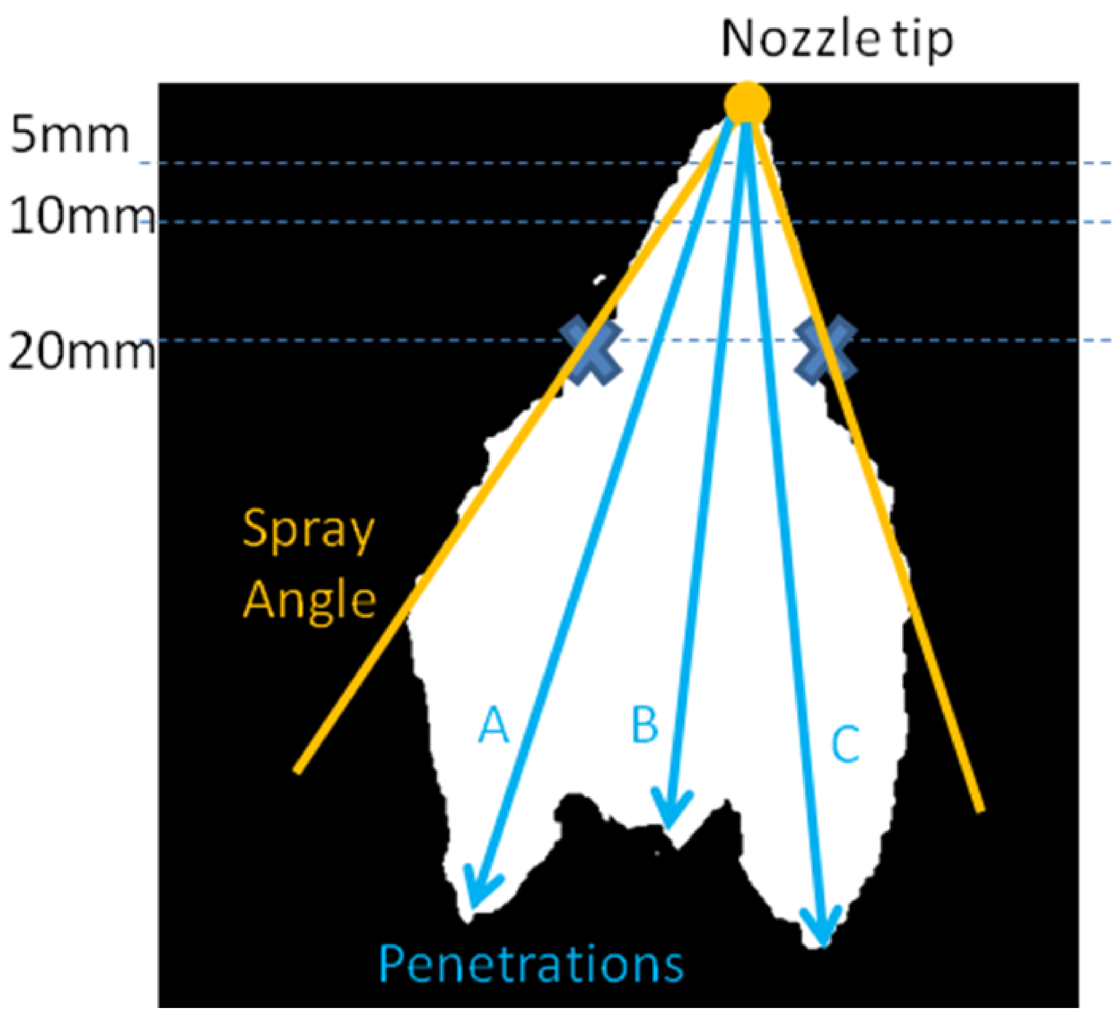

Figure 1) Spray penetration and spray angle

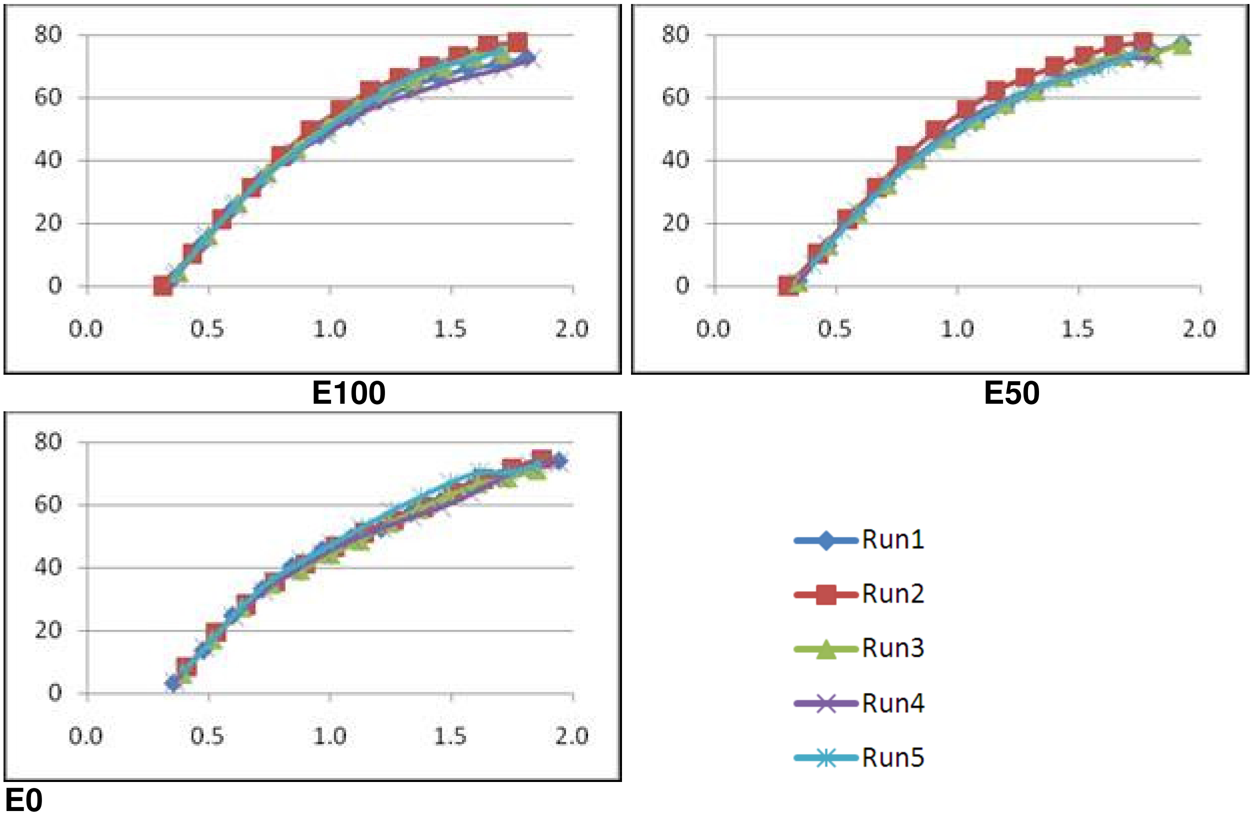

<u>Figure 2)</u> Results of averaged penetration (time (ms) VS penetration)

<u>Spray Penetration</u>

The penetration distance for the three test fuels were very consistent at the early stage of injection (see Fig. 2). At 0.3ms ASOI (After Start of Injection), some variations were observed. The more ethanol content, the more variation was observed at the later stage of injection

<u>Spray Angle</u>

The spray angles at 5mm and 10mm down from the tip were very consistent for the three test fuels. However, there was variation at 20mm, which is shown in figure 3. The spray angles of ethanol content fuels were more consistent than E0. It is believed that smaller components of gasoline are easier to evaporate and the development and transfer of vapor are influenced by random turbulence motion.

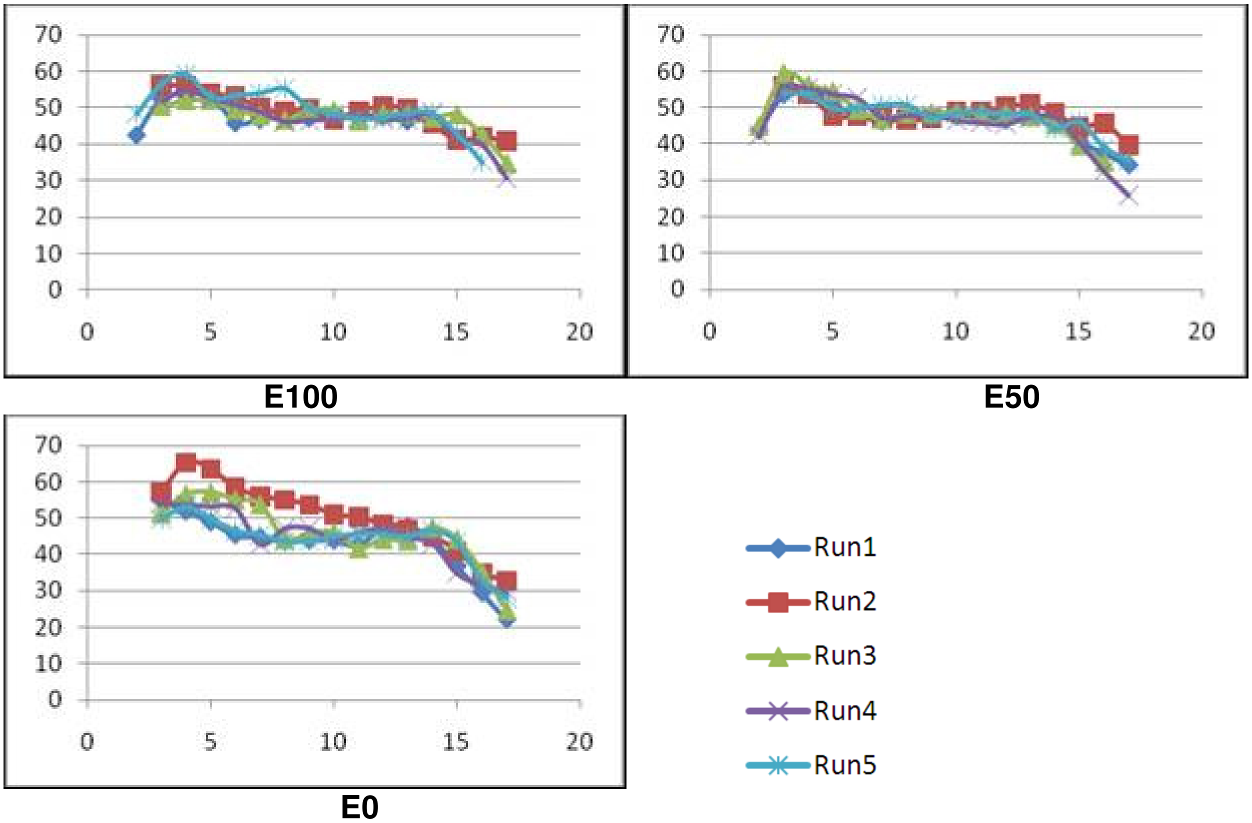

Figure 3) Results of spray angle

Spray Characterization for selection of Phase IV test hardware.

The new E85 (N72-003) injector has been tested using high-speed Schlieren visualization technique. Experiments were run under the following conditions:

- Pch=1, 1.5, 3.2bar, Tch=25, 100C
- Pinj=10MPa, Tinj=25, 40, 60, 80C
- Mass=3, 5, 7, 10, 20mg
- Fuel= E0

Several observations can be made based on this work:

As expected, chamber pressure has a strong effect on the spray penetration. Both liquid and vapor area penetrated less for higher chamber pressure because of higher resistance of ambient air.
The chamber temperature also has some influence on the spray structure especially in the vapor phase. More vaporized spray envelop was observed in higher chamber temperature case. This result will be clearer when the temperature rises to 200C.

Development of vapor depends on fuel temperature, as well as chamber temperature. The higher fuel temperature spray shows more in-homogeneity in spray core area, which implies existence of vapor. E100 spray will show it more noticeably at 80C because the boiling temperature of ethanol is fixed at 78C.

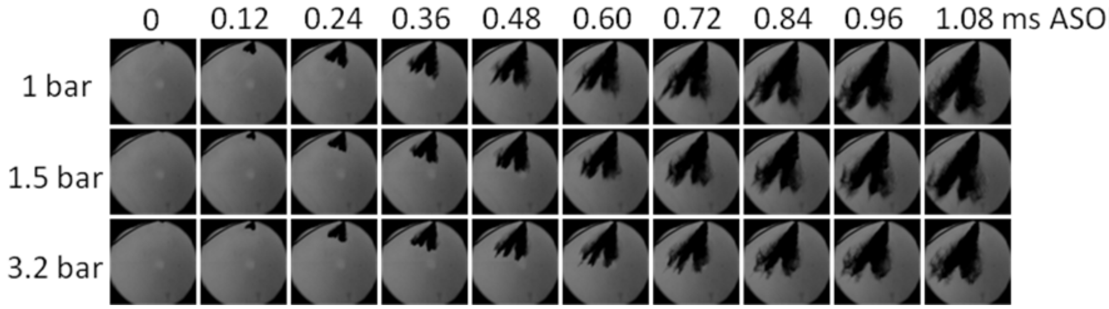

Effect of chamber pressure (Tch=100C, Tinj=60C, Mass=20mg, Fuel=E0)

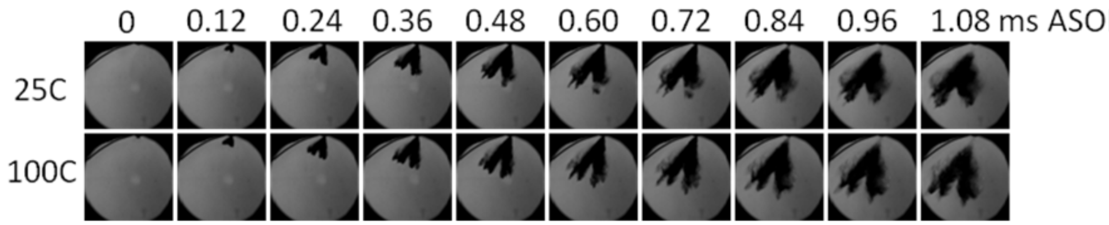

Effect of chamber temperature (Pch=3.2C, Tinj=60C, Mass=10mg, Fuel=E0)

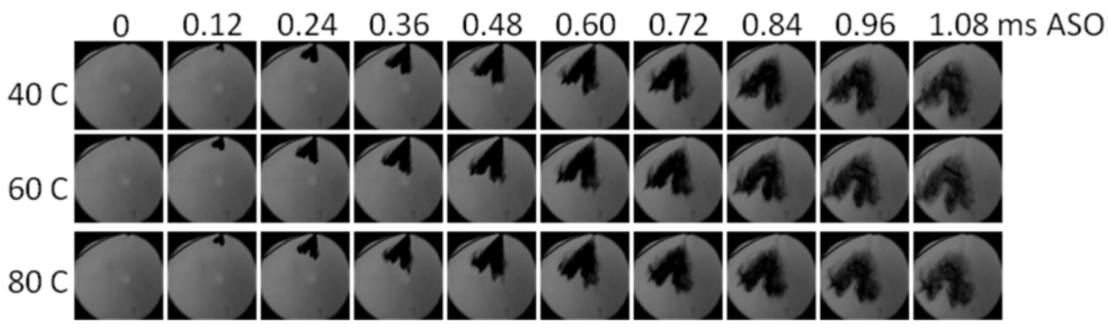

Effect of fuel temperature (Pch=1.5bar,Tch=100C, Mass=7mg, Fuel=E0)

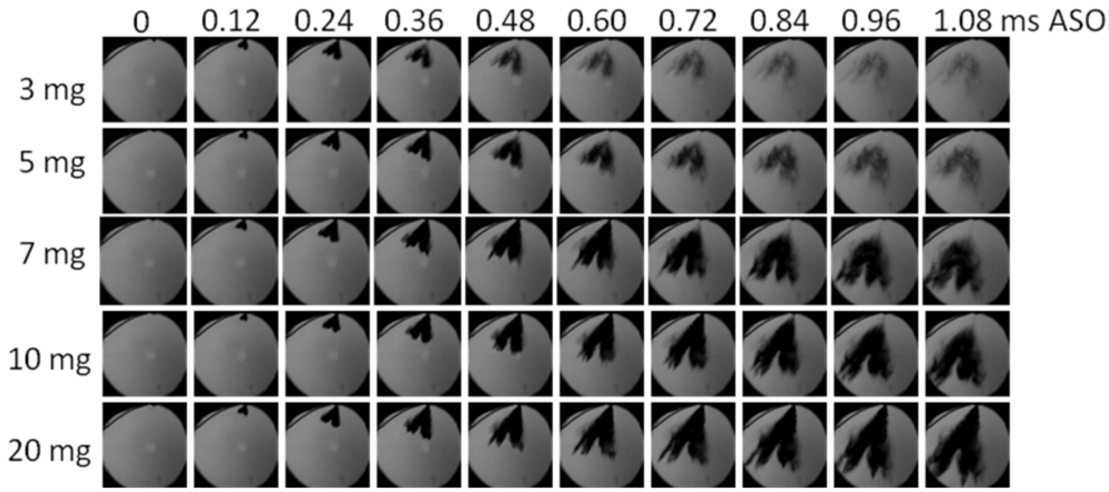

Effect of injected mass (Pch=1bar,Tch=25C, Tfuel=40C, Fuel=E0)
(3-7mg injected at stratified mode, and 10-20mg will be for homogeneous mode. These images will be compared with the results of piston impingement testing and OAE testing)

Figure 4) Progression spray images of N72-003 injector

Phase 3 Task 3.0 –Steady State Engine Characterization using Optical Engine (Revised date 5/31/09 as reported in Q1 2009)

The optical engine is being tested using continuous lighting, due to a Copper Vapor laser high-voltage power supply breakdown. The 25kHz laser is waiting to be repaired. In the meantime, CFD models were developed and used to simulate the charge motion inside the modified engine combustion geometry. The following cases identify the spray plume interaction with charge motion (see Fig.5). As a result of the interaction of tumble and the piston wall, the spray penetration is impeded by the reverse flow if the multiple injection strategy is employed.

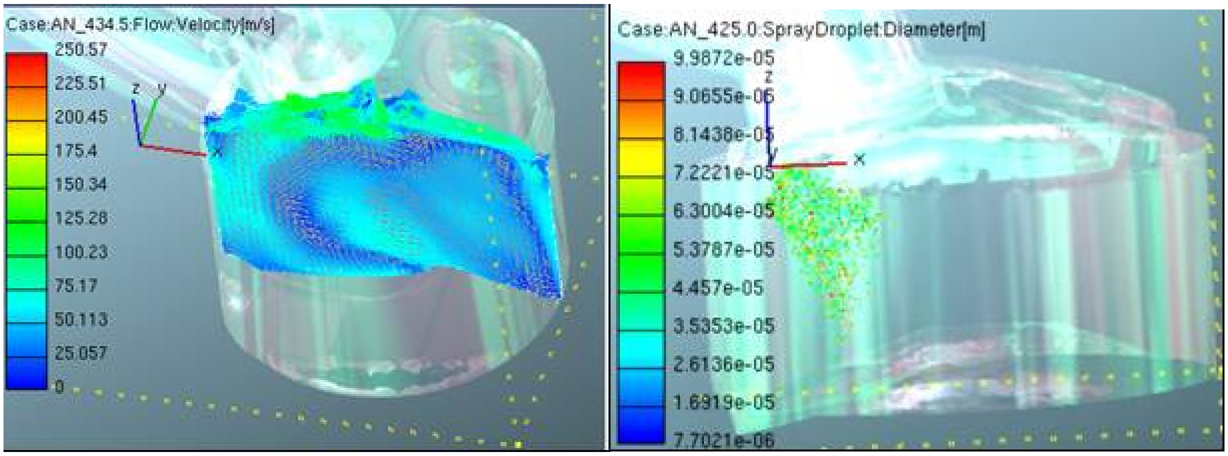

<u>Figure 5:</u> Optical engine and CFD Visualizationunder 1400 rpm, IV: 400-64CA. Fuel Inj : 420-424CA, 0.8mg.

Once cams with the final profiles and injectors with the final spray pattern are available, the optical engine will be retrofitted and these new systems verified.

<u>Phase 3 Task 4.0</u> –On Engine verification of Injector Spray Optimization (4/15/09 – 8/31/09)

<u>Injection Timing Studies</u>

Initial testing was done with the 736 injector; injection timing sweeps indicated an optimal injection timing of 300 deg bTDC firing. This provided a good tradeoff between low soot and combustion stability. The Coefficient of Variation (COV) of IMEP was less than 1% for the majority of operating conditions tested. COV did exceed 3% at higher speeds and low loads. This will be discussed further in the next section. The 736 injector was used to map E85 and 87 PON (Pump Octane Number ≈ 91 RON) gasolines. Unthrottled, unboosted operation was the focus since it is the region used for typical driving. The enhanced Delphi valvetrain strategy provided unthrottled operation from 2-12.7 bar BMEP for E85 and encompasses over 80% of the range of typical operation. These results will be further discussed in the next section.

One of the drawbacks identified with the EIVC (Early Intake Valve Closing) strategy was a reduction in charge motion that resulted in slower mixing and flame propagation. An investigation with the N72 injector was done to investigate its effect on combustion stability. The N72 injector has an increased skew angle, spray images indicated its ability to entrain flow and enhance mixing in the combustion chamber. The SOI (Start of Injection) was varied to identify the smoke limited window using both the EIVC and LIVC (Late Intake Valve Closing) strategies. The LIVC strategy, which is intended for higher speeds and loads exhibits good mixing and fast flame propagation. This was observed over the load domain tested with the 736 injector. The EIVC strategy suffered from slow burn durations especially at low loads.

Figure 6 shows the LIVC timing sweep, the injection window was robust to particulate (FSN) from 280 – 140 degrees before TDC, minimal emissions of HC, CO and best BSFC were identified at 260 degrees before TDC. No significant effect on burn duration or combustion stability was observed in the conducted test.

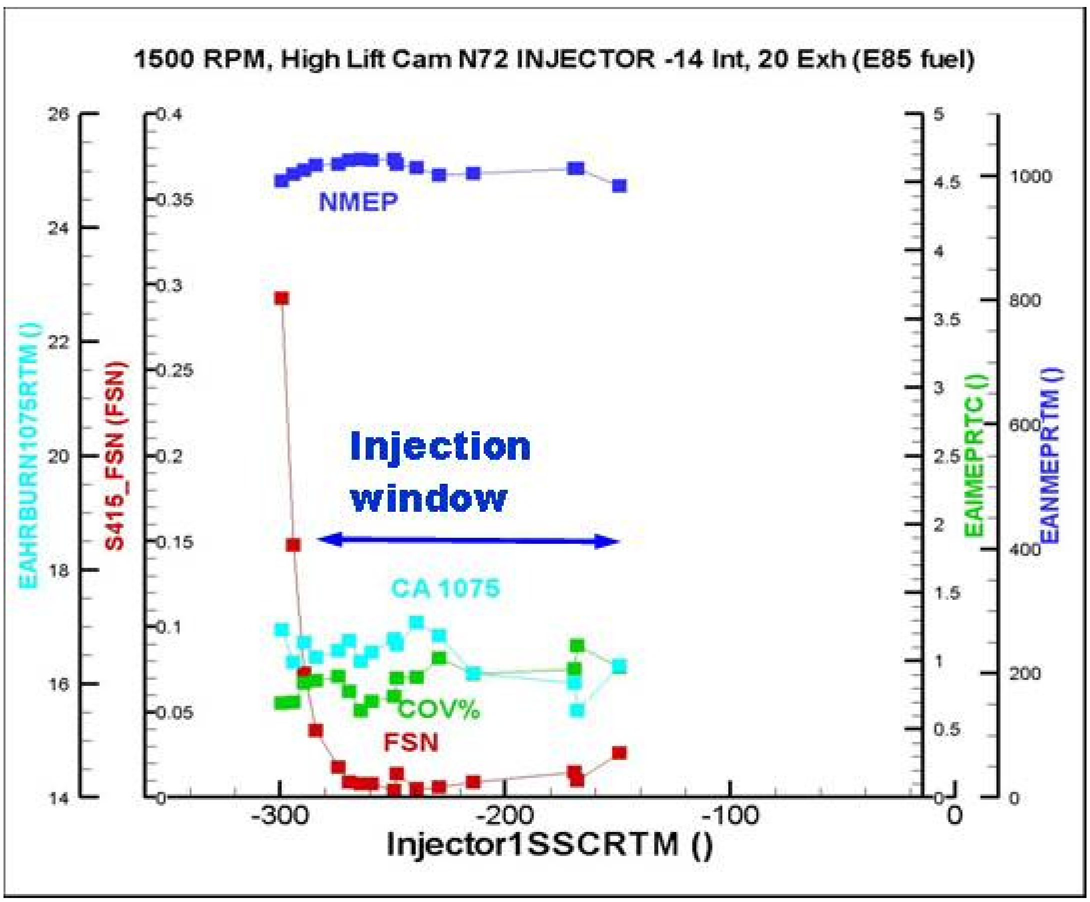

<u>Figure 6)</u> Effect of injection timing on combustion stability, Soot, IMEP and burn duration . Single injection, LIVC strategy, 1500 RPM.

The results of an injection timing sweep with the EIVC strategy are shown in Figure 7. The results demonstrated a higher degree of sensitivity to injection timing. Although an adequate soot window was found, later injection timing was found to reduce both COV and combustion duration indicating that spray induced charge motion can be effectively used for combustion optimization. Additional testing is needed to investigate the potential for mixing control at other speed load points and different fuels. At the later combustion timings the flame speed is comparable to the LIVC strategy.

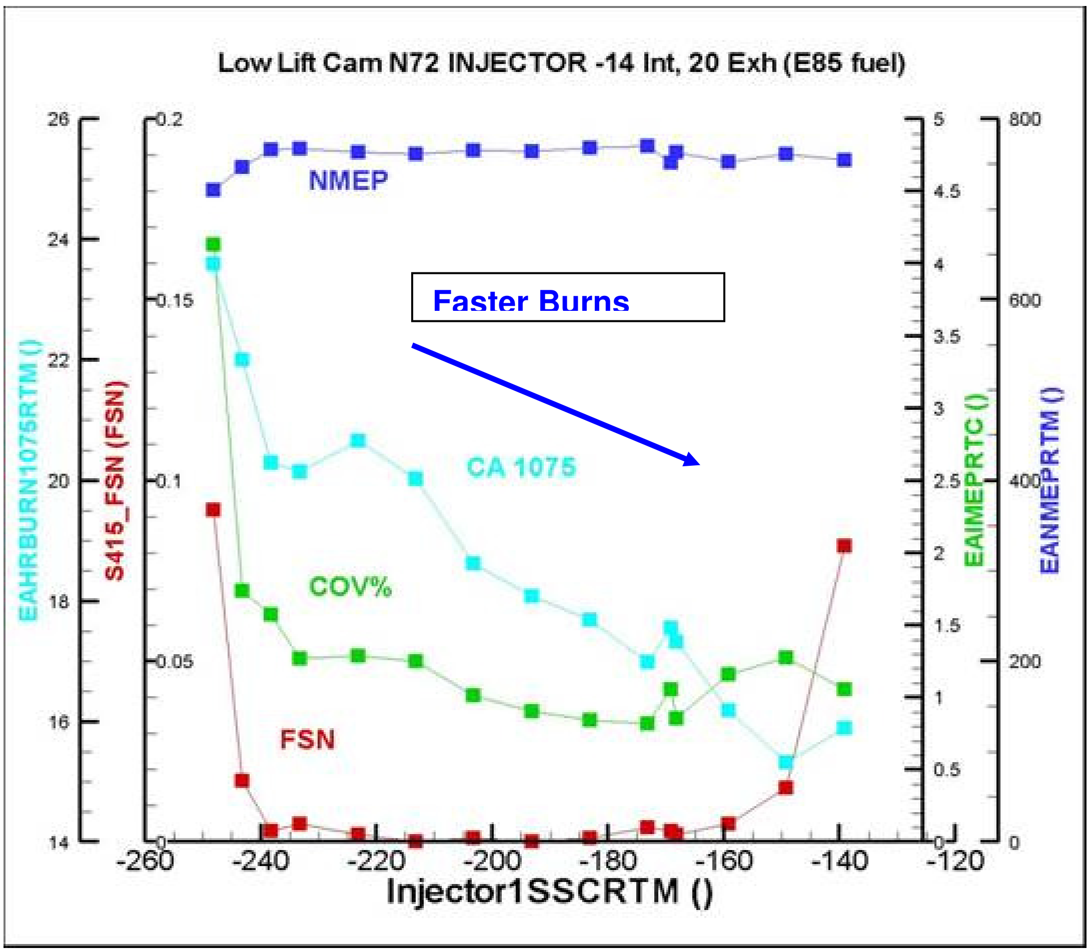

Figure 7) Effect of injection timing on combustion stability, soot, IMEP and burn duration . Single injection, EIVC strategy, 1500 RPM.

Figure 8 shows a composite figure of pressure data from the injection timing sweep with the EIVC valvetrain strategy. Pressure versus crank angle is shown in the top left figure. The top right shows apparent heat release, which highlights the faster combustion. The lower left figure is the cumulative mass fraction burned curve and the lower right is the PV diagram.

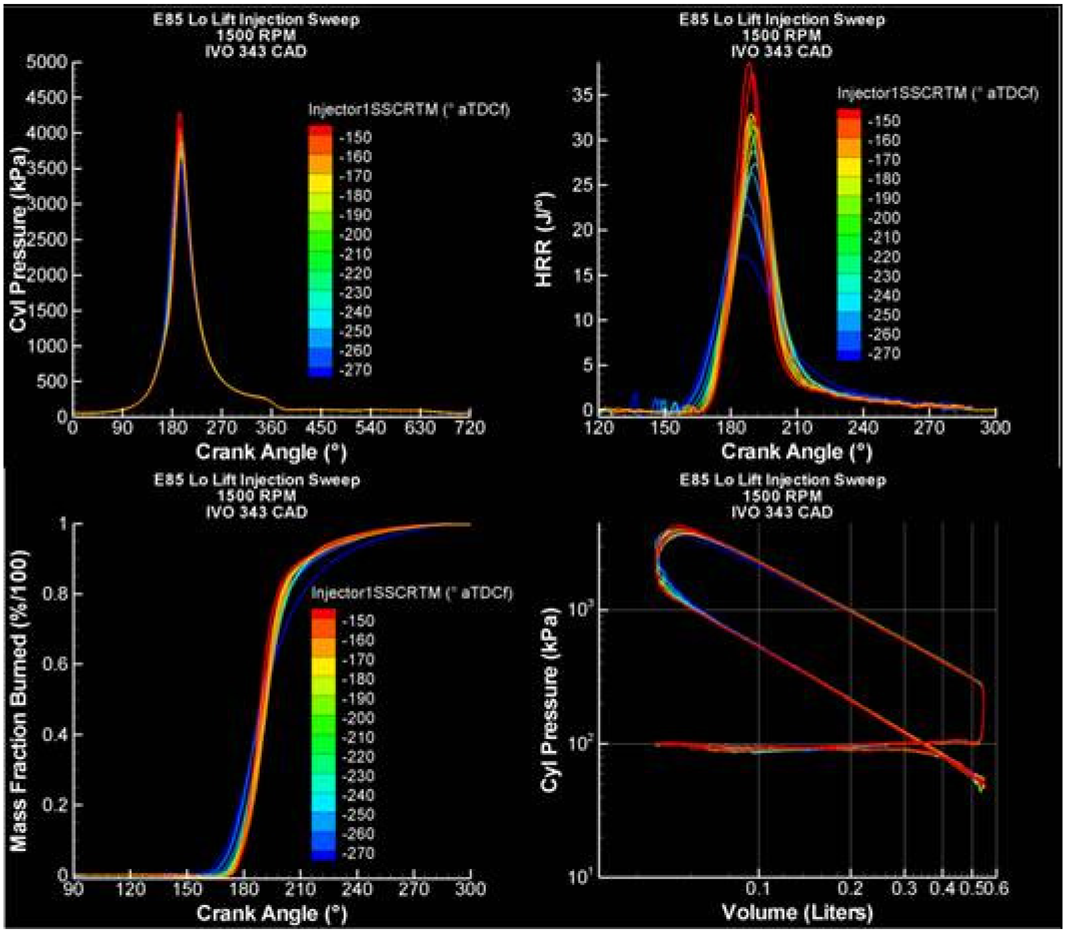

<u>Figure 8)</u> *Effect of injection timing (Single injection, EIVC strategy, 1500 RPM) Cylinder pressure vs. crank angle degrees (CAD), Heat release Rate curve, Cumulative Burn Fraction curve, Log PV Diagram*

Injection timing optimization work as well as the study of multiple injections will continue once the engine is operational in the new dynamometer facility at Delphi's CTCM facility in Auburn Hills Michigan.

Phase 4 Task 1 –Implementation and Test of Ethanol-Optimized Engine (7/09 – 12/31/09)

Cam Phasing Evaluation

The engine was operated in an unthrottled condition to evaluate the domain of load control enabled by the Delphi valve train strategy. Testing was done with the 736 injector using the previously established injection timing of 300 deg bTDC. An effort to further refine injection timing at each operating point was deferred until the domain and potential combustion constraints were identified. Mapping was done with E85 and PON 87 (91 RON) gasoline. The engine was operated in an unthrottled condition with the turbocharger waste gate fully open and the compressor bypass valve completely removed. Figure 9 shows the operating map for E85. The cam phaser position is indicated by the colored contours. The area below the black line shows the preferred operating loads for the low lift (EIVC) strategy, above the black line is the area controlled by the high lift (LIVC) strategy. The black line indicated the cam switch point, where the load is identical for either cam and they can be switched without a torque fluctuation. The low lift (EIVC) cam results agreed well with the GT power simulation done in phase 1 of this project. The extended range phaser enabled operation from 2-9 bar BMEP at 2000 RPM. Lower flame speeds were observed with the low lift cam, presumably from lower charge motion. This was anticipated based on flow test of the head done in phase 2 of the project. Figure 10 displays the burn duration which is noticeably slower on the low lift cam, especially at low loads where the valve is closing very early. The high lift (LIVC) had a higher operating window than predicted from the phase 1 GT power results. A potential cause for this difference may be the intake's outflow coefficients used in the simulation. The cylinder head was not flowed in this configuration (flow out of the intake port) during initial flow tests. This additional flow test is planned with the hopes of resolving the variation in the experimental and computational results. Regardless of the reason, the increased torque, especially at low RPM, is desirable especially for an E85 engine which does not require spark retard for knock control.

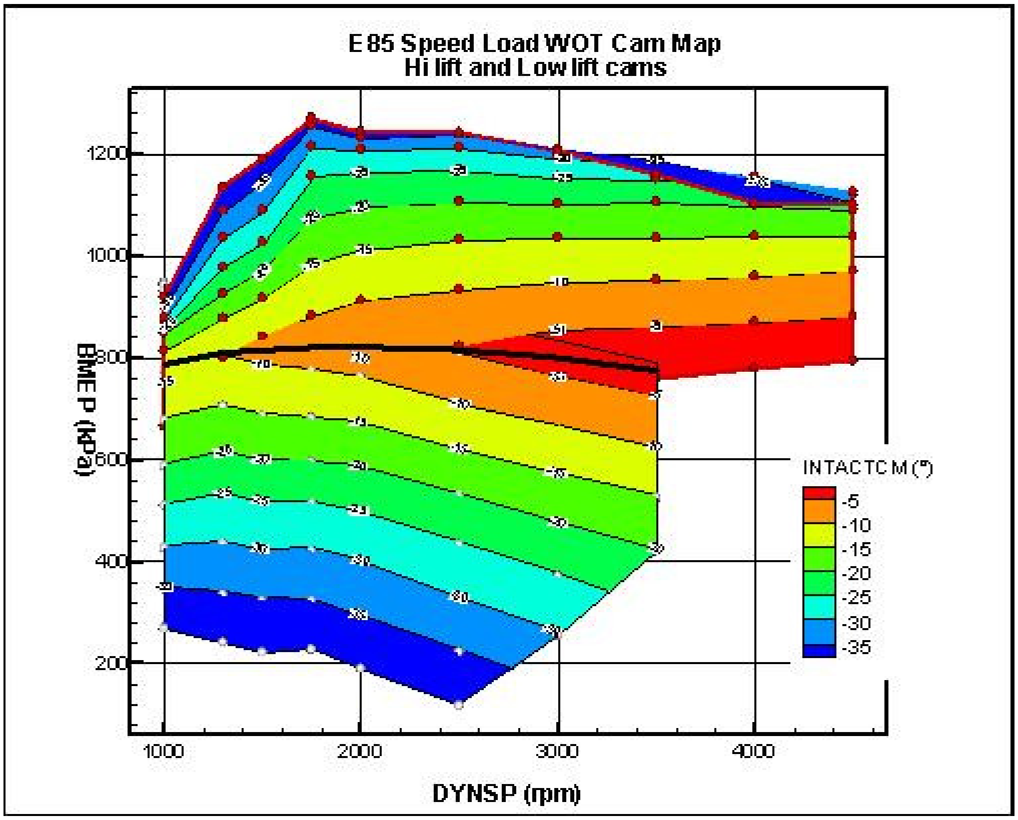

Figure 9) Speed versus load map of E85 (un-boosted / un-throttled) showing valve phasing and valve lift selection

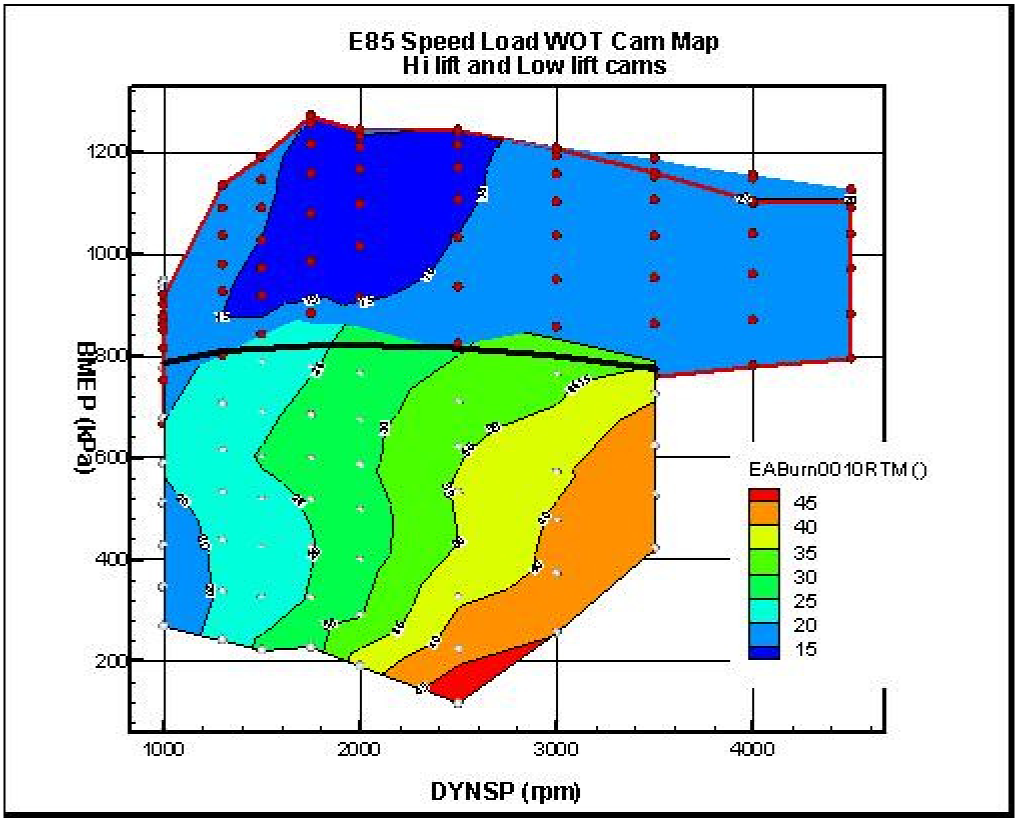

Figure 10) E85 Speed versus load map showing 0-10% burn durations (CAD)

Figure 10 also gives some evidence of the nature of the initial flame development. The high lift cam (LIVC) initial flame development speeds up with RPM such that the burn duration in crank angle degrees is relatively constant. Conversely the low lift (LIVC) burn duration is not significantly affected by RPM and the burn duration in crank angle degrees gets progressively longer. This initial speed load map was for fixed injection timing so any potential benefit of spray induced charge motion is not realized.

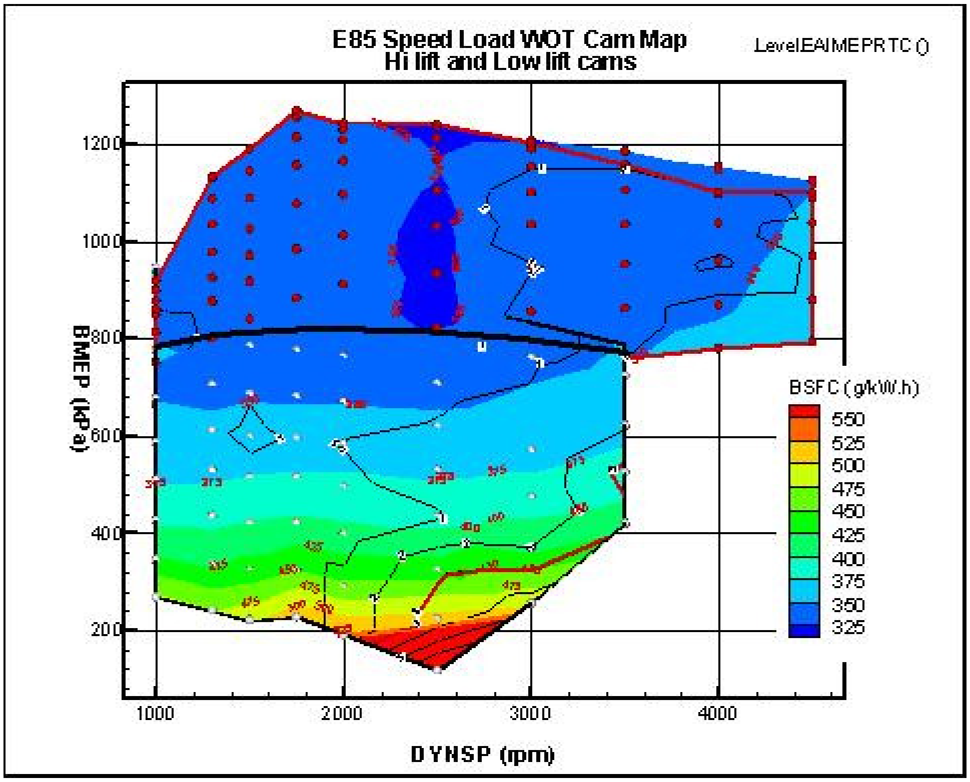

Figure 11) E85 Speed load map showing BSFC and COV of IMEP

The brake specific fuel consumption (BSFC) over the speed load map for E85 is shown in Figure 11. No knock was observed, even at low RPM, high load conditions therefore MBT spark timing was maintained over the entire operating map. The low load, higher speed region of the low lift cam did suffer from unacceptable combustion stability due to poor mixing and long combustion duration. The COV of IMEP was typically below 1% as shown by the black contour lines. The 3% COV limit is highlighted by the bold red line. Additional work to improve combustion stability, including spray strategies and throttling will be required to refine the light load region.

The Burn behavior is shown in the following composite figures. Figure 12 demonstrates the low lift early intake valve closing (EIVC) strategy and Figure 13 the high lift late intake valve closing (LIVC) strategy.

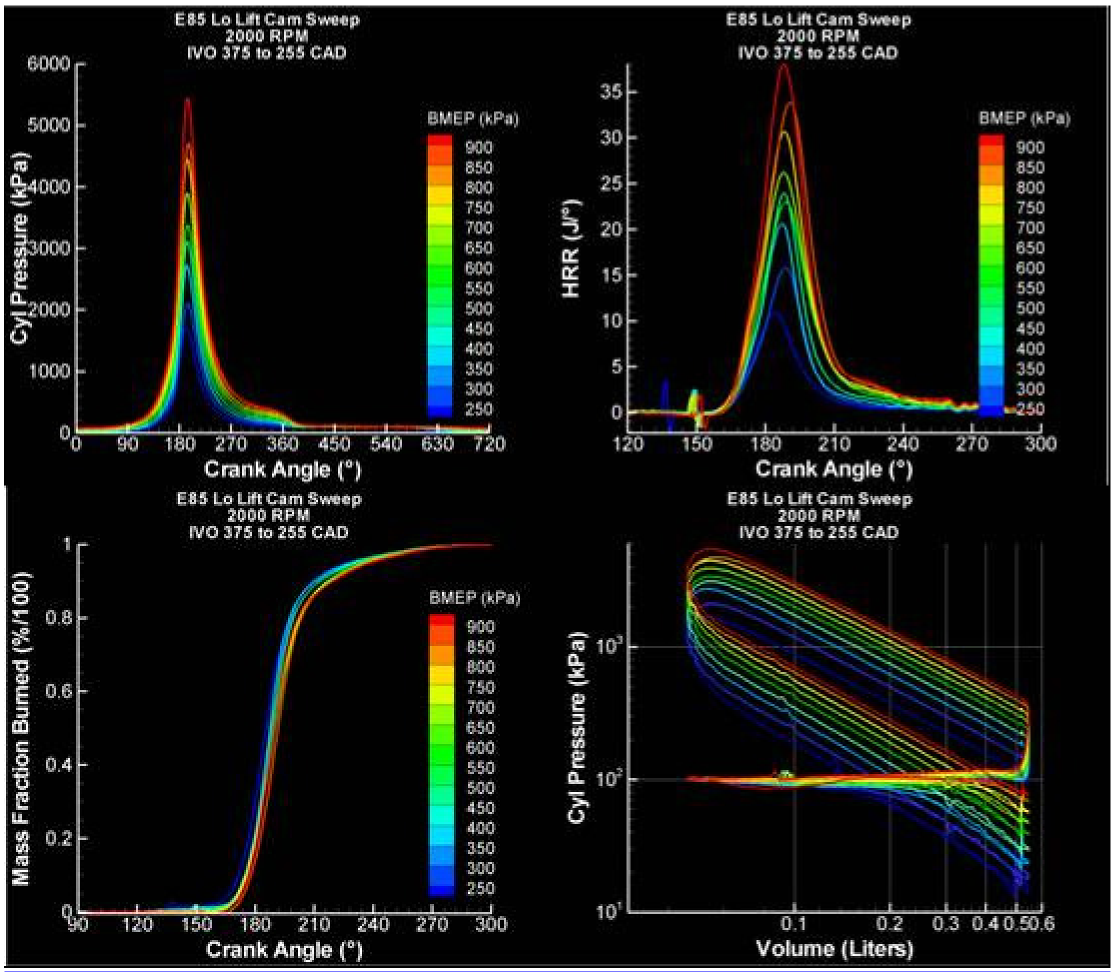

<u>Figure 12)</u> Effect of cam phasing (EIVC strategy, 2000 RPM)
Cylinder pressure vs. crank angle degrees (CAD), Heat release Rate curve, Cumulative Burn Fraction curve, Log PV Diagram

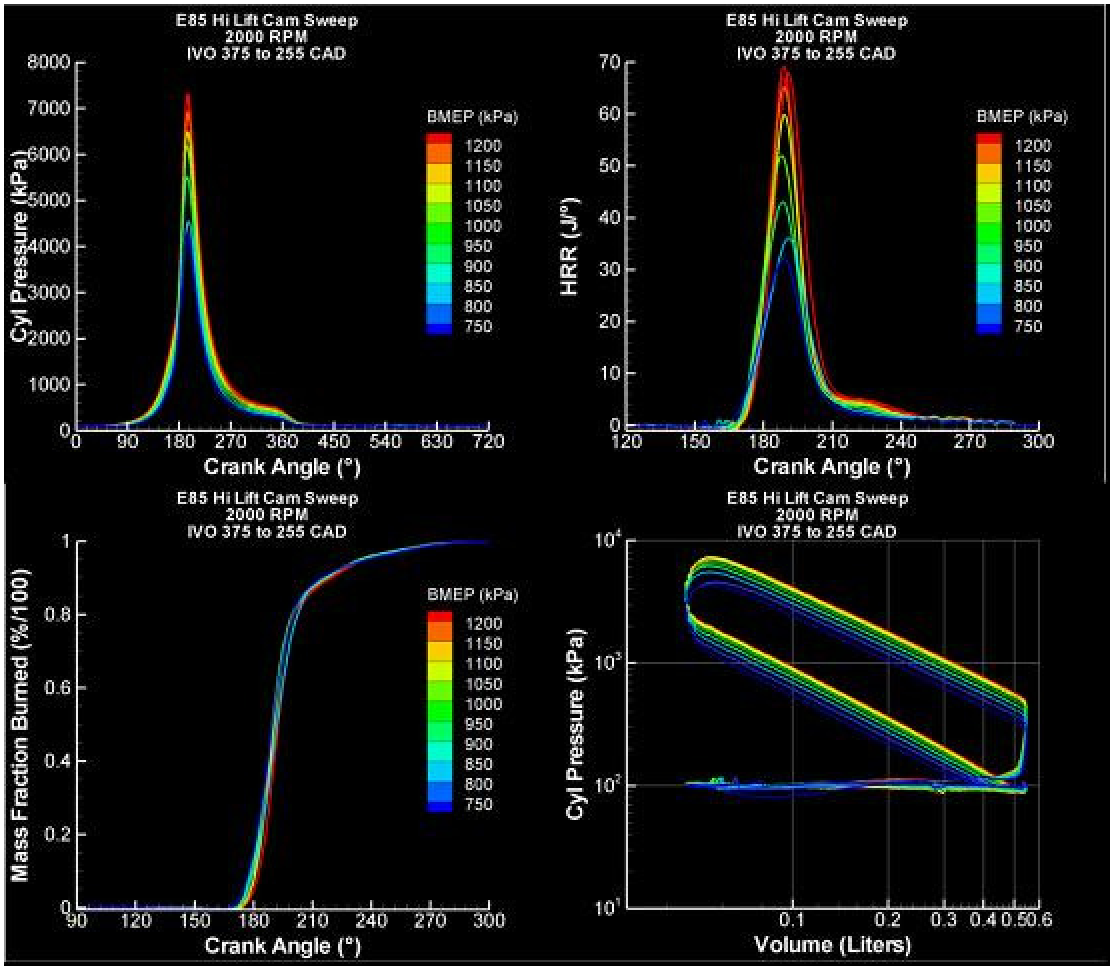

Figure 13) Effect of Cam Phasing (LIVC strategy, 2000 RPM)
Cylinder pressure vs. crank angle degrees (CAD), Heat release Rate curve, Cumulative Burn Fraction curve, Log PV Diagram

The PV diagrams in Figures 12 and 13 illustrate the nature of the load control via cam phasing for each strategy. The EIVC demonstrates a minimal pumping loop and the vacuum associated with the expansion after the valve closing event. The LIVC strategy also has a minimal pumping loop with the effective displacement and CR controlled by the valve timing. Between the two strategies, an effective displacement control mechanism which provides from 20 to nearly 100% is achieved.

BSFC Optimization

During Phase 1 of the project, a simulation to identify the optimal load control strategy for minimal fuel consumption was run; Figure 14 shows that data. One of the interesting conclusions was that at light load, it may be advantageous to preferentially use throttling over cam control for minimal fuel consumption. The Y axis is the manifold pressure (MAP) while intake cam phasing is on the X axis. The colored contours with the black labels indicate BMEP. The results indicate that a tradeoff curve between the two strategies can be used for load control. The white line indicates the optimal load control path. The open white circles are within 1% of the best answer and the +'s indicate values within 2% of optimal.

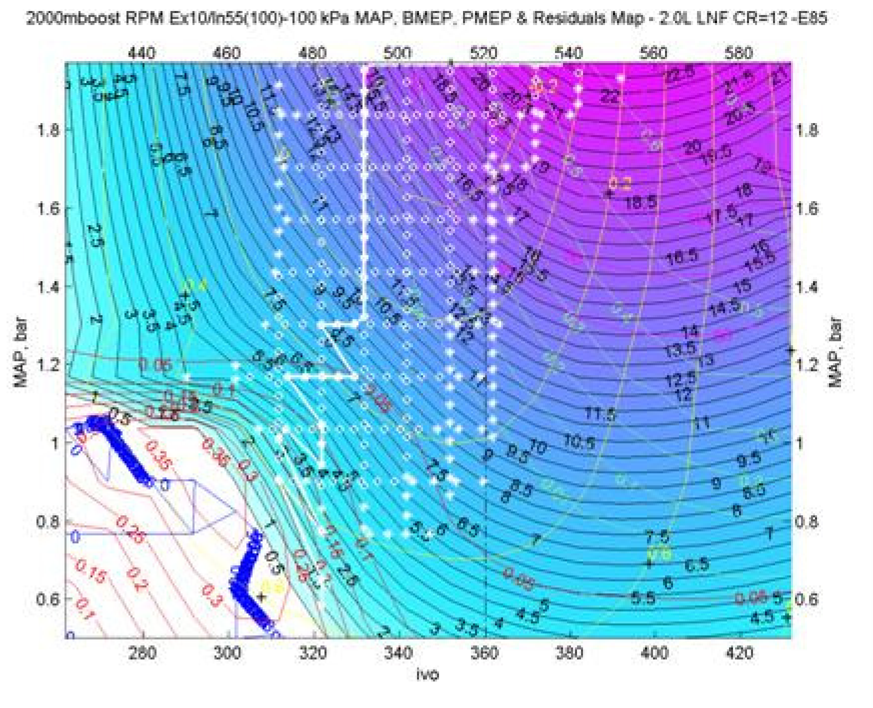

Figure 14) GT power Cam Phasing vs. MAP load control simulation

To investigate this predicted result, testing was done at fixed fuel pulse width while cam position and throttle were traded off to control load. Figure 15 shows the results from the tests confirming the model predictions. The engine was adjusted to provide airflow such that stoichiometric operation was maintained at MBT timing. A more thorough evaluation is needed to understand the result but the initial assessment is that the increase in internal EGR resulting from throttling advantageously offsets the throttling loss by reducing flame temperatures and their associated heat loss and dissociation. The minimal BSFC, (best power) was observed at a light throttle (90 MAP). The result indicates that to optimize the control strategy a more detailed mapping is needed to reach optimal operating conditions.

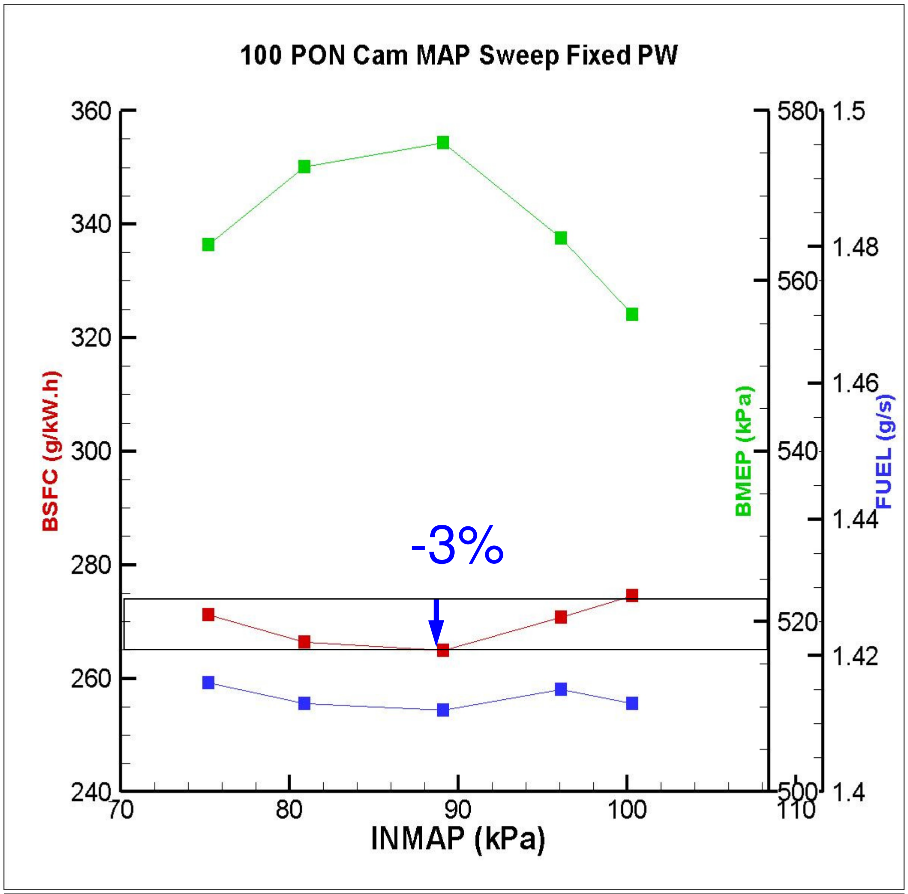

Figure 15 Fixed Pulse Width Cam Phasing vs. MAP Sweep

Gasoline Testing

Testing on 87PON (91 RON) gasoline was significantly more challenging due to knock limited performance at high loads and combustion stability at low load higher speeds resulting from slower combustion. All testing was done at stoichiometric conditions. Spark was retarded from MBT to avoid knock only if necessary at the higher loads and compression ratios. Although the geometric compression ratio of the engine is 11.85 it can be reduced via the valvetrain to a lower effective compression ratio via either the EIVC or LIVC strategy. Since the full 11.85 expansion ratio is maintained, improved efficiency is possible due to more fully expanded cycles. In fact, at low load the cycles are fully expanded at the time of Exhaust Valve Opening (EVO).

The speed load map showing BSFC is shown in Figure 16. Output, relative to E85, is down about 10% as a result of the reduction in air flow from charge cooling and the efficiency loss associated with spark retard to control knock. At low RPM, high load conditions the BSFC begins to increase significantly. A penalty is also noticeable at higher speeds where an increase in breathing causes the compression ratio to rise requiring more spark retard. The net effect is a decrease in output and increased fuel consumption at aggressive cam phasing.

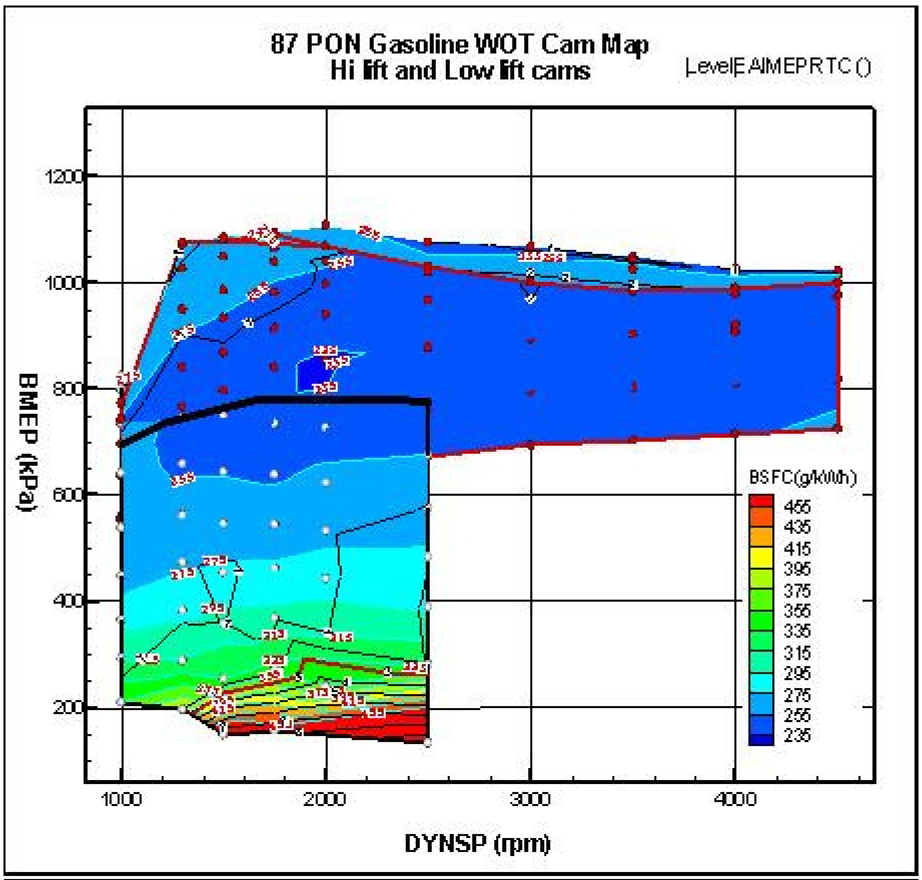

Figure 16) Gasoline PON 87 (91 RON) Speed Load BSFC Map

A composite combustion analysis is shown in Figure 17. The effect of spark retard on all of the diagrams is evident.

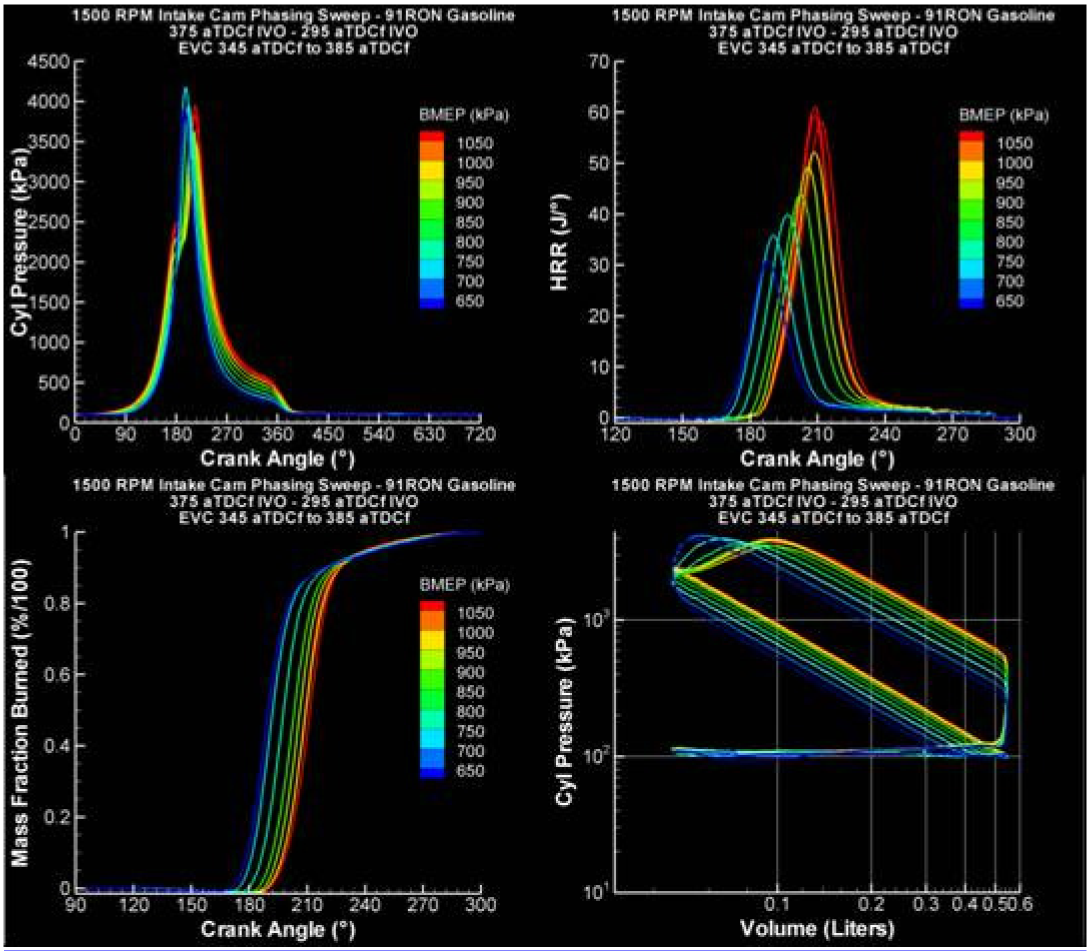

Figure 17) Effect of spark timing (LIVC strategy, 1500 RPM)
Cylinder pressure vs. crank angle degrees (CAD), Heat release Rate curve, Cumulative Burn Fraction curve, Log PV Diagram

Fuel Consumption Improvement Comparison

To evaluate the system level improvements to date, a comparison is made between the baseline engine and the E85 optimized engine with different fuels. The engine was tested, before modification, on 87 PON fuel and compared to the OEM specification. The baseline "out of the box" engine came in about 3%

higher than the OEM numbers for the load sweep shown. Since the production engine was not ethanol capable, no OEM production baseline was possible for E85. To estimate the fuel efficiency of E85 fuel on an OEM calibration an adjustment was made for the reduced fuel energy content (as shown in the yellow line in Figure 18). This calculated curve then acts as the baseline against which all E85 optimization will be compared.

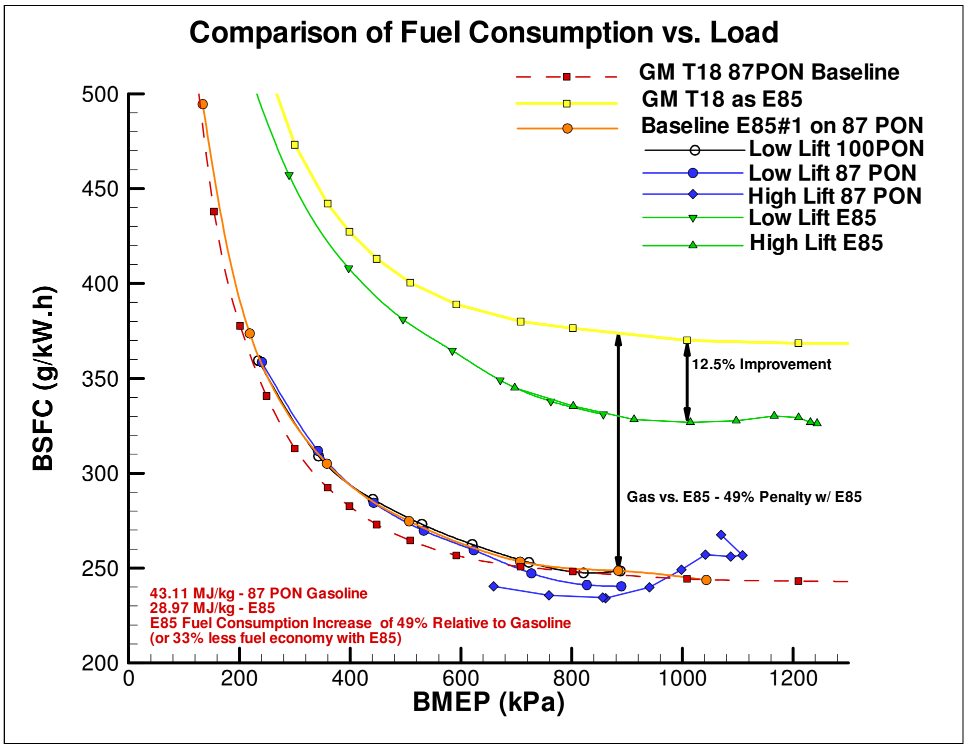

Figure 18) BSFC Comparison 2000 RPM Different engine configurations and test fuels.

Testing was conducted on the E85 optimized engine with E85, 87 PON and 100 PON gasolines. All testing was done at net stoichiometric conditions and MBT or knock limited timing. The 100 PON (106 RON) fuel was used for break-in and initial calibration development since it is highly resistant to knock and allowed safe operation during the initial testing. The 100 PON had similar BSFC performance to the initial engine, part of this was due to the higher engine efficiency being offset by a lower heating value partially attributable to its alcohol content (10%). The 87 PON fuel also had similar BSFC at low loads and reduced fuel consumption between 7 and 10 Bar BMEP. At higher loads the fuel consumption degraded due to spark retard for knock control. The E85 fuel was able to maintain MBT and resulted in a net fuel consumption reduction of 12.5% comparable to the calculated baseline. While a fuel consumption gap still exists between E85 and gasoline, further optimization will continue. Gains from optimization however are anticipated for both E85 and gasoline as the calibration matures. To fully leverage the E85 optimized engine the low end torque improvement with E85 should be leveraged by down speeding the vehicle. Use of more aggressive shift schedules on the vehicle can improve fuel economy when running on E85. This will be further refined as the project proceeds.

Emissions

Emission data was collected for the speed load maps presented. HC, CO, NOx, CO2, O2 and FSN were measured. In general, the emissions were acceptable and could be treated with a 3-way catalyst since the operation stoichiometric. NOx emissions were higher due to the increased temperature form the higher compression ratio at high load. The E85 NOx emissions were higher than gasoline although much of this is due to the required spark retard with gasoline. Particulate emissions for E85 were excellent and produced FSN numbers under 0.01 for the majority of the operation. Gasoline particulate was higher but still under 0.2 for the majority of the map. One exception was under low speed high load conditions. These conditions had late ignition timing (to control knock) and some scavenging which produced a higher in-cylinder equivalence ratio. An example of emission data is shown for the particulate FSN number for the gasoline speed load domain in Figure 19**.** Work will continue at the CTCM facility to improve the steady state calibration and move toward boosted and transient control.

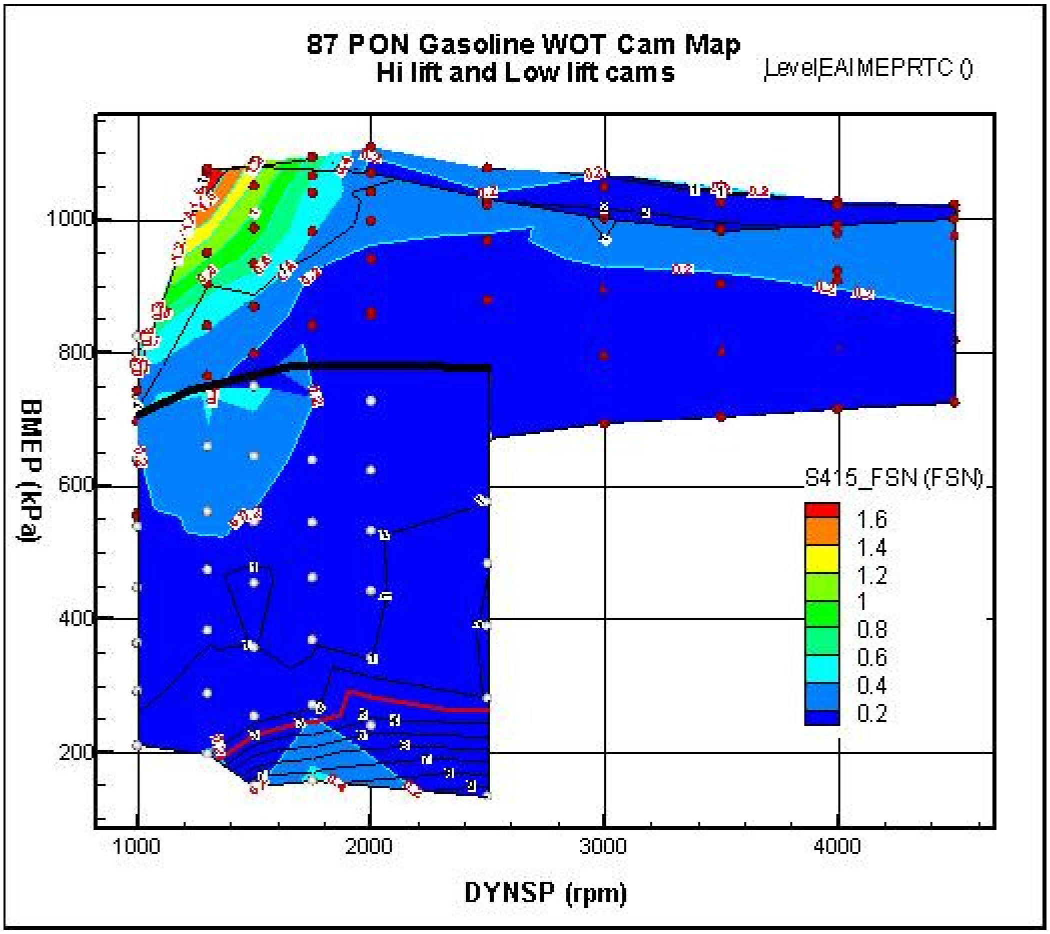

Figure 19) FSN Particulate for Gasoline speed load map

Quarter 4 2009

Phase 3 Task 3.0 –Steady State Engine Characterization using Optical Engine (7/09 – 12/31/09)

The optical engine is being tested using continuous lighting, due to a Copper Vapor laser high-voltage power supply breakdown. The 25kHz laser is waiting to be repaired. In the meantime, CFD models were developed and used to simulate the charge motion inside the modified engine combustion geometry.

Since regular projection lamps were used for light sources, only liquid phase was visible. The injected fuel was 100% pure Ethanol for all the OAE testing.
An image sequence of every 1.5 Crank Angle Degree (CAD) for homogeneous injection is shown in Fig. 11. The OAE was running at 1000RPM and 20mg of Ethanol was injected starting at 60CAD after intake TDC. The process of spray development and mixture formation was well visualized. Mixture of Injector B had less tumble motion because Injector B was aiming a point closer to the center of the cylinder. In other words, “off-centered” injector A added more momentum on the tumble motion drawn by the piston movement. Even though larger tumble motion preferred for better mixing, sprays targeting far from the center will hit the walls and become a source of unburned Hydrocarbon. Actually, the revised spray targeting of Injector B avoided the side wall wetting as Fig. 12 shows.

Images of injections with the same amount of fuel at different engine speed are shown in Fig. 14. In this figure, images are lined up with actual time elapsed after the injection. There is no clear difference in the spray shapes during the injection. However, after the injection, the images of 1000RPM show more fuel existence at the center of the cylinder than 600RPM. One reason to explain this is less surface wetting because of faster movement of the piston. And another reason should be enhanced tumble along the cylinder surface and the piston top preventing a spread of fuel droplets.

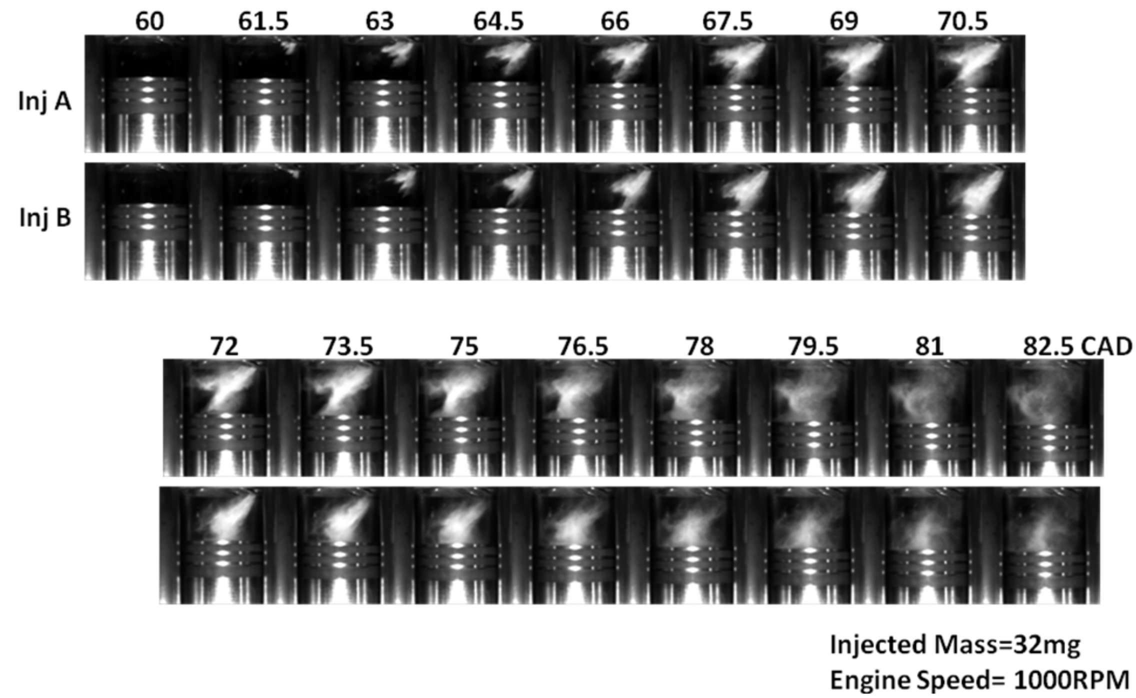

Figure 11) *OAE Spray visualization of early injection case (SOI: 60°ATDC) with different injector*

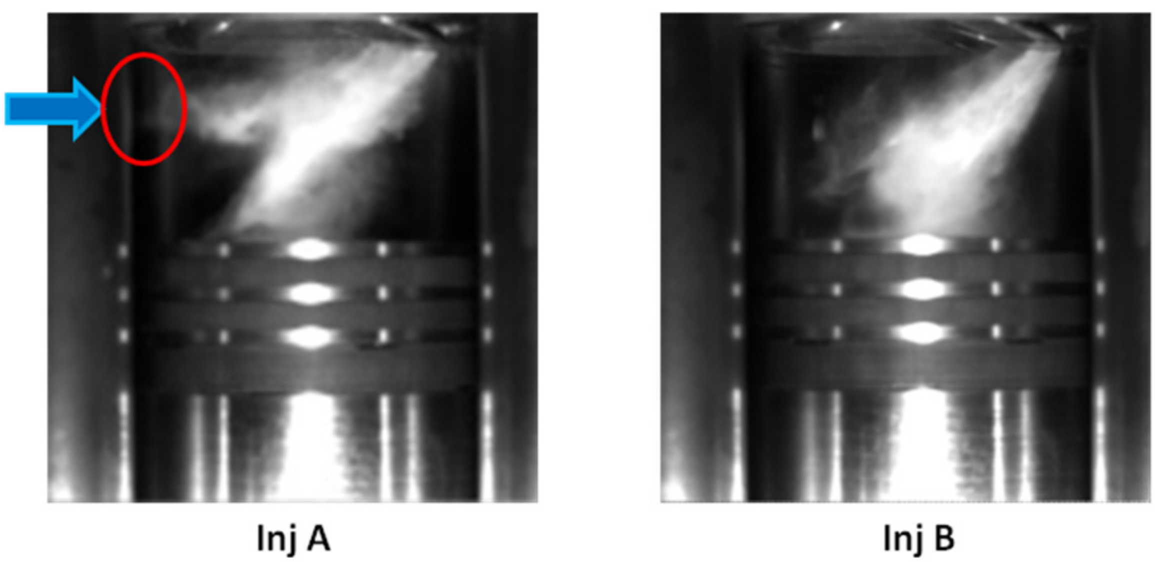

Figure 12) *Side wall wetting for OAE early injection case (SOI: 60° ATDC) taken at 12° ASOI*

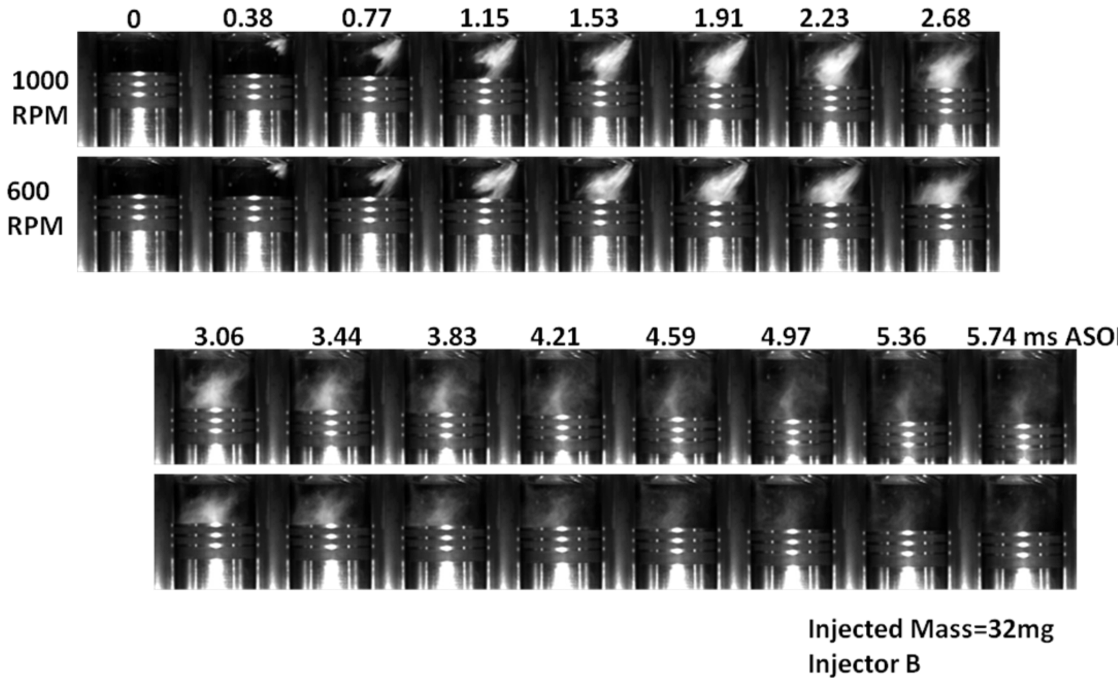

<u>Figure 13)</u> OAE Spray visualization of Early injection case (SOI: 60^o ATDC) with different speed

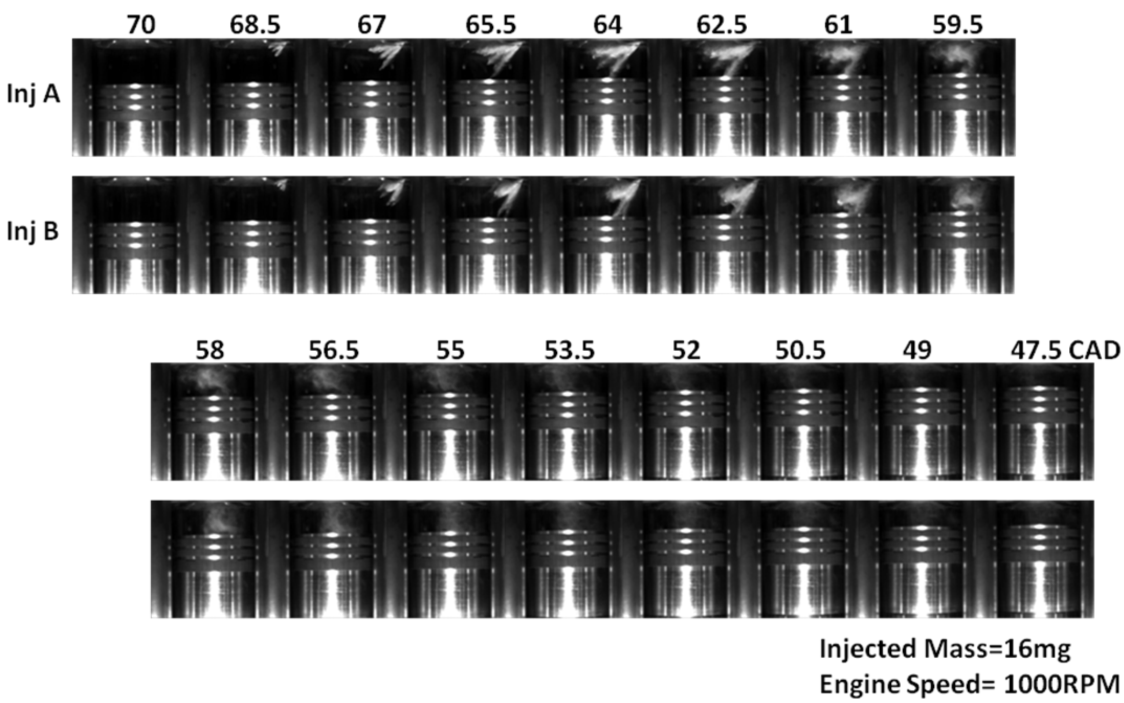

<u>Figure 14)</u> OAE Spray visualization of Late injection case (SOI: 70^o BTDC) with different injectors.

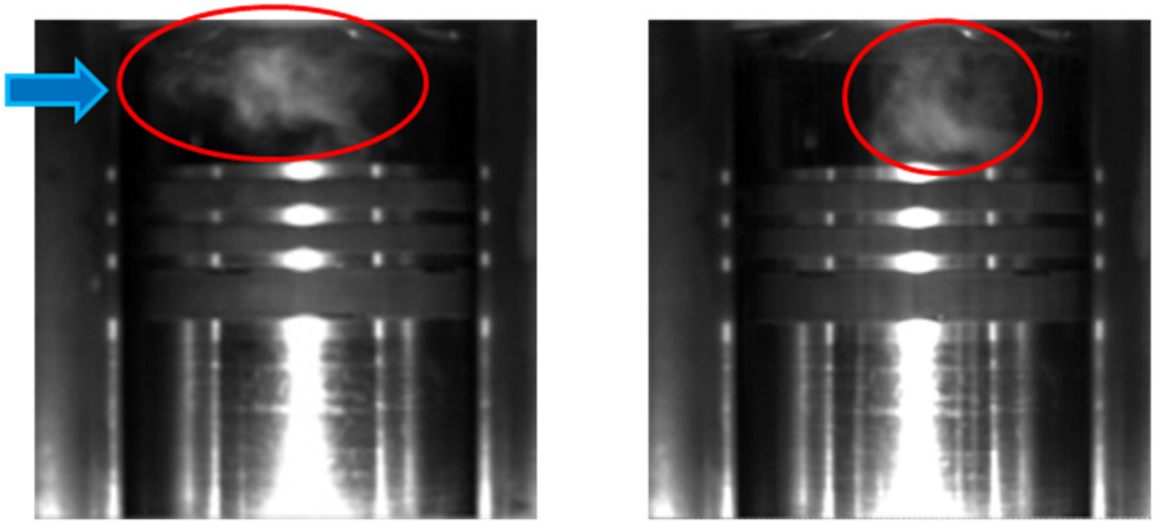

<u>Figure 15)</u> Mixture accumulation of Late Injection (SOI: 70^o BTDC) taken at 15^o ASOI)

Fig. 15 shows a stratified injection starting at 70deg before compression TDC. The injected fuel was 16mg of Ethanol and the engine speed was 1000RPM. Since the fuel was injected at compression stroke, the higher ambient pressure suppressed the spray propagation shorter and narrower. At 64CAD, lower spray hit the piston top. A piston impingement must be managed well in order to avoid hydrocarbon emissions as discussed in [4]. As Fig. 16 shows, the spray of Injector B tended to accumulate in the center of the cylinder due to the spray targeting. This is very critical advantage if the engine is running at stratified mode which needs fuel mixture near the spark plug.

Typical CFD simulation, using KIVA with Automotive Grid Refinement, is used to validate the in-cylinder fuel spray and mixing visualization and are shown for the new injector in Figures 16 for the liquid spray behaviors and compared to OAE visualization suing continuous lighting. Figure 17 shows the equivalence ratio evolution at this condition. More validation of the CFD and OAE experiment will continue for the next phase to improve the engine performance using mixture motion and multiple injections.

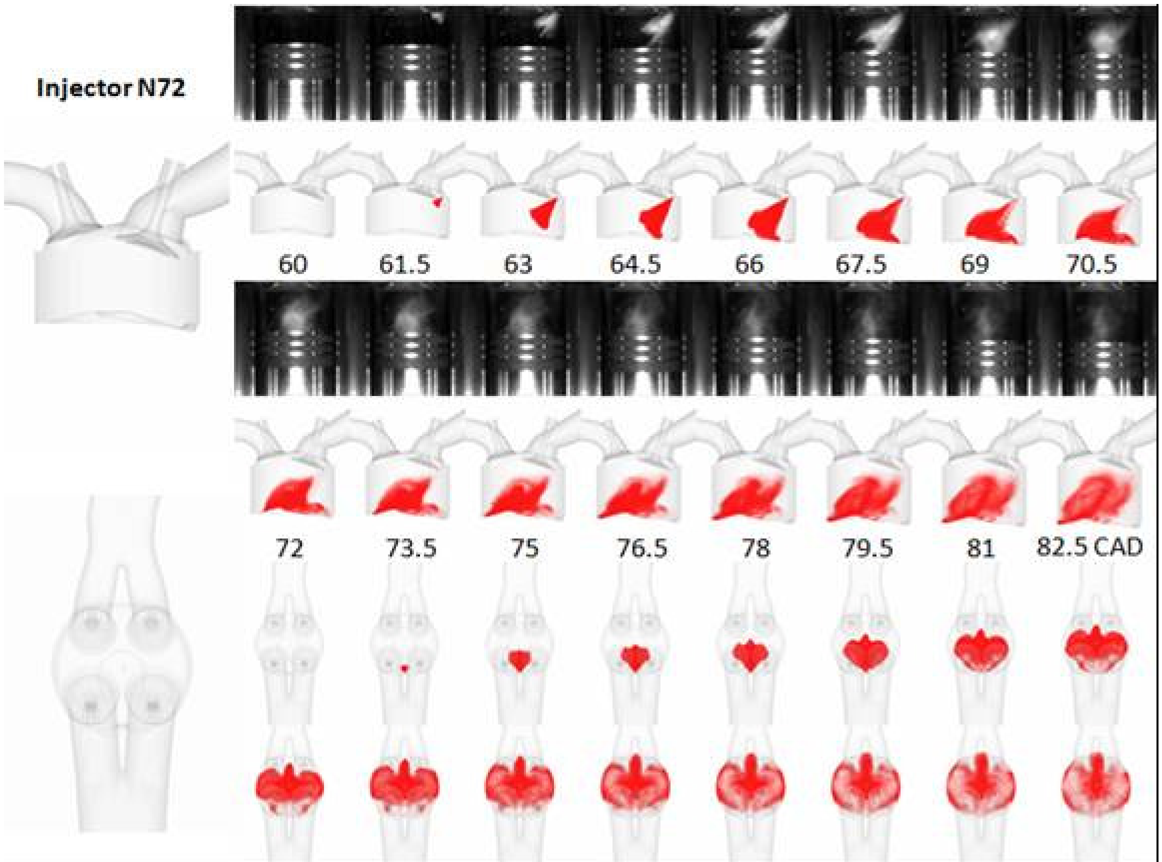

Figure 16) *comparison of fuel spray interactions with mixture motion and combustion chamber for early injection case (SOI at 60° ATDC, 1000 rpm 20 mg)*

Figure 17) Fuel-Air mixing simulation for early injection case (SOI at 60^o ATDC, 1000 rpm 20 mg)

Phase 4 Task 1 –Implementation and Test of Ethanol-Optimized Engine (7/09 – 12/31/09)

Spray timing studies

Work continued to refine the engine operation by determining the effects of injection timing on engine performance. Optimal injection timing to minimize combustion variation, fuel consumption and emissions was studied over the range of operation most important for normal driving. Work carried over from the previous quarter to identify trends in injection timing for 2 sets on injector designs with both LIVC (Late Intake Valve Closing) and EIVC (Early Intake Valve Closing) strategies for E85 and 91 RON E0 gasoline.

Studies with the LIVC strategy showed robust operation on E85 and gasoline due to high rates of charge motion which promoted good mixing and AF homogenization. Wide injection timing windows were identified with low soot and good combustion stability allowing injection timing to be optimized based on power or fuel economy. Figure 18 shows an example with the N72 injector at 1500 RPM on the high lift LIVC Cam.

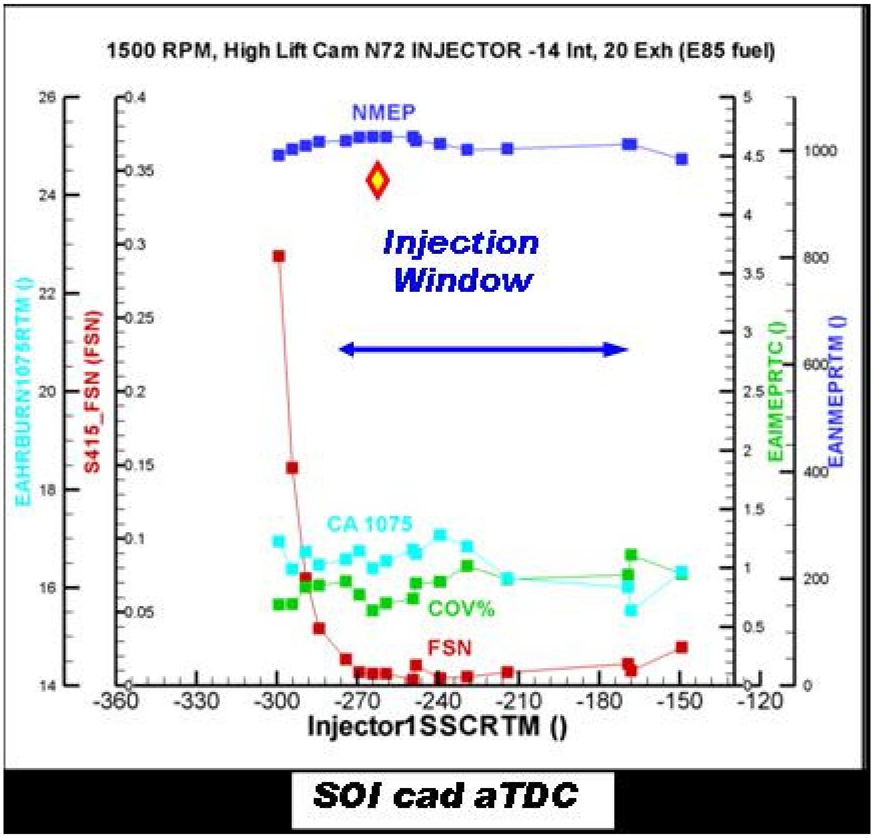

Figure 18) Effect of injection timing on soot and combustion stability window. 1500 RPM, LIVC, N72 Injector, E85 Fuel, Diamond indicates timing selected for best power.

The low lift cam resulted in lower charge motion and reduced the injection window. At higher loads, optimization of the spray timing could be used to enhance mixing and charge motion. Figure 19 shows an injection timing window on the low lift cam for E85 fuel and the N72 injector. The window is shifted later, thus allowing more time for piston clearance. It is also evident that the later injection provides spray induced charge motion which promotes mixing and enhances flame speed.

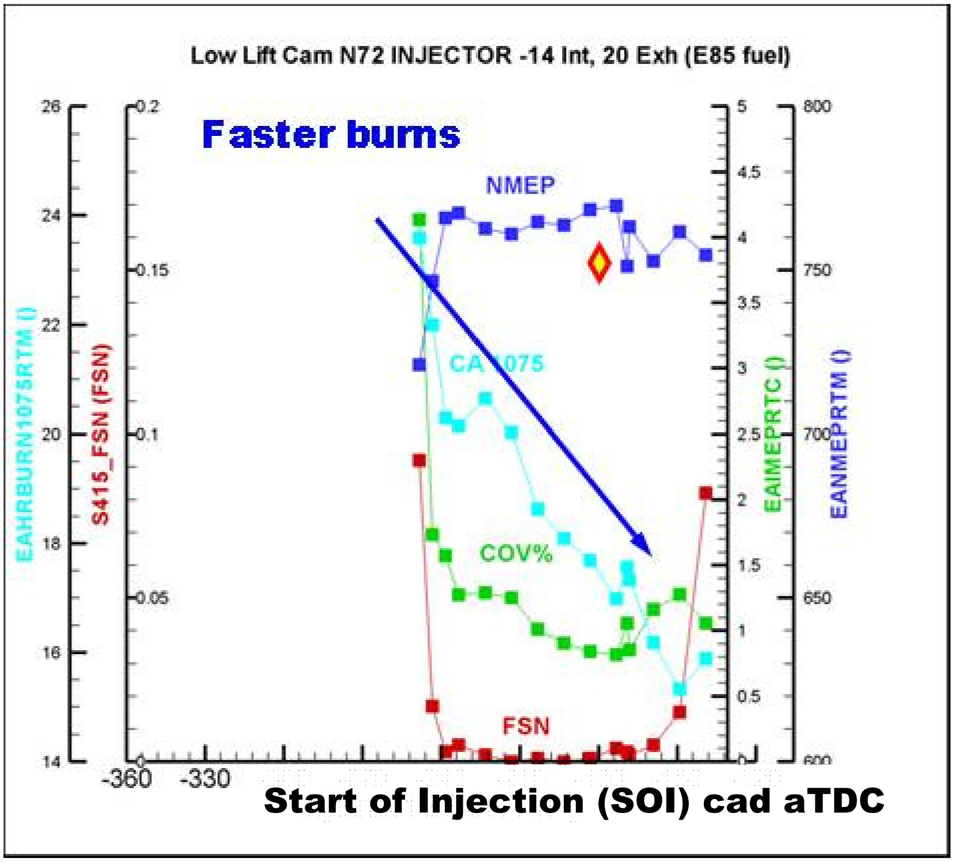

Figure 19) Effect of injection timing on soot and combustion stability window. 1500 RPM, EIVC, N72 Injector, E85 Fuel, Diamond indicates timing selected for best efficiency.

Concern over the smaller injection timing windows on the EIVC cam prompted a study with gasoline at different operating conditions. Injection timing sweeps were conducted at 3 loads; nominally 2, 4 and 6 Bar BMEP on the EIVC cam using un-throttled operation. The 6 bar operating point provided an acceptable injection window however as the load was reduced the injection window was smaller and soot emissions increased to an unacceptable level. These results are presented in Figure 20.

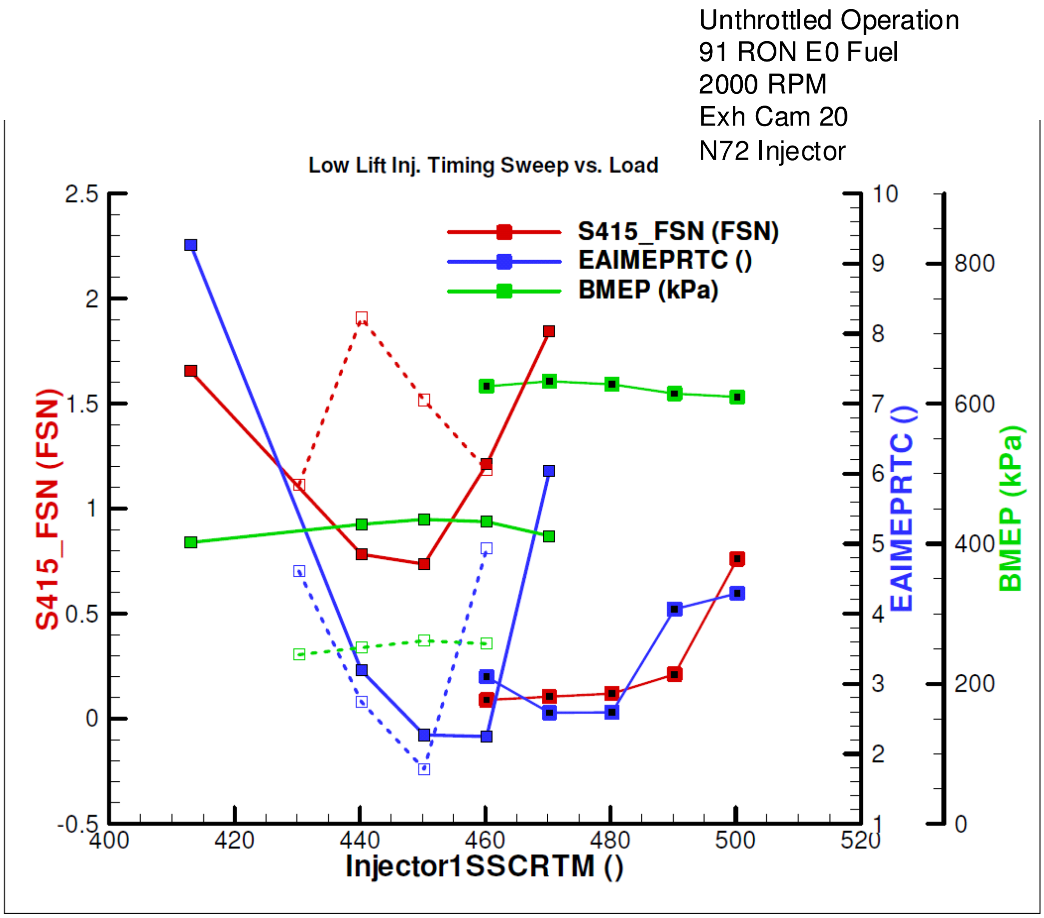

Figure 20) Effect of injection timing on soot and combustion stability window. 2000 RPM, EIVC, N72 Injector, Gasoline, 3 different loads.

Lower soot numbers were achieved under un-throttled conditions with the 736 injector however low loads still presented a combustion stability problem under un-throttled conditions. Because of the better gasoline soot robustness, the 736 injector was focused on to further optimize engine performance.

The 736 injector's optimal timing window was typically shifted earlier due to its lower skew angle which did not require waiting for the piston to clear the spray plume. Typical injection timings were -295 +/- 15 deg before TDC firing (425 cad). At lower loads the optimal injection timing shifted earlier for best fuel consumption for E85. At low loads the injection window also narrowed with the 736 injector. Figure 21 shows a low load timing sweep with E85 using a fixed pulse width sweep, the most efficient timing was an early Injection.

Full optimization work for spray timing was completed on the 736 Injector for E85 operation and will be discussed later in the report. In general, for best fuel consumption, the timing shifted earlier as the load was reduced.

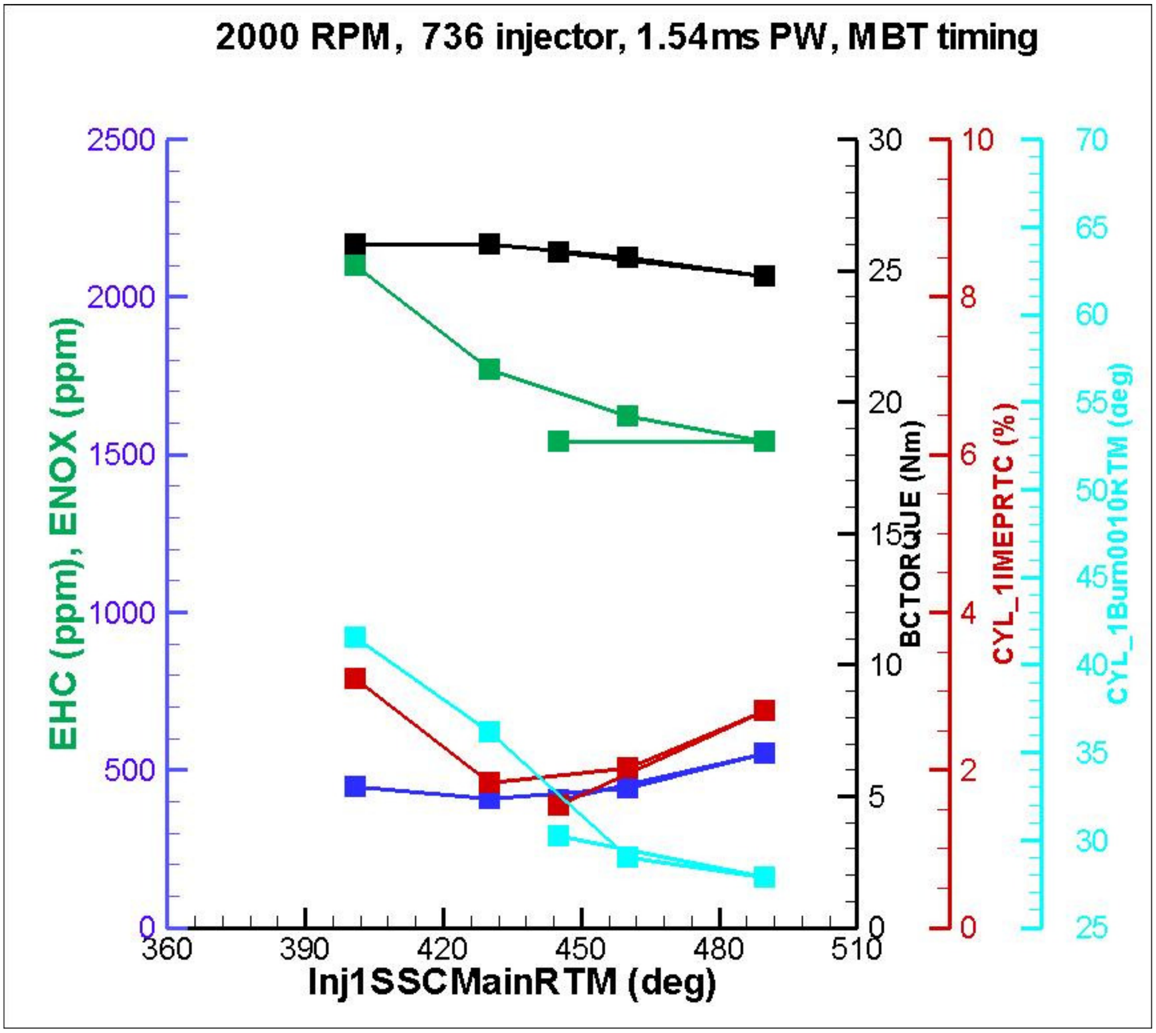

Figure 21) Effect of injection timing on soot, emissions and combustion stability window. 2000 RPM, EIVC, 736 Injector, E85 fuel.

Cam throttle studies

To improve fuel consumption load control via cam phasing was compared to traditional throttle control and the tradeoffs were evaluated. Modeling and previous work had demonstrated the potential for improved fuel consumption by optimizing the cam phasing and using throttle primarily to control internal EGR; this resulted in a decrease in fuel consumption as well as a decrease in NOx production. At low loads, where charge motion was poor, throttling required a longer stroke using the EIVC strategy which provides better mixing. Two tests were run at the switch point for the cams under un-throttled conditions. Fixed fueling sweeps were evaluated to identify the best fuel consumption. These tests were done with fixed injection timing to isolate the throttling tradeoff. Figures 22 and 23 are for the LIVC and EIVC strategy respectively. Optimal cam timing resulted in partial throttle producing a map of 85-90KPa. The LIVC strategy (Fig. 22) was superior for charge motion, which reduced soot and fuel consumption relative to the EIVC strategy. HC's and NOx were similar. The LIVC strategy did show good dilution tolerance enabling low NOX but the high residual rates produced EGR induced knock which required spark retard which hurt efficiency even though throttling was decreasing. Due to E85's high knock resistance, higher EGR tolerance may be enabled with MBT spark timing, this will be evaluated in future work.

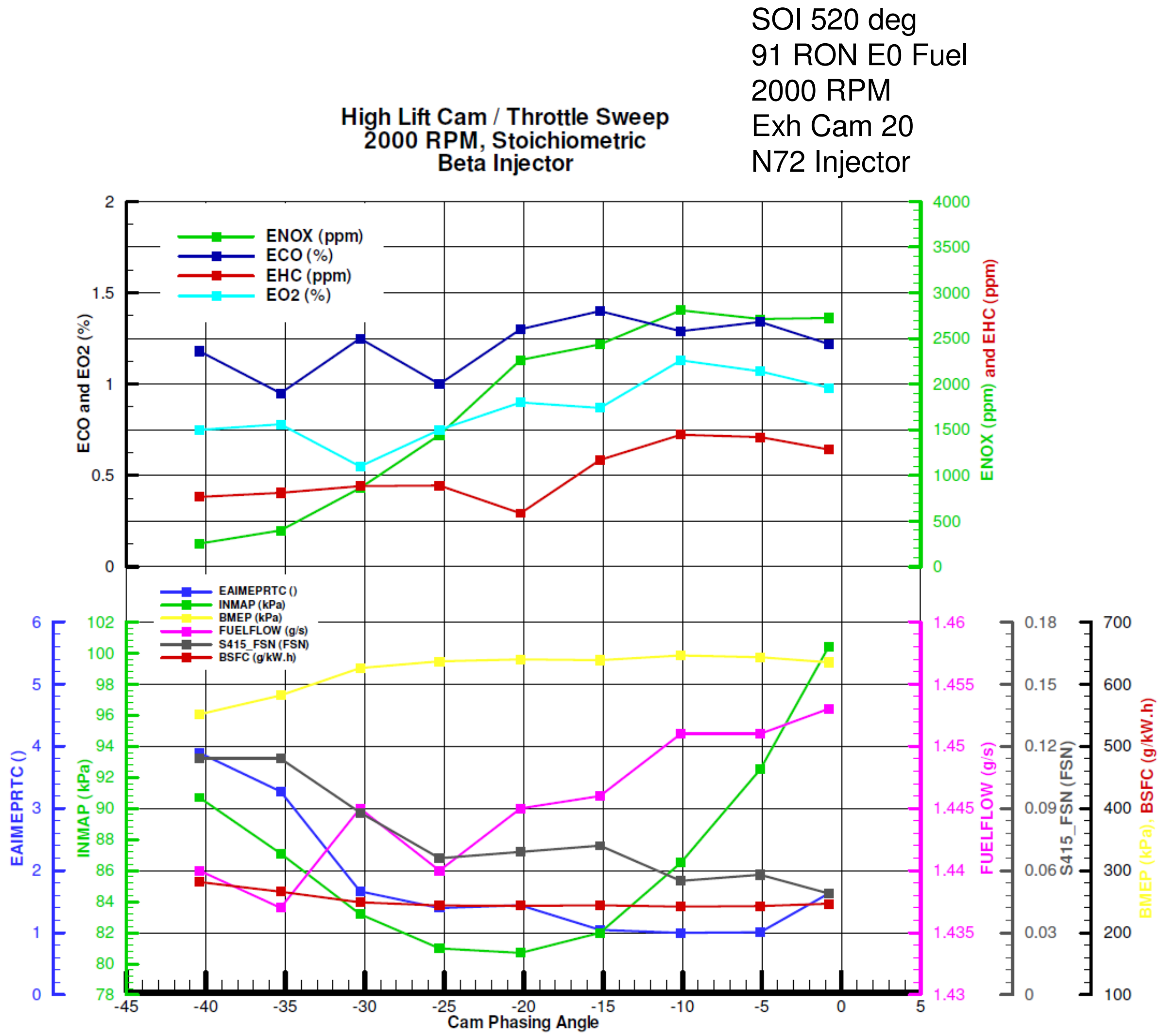

Figure 22) *Effect of cam / throttle tradeoff on soot, emissions and combustion stability 2000 RPM, LIVC, 736 Injector, Gasoline.*

The EIVC strategy, (Fig. 23) results in an increase in NOx as the system is throttled since a larger stroke is required thus reducing valve overlap. The fuel consumption is still reduced, presumably due to the significant reduction in HC's and soot and improved combustion stability.

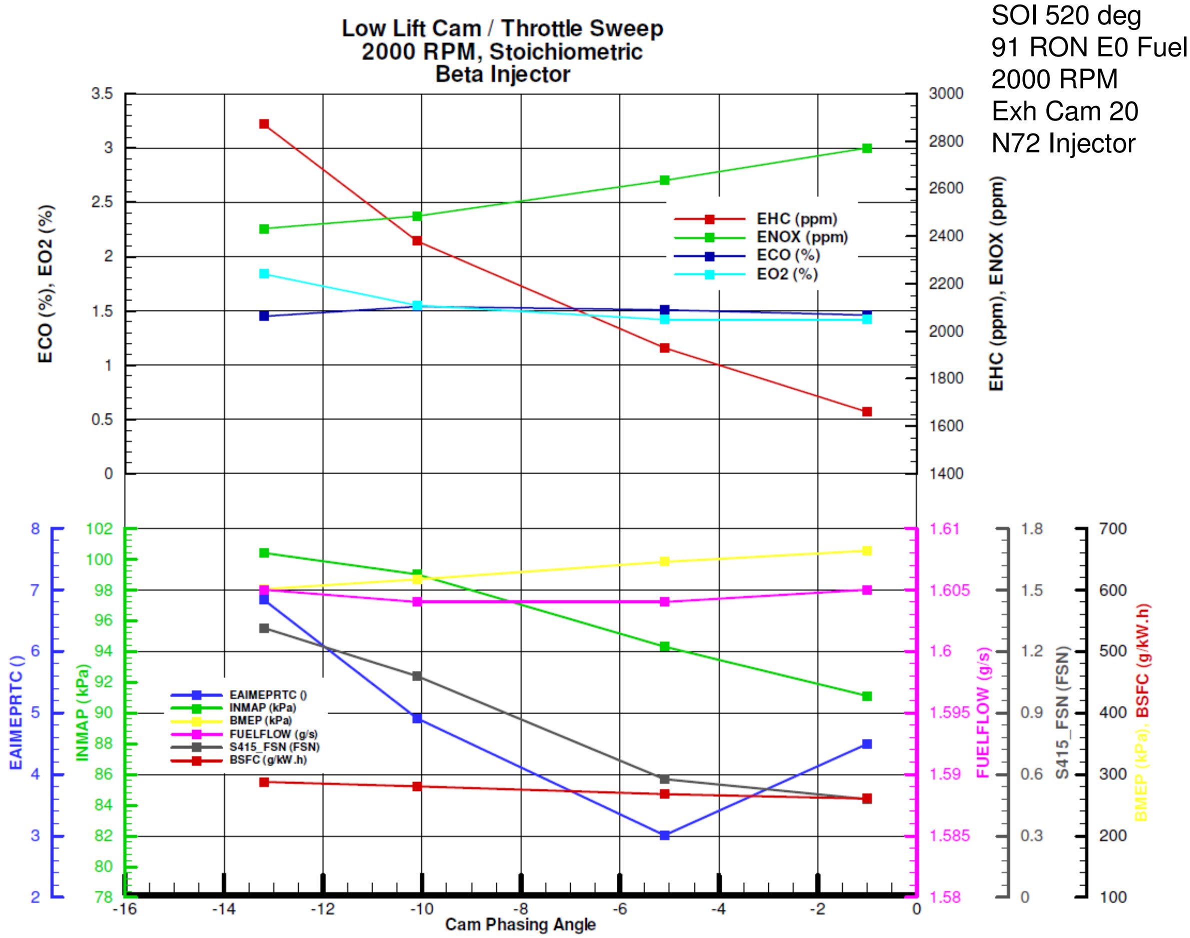

Figure 23) Effect of cam / throttle tradeoff on soot, emissions and combustion stability 2000 RPM, EIVC, 736 Injector, Gasoline.

Cam optimization

To minimize fuel consumption, optimization of the cam phasers, throttle, injection timing, injection pressure and spark timing is required. To demonstrate the nature of the cam phasing relationships, a study is presented based on the use of the LIVC cam on E85 fuel with the 736 injector. The study was conducted nominally at a 2 Bar BMEP point using a fixed fueling strategy to accelerate testing. Figure 24 shows the cam domain that was tested. The cam phasers allow the engine to run in different residual retention regimes including conventional valve overlap and NVO (Negative Valve Overlap). (Note the valve icons included on the chart for clarity.) The dark crosshairs on the chart indicate the appropriate phasing for exhaust valve closing at TDC and intake valve opening at TDC. For this study MBT timing was maintained at all test points and injection timing was maintained at 295 deg before TDC firing which showed to be robust for all cases. Fueling was fixed and throttle was adjusted to maintain stoichiometric operation in all cases. Load was allowed to float, thus the highest output produced the lowest BSFC. Combustion stability was good for the entire map typically less than 2% for all cylinders; one cylinder reached the 3% COV limit at the highest overlap point which also produced the lowest BSFC.

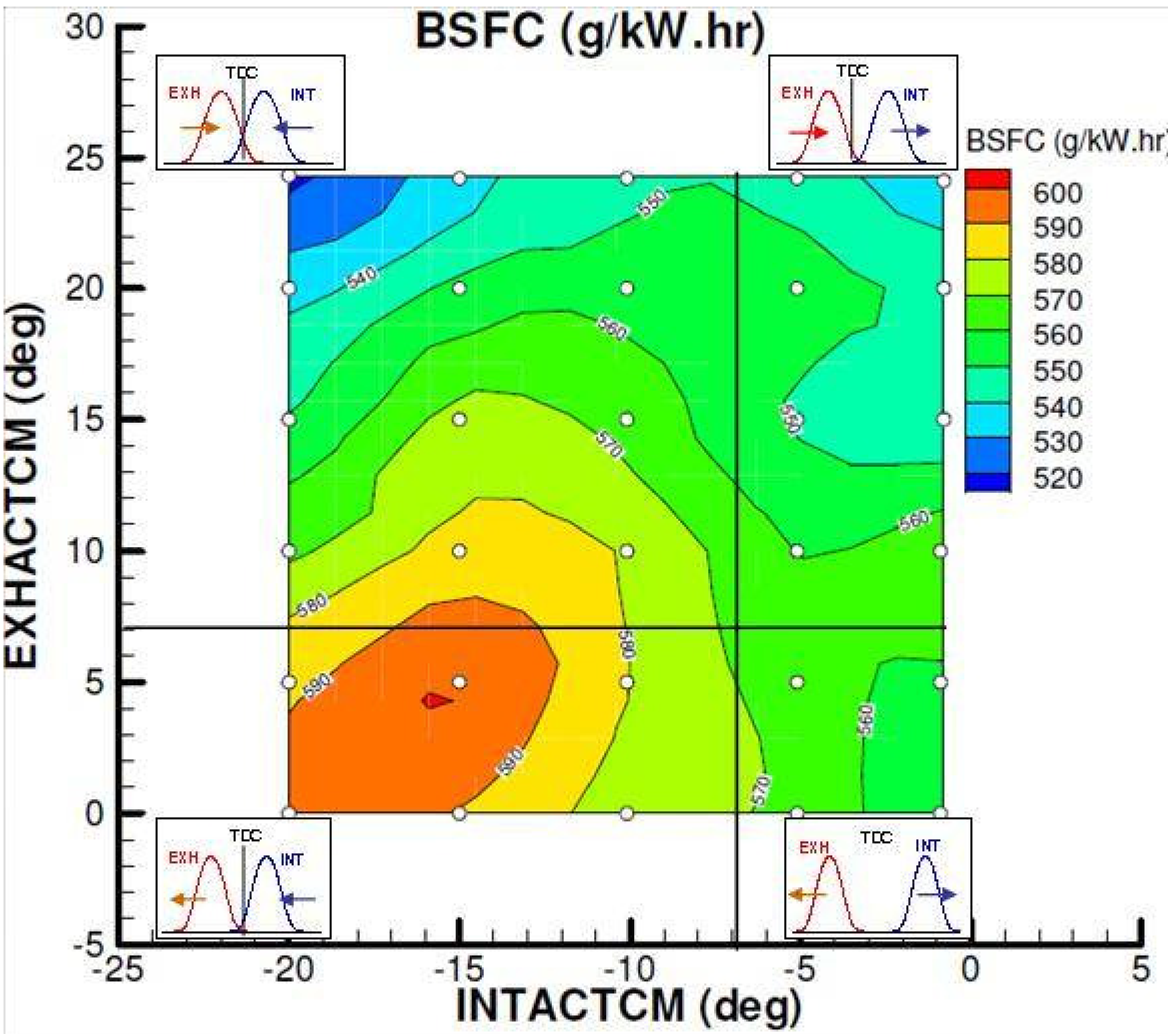

<u>Figure 24)</u> Cam optimization 2 bar Nominal BMEP Fuel consumption map 2000 RPM, LIVC, 736 Injector, E85, fixed fuel, stoichiometric, MBT timing 295 bTDC SOI

The high overlap condition was also highly advantageous for NOx due to high internal EGR rates. Figure 25 shows the NOx map over the domain tested. Low NOx (under 150ppm) was produced at the minimum BSFC point. This result was compared to optimized results for the EIVC strategy and produced similar BSFC (+½ %). Soot and HC emissions were low over the domain tested. Additional testing at other loads is planned to evaluate the potential of LIVC with high internal EGR for fuel consumption reduction over the EIVC operating domain.

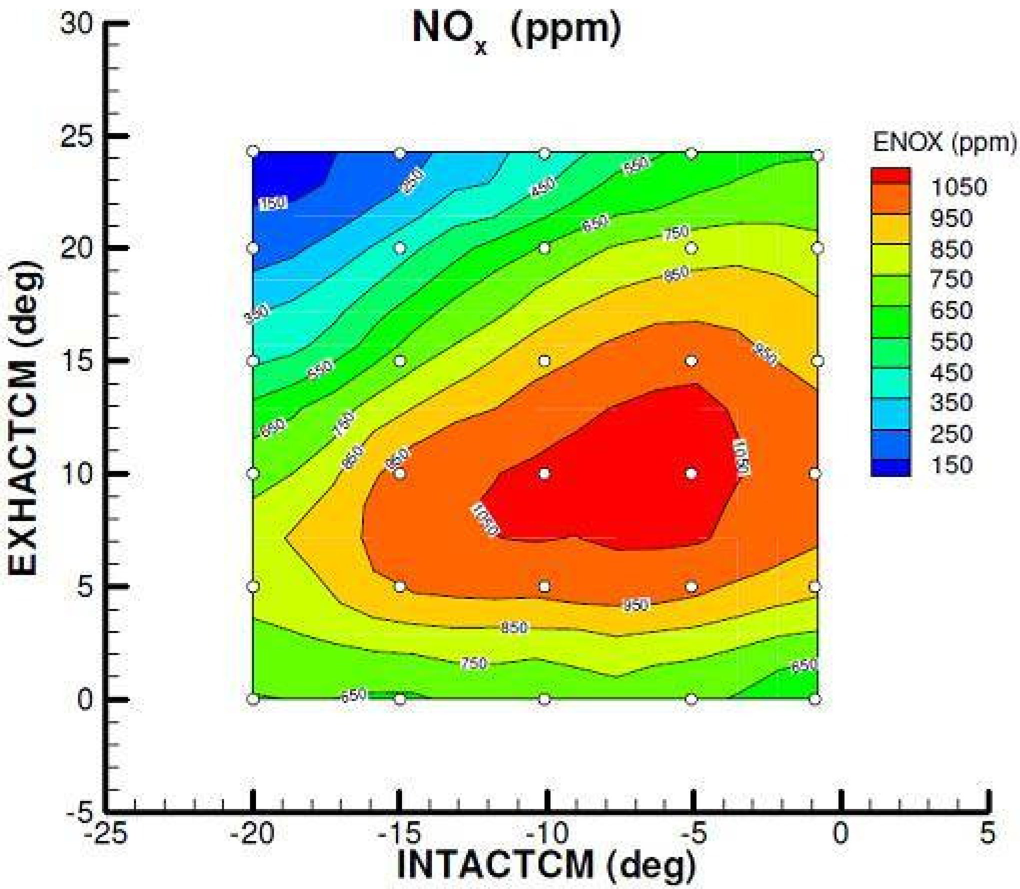

Figure 25) Cam optimization 2 bar Nominal BMEP Fuel consumption map 2000 RPM, LIVC, 736 Injector, E85, fixed fuel, stoichiometric, MBT timing 295 bTDC SOI

Engine control optimization

A full optimization of cam timing, throttle, spark timing and injection timing was completed from 1000-3000 RPM and from maximum load to idle using the EIVC strategy with the 736 injector operating on E85. Fuel consumption was minimized while maintaining good combustion stability (typically under 2%) and near zero soot emissions. NOx was also significantly reduced due to the use of internal EGR. Internal EGR was also beneficial for fuel consumption.

Hydrocarbon emissions were low at all conditions other than an acceptable increase at low speed idle. Fuel consumption was reduced up to an additional 5% relative to un-throttled operation, thus extending the speed load domain showing an increased improvement over the base engine.

Comparison to un-throttled operation

A comparison is made between pure un-throttled operation and the optimized results. Figure 26 shows the combustion stability map for the optimized calibration and the un-throttled operation. By using cam phasing and optimal injection timing, good combustion stability was maintained and the high speed low load issue was eliminated. At idle, spark was retarded 20 degrees from MBT to confirm authority for idle speed control across zero net torque*.

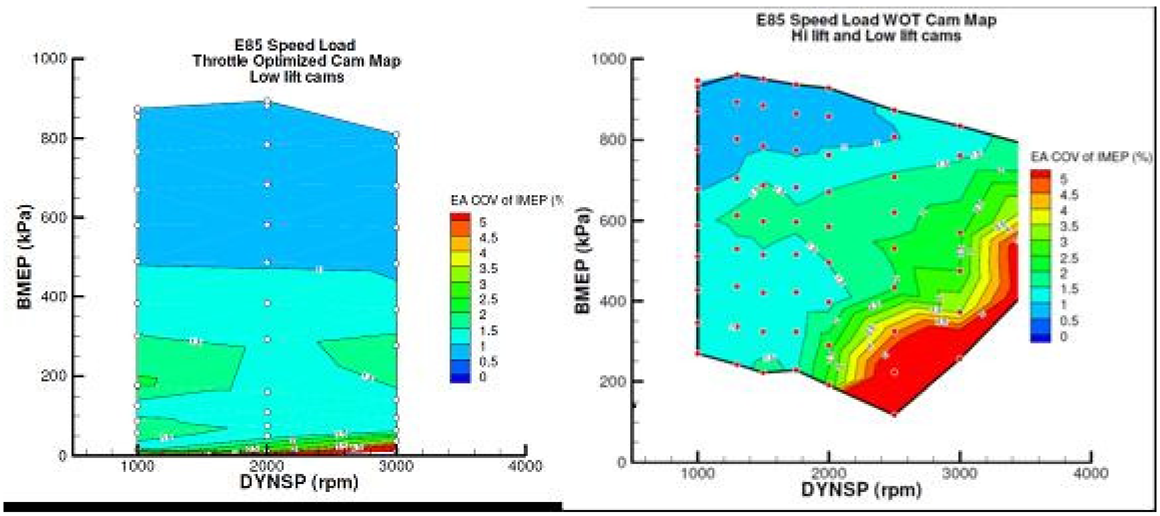

*Figure 26) Control optimization vs. Un-throttled combustion stability map, EIVC, 736 Injector, E85, stoichiometric, MBT timing**

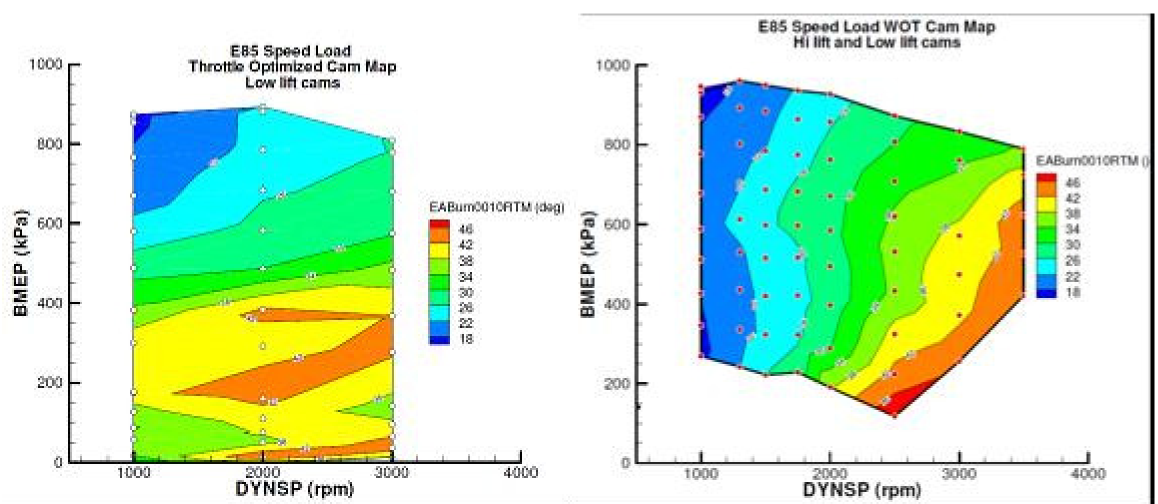

*Figure 27) Control optimization vs. Un-throttled 0-10 Burn Duration map, EIVC, 736 Injector, E85, stoichiometric, MBT timing**

Figure 27 shows the difference in initial flame development. Where allowable, internal EGR was used, which resulted in slower burns. By optimal use of cam timing and injection timing combustion stability allowed increased internal EGR resulting in lower NOx emissions, Figure 28.

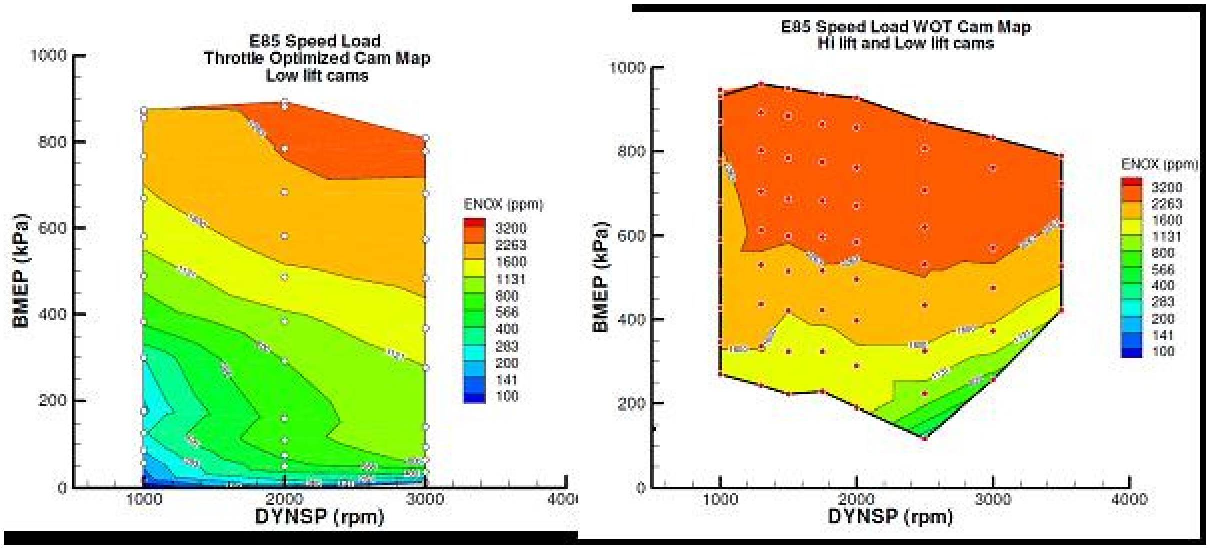

*Figure 28) Control optimization vs. Un-throttled 0-10 Burn Duration map, EIVC, 736 Injector, E85, stoichiometric, MBT timing**

Engine control parameters

The control parameters for the optimized calibration are shown in Figures 29-32. Intake cam phasing, exhaust cam phasing, injection timing and MBT Spark were optimized for E85 fuel with the 736 injector using the EIVC cam.

These calibration maps are based on a single injection strategy and provide a good baseline as work progresses towards evaluating the use of multiple injections and enhanced charge motion which offer potential for further improvements in fuel economy.

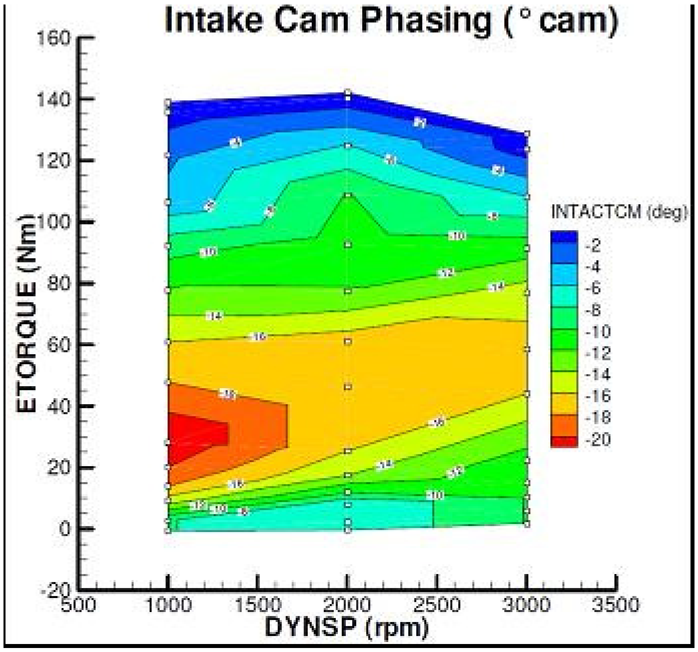

Figure 29: The intake cam operates with very light throttle down to 3-4 bar BMEP (48-64 NM). As it is phased earlier it is also increasing the valve overlap thus allowing retention of internal EGR. At 2-3 bar BMEP (32-48 NM) the stroke is increased to improve charge motion for combustion stability.

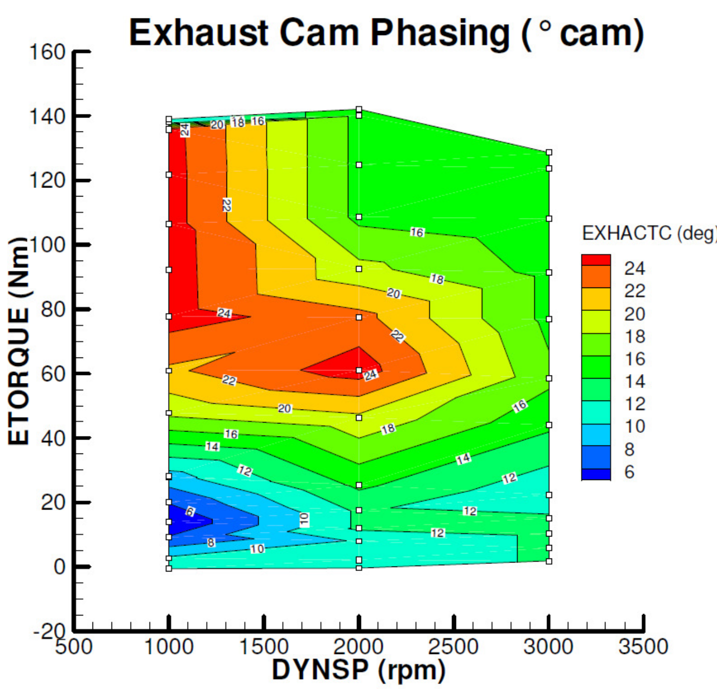

Figure 30: The exhaust cam is used for control of internal EGR, maximum authority is used at 3-5 bar BMEP. Valve overlap is reduced at low loads to

maintain combustion stability. A significant increase in throttling is required at loads below 3 bar BMEP due to the reduced use of overlap for internal EGR.

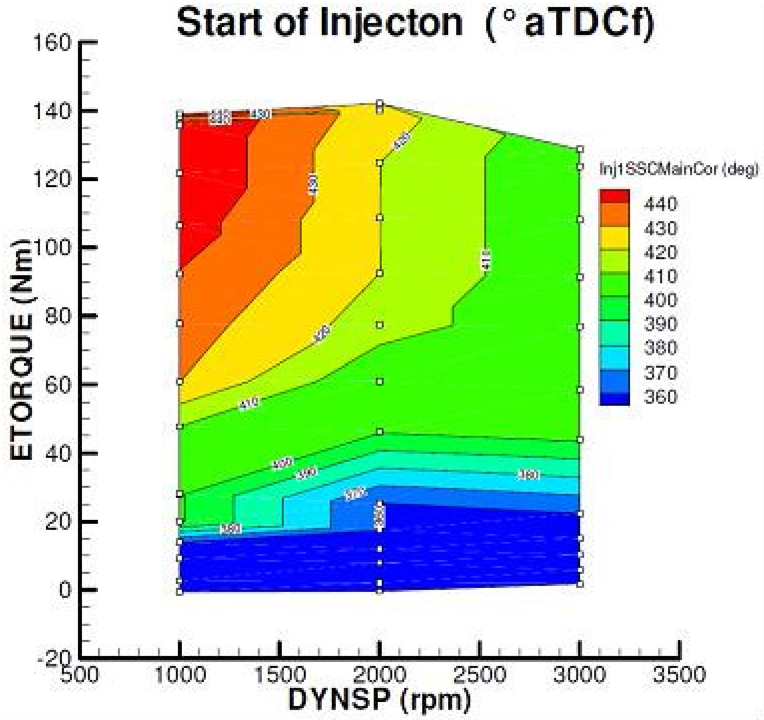

Figure 31: Injection timing 360 =TDC gas exchange, 440 =280 cad bTDC firing. Injection timing was selected for best BSFC.

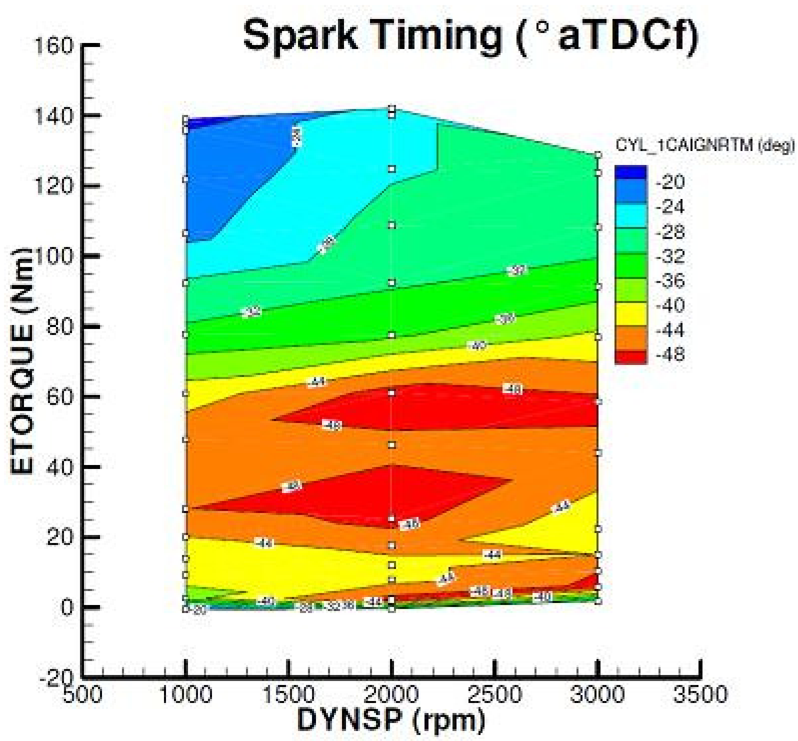

Figure 32: MBT Spark timing map.
Advanced spark results from high internal EGR at lower loads.

Fuel consumption and Emissions status

The current best BSFC map is shown in Figure 33. Although not the entire operating range of the engine it is the most important portion as it relates to real world driving and fuel economy. Figure 34 shows a comparison of fuel consumption improvement to date at 2000 RPM. By optimizing control with internal EGR additional gains of up to 5% were achieved (red line in figure 32) over un-throttled operation and extending the operating window showing a 12% + improvement over the base engine. Additional work will focus on further improvement in the base engine operation. In addition due to the high low end torque without spark retard vehicle optimization using down-speeding with E85 offers additional fuel economy improvements.

Emissions for HC's (Figure 35) and NOx (Figure 36) are also presented. E85 is very good for particulate emissions which are very low.

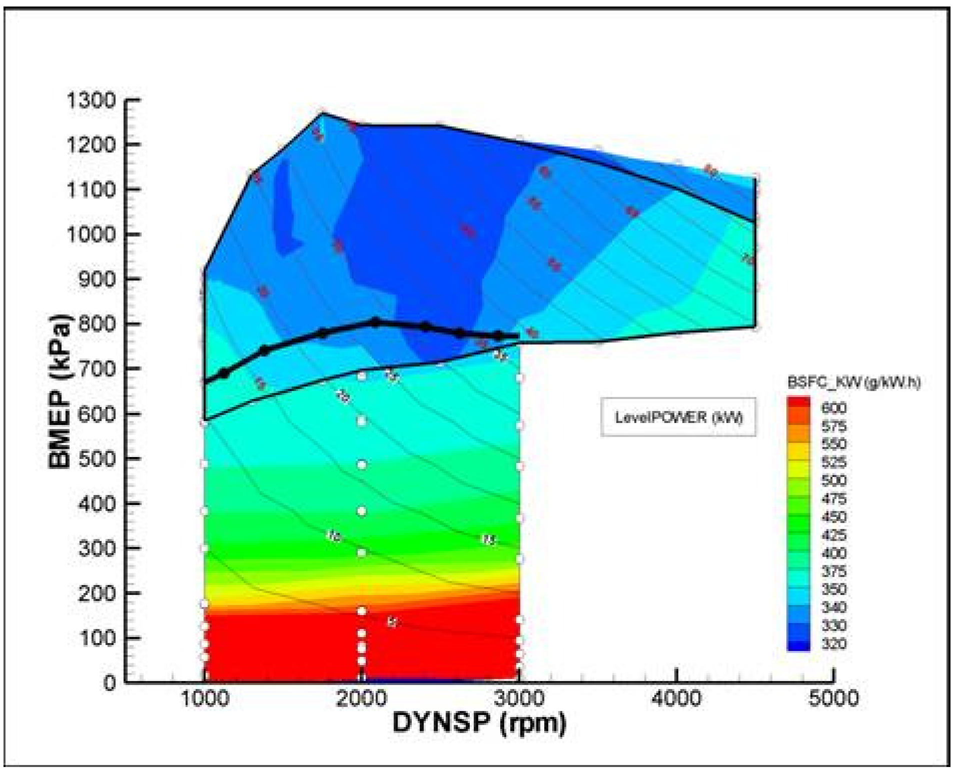

Figure 33) BSFC Map for E85 Fuel, 736 injector, single injection optimized calibration as of Q4 2009

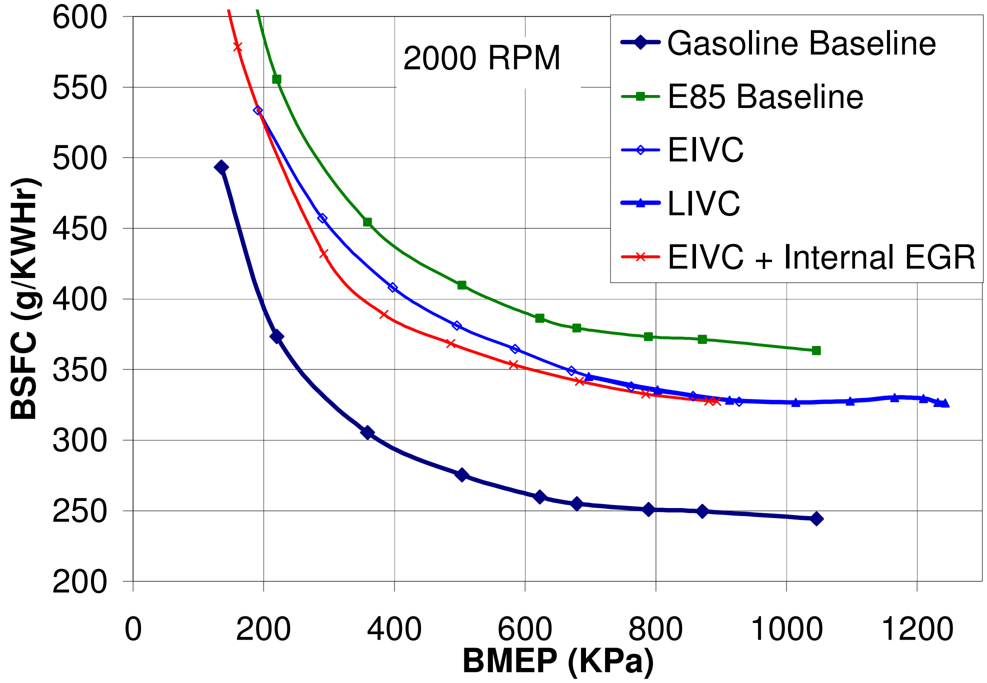

Figure 34) BSFC improvement 2000 RPM for E85 Fuel

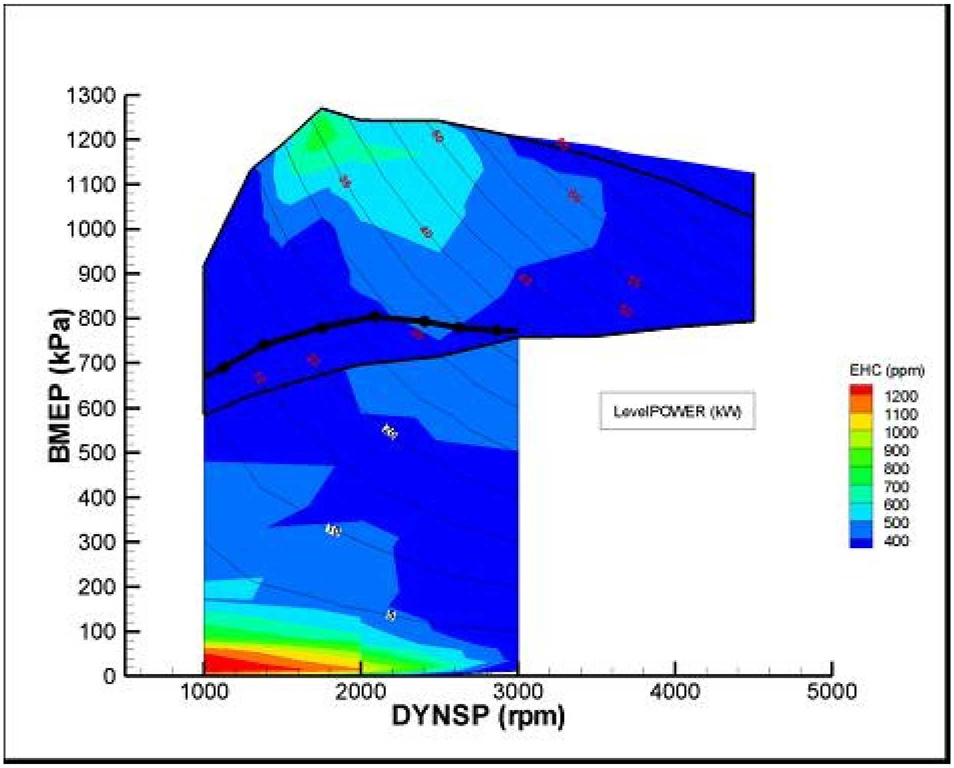

Figure 35) Hydrocarbon emission map E85 Fuel

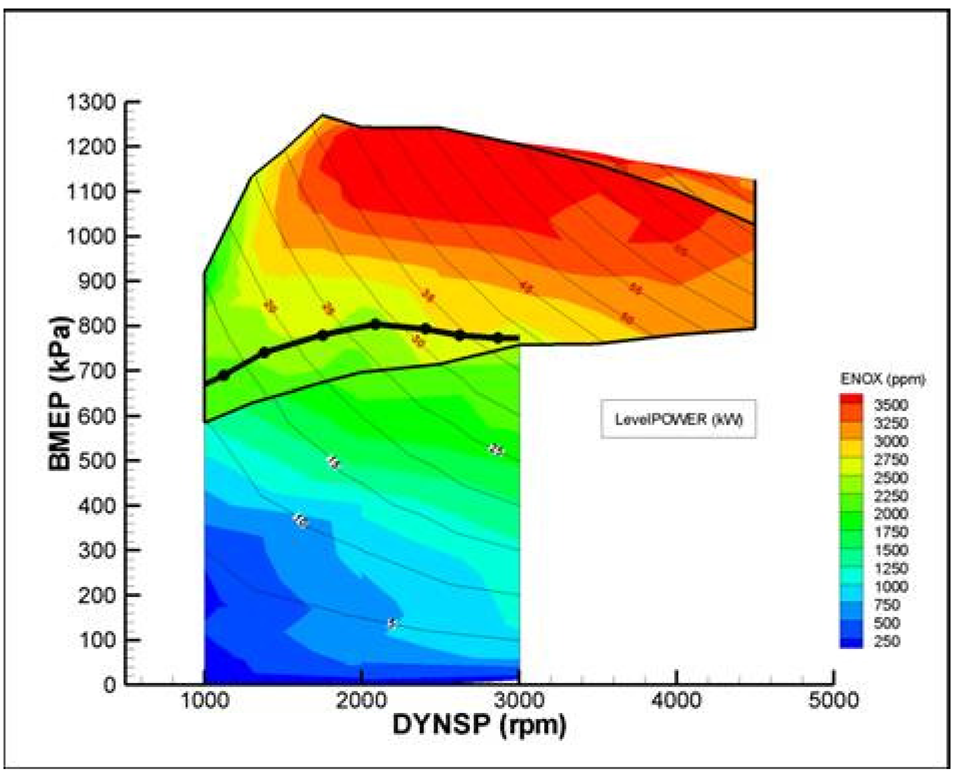

Figure 36) NOx emission Map E85 Fuel

Quarter 1 2010

Phase 3 Task 3.0 –Optical engine charge motion study (1/1/10 – 3/31/10)

Optical engine tests were carried out to investigate the effects of injection timing on the bulk flow and charge motion, in order to better correlate and interpret the observed multi-cylinder dyno engine test results, and to validate the CFD predictions. Examples using Mie scattering from the injected in-cylinder liquid spray are shown below in Fig. 1. If the fuel is injected after 120CAD, no significant wall impingement was observed, the ideal scenario of the spray chasing the piston and contained within the cylinder wall result in minimized wall impingement. This is confirmed by the multi-cylinder dyno engine tests, where the reduction in wall impingement manifested as lower unburned hydrocarbon and soot emissions. There are also significant differences in the mixing pattern for injection between the window of 120 and 180CAD.

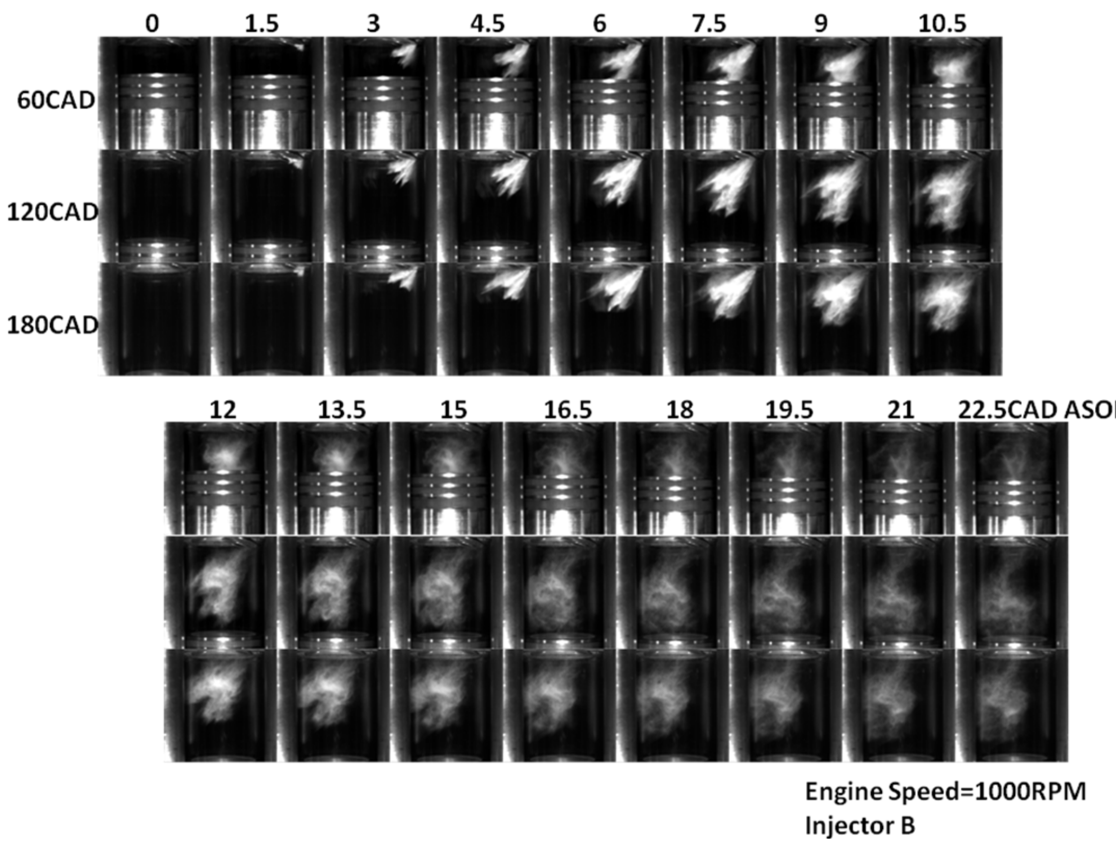

Fig. 1 Effect of injection timing for the homogeneous operation

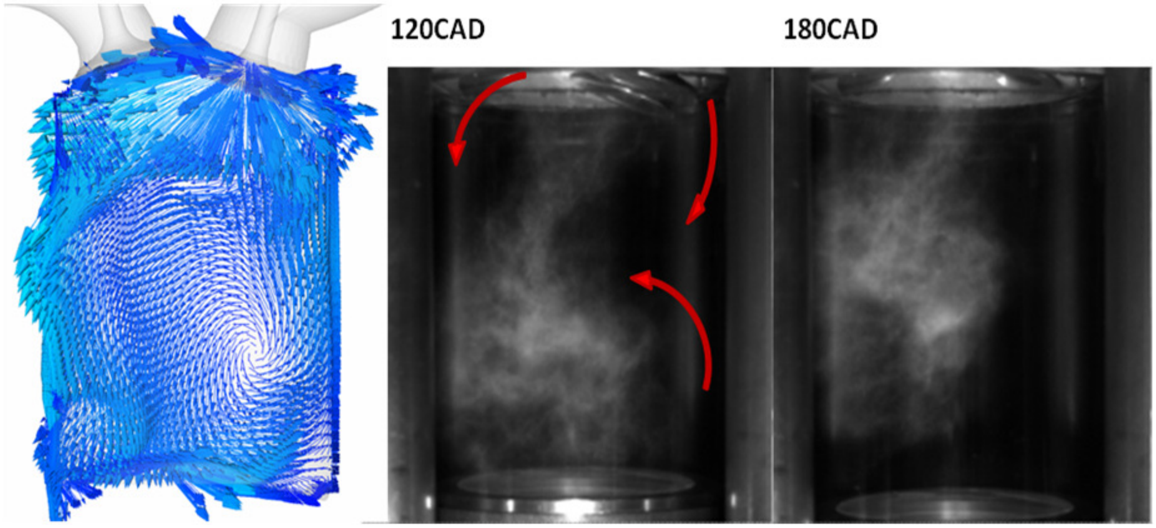

Fig. 2 Effect of injection timing on mixing at 22.5CAD after start of injection

Figure 2 shows the images at 22.5CAD after start of injection (ASOI) for two injection timings along with the velocity vector plots from CFD at the center plane for 120CAD injection. Injection during the intake stroke after the bulk tumble flow motion become the strongest, ca. at 90 CAD ATDC is shown to assist with the mixing process.

The effect of injection timing on bulk flow motions and fuel-air mixing can be better visualized using CFD. Post-processing the integral analysis to obtain the wetted fuel footprints and mass is shown in Fig. 3, and the tumble ratios and turbulent kinetic energy, is shown in Fig. 4. A large amount of liquid film forms on the surface due to the relatively short injector-piston distance for the early injection case (e.g., at 60CAD ATDC). Because of spray targeting Injector B has more wall wetting than Injector A at this timing as shown in Figure 3. This piston wetting can be reduced by retarding the injection timing. If the injection timing is set to 120CAD, the maximum film mass is reduced by 62% for Injector B. Since the spray injected at 120CAD and later was not found to touch the piston, the film mass could be located on the side wall.

Compared to swirling flow, which is very weak for the current engine and most DISI engines, the tumble flow is known to be better in converting the mean flow energy into turbulence kinetic energy which enhances fuel-air mixing and speeds up combustion. The latter mechanism is more prominent near the end of compression stroke, after the ignition has taken place, when turbulence motions wrinkle the flame-fronts and increase the flame surface areas. Comparing to the baseline motoring case, injection too early (e.g., 60CAD BTDC) reduces the tumble flow and the resultant turbulence intensity at the end of compression stroke, as shown in Fig. 4. For much later injections after 240 ATDC; e.g., for the stratified charge mode, neither the enhancement of tumble ratios and turbulent kinetic energy is observed at or after compression TDC.

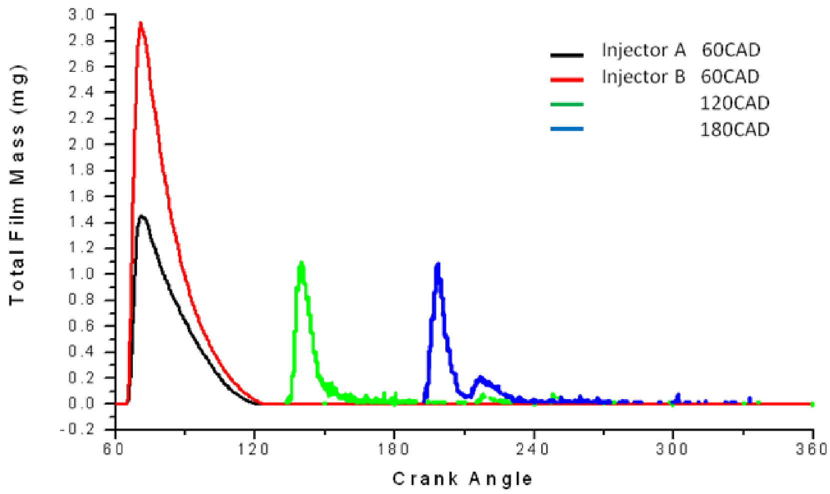

Fig. 3 Total liquid film mass for homogeneous injection

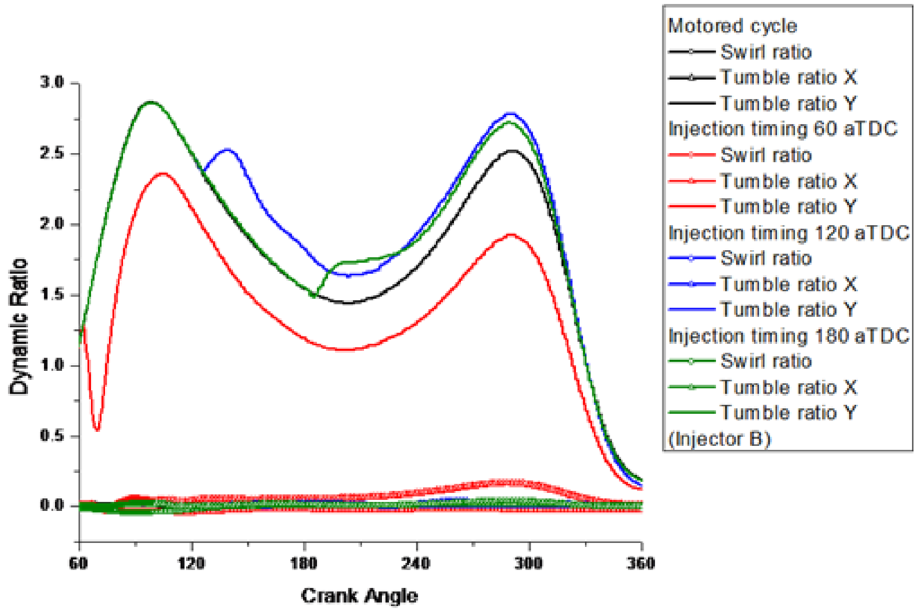

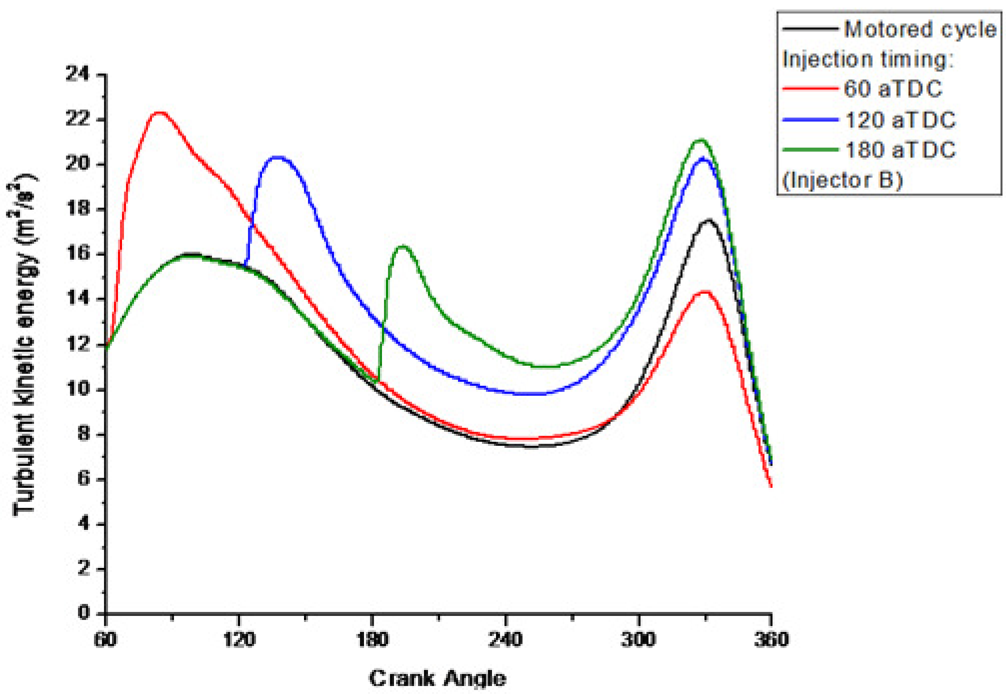

Fig. 4 Bulk flow integral dynamic ratios and turbulent kinetic energy of homogeneous injection at various timing (Injector B)

The high-rep rate Copper Vapor laser has also been repaired and will enable us to carry out light sheet visualization.

Phase 4 Task 3.0 –Multiple cylinder engine charge motion study (1/1/10 thru 3/31/10)

Injection studies

Injection timing windows were evaluated at several speed-load points documenting the emissions, burn characteristics and performance. This was done for both cam strategies for load control, Early Intake Valve Closing (EIVC) and Late Intake Valve Closing LIVC. The test points are shown in Figure 5. Injection timing sweeps were performed at each point to identify optimal injection timing to maximize efficiency with minimal emission impact. Cam optimization was also done to minimize fuel consumption while maintaining acceptable combustion stability. The Low lift EIVC cam was evaluated at the points shown in blue. The high lift LIVC cam was evaluated at the points outlined in red. Initial testing was done with E85, but the focus was changed to E0 Gasoline because of its increased sensitivity due to reduced dilution tolerance and propensity for soot formation. The desire to maintain a full flex-fuel capability thus shifted our focus to the more challenging fuel. The test points will be used for comparison to improved charge motion alternatives to be tested. The Early Intake Valve Closing (EIVC) strategy suffers from poor charge motion at low loads where spray induced charge motion is minimal. High speeds over 2500 rpm are the most problematic due to long burn durations. Later testing will include Valve deactivation effects and modifications to the intake to improve charge motion to extend the dilution limit and improve efficiency. The valve deactivation test are planned for the first weeks of Q2 2010.

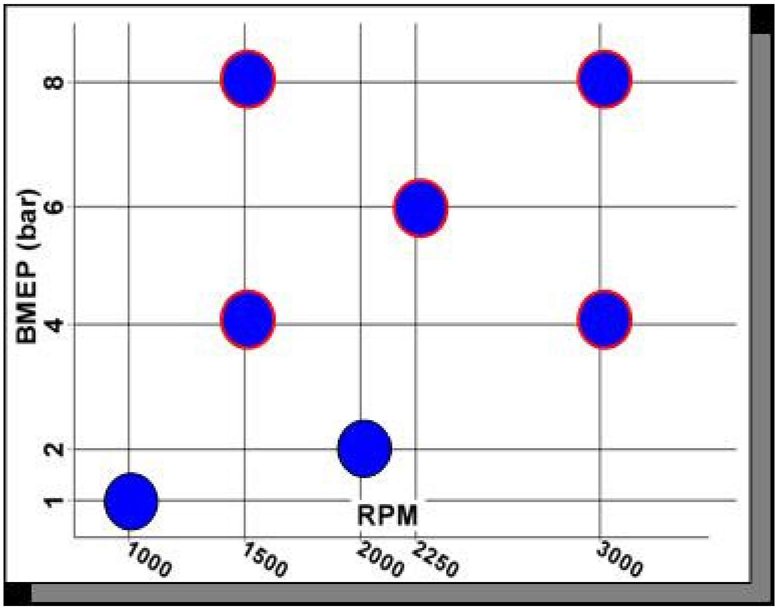

Figure 5 Speed load points tested for comparison of charge motion strategies.

A subset of data for the high and low valve lifts are shown in figures 6 and 7 respectively for E85 fuel. The highlighted windows show the injection window with acceptable injection stability and low fuel consumption. Hydrocarbons are also low in this region, earlier injections lead to liquid impingement on the piston which produces increased hydrocarbons and increase the potential for pool fires contributing to soot formation. Later timings show an increase in hydrocarbons and deteriorating combustion stability, likely the effect of wall wetting of the cylinder bore.

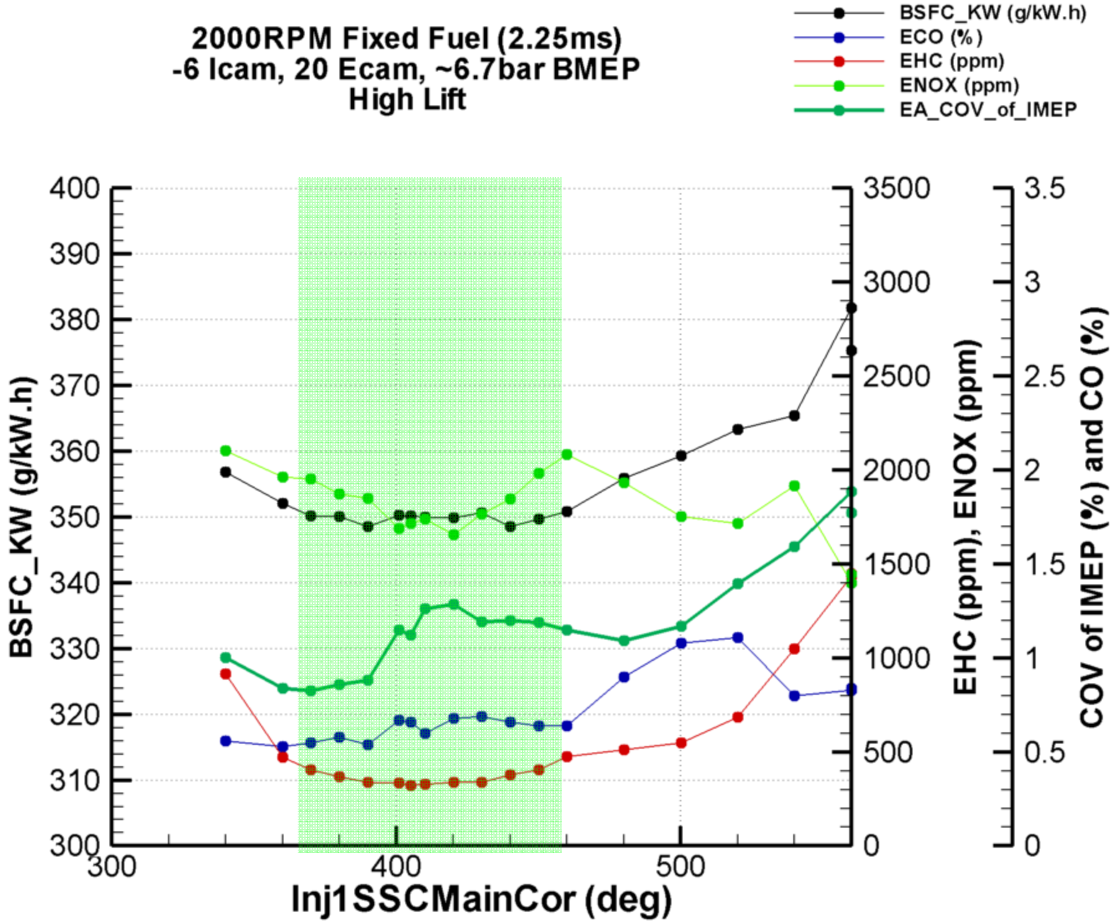

Figure 6 Injection timing sweep, E85 Fuel, High Lift cam at LL-HL Cam switch point. 736 injector.

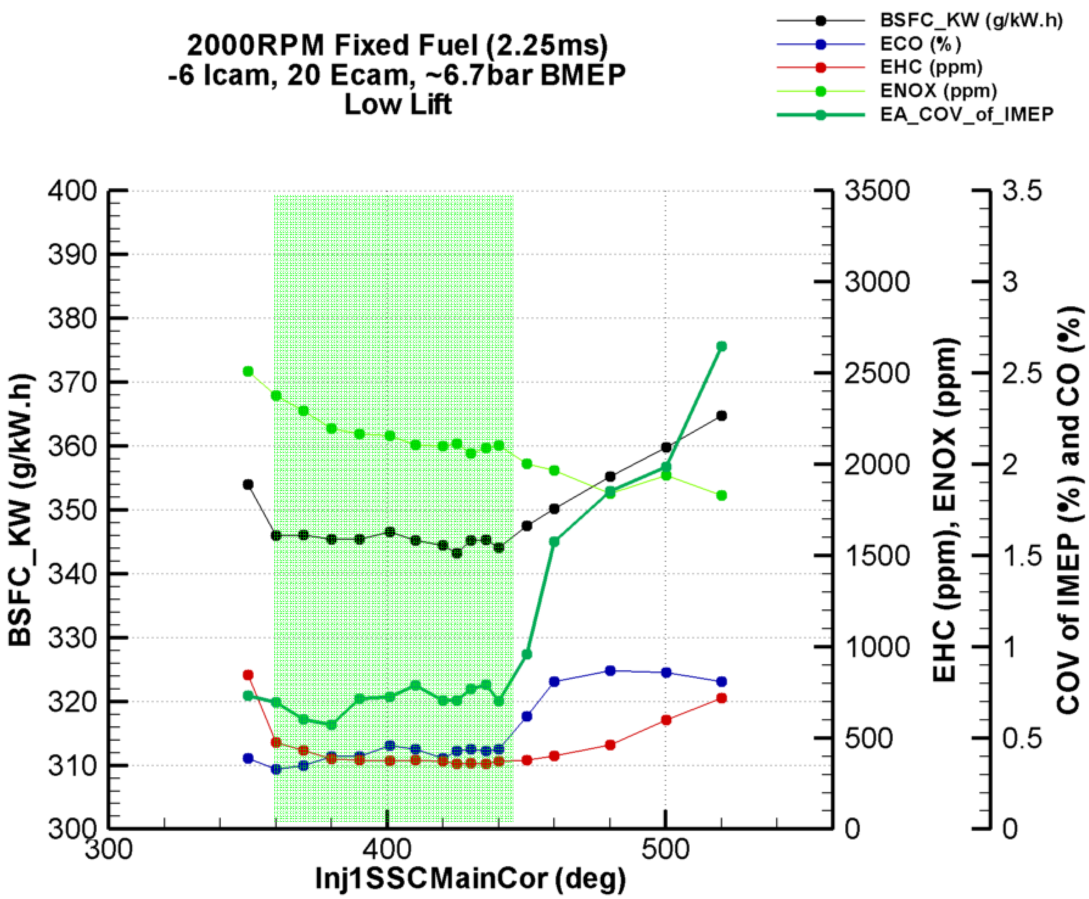

Figure 7 Injection timing sweep, E85 Fuel, Low Lift cam at LL-HL Cam switch point. 736 injector.

. Additional figures 8-12 are shown during operation on gasoline. Soot measurements taken with an AVL415 smoke meter are also included as an FSN, (Filter Smoke Number). Operation on gasoline resulted in smaller acceptable injection windows, bounded by soot formation with early injections and deteriorating combustion stability and BSFC at later injection timings. Figure 7 shows a similar operating point to Figure 8, these were run on E85 and gasoline respectively. Figure 9 is comparable to Figure 6. The gasoline fuel tended to produce higher hydrocarbon levels on the high lift cam as the timing was retarded and were constrained by soot at the earlier timings the best timing was typically as early as possible before reaching the soot limit. The same constraints were observed for most operating points. At higher loads the base soot (FSN) numbers did not produce a satisfactory injection timing even though other metrics were acceptable, see figure 10 for an example.

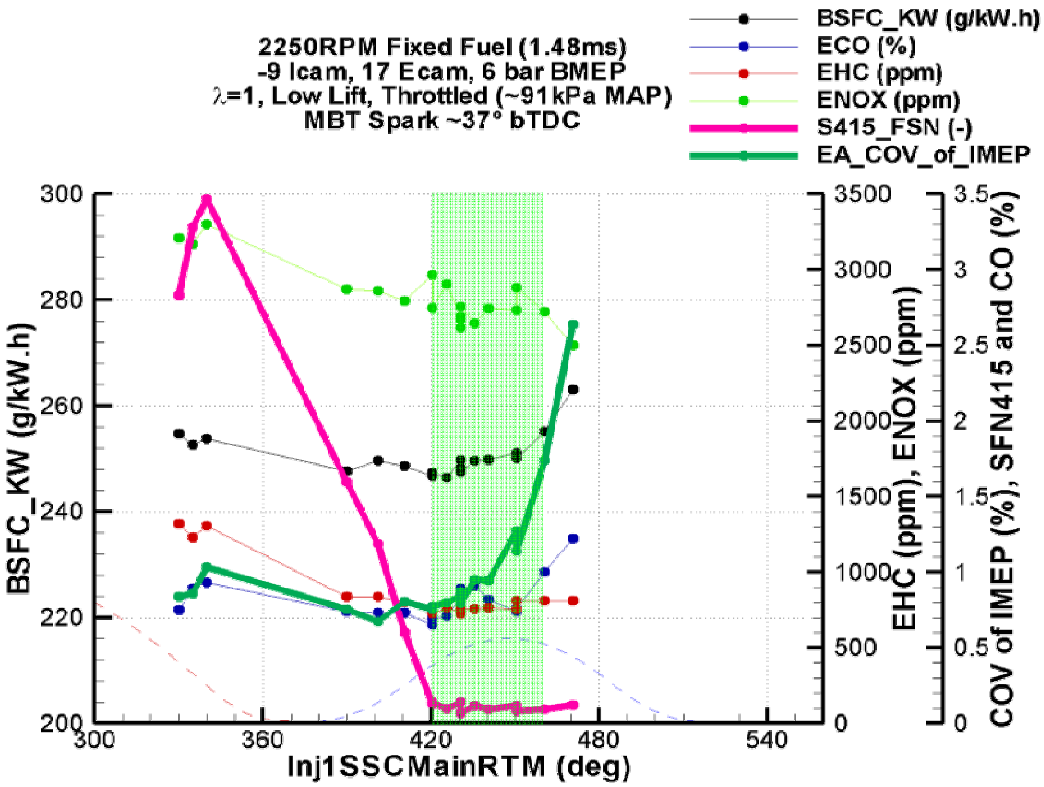

Figure 8 Injection timing sweep, Gasoline, Low Lift cam, 736 injector.

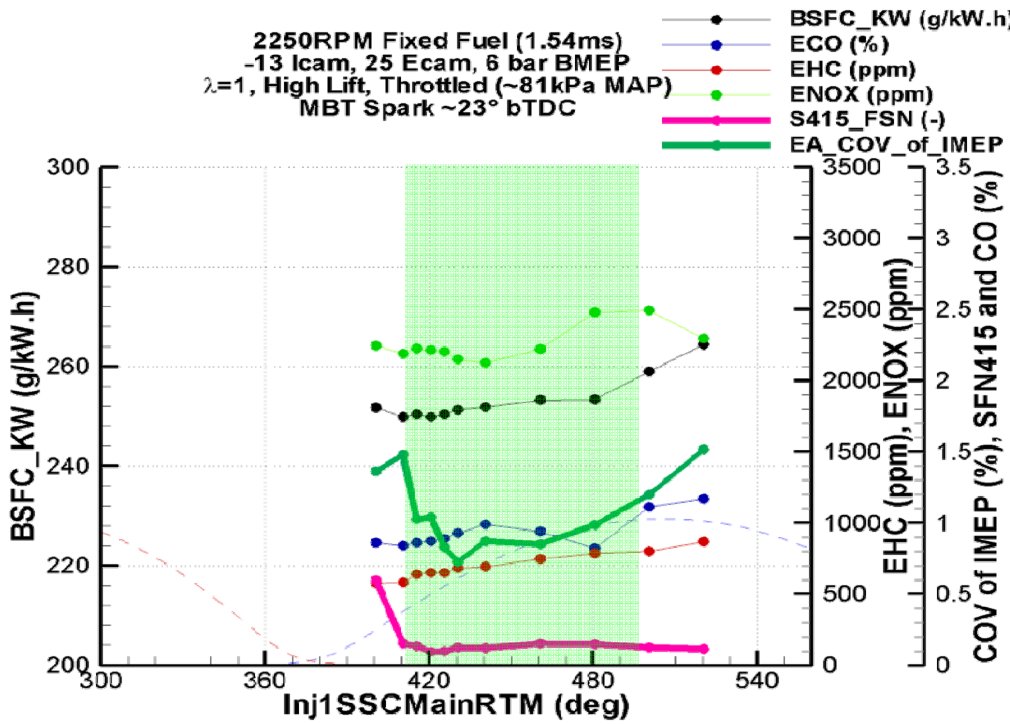

Figure 9 Injection timing sweep, Gasoline, High Lift cam, 736 injector.

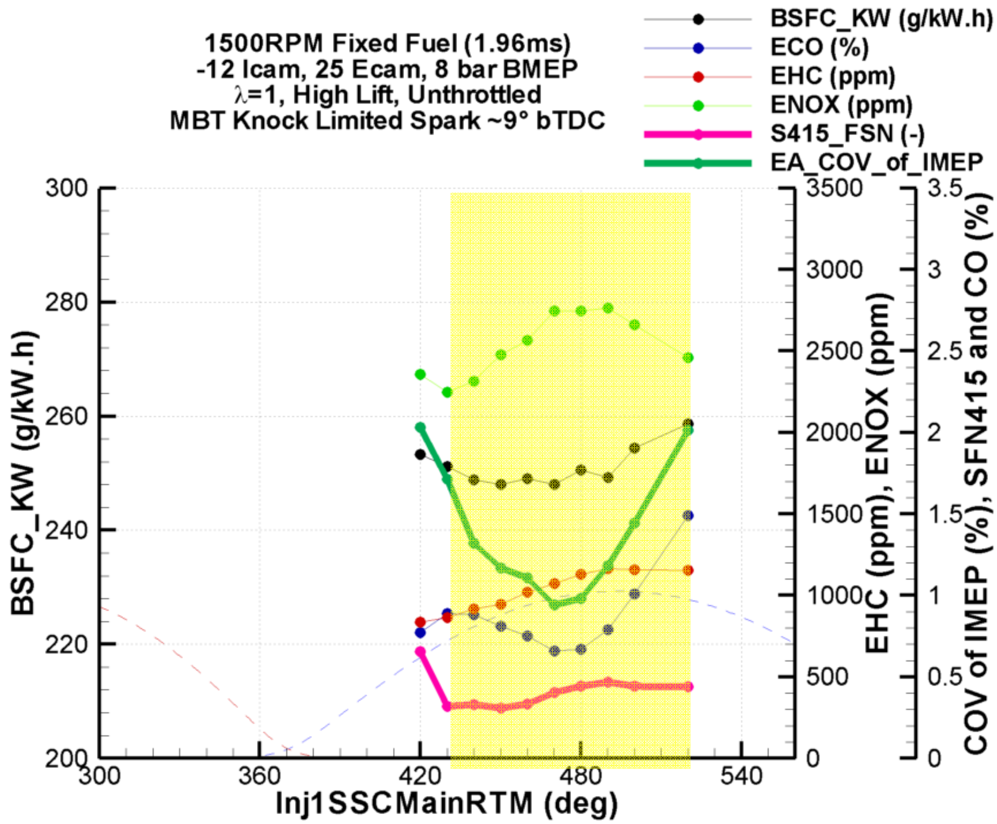

Figure 10 Injection timing sweep, Gasoline, High Lift cam, 736 injector. 1500 RPM, 8 Bar BMEP

For higher speed operation at lower loads the acceptable timing window on the low lift cam collapsed. This required a compromise between combustion stability and soot formation, see figure 11. This was not observed on E85 due to its reduced sooting tendency. Figure 12 shows the same operating condition with the high lift cam. The injection timing window is significantly broader and did allow stable operation with low soot, however an increase in fuel consumption of about 2% was observed relative to the low lift cam. The need for enhanced combustion stability and increased flame speed is evident during low lift operation. Comparisons of these operating points will be made with valve deactivation to access the potential of valvetrain strategies for minimizing fuel consumption.

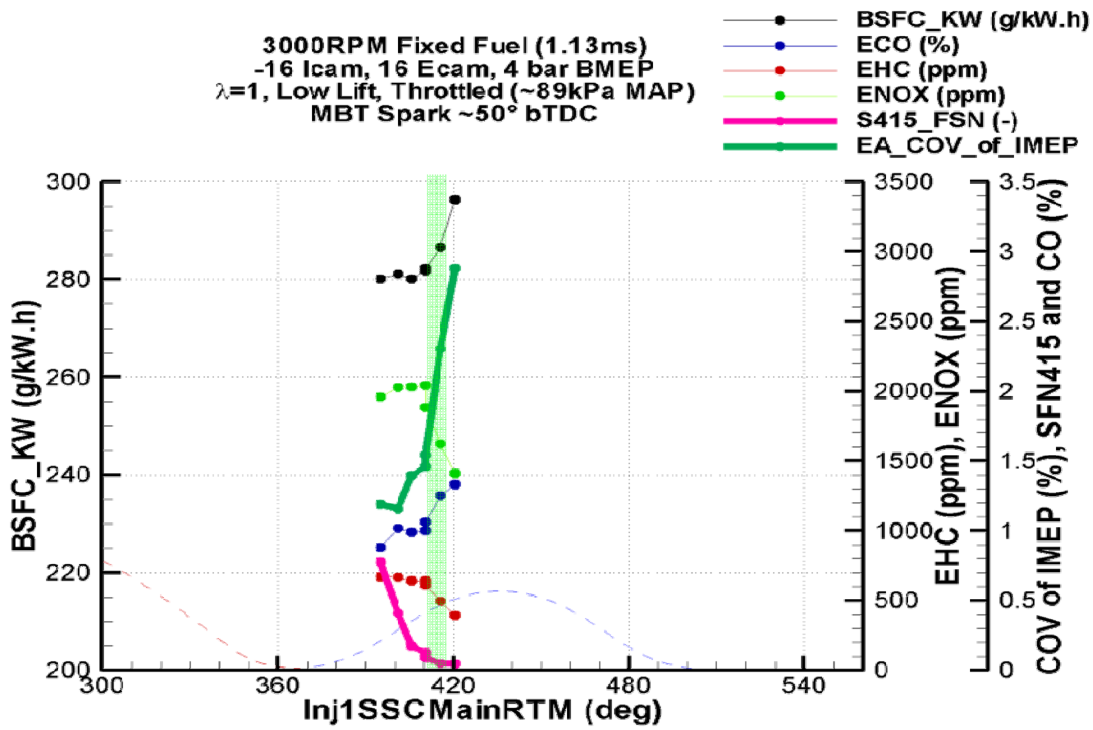

Figure 11 Injection timing sweep, Gasoline, Low Lift cam, 736 injector. 3000 RPM, 4 Bar BMEP

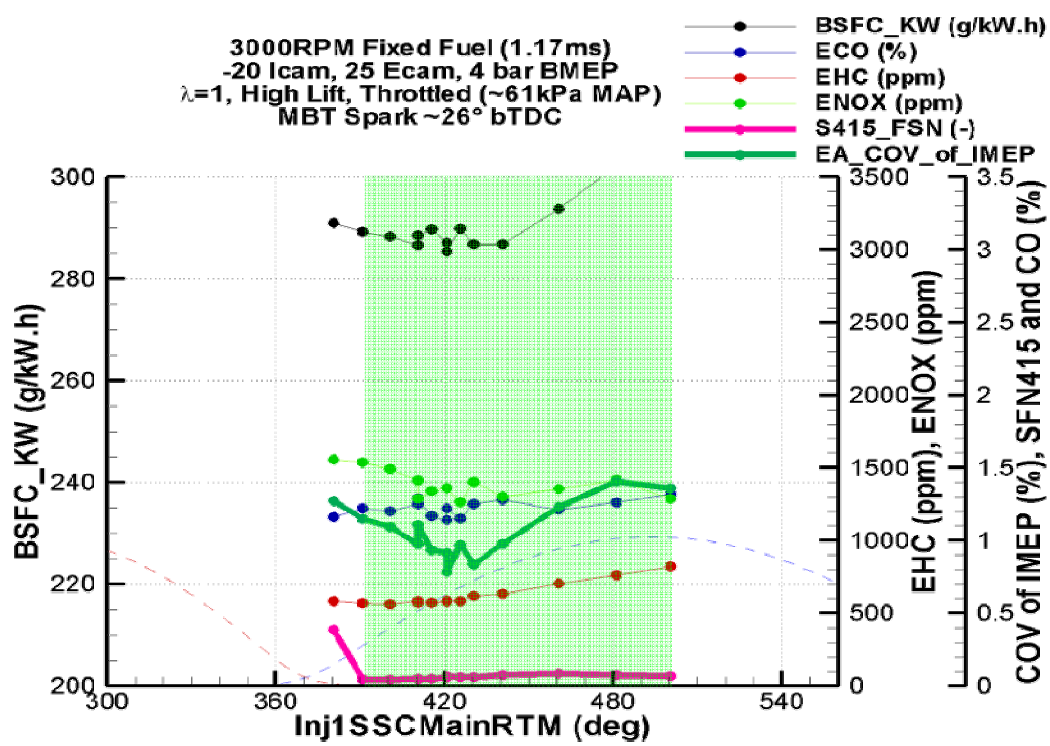

Figure 12 Injection timing sweep, Gasoline, High Lift cam, 736 injector. 3000 RPM, 4 Bar BMEP

NA Peak power cam optimization

Cam optimization to improve peak torque was conducted from 1000 to 3000 RPM on the high lift cam for E85 fuel. A maximum overlap condition with maximum stroke on the intake cam produced the maximum torque above 1500 RPM, at lower speeds reduced overlap was beneficial to reduce over scavenging. Injection timing was also adjusted to maximize Volumetric efficiency. The resulting torque curve is shown in Figure 13. The torque peak is slightly broader than previous tests from 1500 to 1750 rpm which offers opportunity for downsizing. Another observation was that the torque curve measured at the Customer Technical Center Michigan (CTCM) facility was lower than that observed at the Technical Center Rochester (TCR) Facility. The setup of the engine was different the CTCM facility, it included the vehicle muffler to represent backpressure which may explain the differences due to reduced scavenging potential.

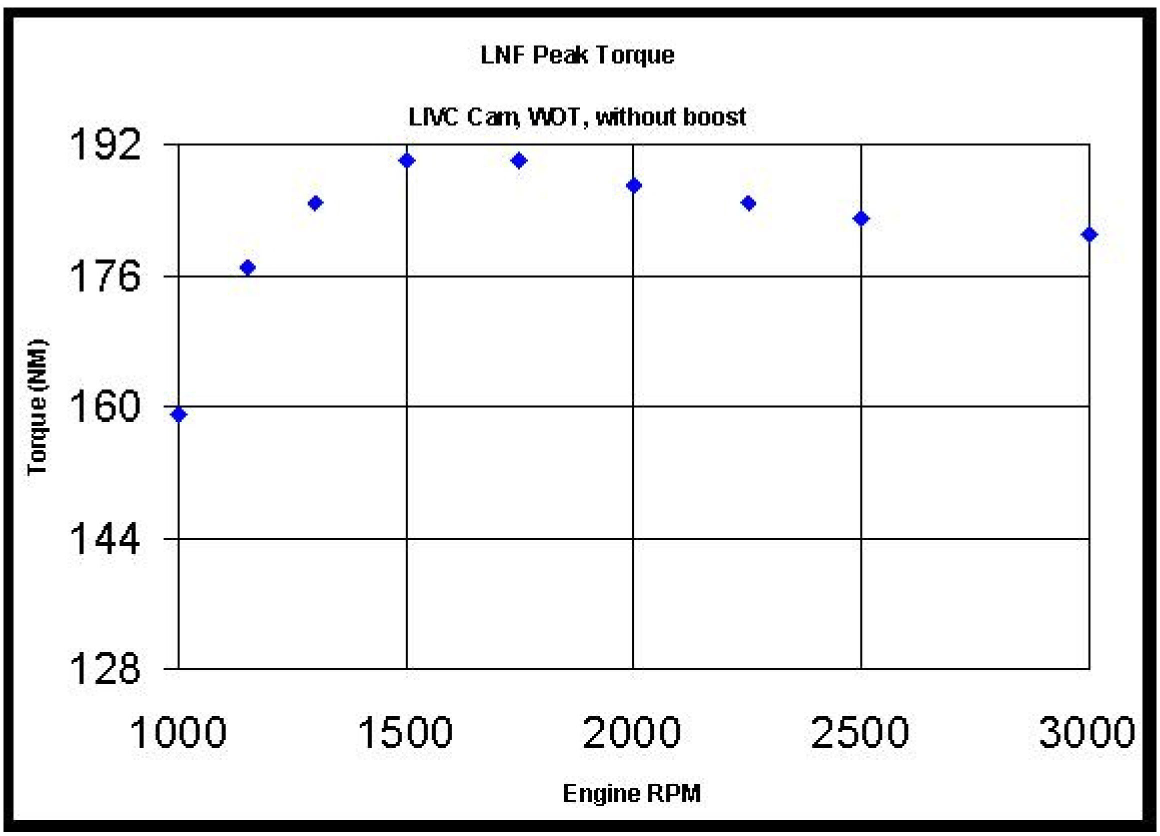

Figure 13 Unboosted Peak Torque curve after cam and single injection timing optimization, LIVC, 736 Injector, E85.

Ignition energy studies

Ignition energy requirements were investigated for E85 at several test points. The production ignition energy was sufficient in all cases and dwell could be reduced 60% to 80% before combustion stability and mis-fire became problematic. In general higher compression pressures and increased charge motion required more ignition dwell, see figure 14.

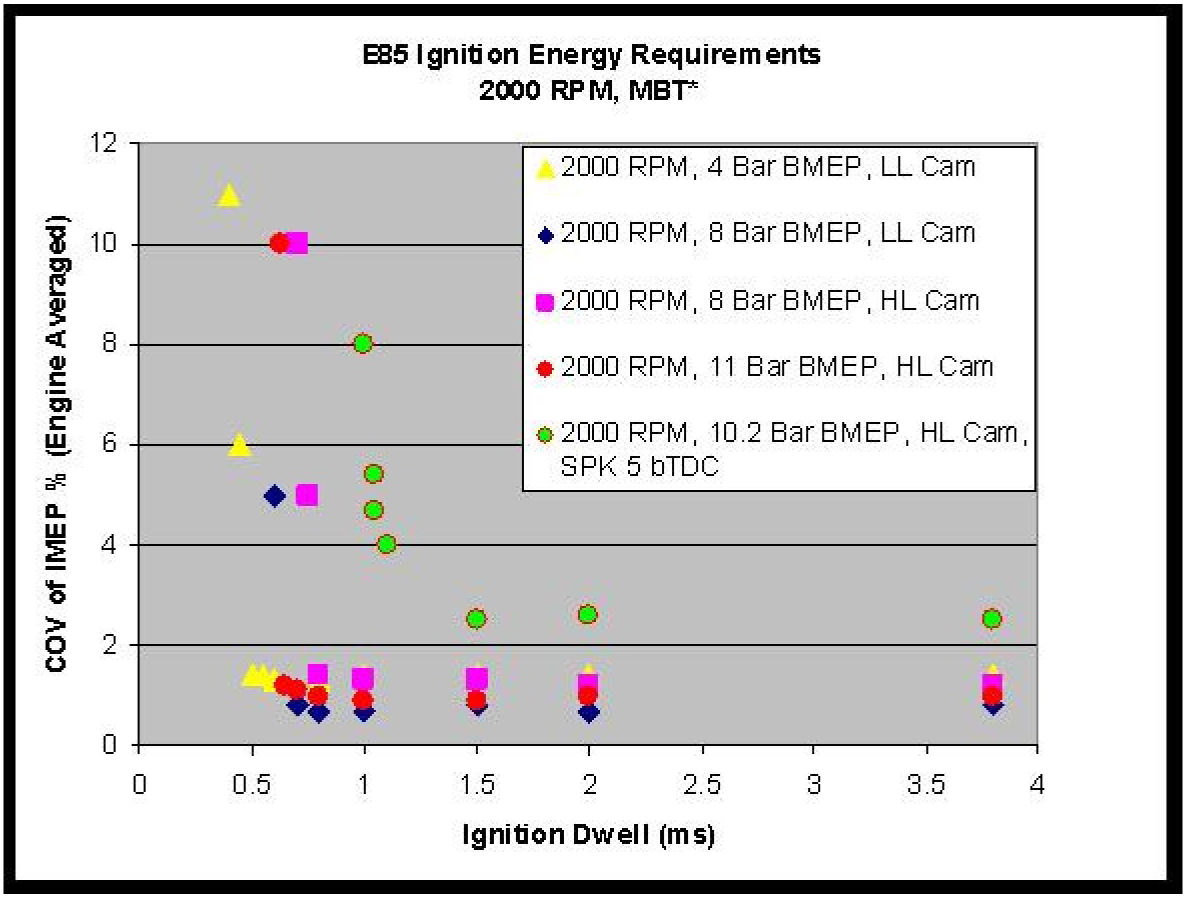

Figure 14 Ignition energy (Dwell) requirements to maintain combustion stability 736 Injector, E85.

Cam timing optimization (Internal EGR) (E85 fuel)

Gasoline was sensitive to EGR induced knock due to the higher compression ratio. On the low lift cam this was not a problem since the EIVC strategy produces a reduced compression ratio as internal EGR is increased with valve overlap. With the LIVC cam increased overlap to control EGR results in an increase in CR which produced EGR and CR induced knock. This limited the ability of the high lift cam to control NOx with internal EGR at mid-high loads for gasoline. This was not a problem when operating on E85 due which allowed significant internal EGR without knock resulting in a reduction of NOX emissions. Figures 15 and 16 show the effect of increased overlap that increases internal EGR resulting in significantly lower NOx emissions 90% and 60% respectively. The increased EGR also was able to reduce fuel consumption from the low EGR condition by 2-5%

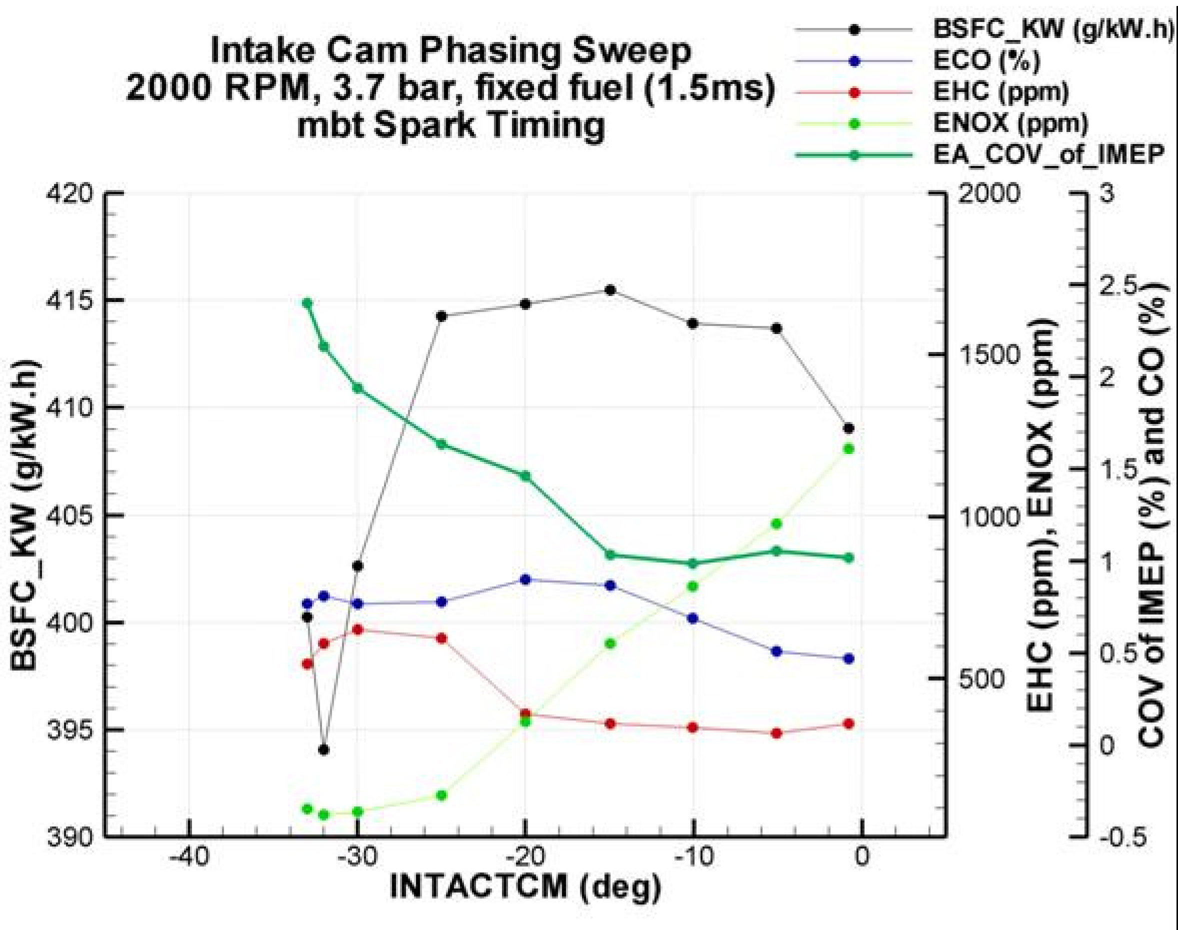

Figure 15 Injection timing sweep, Gasoline, High Lift cam, 736 injector. 3000 RPM, 3.7 Bar BMEP

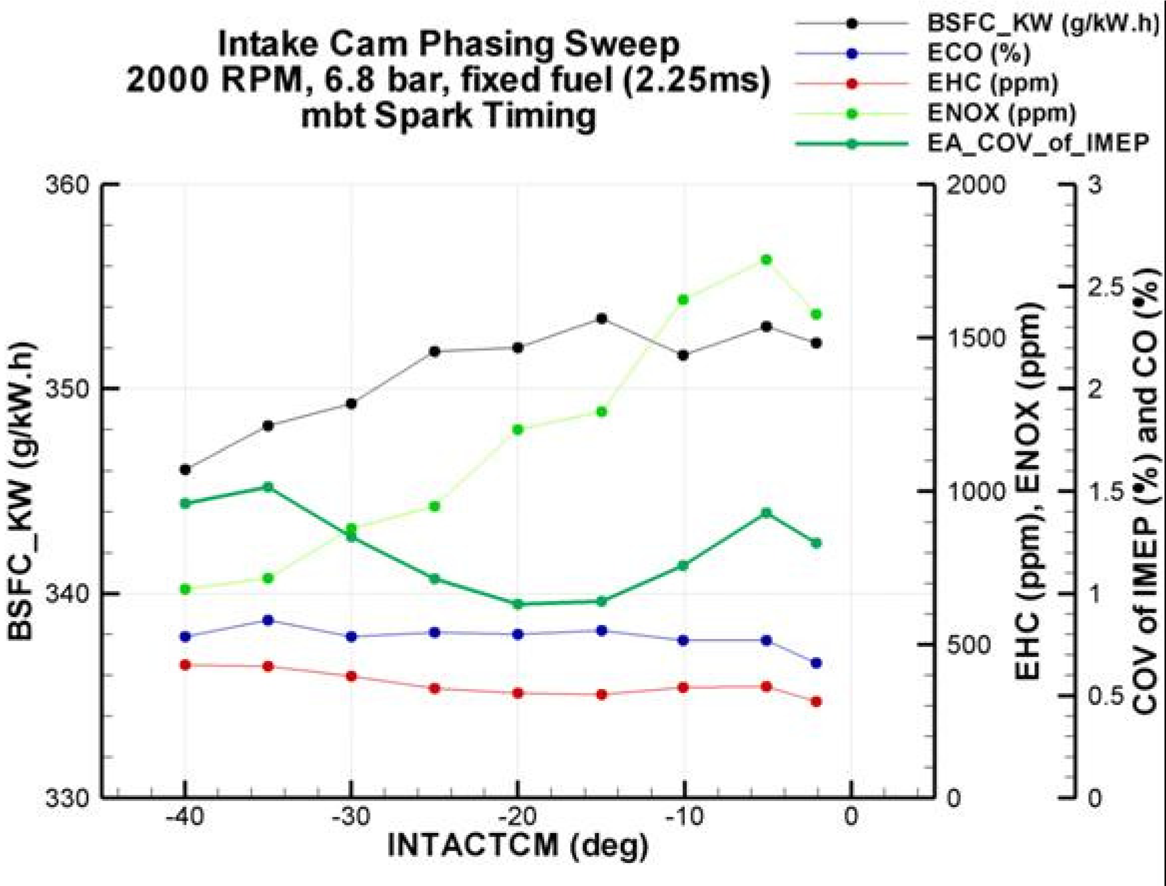

Figure 16 Injection timing sweep, Gasoline, High Lift cam, 736 injector. 3000 RPM, 6.8 Bar BMEP

Intake manifold modification

Intake manifold modifications to evaluated enhanced charge motion are in process. Modifications are intended to increase the swirl and/or tumble in the intake for improved low load combustion stability. Alternative design variations are being fabricated and will be initially evaluated on a flow bench before evaluating promising alternatives on the engine.

Engine Status

The engine has been converted to operate with an intake valve deactivated, testing will proceed next month.

Optimization algorithm development

Algorithm development to optimize the multi-dimensional control space is being developed and evaluated in simulation. As the number of independent control parameters is increased optimization becomes more time consuming. The additional of multiple injections significantly increases the complexity requiring more efficient optimization during testing. This development will be integrated into the engine controller to speed development. The figure below represents the optimization technique in which a fractional DOE is used to identify the local gradients (1) that gradient is followed until curvature is identified and repeated to identify the new gradient to optimize on a best multidimensional solution. The figure represents a 3D optimization but the technique and algorithm has been applied on simulated data sets with various degrees of complexity in higher dimensional space.

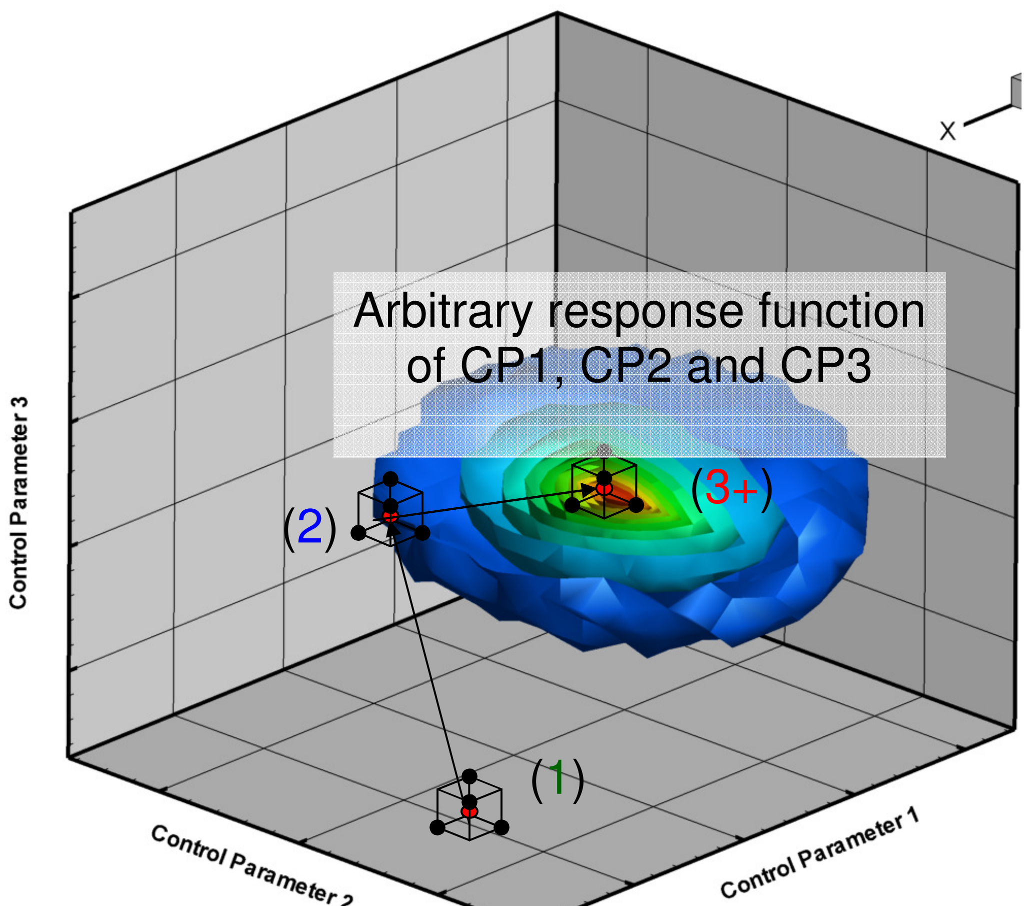

Quarter 2 2010

Phase 4 Task 2 – Optical engine charge motion study_(4/1/10 – 6/30/10)

Optical engine tests were carried out to investigate the effects of injection timing on the bulk flow and charge motion, in order to better correlate and interpret the observed multi-cylinder dyno engine test results, and to validate the CFD predictions. The low-lift valve generates stronger valve flow and therefore more turbulence during the intake process, while one valve deactivated creates more swirling flow and further increase the turbulence which is helpful during the mixing processes. The high-lift valves, however, generate more tumble motion which will be more efficiently converting the mean flow energy to turbulence kinetic energy at the later stage of compression stroke, which is more helpful to increasing flame speed near the TDV. The comparison of the interactions of charge motion with DI fuel injection is illustrated in a typical example below. Figure 1) shows that the stronger swirling flow is better at confining the spray to the center of the combustion chamber, minimizing wall wetting and increasing the mixing and vaporization at the same time. The integral flow dynamic ratios and mass-averaged TKE computed by CFD are plotted in Figures 2) and 3) respectively, which describe the phenomena which agree with optical engine and correlated with multi-cylinder engine results.

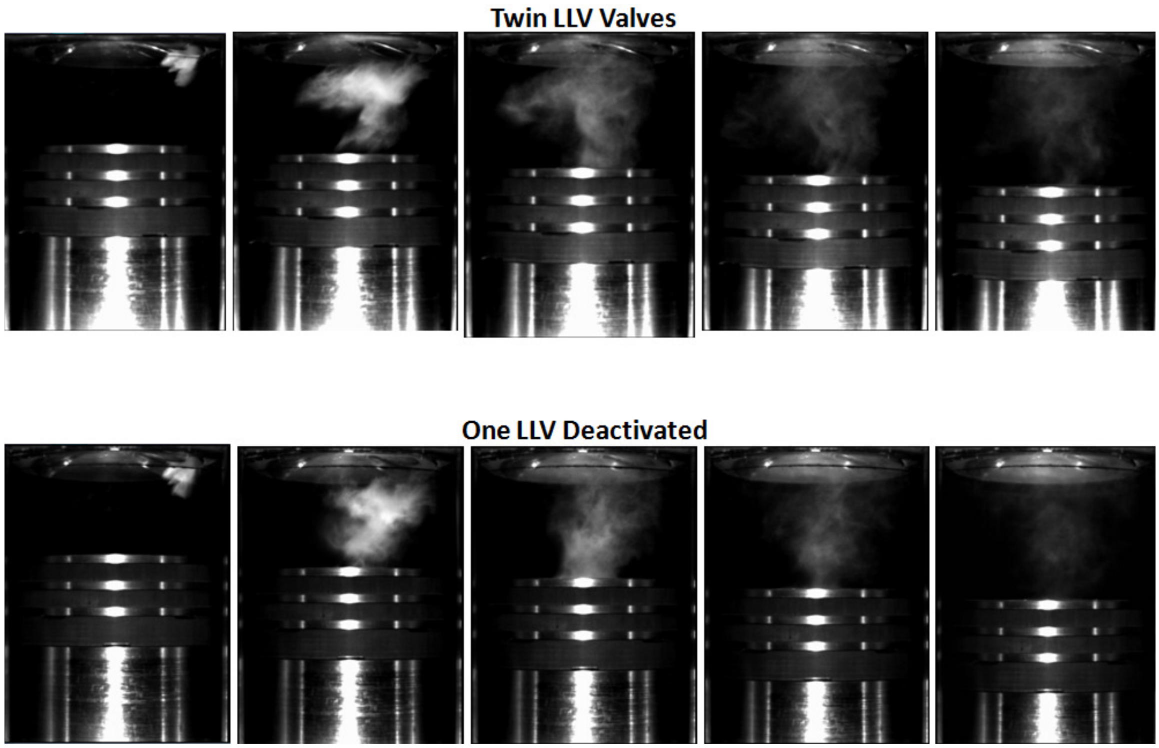

Figure 1) Comparison of Charge Motion-Mixing Interactions due to valve deactivation. (SOI timing 420 ATDC; Top: LLV; Bottom: LLV deactivated)

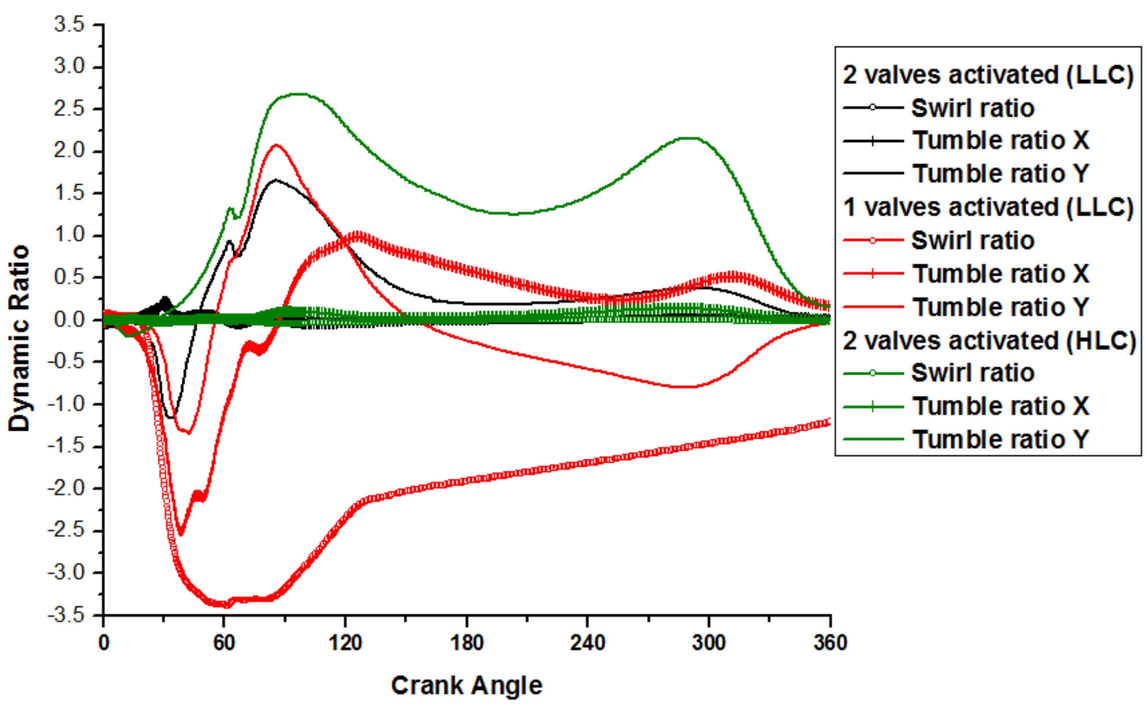

Figure 2) The integrated fluid motion dynamic ratios for different valve conditions

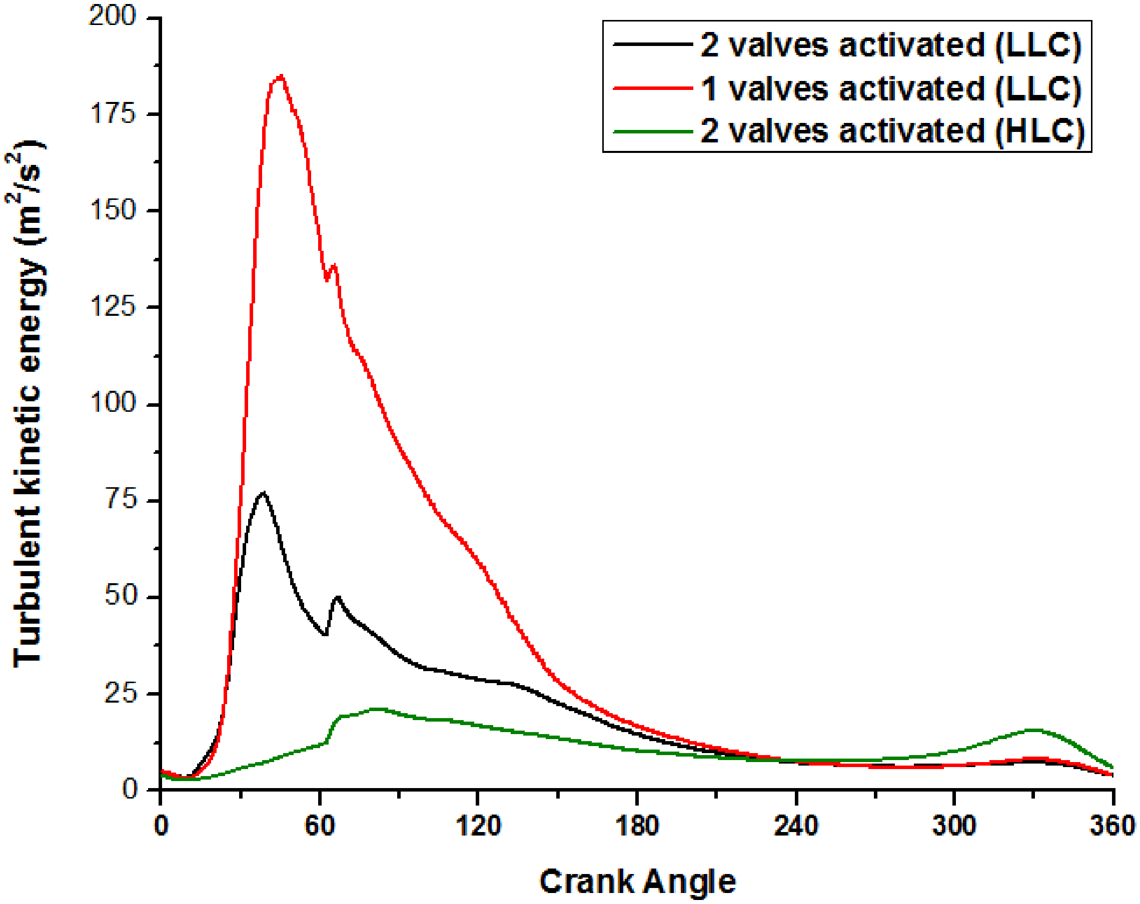

Figure 3) mass-averaged turbulence kinetic energy for different valve conditions

<u>Phase 4 Task 3.0</u> –Multiple cylinder engine charge motion study (4/1/10 thru 6/30/10)

Operation of the engine with over-expanded cycles using Early and Late Intake Valve Closing (EIVC and LIVC) had revealed difficulties with combustion stabilities at low loads using EIVC which was intended for efficient low load operation of the engine. To address the slow flame propagation one strategy evaluated consisted of valve deactivation to improve in-cylinder mixing. Flow bench measurements had identified significant increases in the tumble and swirl indices when an intake valve was deactivated, see Figure 4.

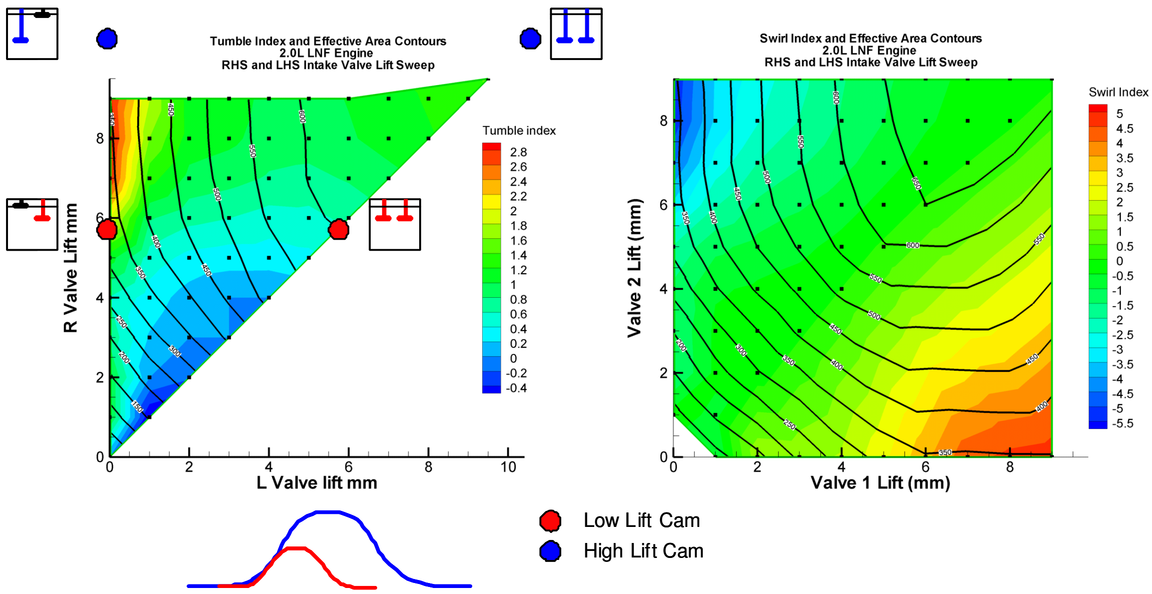

Figure 4 Tumble (LH) and Swirl (RH) maps for the LNF head. The red and blue circles indicate the lifts of the LIVC and EIVC cams respectively.

To evaluate the charge motion effect on the multi-cylinder engine the valvetrain was modified to operate with an intake valve inactive for each cylinder. Testing was done to evaluate the effect of valve deactivation on injection timing windows, emissions, fuel economy and peak torque.

Injection timing widow testing

To evaluate the effect of charge motion, injection timing windows were evaluated over a range of operating points for both the EIVC and LIVC strategies. The LIVC strategy was evaluated at 5 operating points and the EIVC strategy was evaluated at 2 additional points at lower loads. Figure 5 shows the test points denoted by the blue dots for EIVC and blue dots with red outline for the LIVC strategy respectively.

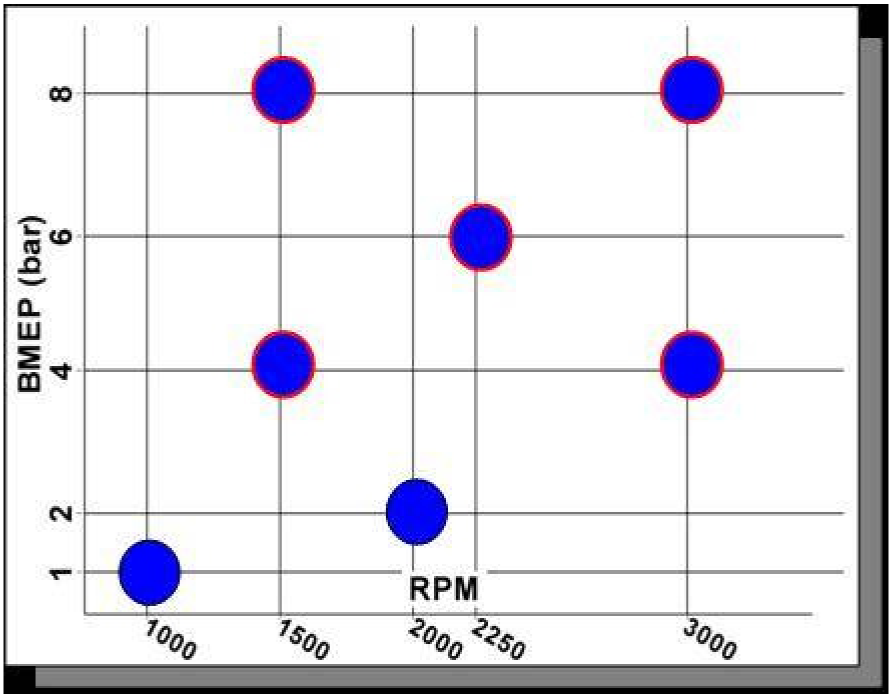

Figure 5 Test matrix for evaluation of valve deactivation.

An example of the effect of valve deactivation during LIVC operation, Figures 6 and 7 illustrates the significant reduction in hydrocarbon and soot emissions when valve deactivation was active at 1500 RPM 8 Bar BMEP. These improvements were observed at all of the operating points tested with the LIVC strategy. The observable difference was more significant as the load and respective fuel mass increased. This testing was done with a 91 RON E0 Gasoline. Testing with E85 has not been an issue for soot emissions.

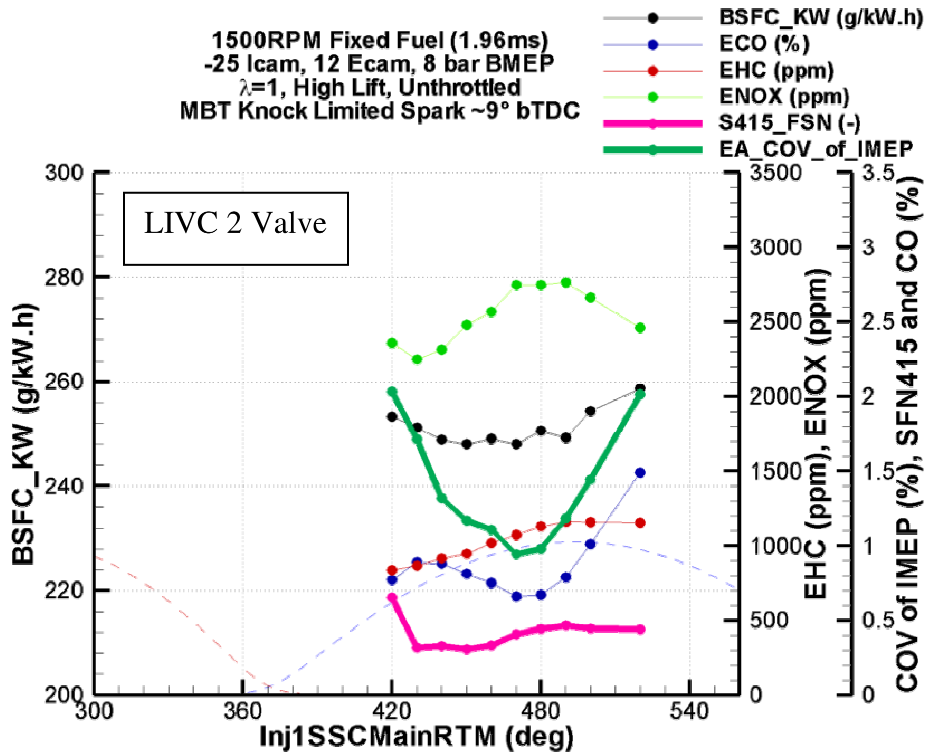

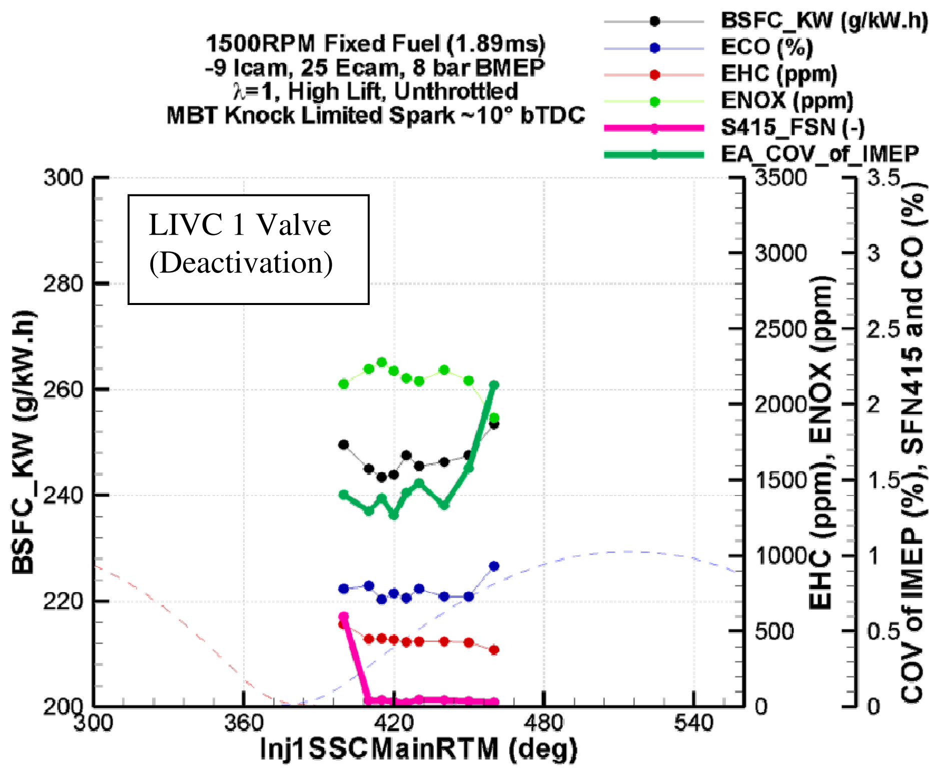

Figures 6 and 7 Comparison of 2 Valve to 1 Valve operation injection timing windows. LIVC Strategy 1500 RPM 8 Bar BMEP, 91 RON Gasoline, 736 injector.

Valve deactivation, while operating with EIVC, produced a significant reduction in burn duration, which improved combustion stability. This enabled a reduction in fuel consumption at low loads. While the injection timing windows were only slightly larger, the enhanced EGR tolerance allowed more overlap, thus reducing the throttling losses. For the 2000 RPM 2 Bar BMEP point this allowed MAP to increase from 53 to 95 KPA, See figures 8 and 9. The reduction in throttling losses resulted in an 8% reduction in fuel consumption at this point. At lower loads particulate emissions were primarily from pool fires if the injection timing was too early. A small but acceptable injection window was possible at low loads with EIVC with a deactivated valve. The other points evaluated also showed improvements but the fuel consumption was most significant as the load decreased down to about 1.5 bar BMEP. For each of the test points evaluated initial cam optimization was done to reduce fuel consumption. Operation at very low loads (<1.5 Bar) required the use of significant throttling and reduced valve overlap to achieve these loads which compromised efficiency.

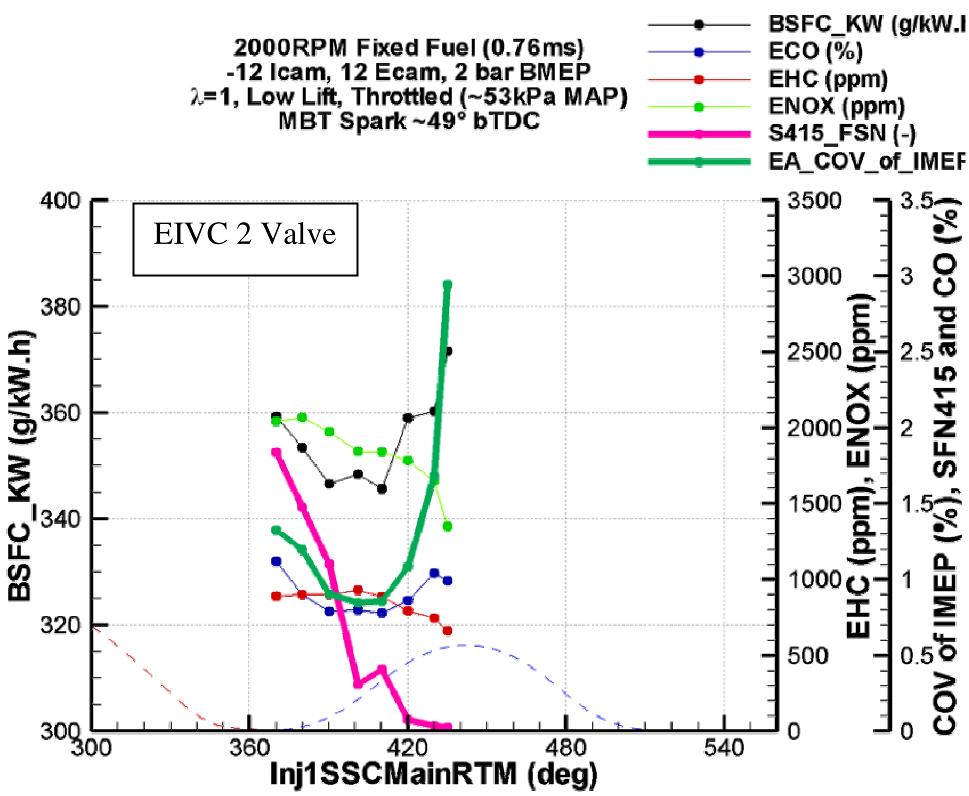

Figure 8 Injection timing sweep for 2000 RPM 2 Bar BMEP, 2 Valves EIVC. 91 RON Fuel, 736 injector

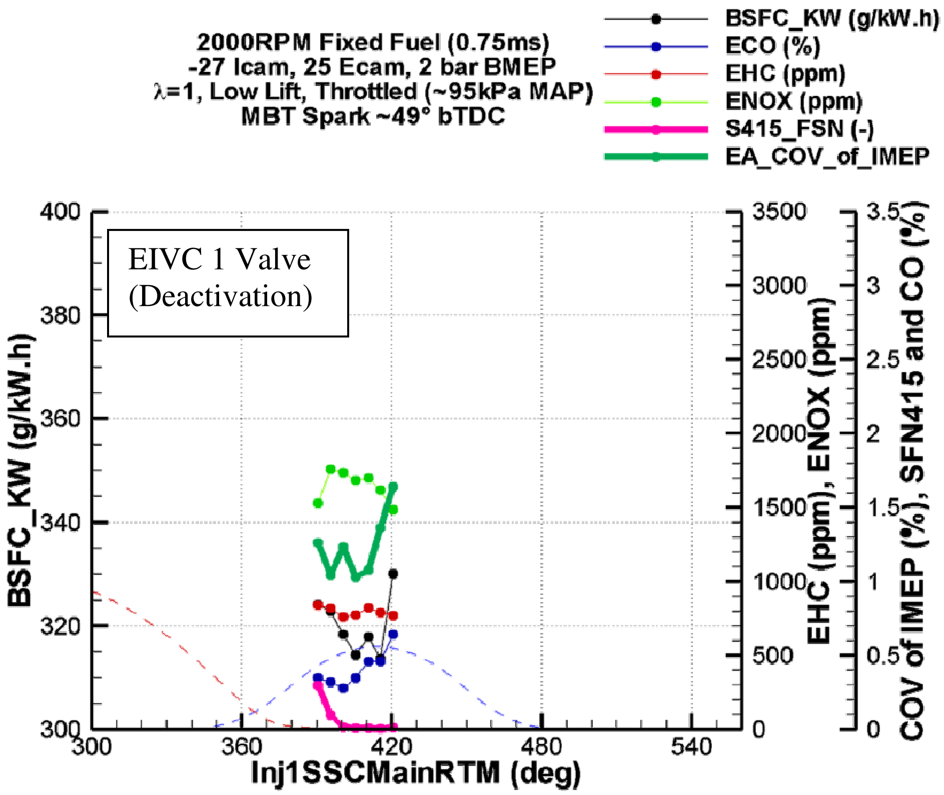

Figure 9 Injection timing sweep for 2000 RPM 2 Bar BMEP, 1 Valve EIVC. 91 RON Fuel, 736 injector.

Enrichment sensitivity testing

To determine the robustness of valve deactivation for reducing soot and hydrocarbons the effect of rich operation was evaluated using gasoline. Figure 10 shows hydrocarbon and soot levels at 1500 RPM 8 Bar BMEP using EIVC Low Lift (LL) and LIVC High Lift (HL) with and without valve deactivation. The most noticeable difference is the contrast with the high lift LIVC cam; in this case the valve deactivation resulted in a decrease in soot and hydrocarbons of 95 and 50% respectively. The low lift cam (EIVC) did not show the same sensitivity. The source of the soot and HC emissions with LIVC is likely the result of bore wetting of the fuel spray which results in a local rich pocket that is inadequately mixed. Results from optical engine work indicate over penetration of the spray with LIVC due to a large flow gradient carrying fuel toward the wall. The use of deactivation appears to reduce penetration as well as providing an additional mixing mechanism that may be able to scrub the wall layer and mix it into the bulk mixture. It is noticeable that the soot level with deactivation did not approach the same level measured for the 2 valve setup at stoichiometric until over 50% enrichment was achieved. This indicates that the bulk AF ratio does not contribute as much as local sources (from bore wetting) that produce an over rich boundary layer.

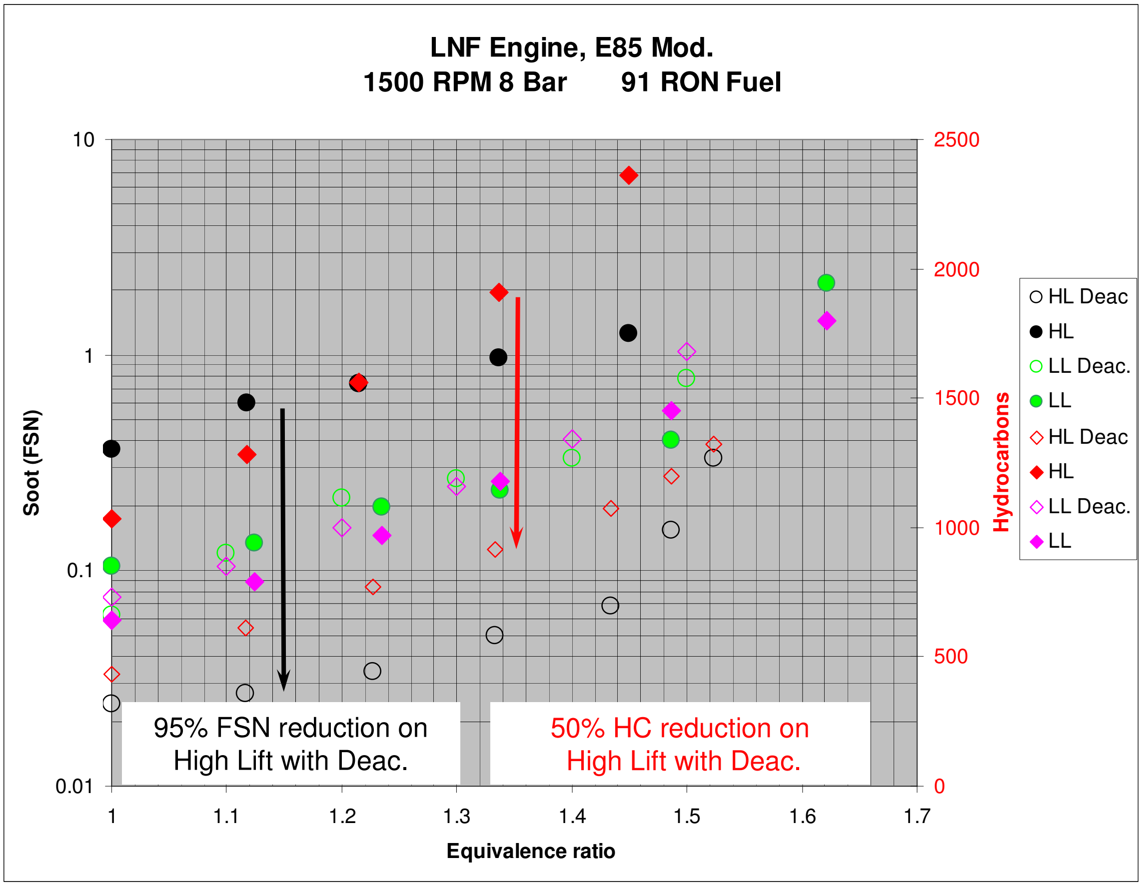

Figure 10 Enrichment evaluation of valvetrain strategies, 1500 RPM 8 Bar BMEP, 91 RON Fuel 736 injector .

Additional work with the optical engine and CFD work is progressing to better define the mechanisms contributing to the differences in soot and hydrocarbon levels observed.

Cam optimization mapping

Cam optimization maps have been constructed at several fixed fueling rates to identify the most efficient modes of operation of the engine. The use of valve deactivation significantly enlarged the cam phasing authority range when operating at low loads with EIVC. Figures 12 and 13 show the BSFC MAP and %COV map for a 2000 RPM 3 Bar BMEP operating condition.

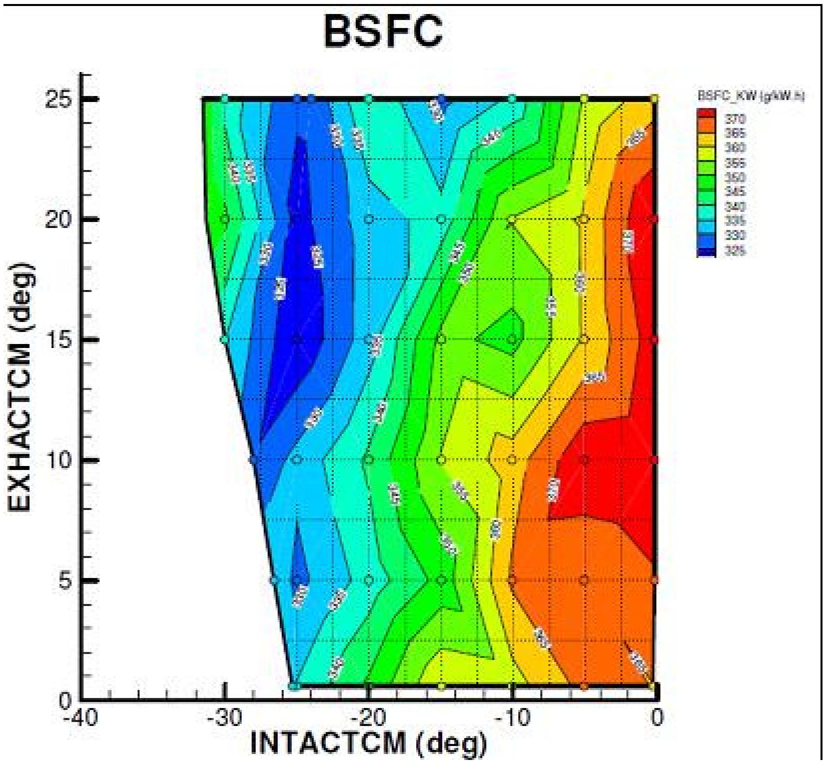

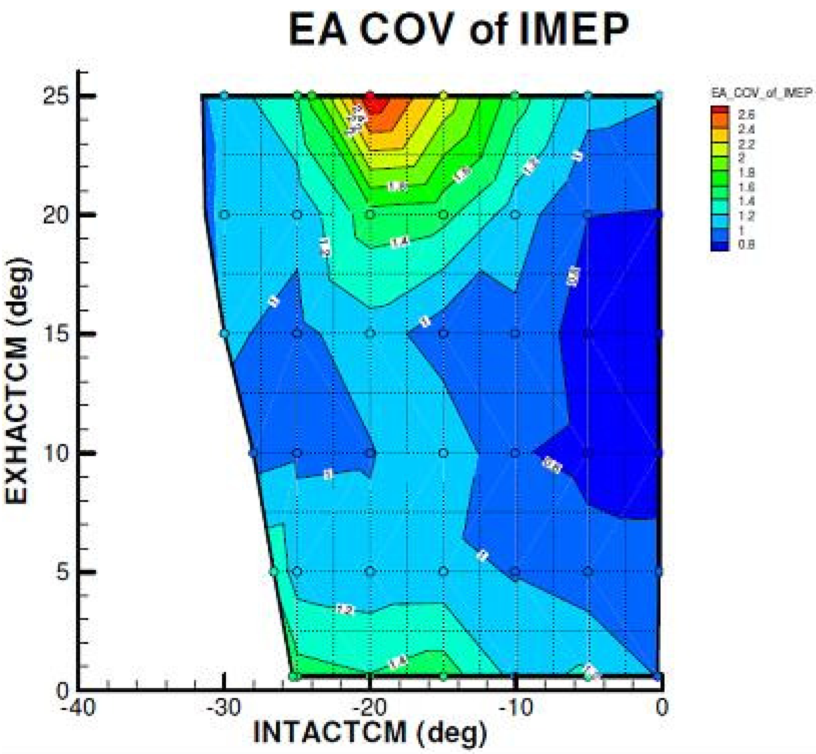

Figures 12 and 13 Cam optimization map, EIVC 2000 RPM 3Bar* BMEP, 91 RON Fuel, 736 injector .

The lowest BSFC region is near untrottled conditions (90-95 KPa) with some internal EGR. The engine will run with acceptable COV except for a small region where internal EGR is too high. BSFC also suffers at this point due to poorer combustion stability. At higher loads the internal EGR level contributing to high COV is lower and best BSFC is typically achieved with the maximum internal EGR level with 90-95 MAP. Since the 3-6 Bar BMEP data indicated best efficiency was limited by lower than desired internal EGR the phasing window of the exhaust cam was adjusted to allow more valve overlap. This sacrificed a region of valve phasing with negative overlap for the exhaust cam that had not shown to be beneficial during testing to date. The piston valve clearance was confirmed to still allow safe valve clearance although the measured exhaust valve to piston clearance was reduced from 2.6 to 0.6-0.7 mm with the adjustment. This clearance was measured under conditions of maximum phasing of the exhaust valves to produce minimum clearance. A procedure was developed to measure this in an assemble engine without removing the head with the entire valvetrain system intact.

At loads below 3 bar BMEP the region with excessive internal EGR increased in size and reduced the acceptable cam phasing region for best BSFC. Figures 14 and 15 show the cam phasing map for a 2000 RPM 1.25 Bar* operating condition. At this condition the internal EGR must be reduced by reducing the exhaust valve phasing to limit internal EGR. This results in earlier valve opening and reduced overlap. At these low loads the engine is actually operating as a fully expanded cycle so opening the exhaust valve earlier does not sacrifice expansion work. Difficulty still remains when trying to reach lower loads with EIVC and the area of near unthrottled operation has unacceptable combustion variation such that the engine must be operated in a condition of near zero overlap with high throttling to produce low load to idle conditions. Additional measures including individual trim control of injector PW to account for variation at low flows also had to be employed at the lowest load conditions; this will be discussed in the following section.

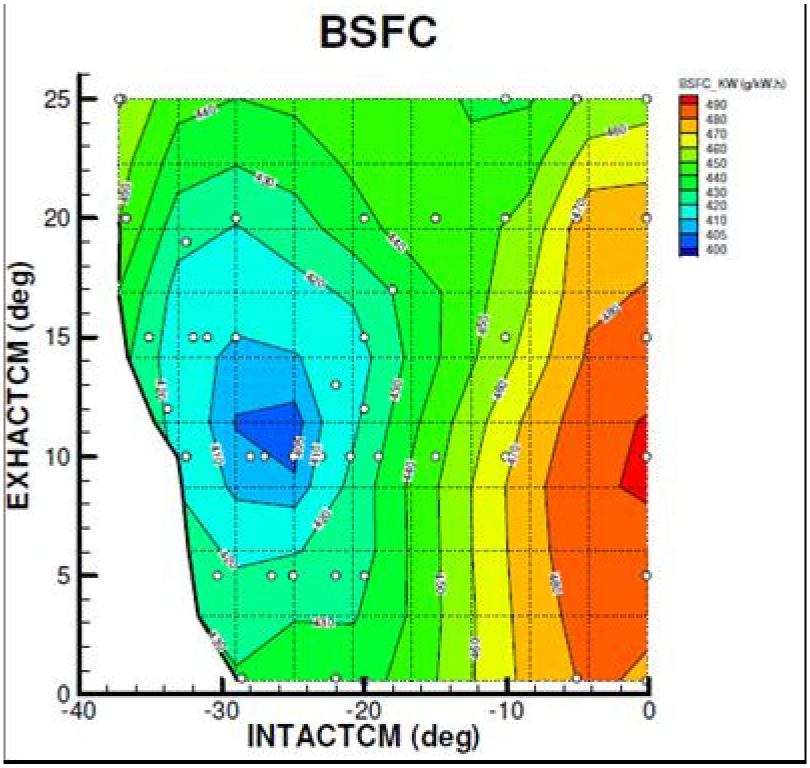

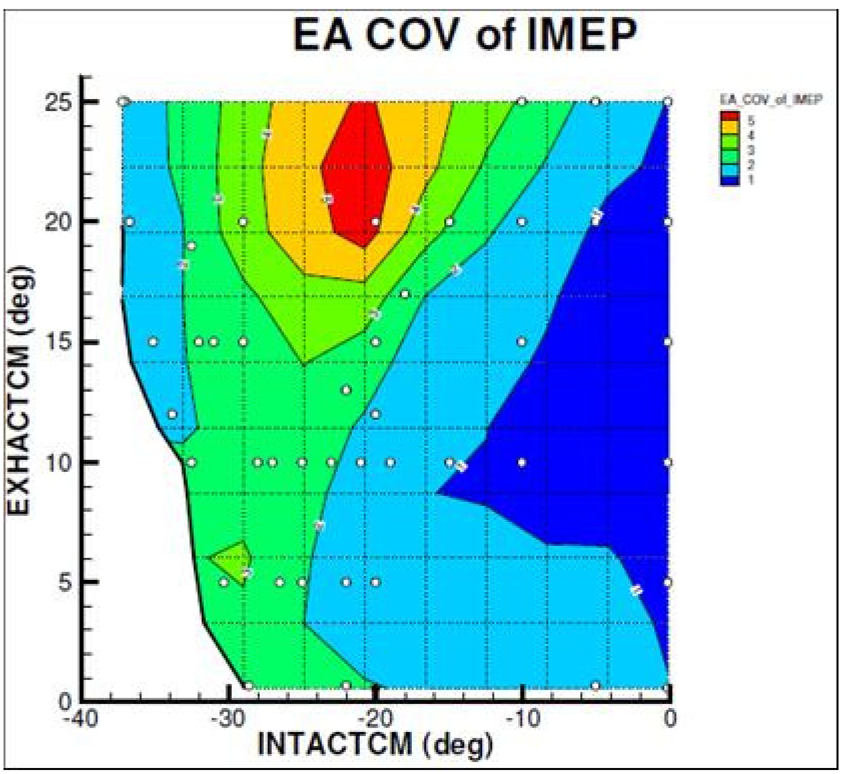

Figures 14 and 15 Cam optimization map, EIVC 2000 RPM 1.25Bar* BMEP, 91 RON Fuel, 736 injector .

Injector Flow Variation

As engine load was reduced variation between cylinders became more significant. Some cylinders exhibited excellent stability while others had high levels of variation which limited the potential of the engine. An effort was made to identify the sources of variation including individual cylinders, spark plugs and fuel injectors. The most significant contribution came from variation in injector flow rate as the injector PW was reduced. A technique was developed to identify the flow rate variation of individual injectors in situ while the engine was operating at a fired test condition. An example of results is shown in Figure 16**.**

At low flows the mass flow rate as a function of injector pulse width becomes more non linear and variation between injectors must be accounted for to assure a stoichiometric fueling to each cylinder. The observed cylinder to cylinder variation was actually the result of air fuel imbalance in the engine with rich cylinders operating well and lean cylinders suffering from poor engine stability.

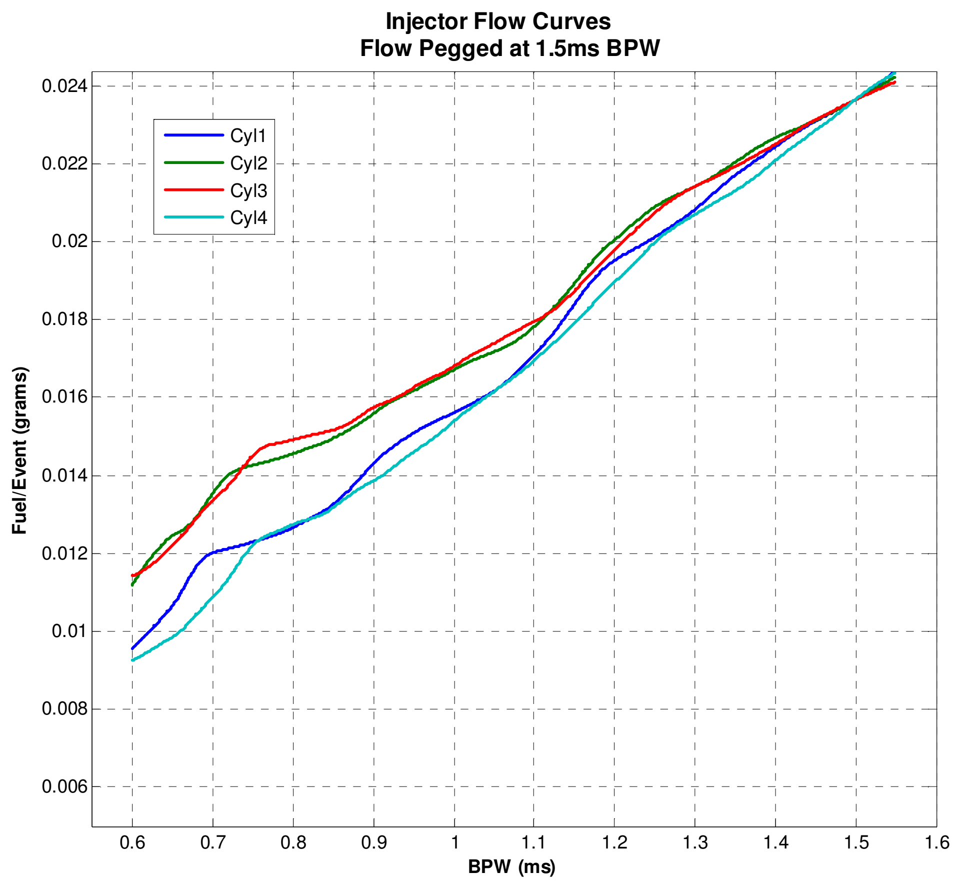

Figure 16 Injector flow rate vs Base Pulse Width (BPW) 736 injectors.

By knowing the fuel mass response this allowed adjustment of the individual injector Base Pulse Width (BPW) to balance the engine. This reduced AF variation between cylinders such that operation was not limited by a lean cylinder(s) contributing to poor combustion stability. The effect of injector flow mismatch is not significant at higher loads but should also benefit from the individual cylinder trim. At low loads (1 bar BMEP) variation in the individual flow curves can contribute to 10-20% variation in the AF ratio between cylinders, thus individual balancing is critical for stable low load performance.

Fuel consumption Improvement

The use of valve deactivation with EIVC enabled significant reductions in fuel consumption at low loads 2-6 bar BMEP. This testing was done for 91 RON gasoline. Improvements over the baseline engine ranged from 10-18 % from 6 to 2 bar BMEP. Figure 17 shows BSFC versus load at 2000 RPM for EIVC and LIVC with valve deactivation. The EIVC strategy is more efficient for loads below 6 bar BMEP.

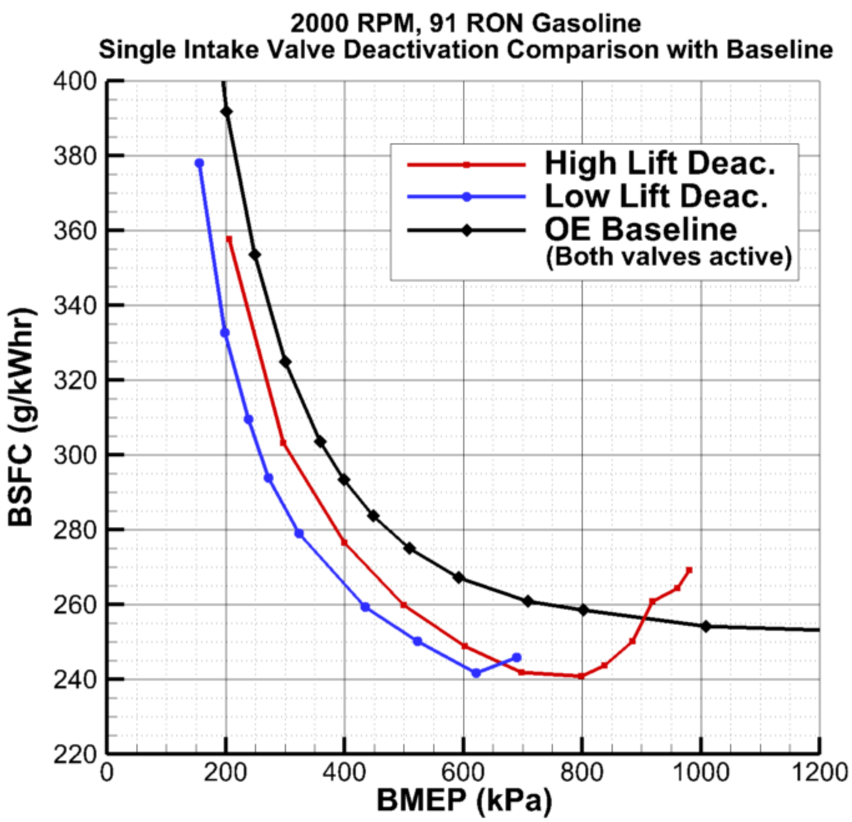

Figure 17 BSFC curves for 91 RON gasoline, 736 injector, unboosted operation.

Peak torque evaluation

Valve deactivation at high loads demonstrated benefits in reduction of particulates and hydrocarbon emissions. To determine the useful operating range that valve deactivation with LIVC provides peak torque was evaluated using E85 as a fuel. This testing was done with E85 fuel under unboosted conditions. Figure 18 shows the peak torque curves for LIVC using valve deactivation and 2 valve configurations. MBT timing was maintained under all test conditions. Valve deactivation provided an increase in low end torque under 2500 RPM with peak torque at 1500 RPM. The torque fell off significantly at speeds above 2500 RPM so a 2 Valve configuration would be preferable. All points are for stoichiometric operation.

Two points are shown for the peak torque curve with valve deactivation; the higher point is maximum torque which benefits from scavenging to increase volumetric efficiency. The peak torque sometimes resulted from over scavenging which produced a rich in-cylinder mixture, for additional power even though the net mixture remained stoichiometric. The lower point is for a condition with minimal scavenging producing the minimum BSFC.

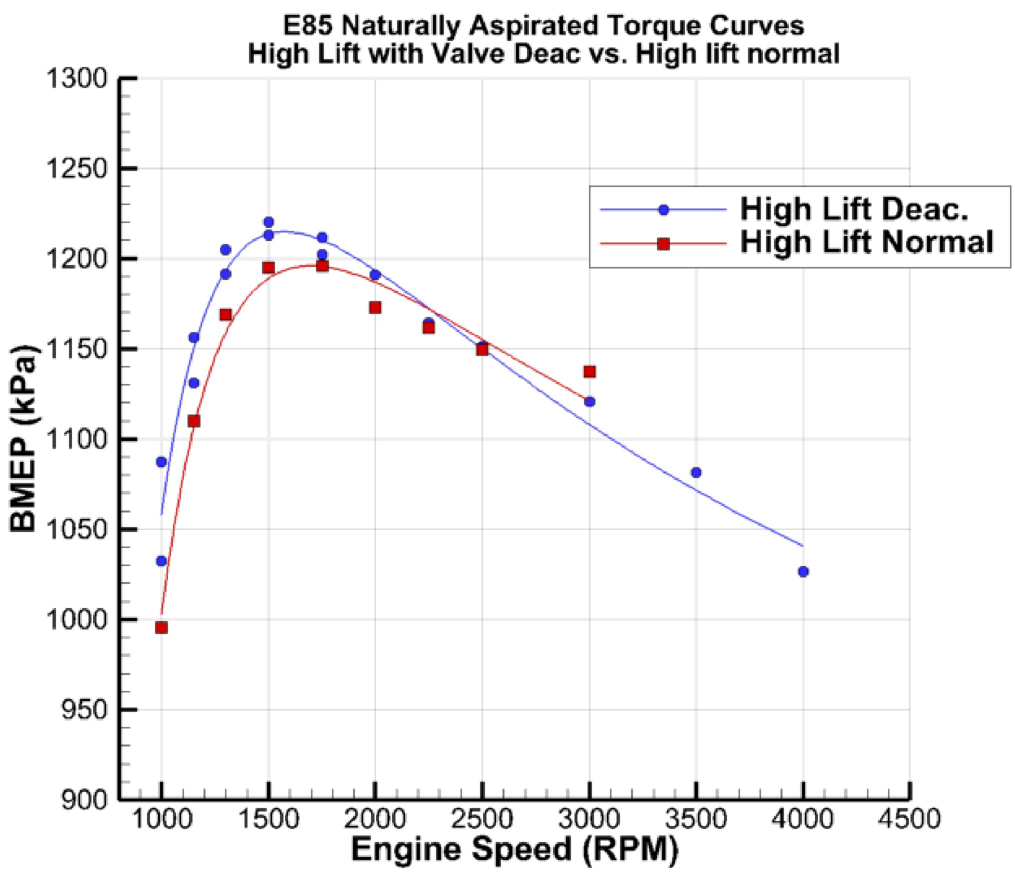

Figure 18 Peak torque curves LIVC strategy, E85 Fuel.

Phase 4 Task 4 – Multi-Pulse Fuel Injection (4/1/10 thru 6/30/10)

The multiple injections will also be investigated at WSU using spray visualization (which were reported earlier) and the injection rate measurements using IAV Injection Rate (IR) Meter. Typical IR results of the single and double injections are show in the figures below which show the injector design and their effects of the injection dynamics.

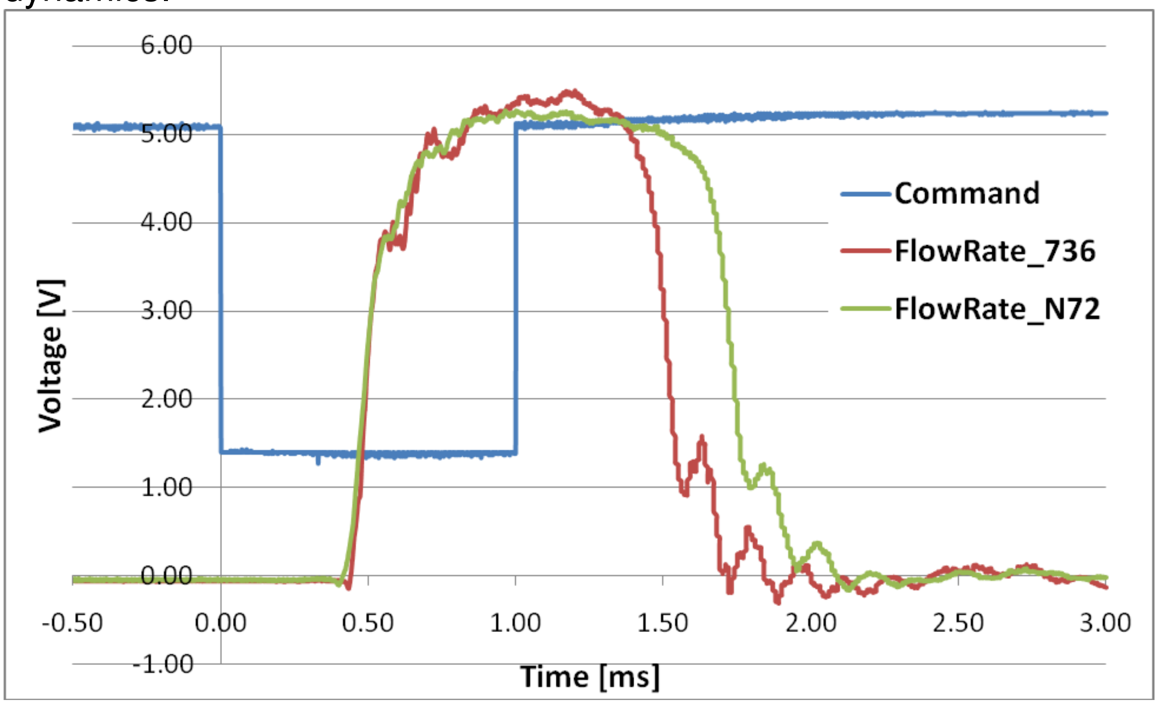

Figure 19. Comparison of injection rates of different injectors under single injection.

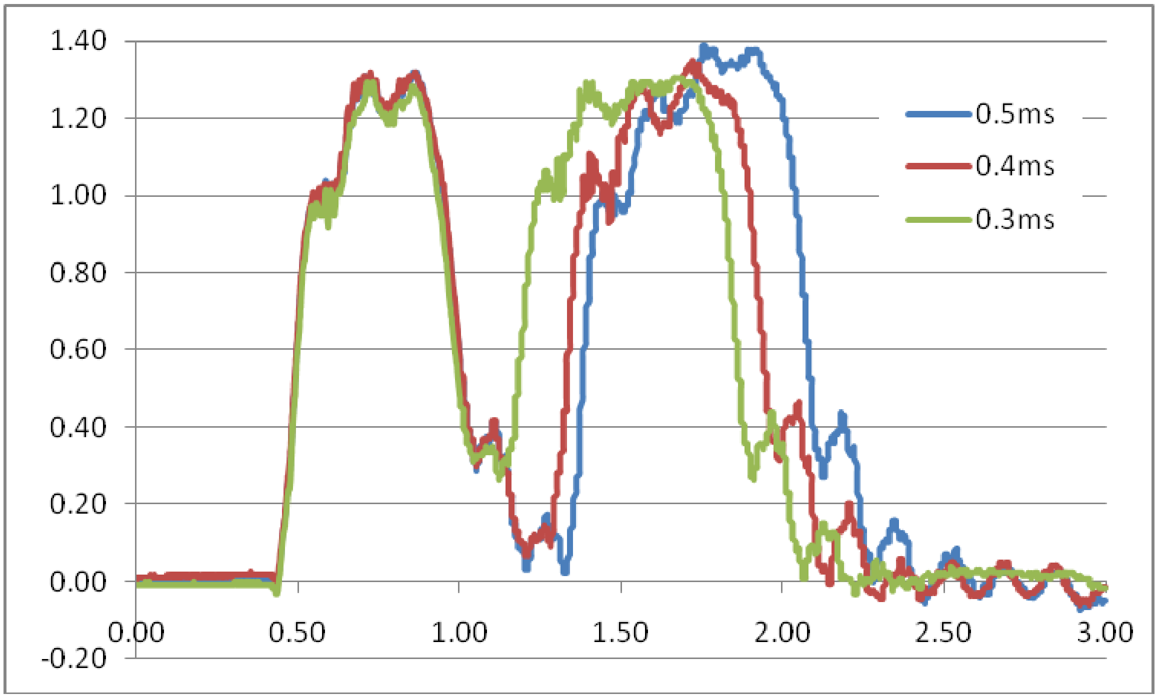

Figure 20. Comparison of split injection rates with different dwell times.

Quarter 3 2010

Phase 4 Task 2 – Optical engine charge motion study_(7/1/10 – 9/30/10)

Fig. 1 shows a typical result of the visualization of the OAE testing, with the side view results on the top and the bottom view below. The injector is placed on the upper right corner of the images in the side view, and it is seen at the center of the right side in the bottom view. The pairs of intake and exhaust valves are on the right and left half of the image respectively. The injection timing was 420CAD, and both intake valves were active for this example. The results clearly show how the spray develops and the mixture is formed inside the cylinder. Symmetric spray cloud of the upper and lower half of the bottom view confirms that the charge motion is tumble dominant.

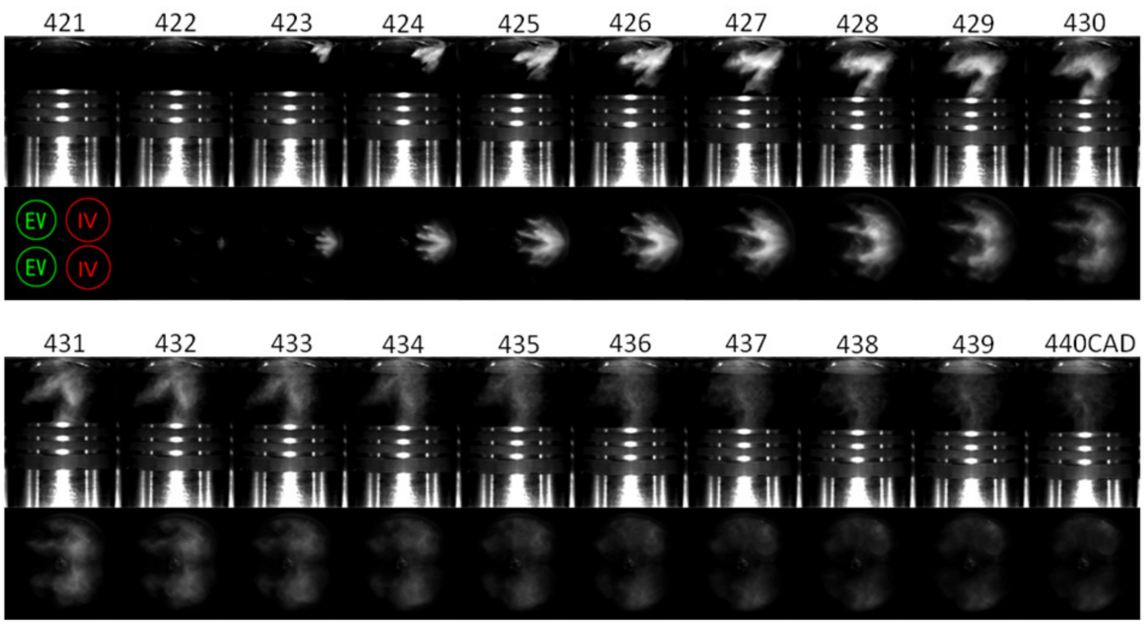

Fig. 1In-cylinder visualization of side and bottom views with the injection timing at 420CAD, with both valves active.

Previous work on the fired engine indicates advancing the injection timing is limited at 410CAD by soot generation, which is believed to be the result of spray impingement on the piston. To study the effect of injection timing on the piston wetting, spray penetrations with the injection timings from 400 to 450CAD were measured and plotted in Fig. 2 along with the piston displacement curve. Penetration was defined as the vertical component of the measured distance from the injector tip to the spray front of the lowest plume. It should be noted that there is some offset for the piston displacement because the origin was defined at the injector tip. The figure indicates that earliest three injection timings have the spray touched to the piston. However, since the injection timing at 420CAD resulted in almost zero soot emissions based on fired engine data, the impingement small enough that wall wetting is negligible.

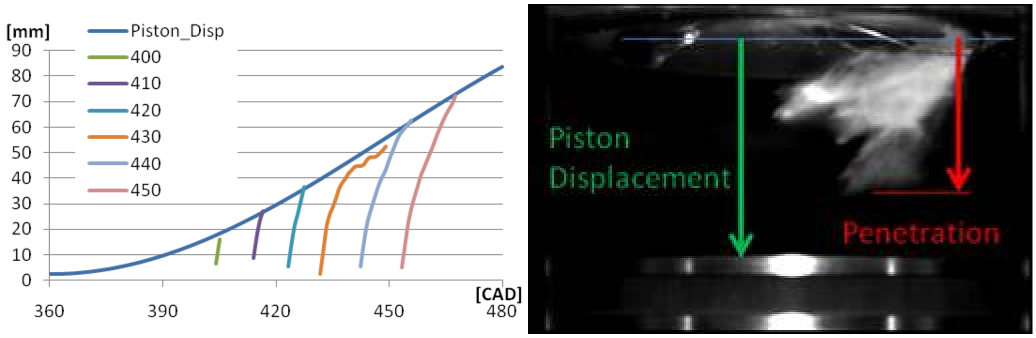

Fig. 2 Penetration of the spray and displacement curve (Left), and the definition (Right)

A big difference was observed between 420 and 430CAD. The spray at 430CAD did not hit the piston, and it stays away from the surface as Fig. 3 shows. The spray broke nicely and the mixture distributed thoughout the cylinder uniformly. When the injection occured at 440CAD, the resultant mixture motion was more dynamic. The in-cylinder air flow carried the mixture at the spray front away, and bulk motion of the mixture was observed at the bottom part of the cylinder which made the extended penetration in Fig. 2. In the right image of Fig. 3, the two images at 25CAD aSOI are superimposed with being colored as red for 430 and green for 440CAD. It is clear that the bulk cloud of 440CAD was located at the bottom of the cylinder and the stretched mixture make the cloud thinner. The same trend was observed for 450CAD case.

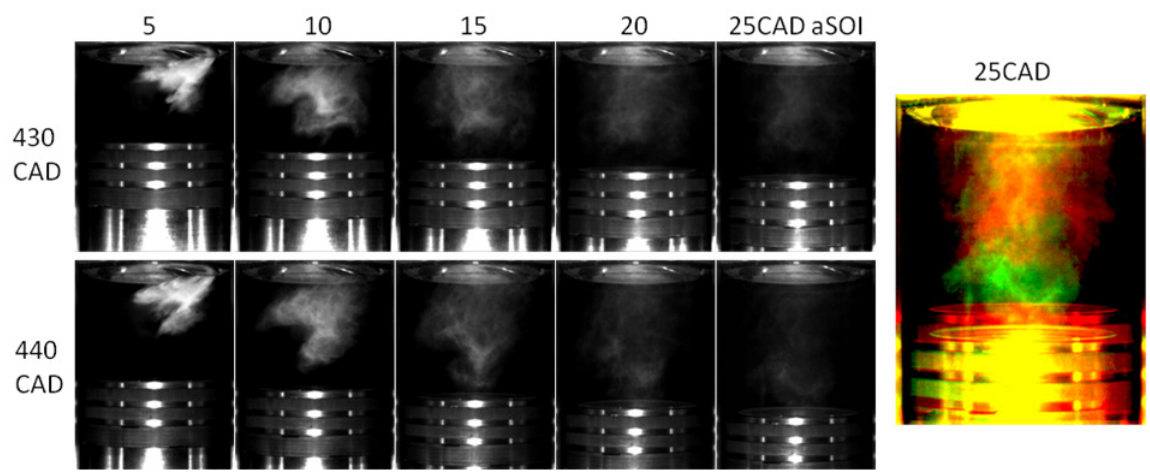

Fig. 3 Mixture visualization with injection at 430 and 440CAD

Fig. 4 shows the in-cylinder visualization with one intake valve deactivated. Only the bottom right intake valve was working. The injection timing was 420CAD. Comparing with the condition of two valves, the spray shape was very different. In Fig. 5, two-valve results were colored in red and one-valve in green. It is reviealed that strong in-cylinder air motion broke up the spray and deformed it significantly. In-cylinder flow sucked up the spray cloud to the top of the cylinder, and blowed it away with the intake flow coming through the valve. This explains why most of the cloud stayed on the right side of the cylinder, but it was vaporized quicker than the two-valve case. The later part of the bottom view shows asymmetrical distribution of cloud with respect to the horizontal center line, which indicates the charge motion consists swirl motion as well as tumble. There is difficulty in following how the mixture is formed optically by such complex charge motion.

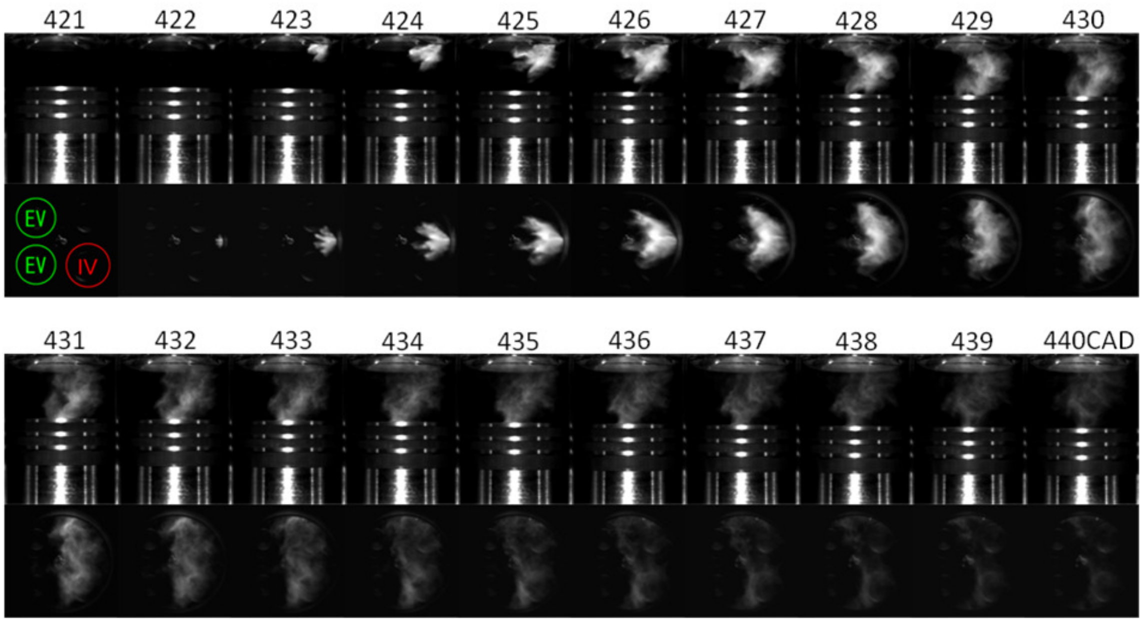

Fig. 4 In-cylinder visualization of side and bottom views with the injection at 420CAD, one valve deactivated

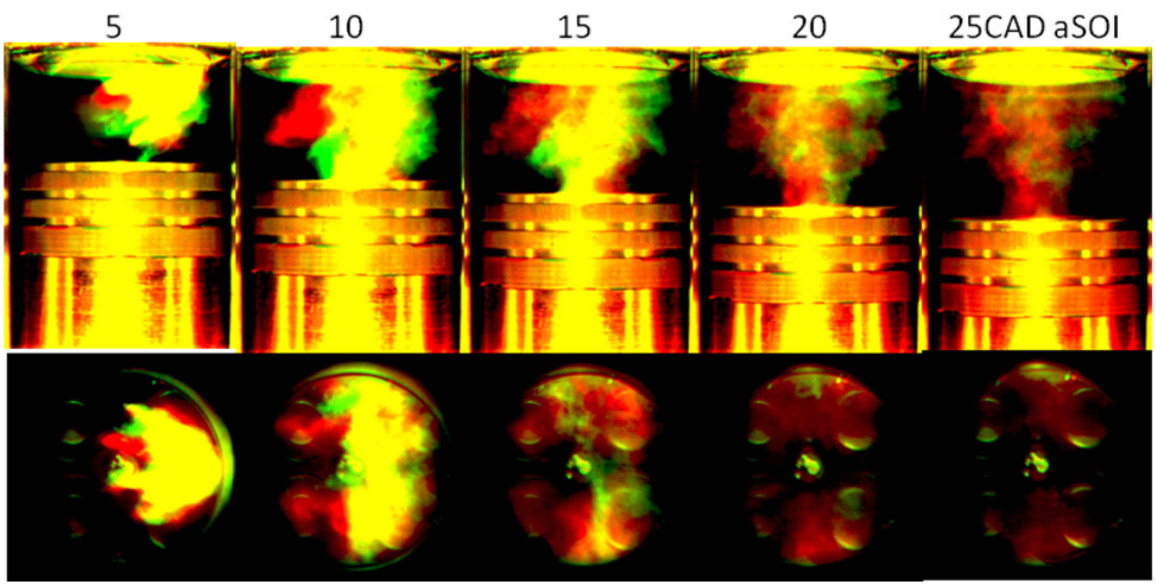

Fig. 5 Comparison of in-cylinder visualization of two valves (Red) and one valve deactivated (Green) with the injection at 420CAD

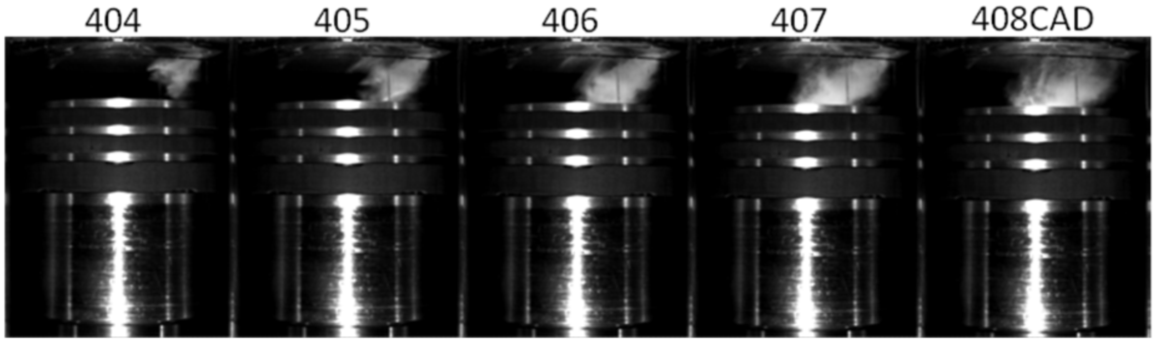

Fig. 6 In-cylinder visualization with the injection at 400CAD, one valve deactivated

The visualization showed strong piston impingement for these condition. (Fig.6), similar to the higher soot emissions measured by the metal engine experiment. The observed phenomena were investigated simultaneously using CFD using selected cases. Fig. 7 and 8 show the effect of injection timing on the bulk flow dynamic ratios and mass-averaged turbulent kinetic energy (TKE) compared to the motoring baseline. The results show that the injection timing has strong effects on the bulk flow. Injection too early cause liner and piston wall wetting. Injection too early or too late both weaken the tumble motion for the intake geometry tested. On the other hand, injection too late also counteracts the tumble motion and suppresses the overall turbulence intensity near compression TDC. TKE are required for mixing and to speed up combustion near the TDC. Injection too early reduce TKE for mixing, but injection too late also reduce it. Within that window of injection sometimes the TKE increases with the SOI angle, which can be correlated to the burning speed (e.g., CA1075 or the crank angle it takes from 10 to 75% burn-fraction of the injected fuel).

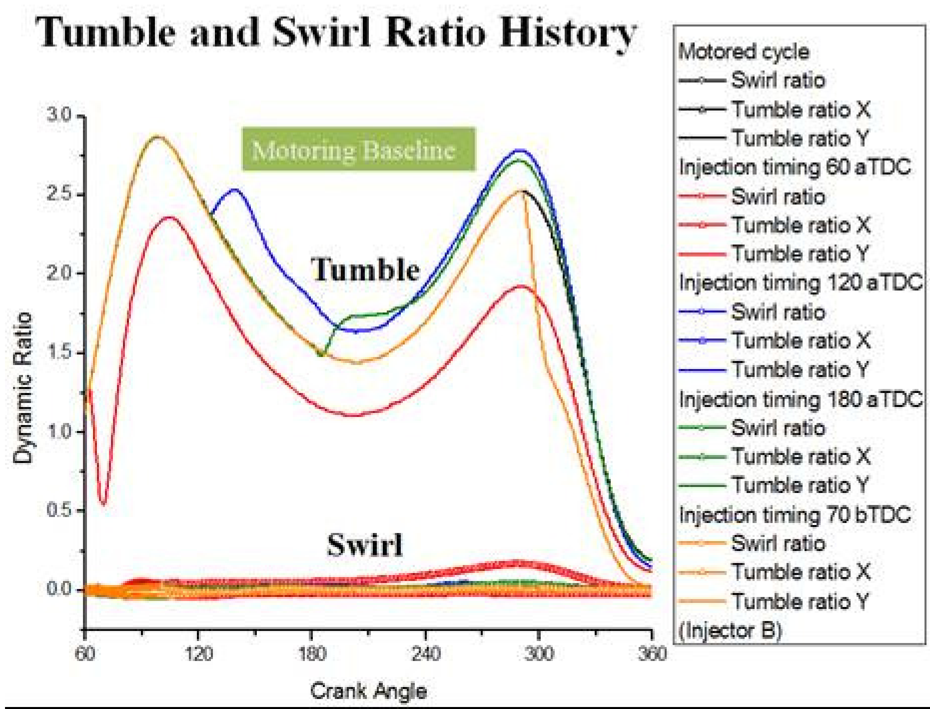

Fig. 7 The effects of injection timing on the dynamic tumble and swirl ratios.

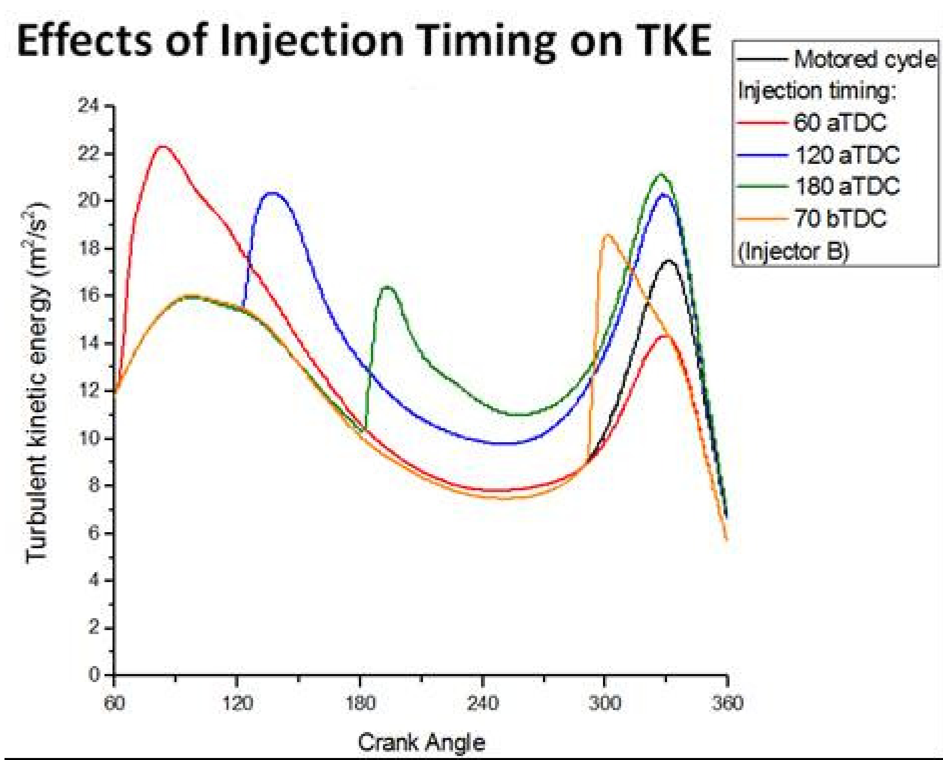

Fig. 8 The effects of injection timing on the turbulent kinetic energy.

CFD was also carried out to investigate the effect of valve deactivation on the charge motion and spray mixing. Four cases of low and high lift cases, with and without valve deactivation were selected for investigation in order to correlate with the metal engine test results. Fig. 9 describes the details of the test conditions and the valve lift profiles. For low-lift and lower load cases the start of injections are both timed at 50 degree after intake TDC; for high-lift and higher load cases the SOI timings are later at 60 and 80 degree after intake TDC respectively. The effects of valve deactivations on the bulk flow are very dynamic, and transform the initial tumble flow into 3-D rotational and tumbling flow as shown in Fig. 10,11. The interactions of the DI spray further complicated the flow structure. The TKE due to induction through the valve opening are generally lower for high-lift cases because of lower velocity within the larger valve gap opening. Valve deactivation increases the intake velocity but also create swirl which is less effective for generating turbulence near the TDC but could be more effective in improving air utilization of the fuel spray plume. Fig. 12 shows that the deactivation reduces the unmixedness as indicated by the standard deviation of excess air ratios (lambda) for both low- and high-lift cases near TDC. The interaction of the DI spray further complicates the mixing structure, as later injection timing improve the tumble and turbulence for mixing, which is evident for the high-lift deactivation case in Fig. 11.

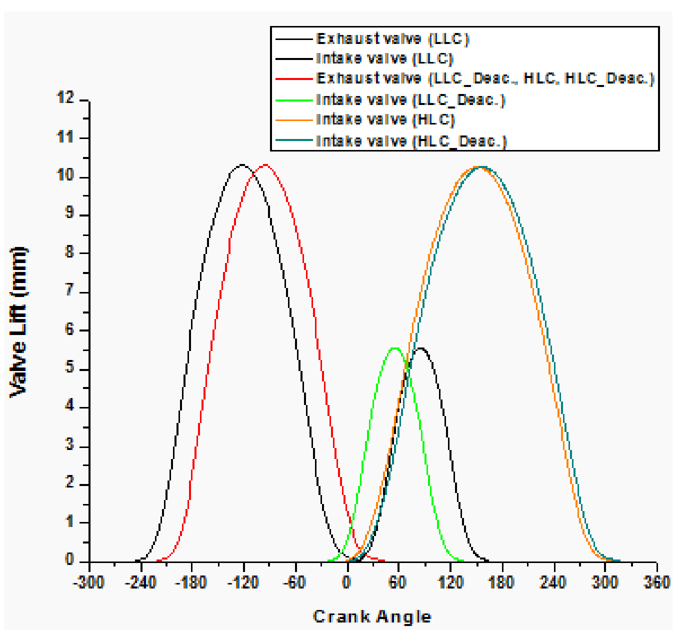

Injection conditions	*LLC*	*LLC_Deac*	*HLC*	*HLC_Deac*
Injection Timing (CAD After intake TDC)	*50*	*50*	*80*	*60*
Injection Duration (CAD)	*9.12*	*9*	*17.64*	*17.01*
Injection Mass (mg)	*10.2*	*10.05*	*27.8*	*26.4*
Fuel	*Gasoline (density 0.7426)*			

Fig. 9 The details of the test condtions and the valve lift profiles cases selected for CFD investigation.

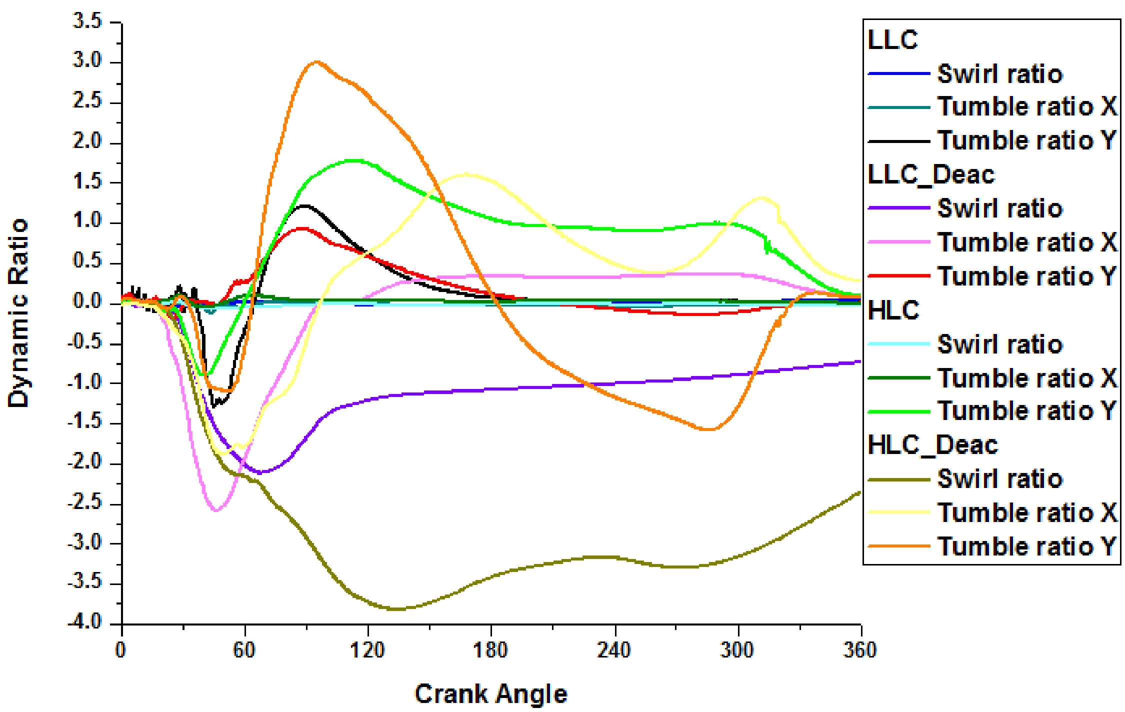

Fig. 10 The effects of valve deactivation and lift on the dynamic tumble and swirl ratios.

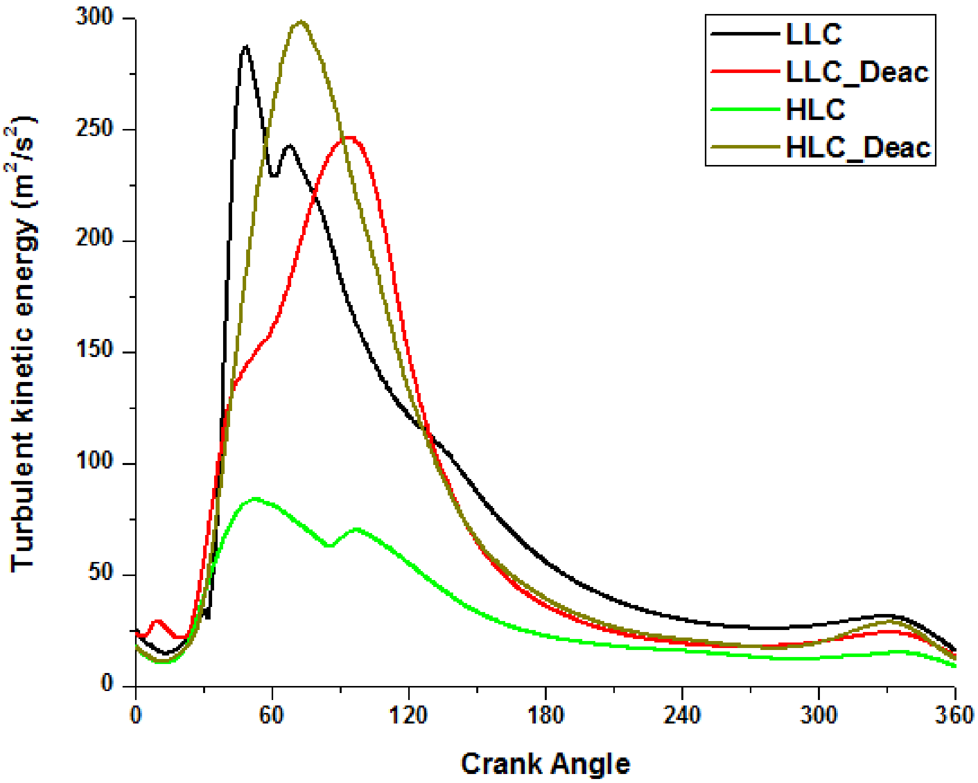

Fig. 11 The effects of valve deactivation and lift on the turbulent kinetic energy.

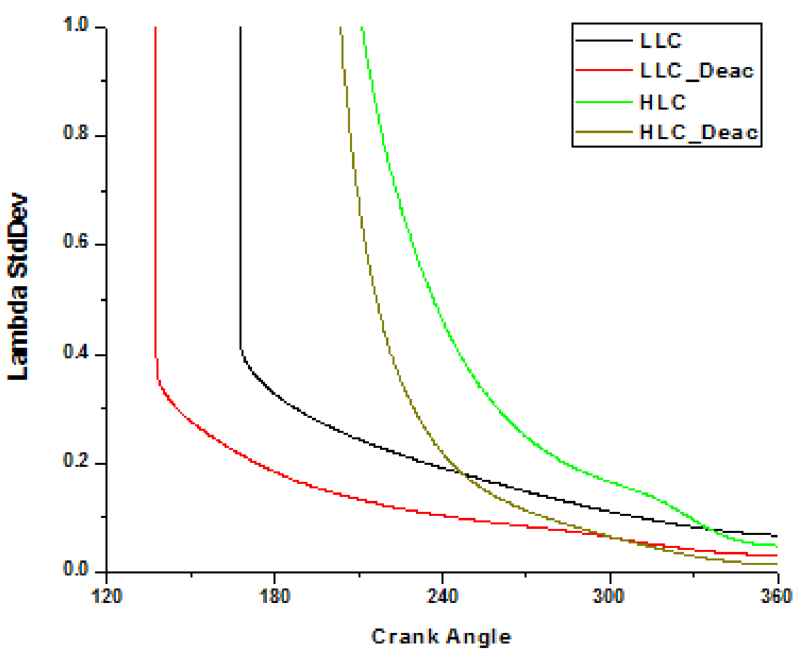

Fig. 12 The effects of valve deactivation and lift on mixing.

The wall-film history for the four selected cases is shown in Fig, 13. Valve deactivation creates swirling charge motion and keeps the spray away from the piston. The wall film on the liner is relatively small for the four cases investigated.

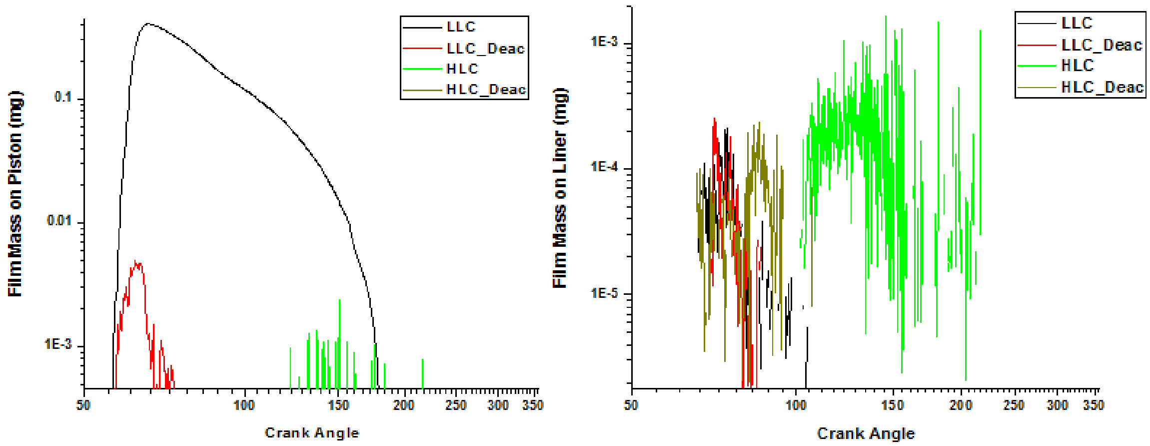

Fig. 13 The effects of valve deactivation and fuel film history on piston (left) and liner (right).

CFD is shown to be very useful in GDi engine design to evaluate effects of injector design, engine speed, and bulk flow and spray-wall interactions, although continuous improvement in flash boiling, wall impingement and combustion models are needed.

<u>Phase 4 Task 3.0</u> –Multiple cylinder engine charge motion study (7/1/10 thru 9/30/10)

The use of valve deactivation proved effective for improving combustion stability with Early Intake Valve Closing (EIVC) enabling significant gains in fuel efficiency at low loads below 5 bar BMEP. Optimization was carried out with and without valve deactivation on the EIVC and LIVC cam. Data from a load sweep at 2000 RPM is shown in Figure 14 comparing a variety of strategies. The preferred strategy below 6 bar was to use EIVC with valve deactivation. At higher loads running LIVC with both valves and light throttle was preferred both for fuel economy and NOx emissions. EIVC with deactivation allowed operation up to 3500 RPM although maximum torque did start to fall off to 5 bar BMEP by this point. Above this load LIVC is used to achieve peak torque by optimization of cam timing.

The relative fuel consumption improvement relative to the base engine up to 3000 RPM and peak load is shown in figure 15. Improvement ranges from 6% at high loads to over 20% at low loads. The area of improvement is most significant in the region of operation typical of low speed city or mild highway driving typical of the FTP city and highway cycle. The region centered on 6 bar BMEP and

2000 RPM is where DICP was used on the base engine to minimize fuel consumption with internal EGR control so the relative improvement is smaller in this region.

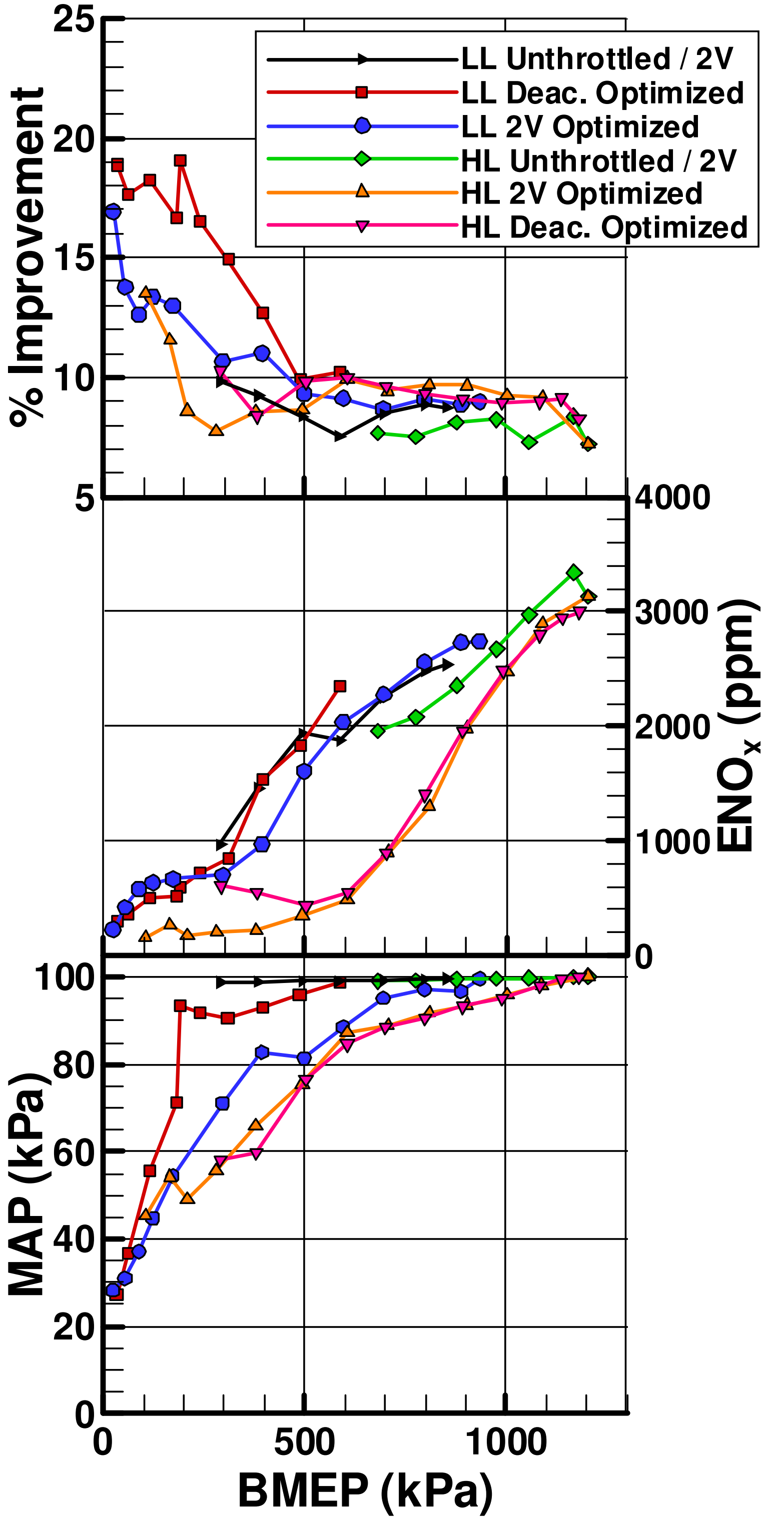

Figure 14 2000 RPM Load sweep E85 fuel comparing valvetrain strategies. (a) Fuel consumption reduction, (b) NOx Emissions, (c) Throttle (MAP)

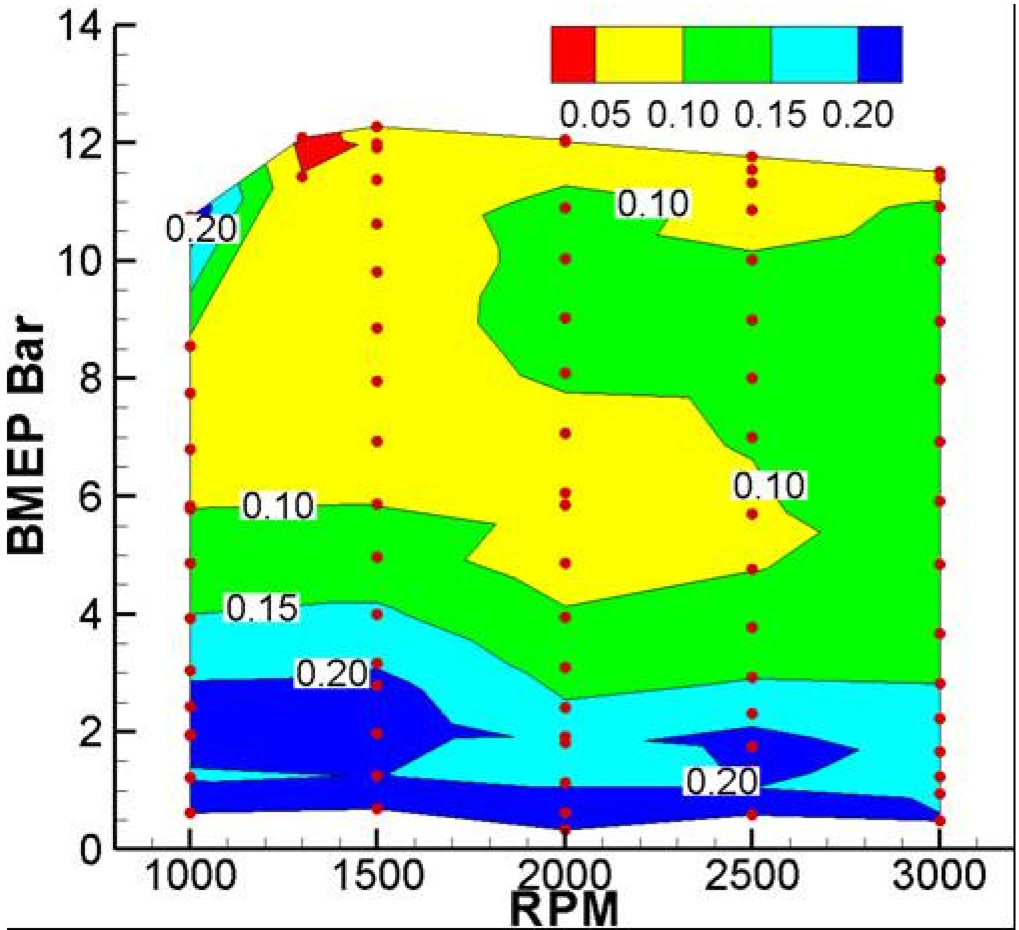

Figure 15 Relative improvement in thermal efficiency relative to the base engine configuration operating on E85.

To investigate the potential improvement in fuel economy of the E85 optimized engine GT-Drive was used for evaluating the fuel economy on representative drive cycles. In addition to the improvements to engine efficiency improvements can be realized by operating the engine in regimes of higher efficiency. This includes modifications of shift schedules and drive ratios to down-speed the engine increasing its load and efficiency. The development of transmissions with 5, 6 or more speeds allows better optimization to improve efficiency and maintain good drivability. To investigate the potential end develop shift schedules the BSFC map of the improved engine is evaluated to determine the most efficient operating strategies Figure 16. In addition to showing the BSFC curves an analysis of preferred operation conditions is presented. With the ability to select between different gear ratios, it would be desirable to operate the engine in the most efficient operating point for the desired power to supply the power demanded by the driver. To evaluate this, a line of constant power is shown by the blue dashed line, in this case 10KW. If we compare the locus of points the most efficient operating condition would be to operate at a low speed and high load. This point is shown by the Yellow line which is the locus of points of most efficient operation as a function of power. While it may not be possible due to transmission capability or even desirable to operate at this load due to NVH issues it is useful as a reference. For comparison the lines with the red labels show the relative fuel economy penalty by operating at different conditions for the same power. For example at the demanded power of 10 KW this can be achieved at 1500 RPM, 4 Bar BMEP which suffers a 5% penalty, 2000 RPM 3 Bar which has a 17% penalty or 3000 RPM 2 Bar which suffers a significant 45% penalty. Figure xx thus provides a useful tool to identify regions that proper selection of the transmission gear and shift schedules can significantly aid vehicle fuel economy. This must be balanced with needs for good drivability; however the combination of good low end torque and improved transmissions offers the potential for both good economy and performance. To leverage this potential, shift strategies to minimize the amount of time at high speed low load conditions with high fuel penalties were evaluated in vehicle drive simulations.

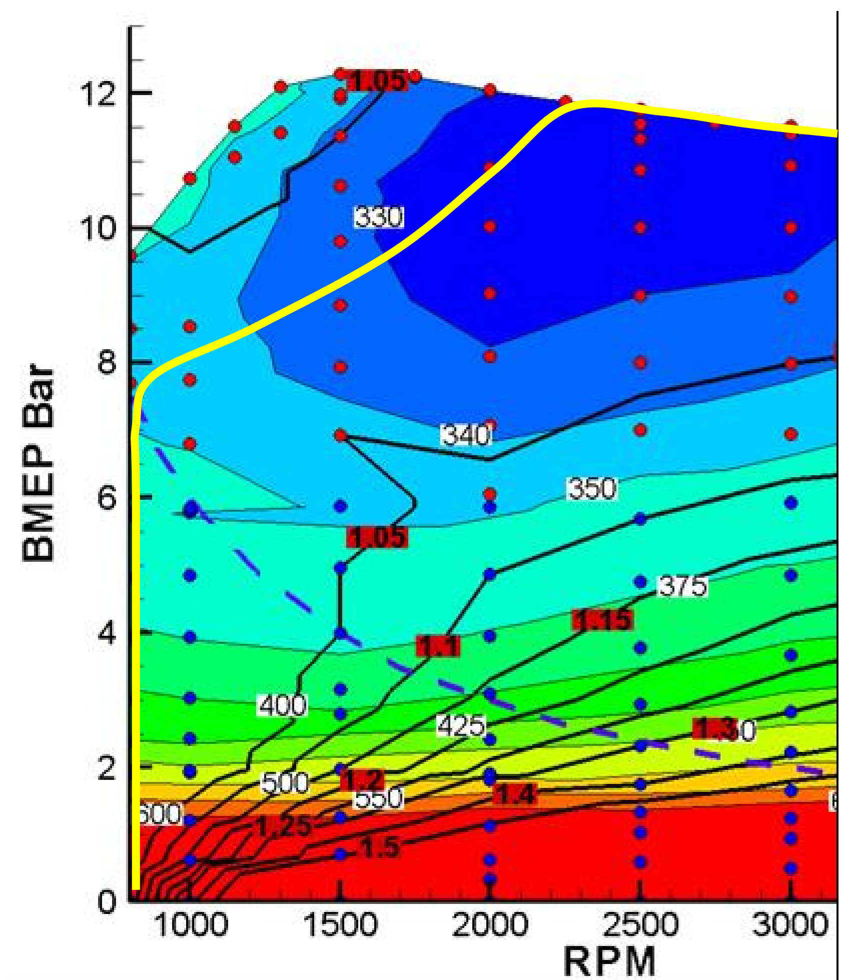

Figure 16 Speed-Load Map of E85 BSFC (Contours) showing relative efficiency (Red Labels) at equivalent power (Blue Dashed Line), Yellow line indicates most efficient path. Red Points LIVC, Blue Points EIVC (Deac).

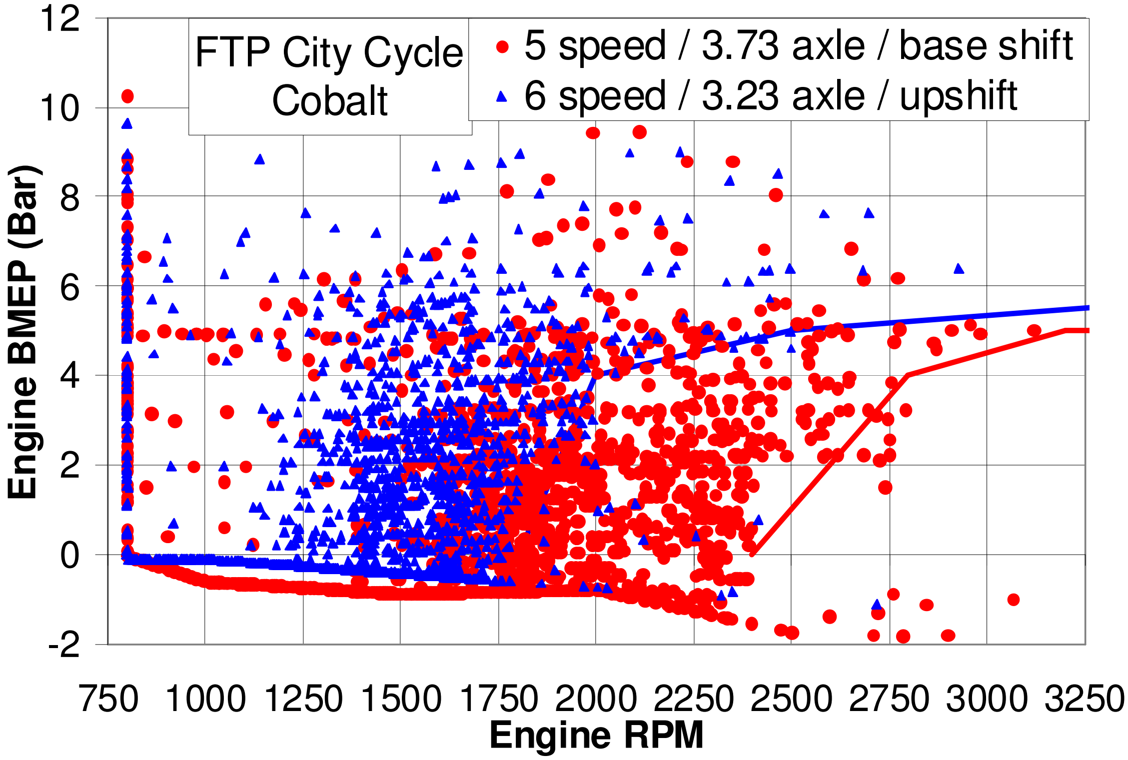

Figure 17 FTP City cycle showing operating points with base and proposed transmission, axel and shift schedule.

Up-shift line, Red (Baseline) Blue (up-shifted)

To illustrate the change of operating conditions the effect of transmission, drive ratio and shift schedules if shown for the FTP city cycle in figure 17. Transmission ratios were selected representing a 5 speed and 6 speed production transmission. A significant reduction of time is spent in the low load region above 2000 RPM where the fuel efficiency penalties are significant. Simulations were run for the FTP city and highway cycles and at steady state road loads of 55, 65 and 75 MPH and these results are presented in figure 18 for a variety of strategies. The fuel economy is relative to the base engine running on E85 with the same thermal efficiency as the base gasoline engine. The benefit of the improved strategies for reducing the disparity between fuel consumption with gasoline and E85 is almost entirely offset on the FTP city cycle but is less effective as the demands of the driving conditions increase. At highway cruise speeds the shift schedule has no effect since the vehicle is in overdrive in all cases, only the benefits of the lower final drive ratio and the engine modifications are evident. The 6 speed transmission's final drive ratio is similar to the 5 speed so its advantage will primarily show up in launch performance not fuel economy

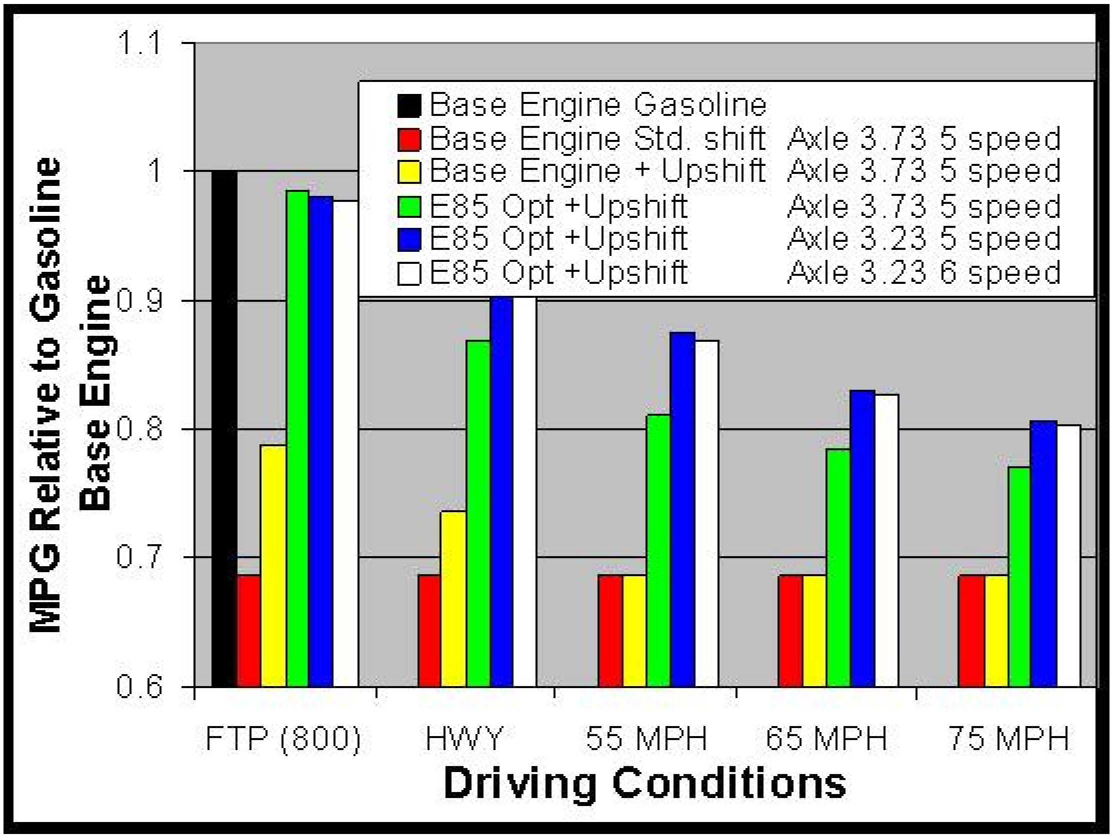

Figure 18 Relative fuel economy to base engine operating on E85 for various operating modes and effect of transmission axel ratio and shift strategy.

Fuel Blend Evaluation

Flex-fuel vehicles must operate on blends from E0 gasoline up to E85. The effect of intermediate blends on engine operation and calibration is an area that must be assessed to maximize performance and efficiency over all blends not just E85 or E0 gasoline. To investigate the effects of intermediate blends a series of tests were run on blends from E0 to E85 including a premium gasoline for reference. During work with gasoline and E85 tests were identified where the performance of E85 and gasoline differed significantly.
The test consisted of the following evaluations:

- Start of Injection (SOI) timing sweeps (EIVC and LIVC) 2250 RPM, 6 Bar BMEP

- EGR tolerance evaluation LIVC, 2000 RPM, 6 Bar BMEP
- Load sweeps to identify knock limited load and compression ratio LIVC, 1500 RPM, 2000RPM
- Knock limited torque vs. speed LIVC, 1000-4000 RPM

Injection timing evaluation

When evaluating injection timing, to optimize efficiency, E85 proved to be highly resistant to particulate formation. This was the case even at early injection timings that would result in piston impingement. This was the case for both the EIVC and LIVC strategies. When testing with intermediate blends up to E50 the early injection timing limited by soot was nearly identical for all blends, thus only E85 showed a wider window of acceptable operation. No effect of ethanol concentration was seen on the late timing limit for EIVC or LIVC. Fuel consumption was dominated by the relative heating value of the blend. Data is presented in figure 19 for the EICV cam injection timing sweeps. Hydrocarbon and NOx emissions did trend lower with ethanol content for all of the testing that was done under MBT conditions. An example will be shown for the load sweeps presented in figure 23.

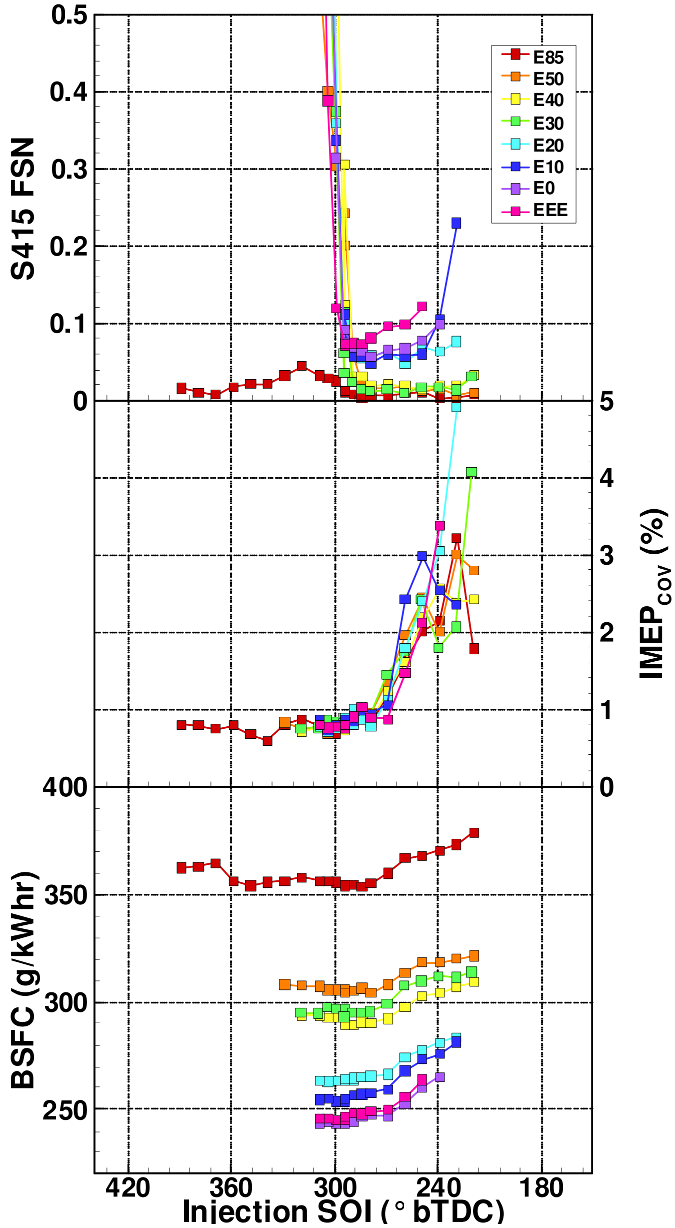

Figure 19 (a) Soot (FSN), (b) Combustion stability (COV%), (c) Fuel consumption (BSFC g/KW Hr) 2250 RPM, 6 Bar BMEP EIVC strategy

Internal EGR Tolerance

E85 showed high resistance to EGR-induced-knock at high loads allowing internal EGR optimization up to peak torque. During E85 cam optimization it was determined that a small operating window existed that allowed high levels of internal EGR, high compression and high MAP where E85 was susceptible to EGR induced trace knock. Slight retard (2-3 cad) to eliminate knock was required for E85. To evaluate the effect of ethanol content this test condition was repeated for the fuel blends to determine the relative knock resistance of the test fuels. The test was conducted as an intake cam phasing sweep which produced an increase in the effective CR and an increase in valve overlap to allow more internal EGR. All conditions are stoichiometric fueling and MBT or knock limited spark. The effect on NOX and BSFC is presented in terms of the effective CR in Figure 20 (a) and (b) respectively. Once the onset of knock was detected spark retard was used to keep knock at an acceptable level. The use of spark retard also results in a reduction in NOx, but both combustion stability (COV) and BSFC deteriorate. Figure 21 (a) and (b) show the required retard in combustion phasing and the combustion stability. For this test condition, ethanol blends above E30 enable a significant reduction of NOx with a reduction in fuel consumption. For gasoline and lower ethanol blends there is a tradeoff because of the reduced knock resistance. The fuel consumption reduction is also partially the result of a reduction of manifold vacuum as overlap is increased resulting in reduced pumping work.

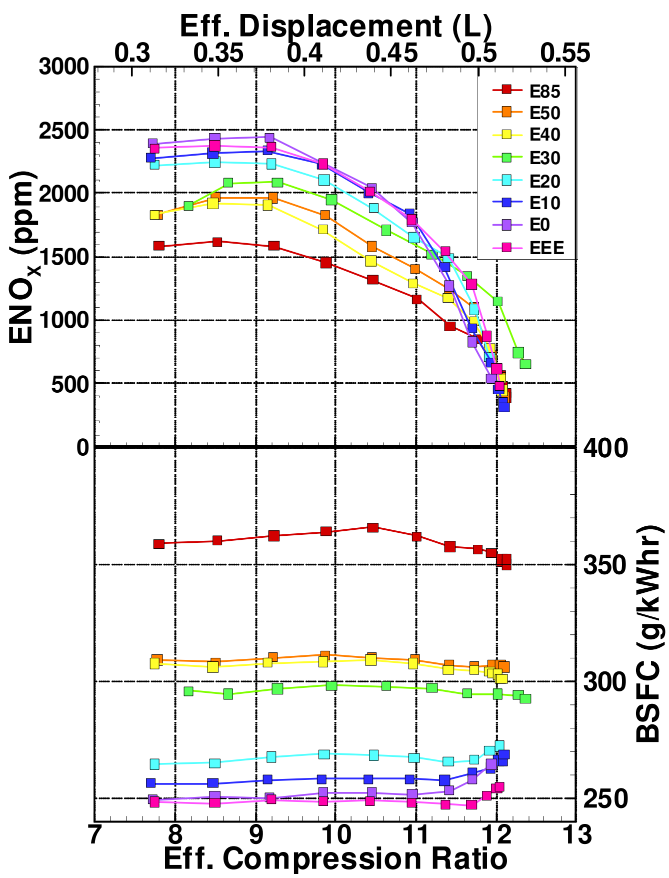

Figure 20 (a) Engine out NOx (ppm) (b) Fuel Consumption BSFC (g/KW Hr) 2000 RPM 6 bar BMEP LIVC cam

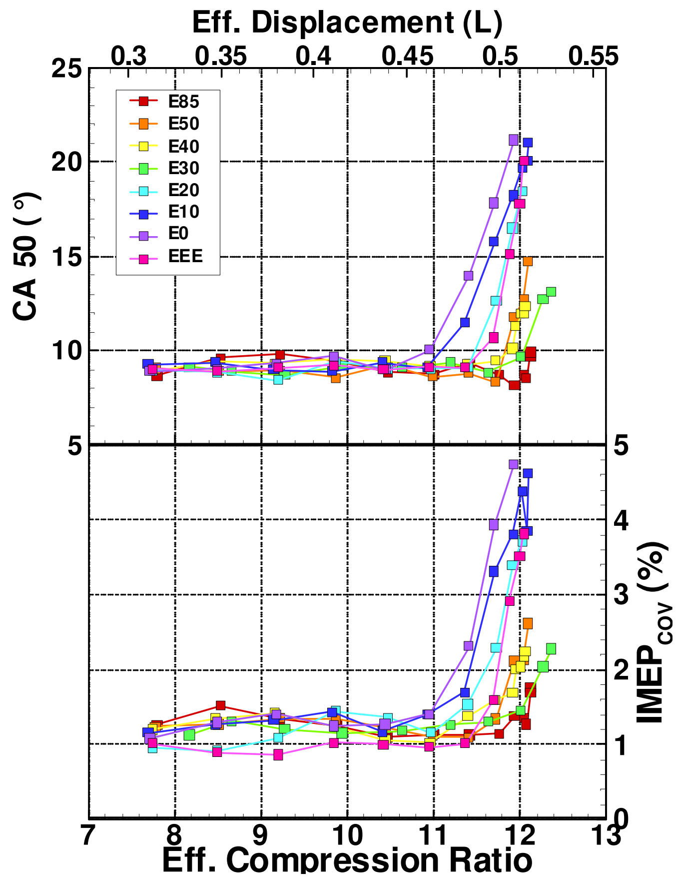

Figure 21 (a) Combustion phasing CA50 (cad aTDC) (b) Combustion Stability (COV%) 2000 RPM 6 bar BMEP LIVC cam

<u>Load – Effective Compression Ratio Sweep (2000 RPM)</u>

To determine the effectiveness of ethanol content for suppressing knock an effective compression ratio sweep of the engine was run at 1500 and 2000 RPM. By adjusting the intake valve closing time the effective compression ratio can be varied from 8-12. The exhaust cam phasing and injection timing were fixed for all cases, to focus on the fuel effects. Injection timing was chosen to avoid the FSN increase resulting from injections being to early. The valvetrain allows the engine to maintain MBT spark without knock for all of the fuels including the E0 91 RON gasoline. As the compression ratio is increased the trace knock limit at MBT or knock limited spark was identified for each fuel. To provide CR specific data the MBT or knock limited combustion phasing with respect to effective compression ratio is shown in figure 22. Of interest is the similar performance of the E10 / 91 RON blend to the 97 RON EEE gasoline, showing the benefits of small quantities of ethanol for increased knock performance. As the ethanol content increased higher effective CR was possible, for the E30 blend and higher no significant spark retard or performance penalty was apparent. E0 gasoline provides minimal fuel consumption up to 9 bar BMEP while E20 provides minimum fuel consumption at peak power. The effect of increasing load via effective compression ratio resulted in an increase in hydrocarbons, NOx and FSN. The emissions were however strongly related to the ethanol content with higher ethanol blends reducing emissions for all 3 constituents, Figure 23 (a, b, c) Testing was also done at 1500 RPM which was more knock prone due to lower speed, similar conclusions are observed at 1500 and 2000 RPM.

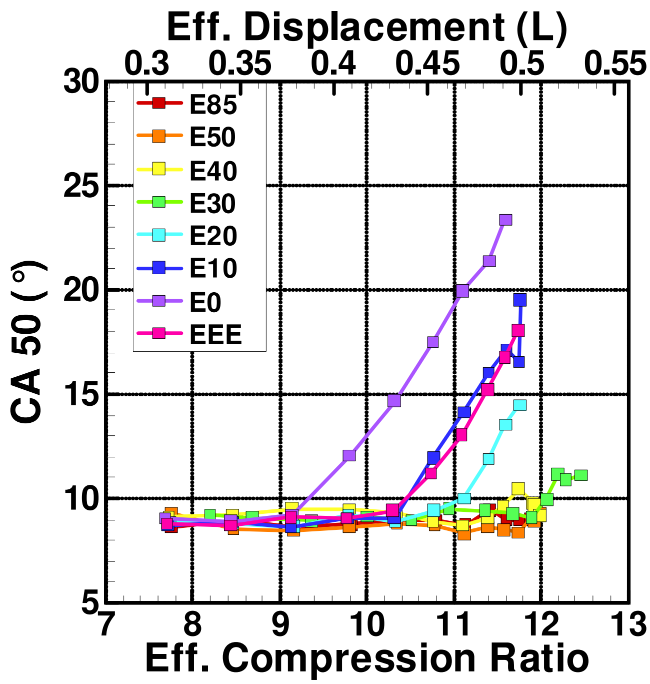

Figure 22 Knock limited CR and combustion phasing (CA50, cad aTDC)

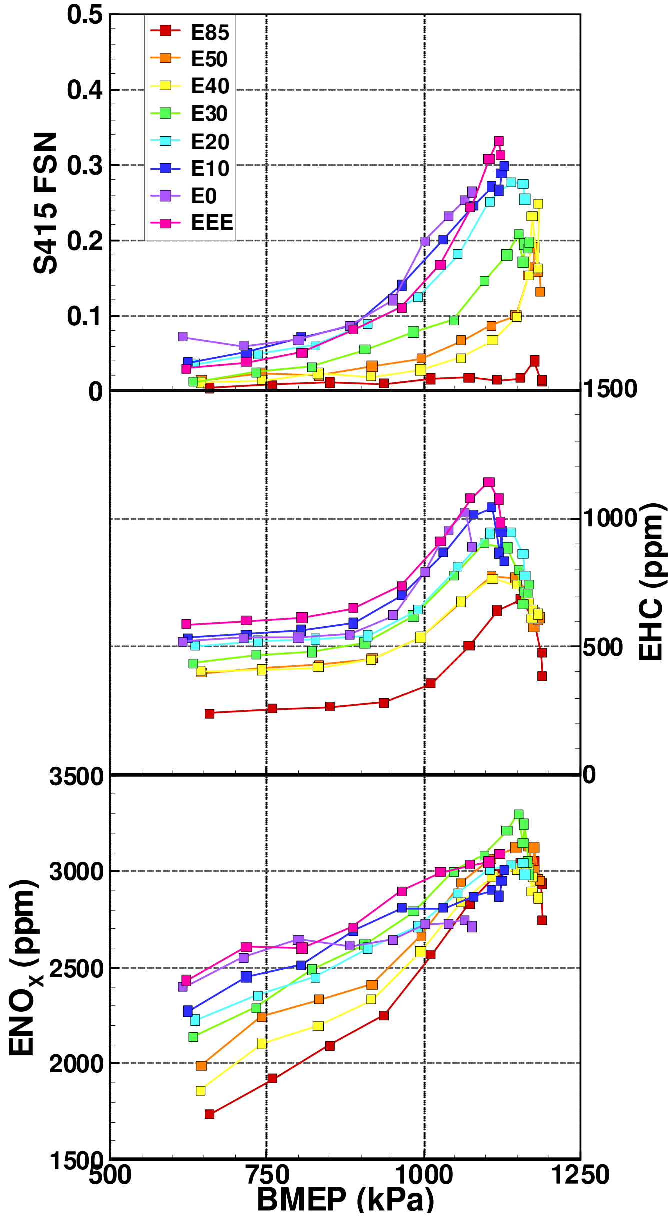

Figure 23(a) Soot (FSN), (b) Engine out Hydrocarbons (ppm), (c) Engine out NOx (ppm)

2000 RPM un-throttled LIVC.

<u>Knock Limited Torque - RPM Sweep</u>

Testing was done over the speed range of 1000- 4000 RPM to identify the knock limited load and compression ratio. Testing was done in a similar fashion to the 2000 and 1500 RPM load sweeps by increasing the effective compression ratio until trace knock was detected. Data was taken with an MBT combustion phasing (CA50; 8-10 cad aTDC). Figure 24 (a,b,c) shows the knock limited BMEP, Combustion phasing and effective compression ratio over the speed range. There is a significant difference in the knock limited CR and associated MBT torque for the ethanol blends. Knock limited torque at MBT is limited to an effective CR of 7.6 at 1000 RPM to 10.5 at 4000 RPM. Increasing the ethanol content shows a consistent effect of allowing a 1 point increase per 10% ethanol addition until the geometric compression ratio of the engine is reached.

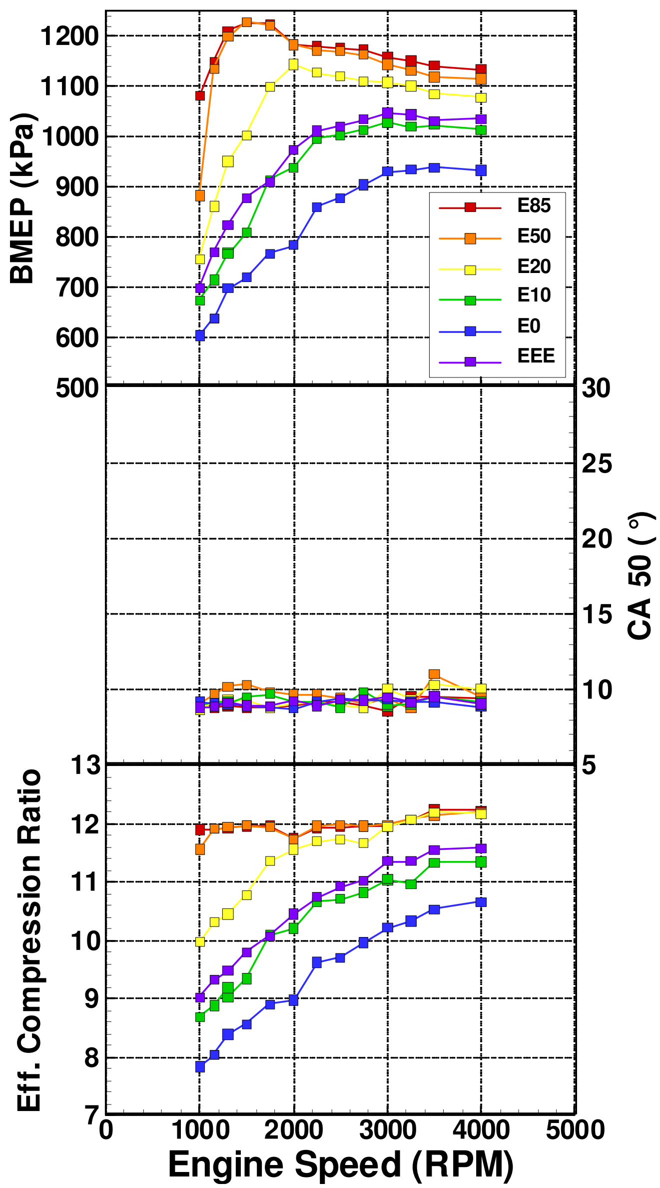

Figure 24 (a) Knock limited load,(b) Combustion phasing(CA50), (c) CR 1000-4000 RPM LIVC Cam

For fuel blends that were knock limited, spark retard was used to retard combustion phasing until maximum torque was achieved. As the effective compression ratio was increased spark retard allowed knock free operation. For the low ethanol blends the effective displacement and CR was limited at low speeds since excessive spark retard was needed as the CR increased. The peak CR was limited to a point in which further increases resulted in a loss of torque. Figure 25 (a,b,c) shows the knock limited BMEP, combustion phasing and effective compression ratio over the speed range. The use of spark retard allowed the effective CR to be increased about 2.5 points before the efficiency penalties associated with spark retard were more significant than the increased displacement. This level of spark retard was typically at a combustion phasing near 24 cad aTDC. Unlike a fixed cam system the use of VVA with LIVC allows cam phasing selection to limit the efficiency loss that results from very late combustion phasing which produces lower torque with increased fuel consumption. For fuel blends above E20 the maximum torque curve was not significantly limited. E20 can provide 97% of the peak torque of E85.

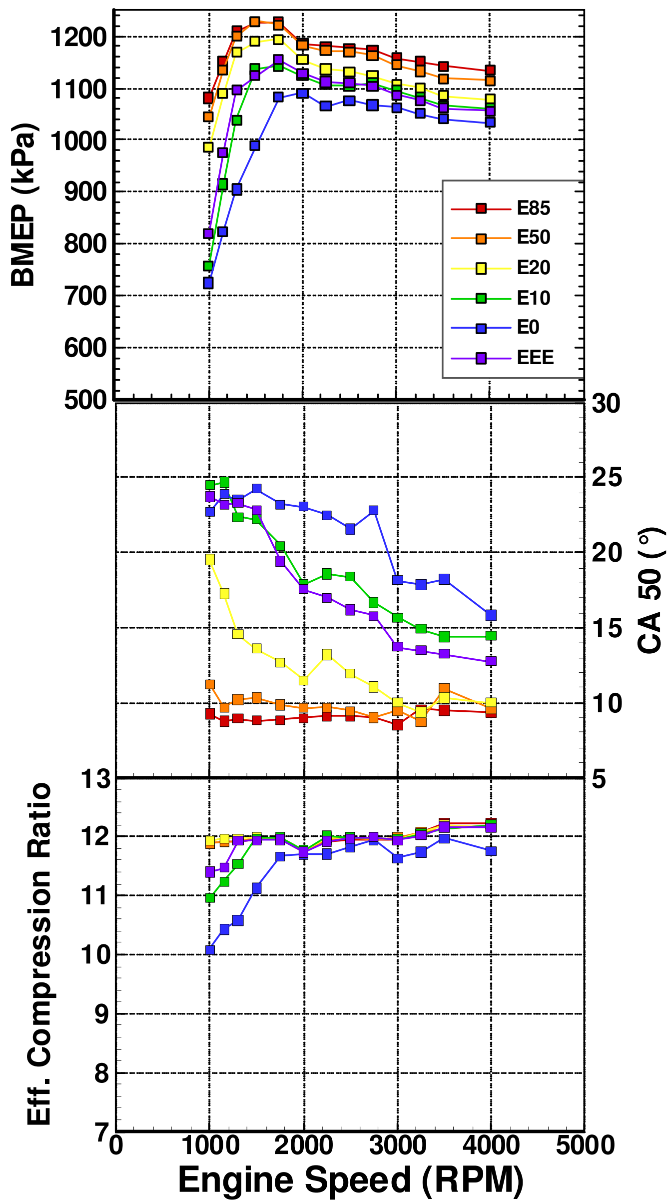

Figure 25(a) Peak Torque, (b) CA50, (c) CR of peak torque vs. RPM

MBT or knock limited torque Stoichiometric operation. 1000-4000 RPM LIVC Cam

Effect of valve deactivation on E20 blends

Under peak torque testing the E20 blend was able to reach performance similar to E85 with a significantly reduced energy density penalty. However the fuel blend testing had still shown an issue with particulate formation for all of the intermediate blends at high loads near the tuning peak. To determine the effectiveness of valve deactivation in this soot prone region the engine was reconfigured for valve deactivation and testing was done with E20 fuel. Data had previously been collected on E0 fuel which had highlighted the issue with particulate formation. Load sweeps were run at 1500 and 2000 RPM with E 20 which were speeds prone to soot formation. Figure 26 shows the 2000 RPM data including the E0 data as a function of load. In both cases the use of valve deactivation also results in a detrimental effect on knock sensitivity. The increase in knock with valve deactivation is likely the result of enhanced in-cylinder heat transfer that raises the end-gas temperatures during combustion. Additional spark retard is required for both fuels which lowers efficiency. This is significant in the case of E0 and a loss of 1 bar in peak torque is observed. For E0 the high load region were particulates were achieved is sacrificed so no benefit is realized. For E20 a small reduction in torque results but soot is significantly reduced at loads above 10 bar BMEP. Testing at 1500 RPM was only conducted with E20. A similar increase in knocking tendency was seen requiring spark retard at 1 bar lower load. The spark retard was not overly severe such that peak torque loss was approximately 0.5 bar BMEP. A significant reduction of Soot and hydrocarbons was observed for both MBT and knock limited loads and is presented in figure 27 along with knock limited combustion phasing.

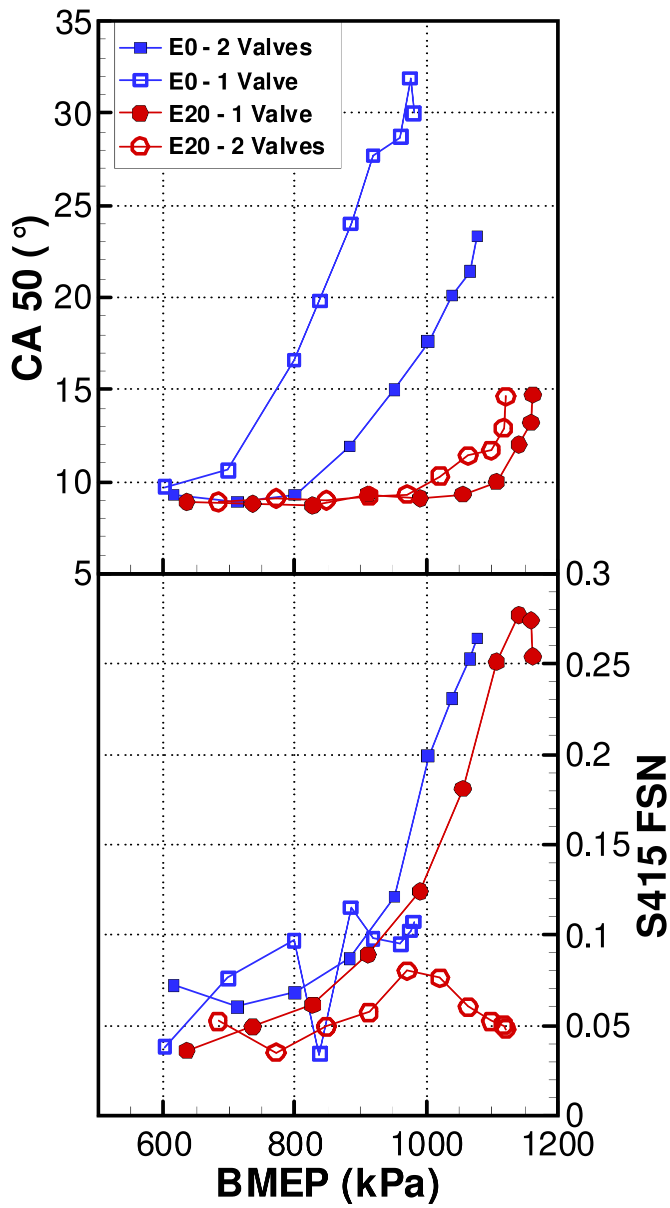

Figure 26 2000 RPM Load sweep, LIVC, E0 and E20 fuel. (a) Combustion Phasing (CA50 cad aTDC), (b) Soot (FSN)

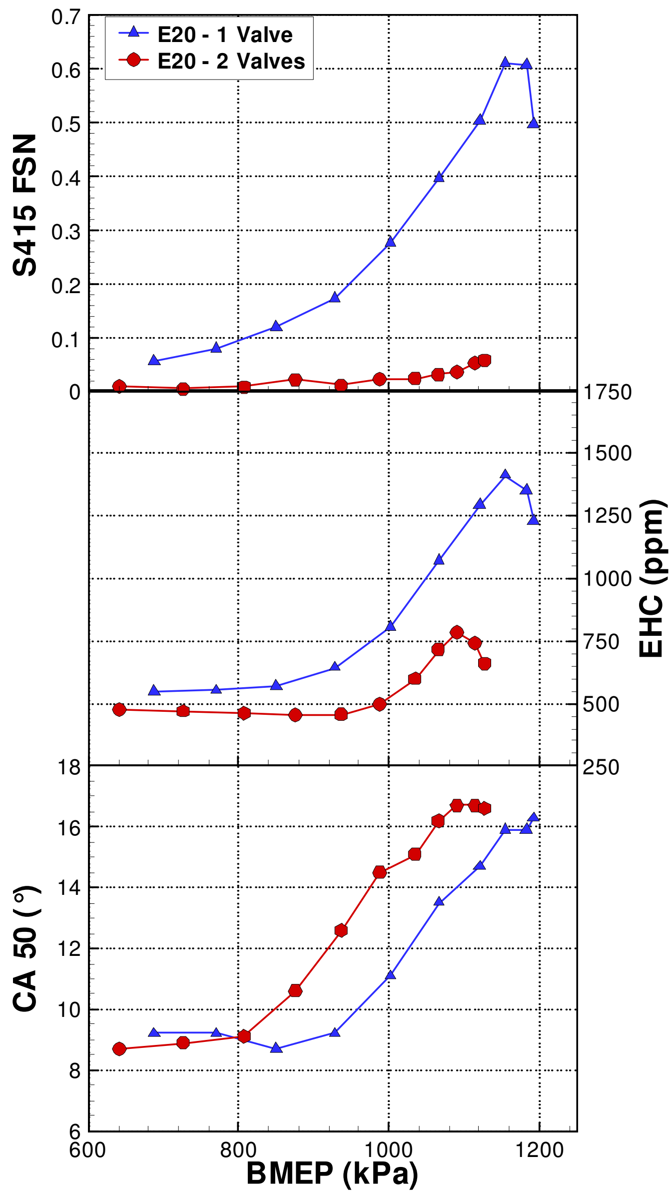

Figure 27 1500 RPM Load sweep, LIVC, E20 fuel. (a) soot (FSN), (b) Hydrocarbons (ppm), (c) Combustion Phasing (CA50 cad aTDC)

Phase 4 Task 4 – Multi-Pulse Fuel Injection

The Drivven Controller has been configured and programmed with multiple injection capability. This will be evaluated for opportunities to better control emissions, knock and improve efficiency in upcoming work.

Quarter 4 2010

Fuel blend testing - Data analysis

Evaluation of test data collected during fuel blend testing highlighted an issue with particulate emissions at knock limited and peak loads. This was an issue for all blends except E85. Figure 1 shows the soot emissions for a variety of fuel blends. The results are a combination of properties relating to the fuel. The inherent soot forming potential is reduced with increasing ethanol content however the allowable load increases with ethanol content and much more spark retard is needed for low ethanol fuel blends or gasoline. The result is that soot emissions are higher for E20 than E0 or E10 since load is higher with less spark retard.

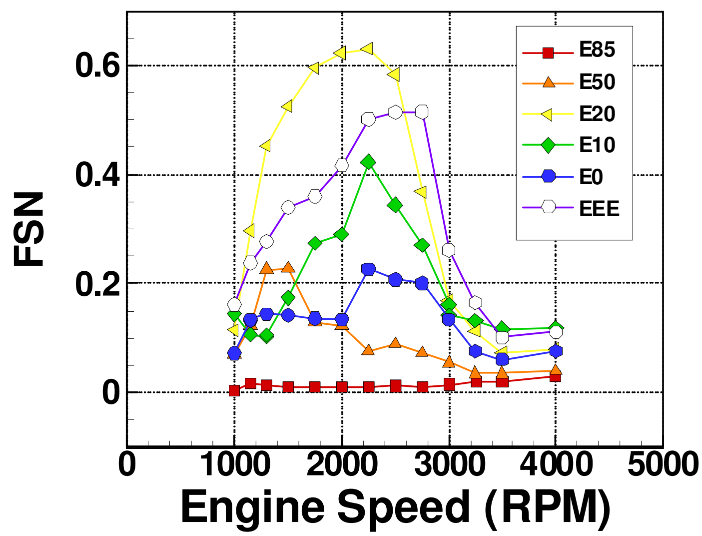

Figure 3 Soot emissions at maximum torque

Data for rated torque at knock limited compression ratio is shown in Figure 2. All combustion phasing was maintained at MBT with a 50% burn duration (CA50) at 9-10 cad aTDC. A similar trend to Figure 1 is observed but in this case it is driven by the competing effects of higher load with increasing ethanol content and the soot forming potential of the fuel.

To address this concern, charge motion has been shown to significantly reduce the soot levels and was tested and reported previously for gasoline and E20. However the detrimental effect of an increased knocking tendency and reduced output and efficiency was shown. To alleviate this compromise the use of multiple injections to promote a more uniform mixture will be evaluated and particle size distributions will be measured. In addition a new cam has been designed which will allow the use of asymmetric valves to determine if this provides a more favorable performance tradeoff. The use of 2-step variable valve actuation with valve independent controls allows for valvetrain operating modes to be selected to optimize emission performance and fuel economy tradeoffs.

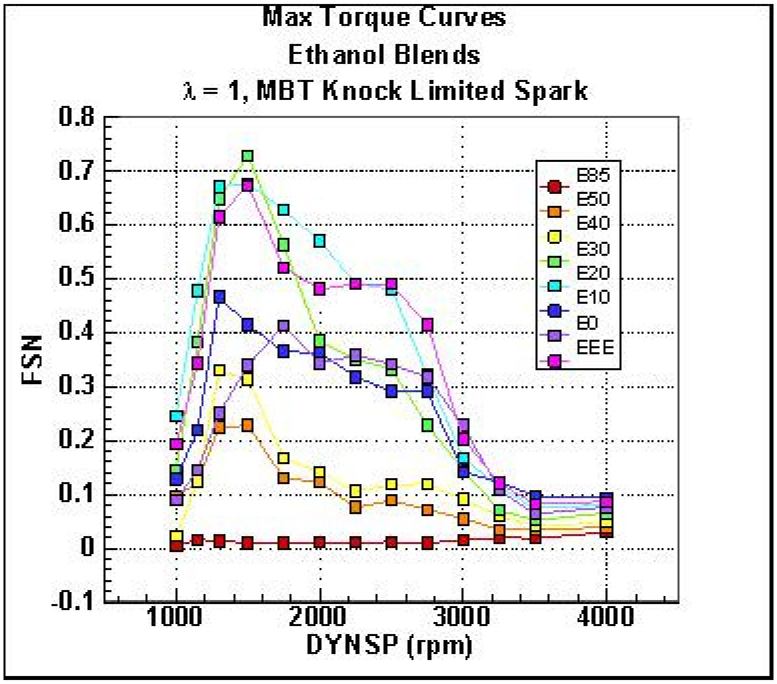

Figure 4 Soot emissions at knock limited compression ratio

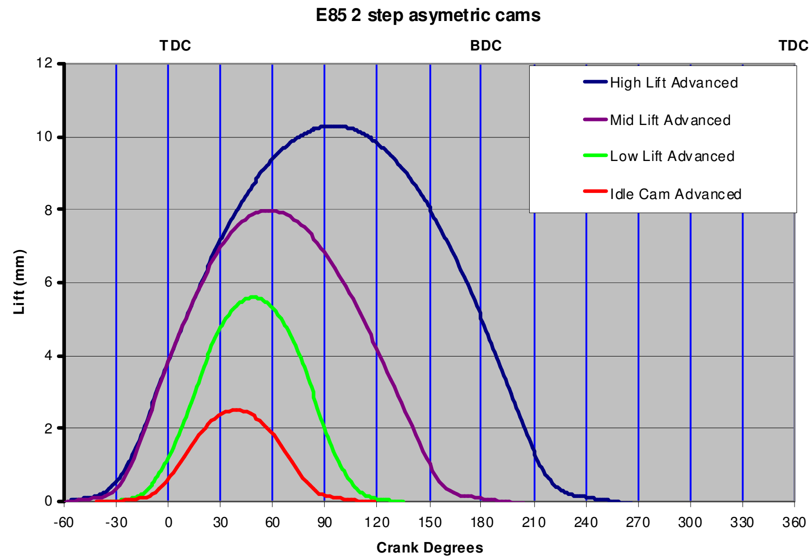

Figure 5 Asymmetric cam profiles

The effect of fuel blends on maximum cylinder pressures is also a strong function of ethanol content. Due to the ability of higher ethanol blends to resist knock, timing can be maintained at MBT, while gasoline and lower ethanol blends require significant spark retard. The peak cylinder pressure at maximum torque is presented in Figure 4. E85 is approaching 80 Bar while E0 Gasoline is 30-55 Bar due to spark retard and reduction of effective compression ratio using variable valve actuation. Peak cylinder pressure for this engine is limited to 100 Bar, therefore boost will be limited to near 1.3 bar while maintaining MBT. To further increase boost, spark retard will be required to reduce cylinder pressure to an acceptable level for the engine.

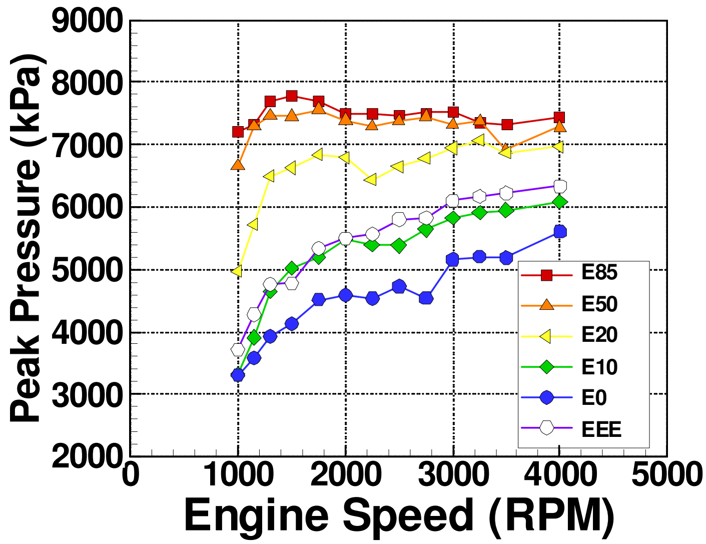

Figure 6 Naturally aspirated peak cylinder pressure of ethanol blends

The effect of spark retard on cylinder pressure is illustrated well in figure 5 which shows a 2000 RPM load sweep and the effect of fuel and spark retard on peak pressure.

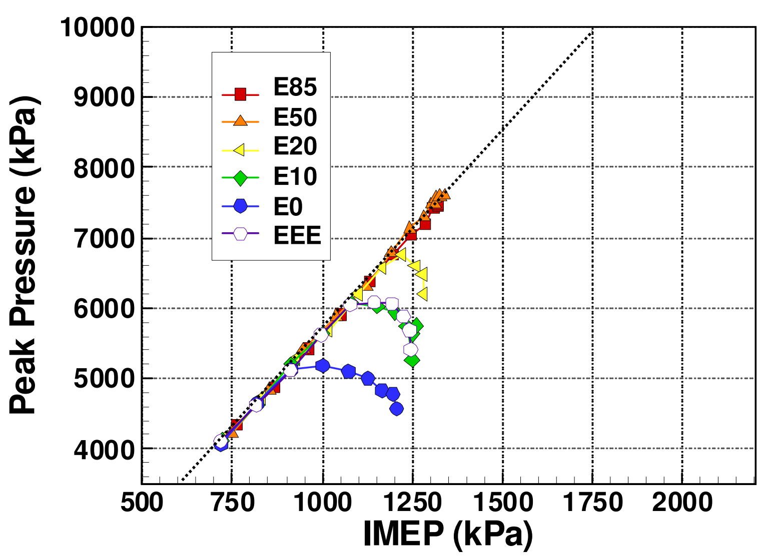

Figure 7 Peak cylinder pressure 2000 RPM load sweep

Without spark retard the peak cylinder pressure increases linearly and will reach the 100 bar maximum cylinder pressure for the engine near 18 Bar IMEP. The effect of spark retard on peak cylinder pressure can be seen when looking at plot

of gasoline (E0) or E10 fuels. As boost is increased for higher loads, above approximately 18 Bar IMEP, spark retard will be needed.
An estimate of allowable boost can be calculated using the following equation:

$IMEP_{(max)} = IMEP*P_{max}$ (100 Bar)/$P_{cylinder}$ (Bar)

The projects development engine is designed to provide a variable effective compression ratio by controlling displacement. In principle, the same load could be achieved at low effective compression ratio (low displacement) and a higher level of boost or a high compression ratio (high displacement) and a lower boost pressure. By using the above equation, the data from the load sweep is evaluated and it is not clear that there is a strong advantage of a high compression ratio (13 bar data) over a lower compression ratio (7 bar data), as seen in Figure 6. This will be a function of the boost capability and efficiency of the turbocharger. The advantage may be most obvious when operating on knock prone fuels, i.e. gasoline. This evaluation will continue during testing under boosted operation. The influence of spark retard on allowable maximum load is illustrated by the predicted loads with spark retard. This will be limited by the turbochargers ability to provide boost and also increases in turbine inlet temperature due to spark retard.

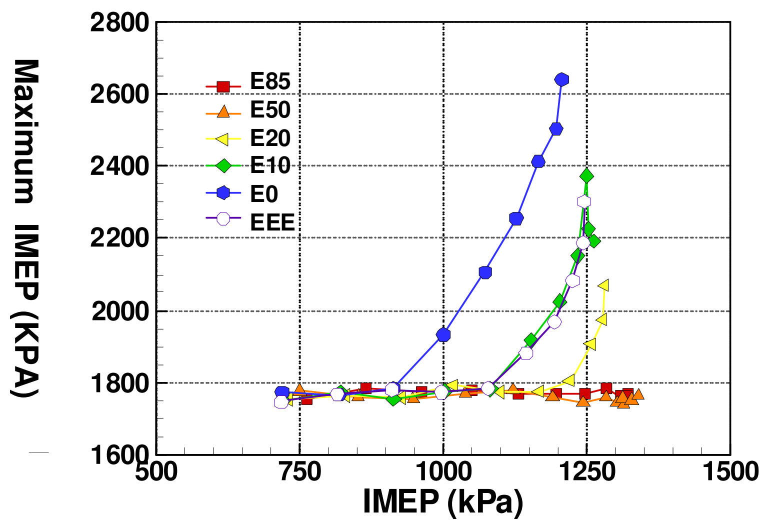

Figure 8 Predicted maximum load limited by cylinder pressure.

Exhaust port temperature is shown in figure 7. The temperatures are still significantly below the turbine inlet temperature maximum of 950 C for the turbocharger. As speed and load are increased during boosted operation it will be monitored. The effect of ethanol content can be clearly seen with exhaust port temperature of gasoline being 80℃ hotter than E85. The temperature difference is a combination of increased evaporative cooling and the ability to maintain MBT spark settings for E85 or higher ethanol blends.

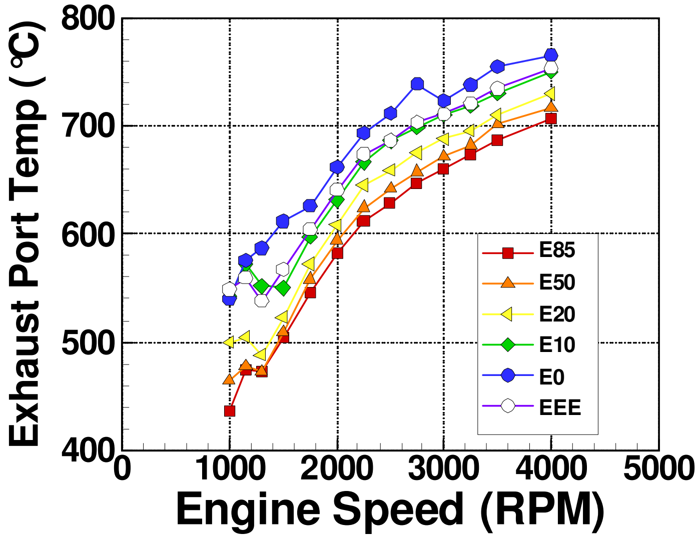

Figure 9 Exhaust port gas temperatures at maximum torque.

Fuel property testing

Fuel testing was completed for the ethanol blends tested. Ethanol content, water content, heating value, density and RON were measured.

From testing on this program and a review of other work it is evident that the benefit of ethanol for suppressing knock as measured by RON testing follows a non linear response with respect to the volumetric blend fraction. Figure 8 shows the results of RON analysis for this study in addition to data pulled from published sources. The results indicate both the nonlinear response of RON to ethanol content and a high degree of variability. A significant increase in RON is observed for the first 20 percent volume ethanol addition; further increases have a diminishing effect. A recently reviewed study suggests that RON and MON follow a more linear blending response when considered on a mole blending fraction. The same data is presented in Figure 9 versus the mole blending fraction supporting the idea of a molar dependence on RON. The high degree of variability in test results still exists and is partially explained by differences in the gasoline blend stock. Variation in the test procedure may also contribute since RON over 100 required additional preparations of reference samples that may lead to increased variation. A further look into understanding the variation may be a useful endeavor to study for the DOE or fuel industry. For industry to take full advantage of the fuel properties of ethanol, improved specifications for E85 blend stocks may be required, especially if it is used in intermediate blends by customer mixing with E0 or E10 as part of a blend pump strategy for intermediate blends.

Figure 10 Effect of ethanol volume fraction on measured RON (Literature review)

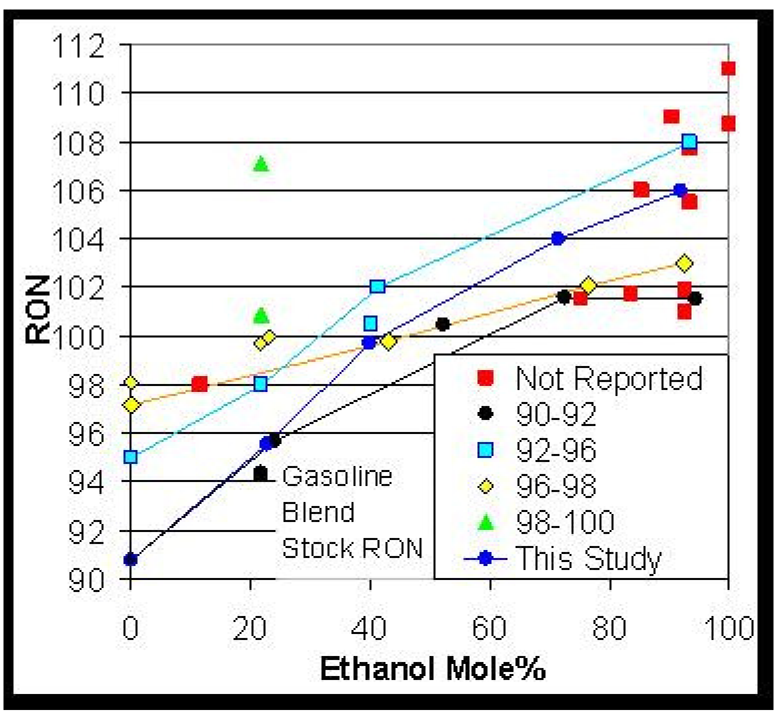

Figure 11 Effect of ethanol mole fraction on measured RON (Literature review)

ERROR: stackunderflow
OFFENDING COMMAND: ~

STACK: